

# **Ultra-High Performance Concrete (UHPC)**

## **Precast Segmental Bridges**

### **- Flexural Behaviour and Joint Design -**

Vom Promotionsausschuss der  
Technischen Universität Hamburg-Harburg  
zur Erlangung des akademischen Grades

Doktor-Ingenieur (Dr.-Ing.)

genehmigte Dissertation

von  
Jaewoo Shin

aus  
Seoul, Korea

2016

1. Gutachter: Prof. Dr.-Ing. Günter Axel Rombach
2. Gutachter: Prof. Dr.-Ing. Uwe Starossek

Tag der mündlich Prüfung: 06. Juli. 2016







## Abstract

Bridges have been built for thousands of years. Nevertheless, new construction methods which enable a very fast erection, a structure which can adapt to the increasing traffic loads, and new materials which improve the durability are still required. An externally post-tensioned precast segmental box girder bridge (PSB) is one solution to these requirements. The great advantages of this type of bridge have made them the preferred construction method for many great elevated highway projects, especially in South East Asia. Normal concrete, having a compressive strength of around  $f_{ck} \approx 40$  MPa, had been used for these structures. In the last years, concrete having  $f_{ck} > 160$  MPa has been developed. This Ultra High Performance Concrete (UHPC) shows significant advantages with regard to strength and durability. While the mechanical properties of UHPC are known, the applications for it are progressing very slowly because of high material cost and lack of design and experience. Thus, this research work focuses on the structural behaviour and the design of UHPC precast segmental bridges.

First, this research gives a brief overview of the material characteristics of UHPC and the suitability for application to segmental bridge construction. The design recommendations of various countries are analyzed. Some examples of UHPC segmental bridges are presented and discussed.

The results from a full-scale test of a Precast Segmental Bridge (PSB) are used to verify a non-linear FE-model of the structure. This numerical model is then adapted to UHPC bridges, having smaller cross-section heights and slab thicknesses. An intense parametric study (slenderness ratio, thickness of slabs,  $E$ -modulus, prestressing force) is conducted to find the most appropriate cross-section for UHPC-PSB. Based on these investigations, a multi-cell box girder with stiffeners is proposed as a viable UHPC precast segmental bridge. The structural behavior, e.g. the deflection, the width of the joint opening after decompression, the compressive and shear stress distribution and the increase of tendon stress for this single span structure is analyzed and discussed. It is demonstrated, that a UHPC-PSB shows significant advantages, such as the significantly reduced dead load, compared to constructions with normal strength concrete.

The capacity of the dry joints between adjacent segments is of crucial importance for the safety of the structure. It is doubtful whether the known design approaches for normal strength concrete can be used for UHPC structures. Therefore UHPC shear-key tests are conducted. Through the comparison of existing designs for UHPC shear-keys, and non-linear FE-simulations, a new design method for shear resistance of UHPC shear-key is proposed.

## Kurzfassung

Brücken werden schon seit vielen Tausenden von Jahren errichtet. Es liegen somit schon viele Erfahrungen vor. Dennoch werden neue Bauverfahren benötigt, die eine schnellere Errichtung der Konstruktion ermöglichen, weitgehend ohne Beeinflussung des vorhandenen Verkehrs. Weiterhin werden Bauwerke gesucht, die die zunehmenden Verkehrs- und Umwelteinwirkungen aufnehmen können und neue Baustoffe, die die Dauerhaftigkeit verbessern und somit die Unterhaltskosten reduzieren. Extern *vorgespannte Segmentfertigteilebrücken* (PSB) sind eine Lösung für diese Anforderungen. Die großen Vorteile dieser Bauweise belegen die vielen Anwendungen in Frankreich, Amerika und vor allem in Südostasien. Viele großen Hochstraße Projekte bestehen aus PSB, wobei bislang größtenteils Normalbeton mit einer Druckfestigkeit von ca.  $f_{ck} \approx 40$  MPa verwendet wurde. In den letzten Jahren wurde Beton mit  $f_{ck} > 160$  MPa entwickelt. Dieser UHPC (Ultra High Performance Concrete) zeigt deutliche Vorteile in Bezug auf Festigkeit und Dauerhaftigkeit gegenüber Normalbeton. Obwohl die mechanischen Eigenschaften von UHPC bekannt sind, vollzieht sich dessen Anwendung in der Baupraxis, u. a. aufgrund der hohen Materialkosten und dem Mangel an Bemessungsverfahren und Erfahrung, sehr langsam. Diese Forschungsarbeit befasst sich daher mit dem Strukturverhalten und der Bemessung von *Segmentfertigteilebrücken* aus UHPC (UHPC-PSB).

Zunächst wird ein kurzer Überblick über die Materialeigenschaften von UHPC und deren Eignung für Anwendung des Baustoffes im Segmentbrückenbau gegeben. Es folgt eine Erörterung der Normen und Richtlinien verschiedener Länder zur Bemessung von UHPC-Bauteilen. Einige Beispiele von Segmentbrücken aus UHPC werden vorgestellt und diskutiert. Um das Trag- und Verformungsverhalten von UHPC-PSB (*Ultra High Performance Concrete Precast Segmental Bridge*) zu studieren wird ein Finite-Elemente Modell entwickelt und anhand den Ergebnissen eines Großversuches, welcher im Rahmen des SES-Projektes in Bangkok stattfand, verifiziert. Ein intensive Parameterstudie (Schlankheitsgrad, Plattendicken, Elastizitätsmoduli, Vorspannkraft) wird durchgeführt, um einen optimalen Querschnitt zu finden. Auf der Basis dieser Untersuchungen wird ein Hohlkastenquerschnitt mit Rippen vorgeschlagen. Das Tragverhalten dieser Brücke, bspw. die Durchbiegungen, die Breite von Fugenöffnungen, die Druck- und Schubspannungsverteilung im Querschnitt und die Zunahme der Spannstahlspannung werden ermittelt und die Ergebnisse diskutiert. Es zeigt sich, dass eine UHPC-PSB deutliche Vorteile, bspw. das erheblich geringere Eigengewicht, im Vergleich zu Konstruktionen aus Normalbeton aufweist.

Die Tragfähigkeit von Trockenfugen zwischen aneinander liegenden Segmenten ist von entscheidender Bedeutung für die Tragsicherheit der Struktur. Es ist unklar, ob die Rechenansätze, welche für Normalbeton entwickelt wurden, auch für UHPC Strukturen verwendet werden können. Daher werden Versuche mit UHPC Schubnocken sowie nichtlineare FE-Simulationen durchgeführt. Es wird ein neuer Rechenansatz zum Nachweis der Querkrafttragfähigkeit von UHPC Schubnocken entwickelt.

# Table of Contents

## Abstract

## Kurzfassung

<b>1</b>	<b>Introduction</b>	<b>1</b>
1.1	Problem statement	1
1.2	Objectives	2
1.3	Thesis organization	2
<b>2</b>	<b>Ultra High Performance Concrete (UHPC)</b>	<b>4</b>
2.1	Development of concrete	4
2.2	Material	7
2.2.1	Composition of UHPC	7
2.2.2	Fibers	8
2.2.3	Effect of heat treatment	10
2.2.4	Types of UHPC	11
2.3	Mechanical properties of UHPC	13
2.3.1	Compressive strength	13
2.3.2	Tensile strength	14
2.3.3	Other material properties and durability	15
2.4	Design values for UHPC	18
2.4.1	Recommendations for design	18
2.4.2	Design values for compressive strength	19
2.4.3	Design values for tensile strength	20
2.4.4	Other design values for UHPC	20
2.5	Applications of UHPC in bridge construction	21
2.5.1	Examples in Germany	21
2.5.2	Examples in other countries	22
<b>3</b>	<b>Ultra high Performance Concrete Precast Segmental Bridge (UHPC-PSB)</b>	<b>25</b>
3.1	Precast segmental bridge (PSB)	25
3.1.1	Introduction	25
3.1.2	Casting of segments	26
3.1.3	Erection methods	27
3.1.4	Development of PSB	30
3.2	Considerations for UHPC segmental bridges	32
3.2.1	Concepts	32
3.2.2	Advantages and disadvantages of UHPC for structural applications	33
3.2.3	Construction techniques	34
3.2.4	Structural concept for UHPC segmental bridges	38
3.2.5	Ultimate failure pattern	40
3.3	Applications of UHPC-PSB	41
3.3.1	Foot bridges	41

3.3.2	Road bridges	43
<b>4</b>	<b>Flexural Behaviour of Ultra high Performance Concrete Precast Segmental Bridge (UHPC-PSB)</b>	<b>47</b>
4.1	Load-deflection relationship of PSB	47
4.2	Finite Element model of PSB	50
4.2.1	Second Stage Expressway System (SES)	51
4.2.2	Material properties used in the FE model	52
4.2.3	Verification	55
4.3	Parameter studies	58
4.3.1	Effect of E-modulus	59
4.3.2	Relationship of member thickness and compressive stress	61
4.3.3	Prestressing force	63
4.3.4	Span-to-depth ratio	65
4.3.5	Comparison of various concrete classes	66
4.4	Numerical analysis of UHPC-PSB	70
4.4.1	Proposed model for numerical analysis	70
4.4.1.1	Numerical model	70
4.4.1.2	Loads and prestressing	72
4.4.1.3	Loading step	74
4.4.2	Single span girder	74
4.4.2.1	Deflection and joint opening	74
4.4.2.2	Longitudinal stress distributions	76
4.4.2.3	Shear stress and rotation	78
4.4.2.4	Normal force variation in webs	79
4.4.2.5	Change of tendon stress	81
4.4.3	Continuous girder	82
4.4.3.1	Deflection and joint opening	82
4.4.3.2	Longitudinal stress distributions	84
4.4.3.3	Shear stress and rotation	86
4.4.3.4	Normal force variation in webs	87
4.4.3.5	Change of tendon stress	88
4.5	Conclusions	89
<b>5</b>	<b>Shear Design of UHPC Joint</b>	<b>91</b>
5.1	Literature review	91
5.1.1	Design models for joint	91
5.1.2	Tests on UHPC joint (flat and keyed joint)	98
5.1.3	Effect of SFRC	101
5.2	Experimental program	102
5.2.1	Test specimens	103
5.2.2	Test procedure	104
5.2.3	Test results	107

5.2.3.1	Test on flat joints	106
5.2.3.2	Test on keyed joints	108
5.2.3.3	Crack pattern and failure mode	112
5.2.3.4	Comparison with test result and design models	114
5.3	Finite element analysis of UHPC shear key	115
5.3.1	Constitutive models for concrete	115
5.3.2	Non-FE model of UHPC shear key	117
5.3.2.1	Material model of UHPC	117
5.3.2.2	Modeling of the shear key specimens	119
5.3.3	Verification of FE models	121
5.3.4	Sliding on inclined contact surface at a key area	124
5.3.5	Shear strength of shear key without confining pressure	126
5.4	New model for shear key design	129
5.4.1	Shear strength of pure shear key	129
5.4.2	Frictional resistance between contact surfaces	131
5.4.3	New proposal	132
5.5	Conclusions	136
<b>6.</b>	<b>Conclusions and prospects</b>	<b>138</b>

## Appendix

A.	Historical Overview of Segmental Bridges	141
B.	UHPC Shear-key Tests	158

<b>References</b>	174
-------------------	-----

<b>Abbreviations</b>	184
----------------------	-----

<b>Notations</b>	185
------------------	-----



# 1 Introduction

## 1.1 Problem statement

Development of new materials can improve the load bearing capacity, serviceability, durability and ease of construction for a structure. Ultra high performance concrete (UHPC) with very high strength, remarkable durability and a ductile behaviour opened new possibilities in concrete construction such as light concrete structures. Since the Bourg-Les-Valence Bridge in France 2001 [Hajar et al. 2004], which is regarded as the first road bridge made of UHPC in the world, small sized PSB had been built in several countries such as France, Japan, USA, Austria and Germany. However, in spite of the excellent material properties, its application is progressing slowly due to the high material cost and a lack of practical design methods and experience.

Figure 1.1 shows the evolution of concrete compressive strength since 1940. With high strength concrete, since 1980s, the compressive strength in practice increases rapidly through the development of UHPC.

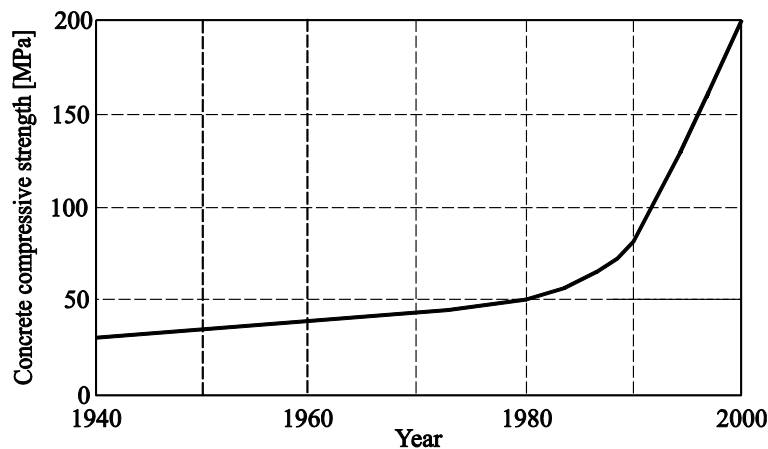


Figure 1.1: Development in the compressive strength of concrete (used on real construction sites) [Acker, Ulm 2011]

In general, UHPC is often used as prefabricated members for modular constructions with joints. However, recommendations or codes for the joint design of very thin members used in practice and for high strength concrete does not exist up to now. For an economic application of UHPC, new design concepts for this material have to be developed. This thesis aims to improve the knowledge in this field.

## 1.2 Objectives

With regard to structural applications of ultra high performance concrete for precast segmental bridges in practice, the main objectives of this thesis are to present concepts and proposals for the design of ultra high performance concrete precast segmental bridge (UHPC-PSB)

Therefore, the objectives of this study are:

- to study the flexural behaviour of precast segmental bridges made of UHPC
  - present the advantages of UHPC material
  - find an optimized cross-section for UHPC-PSB
  - develop a nonlinear finite element model to study the flexural behaviour of UHPC-PSB
- to develop a new method for joint design of UHPC-PSB
  - check and compare the existing joint formulas for application of UHPC
  - conduct experiments with UHPC keyed dry joints
  - study the behaviour and the failure pattern of UHPC shear keys
  - validate the test results through finite element analysis
  - develop a new approach for design of keyed dry joints (for various concrete classes including HSC, UHPC and as well as NSC).

This study will demonstrate the great potential of optimized precast segmental bridge made of UHPC through suitable construction types, such as dry joints, external tendons and span-by-span construction method.

## 1.3 Thesis organization

The thesis consists of six chapters and two appendices.

The first chapter gives an introduction to the field of research, the objectives and the organization of the thesis.

Chapter 2 focuses on the construction material ‘UHPC’. First the development of UHPC is presented shortly. Furthermore the most significant mechanical properties as well as design values are given. Some field applications of UHPC structures are presented.

A brief introduction to PSB, the concepts and the suitability for application of UHPC in segmental bridge construction is given in chapter 3. Several examples of UHPC segmental bridges are presented.

Chapter 4 deals with the flexural behaviour of UHPC-PSB with external tendons and dry joints by means of a nonlinear finite element model. First the complex FE model is verified based on the results of full-scale test of a standard span of the SES project in Bangkok. A very good agreement



between simulation and real behaviour had been obtained. Then parameter studies had been conducted, where the effect of E-modulus, the relationship between member-thickness and concrete strength, the span-to-depth ratio and the tendon stresses etc. are studied. Based on these investigations an optimized cross-section for a UHPC-PSB, which has very thin sections, is proposed. Finally, the flexural behaviour of this UHPC-PSB is studied by numerical simulations. These investigations are focused on the change of normal stresses at mid-span caused by deflections and joint openings.

Chapter 5 focus on the design of UHPC keyed dry joints. Experiments and numerical simulations have been conducted to assess the shear strength and deformation behaviour of the joint. The studies included flat joints (without shear-key) for the estimation the friction coefficient of UHPC and keyed joints with the different levels of normal stresses. The shear capacity, structural behaviour and crack patterns of dry joints in UHPC precast members were investigated. The results obtained in these tests are compared with existing design approaches. Finally a new design formula is proposed.

Chapter 6 presents conclusions and prospects for further research in this field.

Finally, a historical overview of segmental bridges (Appendix A) and detailed information on the experimental program (Appendix B) are added to this thesis.

## 2 Ultra High Performance Concrete

### 2.1 Development of concrete

Generally, high performance concrete (HPC) is often said to be comparable to high strength concrete (HSC). However, the ability of HPC is not limited to compressive strength of concrete as it has an improved microstructure for enhanced durability.

As time went on, the development and the definition of High Performance Concrete have changed. In the 1950s, concrete compressive strength was limited to  $f_{ck} \approx 34$  MPa. In the 1960s, concrete having compressive strength of about 50 MPa was used in practice. In the early 1970s, concrete of 62 MPa was already produced. The application of such high-strength concrete has mostly been used in the columns of tall buildings in order to reduce the column size. It has been shown that the use of more expensive HSC is more economical than increasing the amount of steel reinforcement. For bridges, too, smaller cross-sections bring significant advantages. A reduction in dead load permits longer spans. The higher elastic modulus and lower creep coefficient result in a reduction of initial and long-term deflections. In prestressed concrete bridges, the initial and time-dependent losses of prestressing force are reduced [ACI 1997]. Generally, HSC refers to concrete having compressive strength in the range of  $f_{ck} \approx 55$  MPa to 100 MPa. In the 1980s, the development and use of high-performance concrete attract world-wide attention due to durability problems and short service life of existing structures made of normal strength concrete [Russell 2013].

Basically, high-performance concrete is composed of the same materials as normal concrete, but it has been engineered to achieve enhanced durability and/or strength characteristics. An optimized concrete technology is used, namely an extremely low W/C ratio and silica fume is added. Nowadays, the use of HSC can result in designs that are more efficient with lower construction costs, faster construction and decreased consumption of resources. Furthermore bridges having longer spans and fewer beams can be built.

In the 1970s, water-reducing agents and superplasticizers were introduced in concrete production. Using these, the W/C ratio could be decreased to about 0.45 to 0.60 without any negative effect on the concrete's workability. Furthermore the compressive strength could be improved to about  $f_{ck} \approx 60\text{--}70$  MPa. In order to obtain yet higher concrete strengths, a further improved technology was necessary. In HPC, the W/C ratio must be decreased to about 0.25 (see Figure 2.1). For this purpose, extremely effective superplasticizers, so-called High Water Reducing Agents (HWRA), had been developed. Considering the well-known correlations between W/C ratio and concrete strength, it is obvious that it is not possible to exceed a concrete strength of 100 MPa by the reduction of the W/C ratio alone.

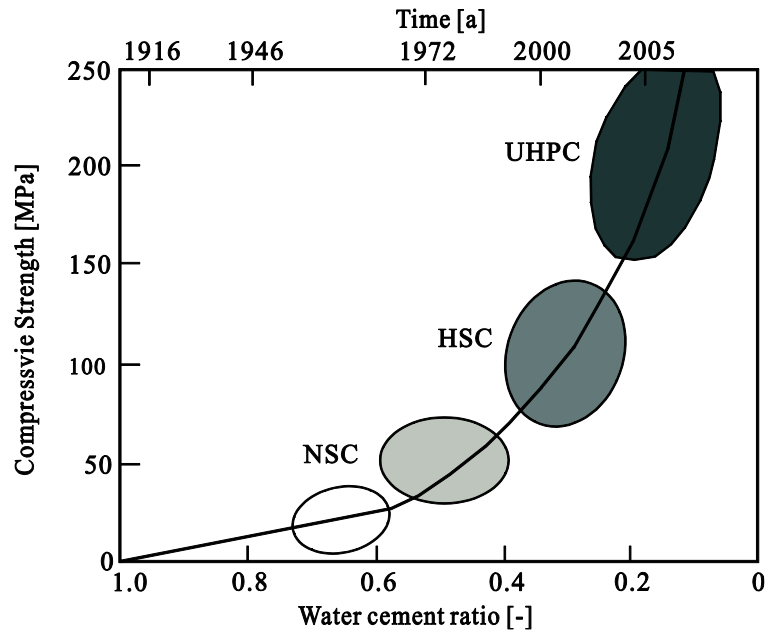


Figure 2.1: Concrete compressive strength by W/C ratio [Freytag et al. 2008]

Due to the improved durability of the concrete, there were applications of HPC in bridges, mainly in Japan, North America and Europe (see Table 2.1). The use of concrete with compressive strength up to  $f_{ck} \approx 78$  MPa in the railway bridges in Japan had also been reported.

HPC was used for the first time in Germany for the columns of the 186 m high rise building, so called “Trianon”, in Frankfurt in 1990 [Breitenbücher 1998]. Almost all applications of HPC have been reported in high-rise buildings. In 1998 the first road bridges, small prestressed slab structures, using HPC in Germany have been built in Baden-Württemberg and in Bavaria [Bernhardt et al. 1999]. Between 1998 and 2001, several bridges with concrete grade C70/85 were realized as pilot projects.

In the past decade significant advances have been made in the field of high performance concretes. The next generation of concrete, the so called ultra high performance concrete (UHPC), exhibits exceptional compressive strength that may exceed 200 MPa, durability, long-term stability, structural efficiency, cost-effectiveness that make it well suited for use in bridge structures.

Table 2.1: Bridges with high strength concrete

Bridge	Location	Year	Maximum design concrete strength [MPa]
Nitta Highway Bridge <sup>1)</sup>	Japan	1968	60
Kaminoshima Highway Bridge <sup>1)</sup>	Japan	1970	60
Ootanabe Railway Bridge <sup>1)</sup>	Japan	1973	78
Fukamitsu Highway Bridge <sup>1)</sup>	Japan	1974	70
Akkagawa Railway Bridge <sup>1)</sup>	Japan	1976	78
Red River Cable-Stayed Bridge <sup>4)</sup>	Guangxi, China	1980	60
Huntington to Proctorville <sup>1)</sup>	W.Va. to Ohio, USA	1984	55
East Huntignton Cable-Stayed Bridge <sup>2)</sup>	East Huntignton, W. Va., USA	1985	55
Annicis Cable-Stayed Bridge <sup>2)</sup>	British Columbia, Canada	1986	55
Tower Road Bridge <sup>1)</sup>	Washington, USA	1987	63
Joigny Bridge <sup>2)</sup>	Joigny, France	1989	60
Braker Lane Bridge <sup>2)</sup>	Texas, USA	1990	66
Liangshui River Highway Bridge <sup>2)</sup>	Beijing-Tianjin, China	1990	60
Normandie Bridge	Normandy, France	1993	60
Louetta Road overpass <sup>2)</sup>	Texas, USA	1994	69
Portneuf Bridge <sup>2)</sup>	Quebec, Canada	1993	60
Confederation Bridge <sup>3)</sup>	Northumberland Strait, Canada	1994	55
Burgerveen <sup>4)</sup>	Rijkswaterstaat, Netherlands	1995	70
Badhaus Bridge <sup>4)</sup>	Tulln, Austria	1997	91
Buchlose Bridge <sup>5)</sup>	Bavaria, Germany	1998	70
Sasbach Bridge <sup>6)</sup>	Baden-Württemberg, Germany	1998	70
Weißeritz Bridge <sup>4)</sup>	Saxony, Germany	1999	70
Griesbach Bridge <sup>7)</sup>	Bavaria, Germany	2000	70
FreihamerAllee Bridge <sup>8)</sup>	Bavaria, Germany	2001	70
Glaubau Bridge <sup>4)</sup>	Saxony, Germany	2001	70

1); [ACI 1997], 2); [Ralls, Carrasquillo 1994], 3); [Tadros, Lester 1997], 4); [König, Tue, Zink 2001]

5); [Zilch et al. 1999], 6); [Bernhardt et al. 1999], 7); [Zilch et al. 2001], 8); [Zilch, Zehetmaier 2002]

## 2.2 Material components

### 2.2.1 Composition of UHPC

UHPC mixtures contain Portland cement, silica fume, quartz flour, fine silica sand, high-range water reducer, and metallic or organic fibers ( $\approx 2\%$  by volume). Materials are usually supplied to the precast concrete producer in three components: premix, superplasticizer, and fibers. The properties of microstructure matrix of UHPC produce a highly compact, dense material within a low porosity matrix. Typical compositions are provided in Table 2.2.

Table 2.2: Mix proportions from various types of UHPC

Material	Types of UHPC			
	M1Q <sup>1)</sup> [kg/m <sup>3</sup> ]	B1Q <sup>1)</sup> [kg/m <sup>3</sup> ]	Ductal® <sup>2)</sup> [kg/m <sup>3</sup> ]	®Cemtec multiscale <sup>3)</sup> [kg/m <sup>3</sup> ]
Portland Cement	733	580	712	1050
Fine Sand	1008	354	1020	514
Basalt 2/8		711		
Silica Fume	230	177	231	268
Ground Quartz	183	325	211	
Quartz Powder		131		
Superplasticizer	28.6		30.7	44
Accelerator	-	30.4	30.0	
Steel Fibers	192	194	156	858
Water	161	148	109	180

1) [Bornemann, Schmidt et al. 2001], 2) [Casanova et al. 2000], 3) [Rossi et al. 2005]

### Water/binder-ratio

Mixtures for UHPC are generally made with a very low water-cement ratio (w/c), even below 0.2, which is significantly lower than the assumed practical minimum value of 0.4. The lower the w/c-ratio; the lower the percentage of cement that can react with water. In spite of a low degree of hydration, very high strength values can be achieved. What counts is the intensity with which hydrating particles are glued together. The evolution of the strength can be correlated to the total contact area between solid particles. As the water to cement ratio is very low, UHPC often does not exhibit any significant drying (no weight loss can be measured) nor drying shrinkage.

### **Silica fume**

Silica fume is the principal constituent of HPC and UHPC in combination with super-plasticizer. Its known superior properties, the micro filler effect and excellent pozzolanic properties, made it possible to produce concrete with outstanding properties. The use of silica fume in concrete increases the calcium silicate hydrate (C-S-H) gel formation that is mainly responsible for the high strength, high durability of concrete members and reduction of pore sizes.

Silica fume is an industrial by product from ferro-silicon alloy producing units, and hence its availability is limited. It also sometimes gives dark color to the concrete, which is due to the unburned coal contained in it, which can be an aesthetical problem. However, specially treated silica fumes are available, but they are expensive.

### **2.2.2 Fibers**

To achieve ductile post failure behavior in compression and to increase tensile strength and ductility of UHPC, often fibers, normally high strength steel fibers, are added. Thus very high flexural strengths can be achieved, particularly for thin structural members. In contrast to this, UHPC without fibers behaves brittle, if no additional measure such as confinement is chosen.

Under addition of fibers the load-displacement behavior and consequently the ductility and fracture toughness can be improved. This can be traced back to the fact that the fibers are able to transfer emerging loads by bridging the cracks. Here the fibers make an impact not until the appearance of cracks. That means after reaching the maximum load the descending arm of the load-displacement curve does not drop down at once. Depending on the kind of fiber, fiber length especially, and the fiber content, slow and even reduction of loads appear, coming along with increasing deformations.

UHPC with fibers shows, depending on the type and quantity of fibers contained in the mix, ductile behavior under compression as well as in tension. Since the pre-peak behavior does not show significant differences, the elastic properties of UHPC with and without fibers can be described in common whereas the influence of fibers has to be described separately. A consequence of the dense material is the improvement of the contact zones between the cement matrix and the aggregates as well as the fiber reinforcement which allows a short length of fibers.

In general the influence of fibers on the compression strength is low. Due to 2.5 vol.-% of fibers, an increase of the compressive strength of about 15 % has been noted.

For UHPC a pronounced descending branch can be developed by the effect of the fibers. The slope of the descending branch depends on:

- Fiber content
- Fiber geometry (length, diameter)
- Fiber length in relation to maximum aggregate size
- Fiber stiffness (in case of fiber cocktails)
- Fiber orientation

Within the fiber geometry a mixture of fiber lengths is preferred [Markovic 2006]. The role of the different fiber lengths is explained in Figure 2.2.

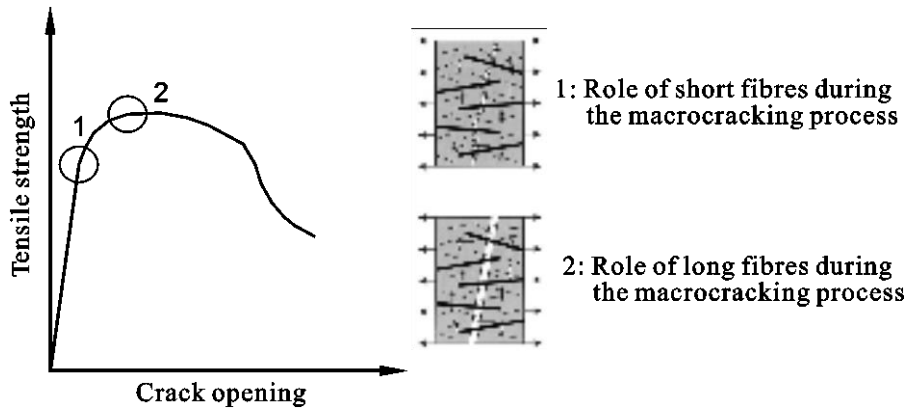


Figure 2.2: The role of fibers in different stages of tensile cracking [Orgass et al. 2004], [Markovic 2006]

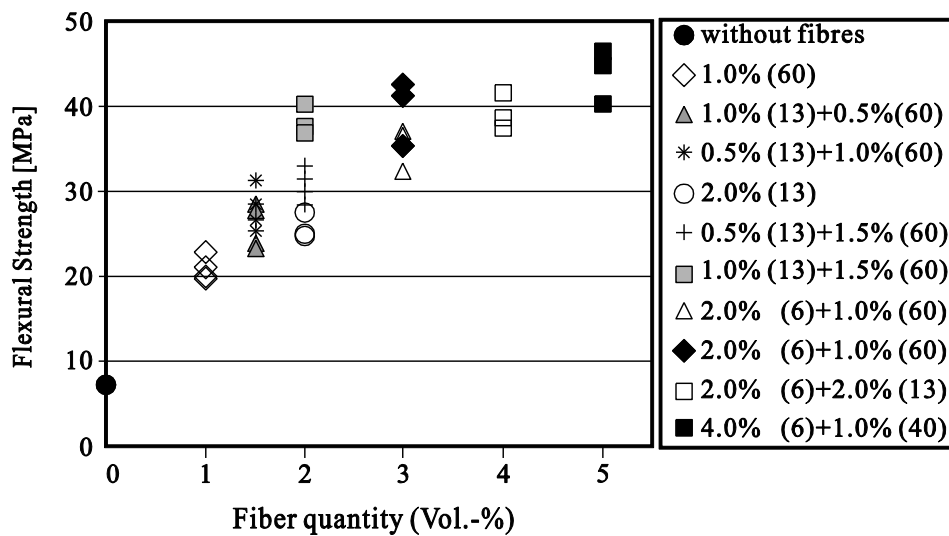


Figure 2.3: Flexural strengths of concretes with one and two types of steel fibers [Markovic 2006]

It is however not necessary to use that high quantities of fibers. Figure 2.3 shows that only slightly lower flexural strength of about 40 MPa can be obtained with a Hybrid-Fiber Concrete, which contains only 2.0 vol. % of fibers. Similarly, the flexural strengths achieved by concretes with 3.0 or 4.0 vol. % of fibers, are almost equal to the flexural strength of the concrete with 5.0 vol. % of fibers. Therefore, the applied combination of fibers is far more important than the applied volume quantity of fibers in an absolute sense.

In the case of the two concretes with in total 1.5 vol. % of fibers, the highest flexural strength was achieved if concrete contained more long fibers. The flexural strength was higher with fiber combination 0.5 % (13) + 1.0 % (60) than with 1.0 % (13) + 0.5 % (60). In Figure 2.3, 1.0 % (13) + 0.5 % (60), for example, contains 1.0 vol. % of fibers with  $l/d = 13/0.2$  and 0.5 vol. % of fibers with  $l/d = 60/0.7$ .

A similar conclusion could be drawn as well for all concretes with 2.0 vol. % of fibers. In this case, the application of a combination of short and long fibers (1 % (13) + 1 % (40)) resulted even in a 50 % higher flexural strength, than achieved by the concrete with the same volume quantity of the short fibers only (2 % (13)). Obviously, the combining of different types of fibers has very positive effects in this case [Markovic 2006].

Due to the fibers and their contribution to the behavior in tension UHPC shows a different tensile behavior than ordinary concrete. This has an important influence on the design of structures in UHPC. It can be concluded that:

- Major tensile stresses should be taken by reinforcement bars or pre-stressed steel to guarantee a reliable and efficient tension bearing.
- The strain hardening effect caused by the fibers leads to a well distributed multi cracking. This eliminates the need of minimal reinforcement for crack distribution.
- The bond between reinforcement and the fiber reinforced cement matrix is about 10 times higher than the bond strength of conventional concrete. This leads to a theoretical short development length, which could make connection of precast elements very easy.
- Shear and punching reinforcement are not needed for minor shear stresses due to the high tensile strength.

From this point on the term Ultra High Performance Fiber Reinforced Concrete will be abbreviated to UHPC. Both “UHPC” and “UHPFRC” are considered to be correct terms since the content of fiber reinforcement is inevitable for the structural application of the material, and therefore, the term “UHPC” is considered to be common.

### **2.2.3 Effect of heat treatment**

Various types of UHPC undergo heat treatment which consists in raising the temperature of components to a relatively high level, with temperatures between 60 and 90°C for 48 to 72 hours, starting a few hours after the concrete has set. This kind of treatment must be carried out only after the concrete has set in order to avoid any risk of delayed Ettringite formation, a form of internal sulfate attack believed to be caused by improper heat curing. Table 2.3 shows the results that were reported by Federal Highway Administration of U.S. Department of Transportation for material property tests of UHPC.

Heat treatment therefore requires good knowledge of the setting time. The main effects of heat treatment are as follows:

- The concrete strengthens faster (compressive and tensile strengths)
- Delayed shrinkage and creep effects reduce substantially once the heat treatment is finished
- Durability characteristics are considerably improved



Table 2.3: UHPC material properties according to curing treatment [Graybeal 2006]

Material characteristic	Steam	Untreated	Supplemental description
Compressive strength (MPa)	193	126	28-day strength
Modulus of Elasticity (GPa)	52.4	42.7	28-day strength
Flexure cracking strength (MPa)	9.0	9.0	305mm span
Tension cracking strength (MPa)	9.7-11.0	5.5-6.9	Axial tensile load
Long-term creep ( $\phi_\infty$ )	0.29	0.78	77-MPa sustained load
Total shrinkage ( $\epsilon_{s,\infty}$ in mm/m)	850	790	Embedded vibrating wire gage
Freeze-Thaw resistance (RDM)	96 %	112 %	600 cycles

### 2.2.4 Types of UHPC

Examples of UHPC currently marketed are given in the following:

- Different kinds of **Ductal®** concrete, including RPC (Reactive Powder Concrete), resulting from joint research by Bouygues, Lafarge and Rhodia, and marketed by Lafarge and Bouygues
- **Ceracem®** concrete, which technology has evolved from BSI "Béton Spécial Industriel" (special industrial concrete), developed by Eiffage in association with Sika.
- **BCV®** being developed by cement manufacturer Vicat and Vinci group. Rather few available data is on hand in literature.
- **Cemtec multiscale®**, developed by P. Rossi et al. [2005], with first available results around 2002 and site application in 2004. It represents one available solution of UHPC with multi-scale (hybrid) fiber reinforcement (with about 10 % total fiber content; about 3 % for the longest fibers).

All of these materials have been used at least once in a real-size project, for either a new bridge or a repair operation. Historically CRC (compact reinforced cement) developed by Bache in Denmark [Bache 1999] has a lot of properties close to those of UHPC.

Considering UHPC (presently available), the sources of difference can be listed as follows:

- The choice of fibers percentage and type, which is mainly governed by the required post-cracking ductility, and also interacts with size of the elements.
- Possible heat treatment, which is especially applied for Ductal®. Hydration is thus boosted during a 48 hours heat treatment (90°C) 2 days after setting, which further strongly reduces

creep and shrinkage deformations. This treatment is of specific interest for pre-fabricated segments assembled by post-tensioning

- Possible addition of organic fibers, in general polypropylene fibers at about 1 to 2% in mass of the cement content, in order to improve fire resistance of the elements by prevention of spalling. This addition has generally little influence on the rest of the mixture proportions.
- Maximum aggregate size: while some Ductal® materials only contain cement or very fine sand (< 2 mm), Ceracem® includes up to 7 mm-sized ultra-hard natural aggregate (but at a rather low content as compared to micro-concrete). These aggregate have a beneficial effect with respect to shear transfer, but they imply using longer fibers.
- Cement type, chemical nature of fine additives and type of silica fume: these choices have generally been optimized in the “premix” industrially available UHPC, however there are still a lot of possible variations depending on possible requirements of chemical durability, economical and local feasibility, etc.
- Super plasticizer type, which induces some differences in the rheological behavior of UHPC at the fresh state. While vibration is generally avoided, due to the risks on the fiber repartition, some UHPC types are definitely self-compacting with a low viscosity, some of them may require adapted casting in order to eliminate bubbles and prevent hardening.

More information on Ductal® is represented below;

A technological breakthrough took place in the 90's with the development of Reactive Powder Concrete (RPC), offering compressive strength exceeding 200 MPa and flexural strength over 40 MPa, showing some ductility. Based on the RPC initial research, the Ductal® technology was then developed. Comprehensive physical analysis and experimental results have confirmed the ability to achieve and combine several properties, usually considered as contradictory.

As a result of the ductility and very high compressive strength of such material, it is today possible to avoid passive reinforcements in structural elements. The Ductal® technology has been introduced as a first reference, in several countries, both in structural and architectural segments of construction and currently developing through innovative applications in large projects at various stages of development. It has local adapted variations under license in Korea, Japan, USA, Canada and Australia where bridge projects have been built.

Ductal® refers to a simple concept, minimizing number of defects such as micro-cracks and pore spaces, which allows in achieving a greater percentage of the potential ultimate load carrying capacity defined by its components and provide enhanced durability properties. To apply that concept, a concrete was proportioned with particle sizes down to less than 0.1 mm to obtain a very dense mixture which minimized void spaces in the concrete.

## 2.3 Mechanical properties of UHPC

The term “UHPC” (Ultra-High-Performance-Concrete) is an all-embracing expression for multiple compositions of mixtures leading to a satisfying “*new material*” with high performance demands. Because of this multiple compositions, it is not possible to discuss all different types. The characteristics of UHPC are therefore discussed in general.

### 2.3.1 Compressive strength

The typical compressive strength of UHPC is in the range of 150 to 220 MPa. Until about 70 to 80 % of the compressive strength, UHPC shows a linear elastic behavior (see Figure 2.4) regardless of the maximum aggregate size. The failure of UHPC without fibers is of explosive nature. No descending branch in the stress-strain-diagram does exist. The modulus of elasticity values have been reported to be in the range of  $E_c \approx 45 - 55$  GPa. Linearity limit and Poisson’s ratio from stress-strain relationship are constant up to  $\approx 80$  % of compressive strength.

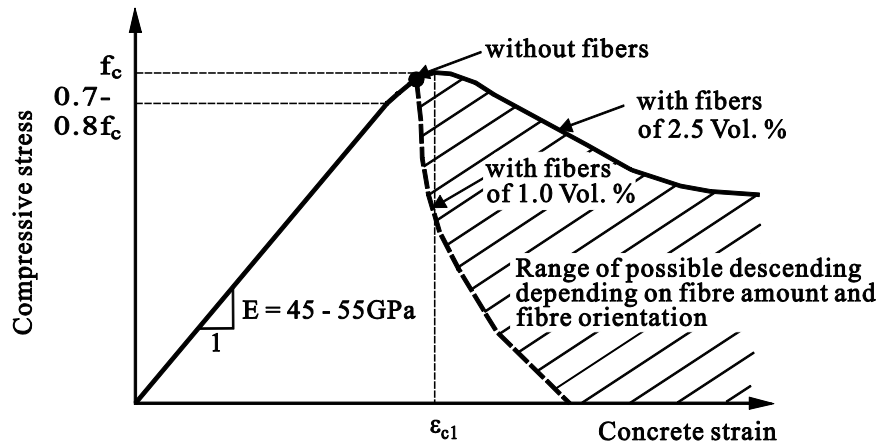


Figure 2.4: Compressive stress-strain relationship of UHPC with different fiber content [DAfStb 2008]

Figure 2.5 shows the behaviour of UHPC under compressive stress in comparison to the behaviour of normal and high-strength concrete. The failure cannot be observed in the stress-strain curve. The typical fracture energy of UHPC fiber-free matrix is almost in the range of mortars.

The addition of fibers to a UHPC matrix leads to less brittle compressive behaviour. The compressive strength is slightly improved by fibers. The non-linear part before failure is more pronounced than with fiber-free matrix due to the improved stress transfer mechanism through the micro-cracks. In general, the compressive strength is reached at a strain in the range of 3.5 – 5 ‰. The post-peak softening behaviour is influenced mainly by fiber content, fiber type (straight or hooked) and interaction of fibers.

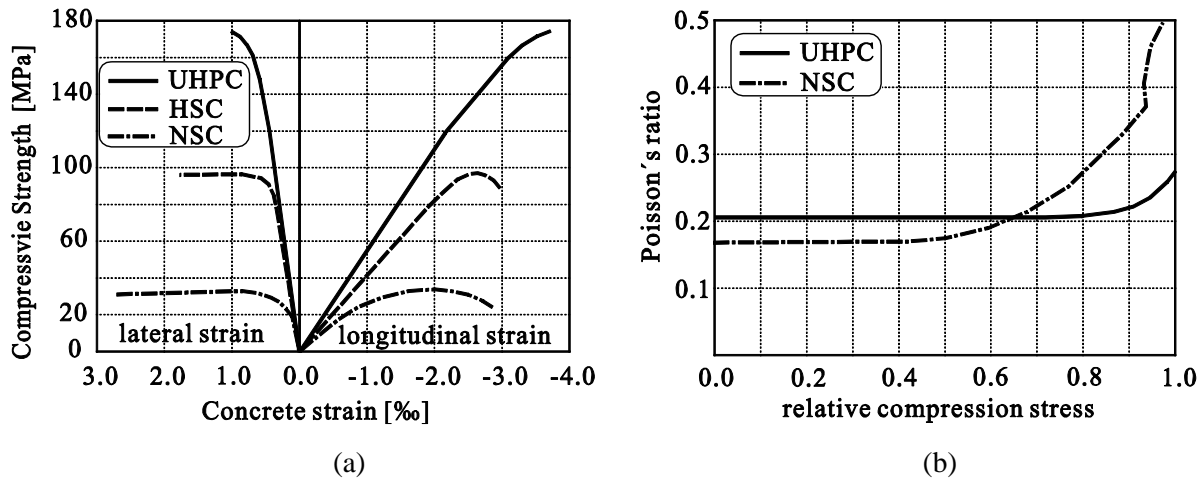


Fig. 2.5: (a) Compressive behaviour, (b) Poisson's ratio of UHPC [Tue et al. 2004]

### 2.3.2 Tensile strength

The tensile behavior of UHPC is characterized by:

- An elastic stage limited by the tensile strength of the cement matrix.
- A post-cracking stage characterized by the tensile strength of the composite material after the matrix has cracked.

The failure of UHPC without fibers is rather brittle, hence without a significant descending branch. Depending on the amount, type and orientation of fibers, the tensile strength of UHPC can be increased beyond the matrix strength. Values in the range between 7 and 15 MPa have been reported. Due to the effect of fibers, the behavior becomes ductile. After onset of cracking, the material may be characterized by the stress-crack-opening-diagram. The typical behavior is depicted in Figure 2.6. It should be noted, that the slope of the descending branch can be very different, depending on the fiber orientation and the content and type of fibers.

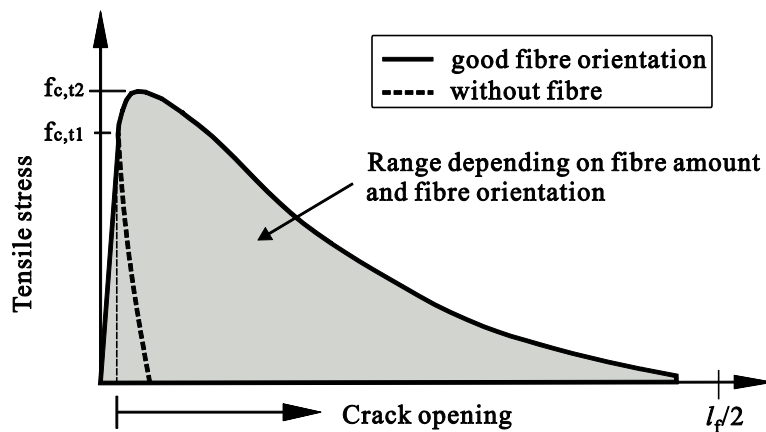


Fig. 2.6: Tensile stress-crack opening relationship [DAfStb 2008]

As mentioned before, the behavior of UHPC without fiber is extremely brittle. The addition of fibers to UHPC matrix leads to a tensile behavior that can be presented as in Figure 2.7. The

maximum stress attained in this regime coincides with the tensile strength  $f_{ctm}$  and it is observed that the first cracking stress is scarcely influenced by the fibers. The part of maximal tensile strength is achieved in this regime, but with a very small part of corresponding deformation ( $\varepsilon_{el} < \varepsilon < \varepsilon_u$ ). The changes of microstructure take place during this deformation as linear-elastic of the modulus of elasticity,  $E_c$ , in compression.

With an further increase of deformations beyond the elastic level, uniaxial tensile stress increases at a much lower rate than in the elastic regime, or remains constant ( $f_{ct} \geq f_{ctm}$ ). The maximum deformation can be attained before strain softening begins and by the strength attained at the level of deformation,  $f_{ct}$ . A typical  $\varepsilon_u$  of UHPC with fibers has a value in the range of 2 – 3 ‰. Both of these parameters ( $f_{ct}$  and  $\varepsilon_u$ ) are functions of the quantity and properties of the fibers, and their interaction with the matrix.

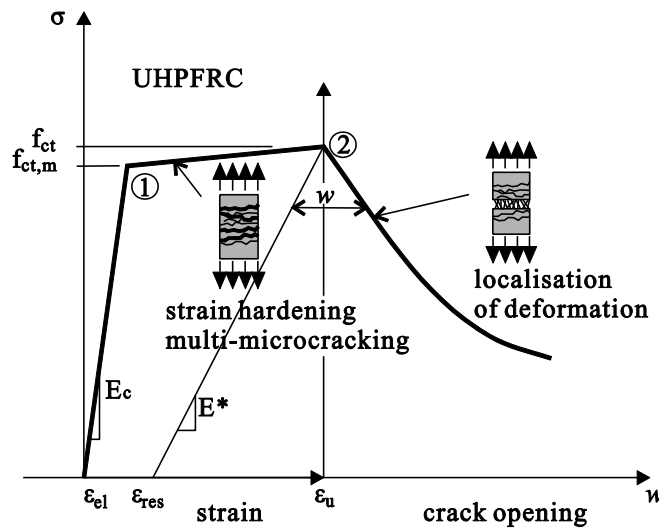


Figure 2.7: Stress-strain relationship of UHPC in uniaxial tensile strength [Spasojevic 2008]

### 2.3.3 Other material properties

#### 2.3.3.1 Creep and shrinkage

UHPC also exhibits very low creep and shrinkage after heat treatment when compared to conventional concretes, making the material suitable for precast/prestressed structures [Acker et al. 2004].

Creep is related to shrinkage as long term behaviour. It is observed that thermal treatment significantly reduces creep [AFGC/SETRA 2002]. The behaviour of creep depends on the age of the material at time of loading. For Ductal®, a creep coefficient of  $\varphi_{\infty} \approx 0.2 - 0.8$  is suggested. A thermally treated UHPC has lower values, on the other hand, non-treatment UHPC has higher values (the creep coefficient of normal concrete is up to 2 to 4). These values mean suitability for applications of prestressed concrete structure.

According to French recommendations [AFGC/SETRA 2002], no shrinkage occurs after early age

due to the low water-cement ratio in UHPC. For thermally non-treatment material with a water-cement ratio of  $W/C = 0.17 \sim 0.2$ , the shrinkage value is  $\varepsilon_{s\infty} \approx 550 \mu\text{m/m}$ . For thermally treatment material, no shrinkage develops according to [AFGC/SETRA 2002]. In general, UHPC with fiber is given  $\varepsilon_{s\infty} \approx 0$  to  $10 \mu\text{m/m}$ .

### 2.3.3.2 Fatigue strength

Normally, fatigue is hardly of interest for conventional, rather massive concrete structures. But since UHPC provides the possibility to design more slender members fatigue may become decisive. Fatigue problems can occur for instance due to traffic loads.

Only a few studies exist on the fatigue behavior of ultra high performance fiber reinforced concretes. This is due to the fact that these materials have only been developed recently and research in that field is still in progress. Fatigue tests under compression concrete stresses at the University of Kassel and TU Munich have shown a rather good-natured behavior [Fehling et al. 2005], [Fitik et al. 2010]. Thus, it can be said, that in contrast to other high strength materials, the high strength of UHPC with fibers does not lead to disadvantages with regard to fatigue.

### 2.3.3.3 Durability

UHPC is very different to the materials which are usually encountered in civil engineering. Apart from being far stronger than conventional concrete, it has outstanding qualities in terms of durability. The durability of concrete is determined to a great extent by its porosity and the related pore radius distribution. These two characteristics have very small values in UHPC compared to concrete with conventional strength classes. The transport of water and solutions, transporting harmful materials as chlorides, takes place in capillary pores. As the value of capillary pores decreases the resistance to transport harmful materials improves. What is more, the first structures built with UHPC about five to ten years old, confirm good durability and natural-ageing results.

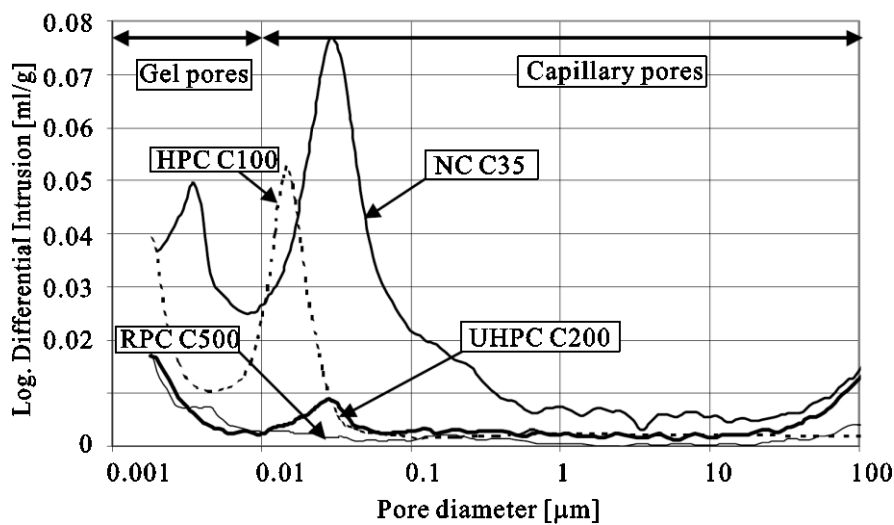


Figure 2.8: Distribution of pores of different size in UHPC, HPC and normal concrete [Fehling et al. 2005]

This performance of UHPC can have interesting applications for structures in highly aggressive environments, as e.g. waste storage tanks or maritime structures. It makes it possible to envisage structural components with very long lifetimes without maintenance or repair. In addition, thin structural elements can be made: the gain in durability compensates the reduction in thickness. Furthermore one can consider a decrease in concrete cover because of the enhanced durability.

Table 2.4: Characteristic durability values for NSC, HPC and UHPC [Schmidt, Fehling 2005]

Indicator	NSC (C35 EN 206)	HPC (C100/115 EN 206)	UHPC
Total porosity [%]	app. 15	app. 8	4 – 6
Capillary pores [%]	app. 8	app. 5	1.5 – 2.
Nitrogen permeability [m <sup>2</sup> ]	10 <sup>-16</sup>	10 <sup>-17</sup>	< 10 <sup>-18</sup>
Chloride-ion diffusion (6h quick-migration test) Depths of intrusion [mm]	23	8	1
Carbonation depth (after 3 years) in mm (20°C, 65% r. humidity)	7	4	1.5
Freeze-salt-resistance (scaling in [g/m <sup>2</sup> ] <sup>1)</sup>	<1500 (air entrained)	150 (air entrained)	20 – 50 (water...heat cured)
Water absorption factor <sup>2)</sup>	60	11	1

1) CDF-test, 28 cycles, limit 1500 g/m<sup>2</sup>      2) DIN52617

The durability of UHPC is related to decreased porosity and improved material homogeneity. It results in a highly improved resistance to the penetration of chlorides, frost and freezing attack, etc. UHPC's excellent resistance to freeze-thaw cycles also develops from the dense matrix, making it ideal for virtually any climate condition. Due to the dense cement matrix and small and disconnected pore structure, UHPC maintains a very low permeability: roughly 1/10 that of granite [Harris 2005]. There is more detailed information given in [Fehling et al. 2005]. Table 2.4 shows some characteristic indicators for durability under comparison with NSC, HSC and UHPC [Schmidt, Fehling 2005].

## 2.4 Design values for UHPC

In this chapter, a brief summary of several recommendations is given. The most important design parameters and approaches given in the various recommendations are presented and compared. Other design parameters, e.g. modulus of elasticity, Poisson's ratio, etc., are mentioned.

### 2.4.1 Recommendations for design

Up till now, there are no internationally accepted recommendations for the design of UHPC members. Partially this is due to insufficient information with regard to the properties of the material. An example of this is the durability of high performance concrete. It is mentioned that designing thin-walled structural elements applying reinforced or prestressed UHPC allows slender and large span structures. If standard recommendations for conventional concrete would be applied for such structures large concrete covers of the reinforcement would be applied and the advantage of using UHPC would be significantly reduced.

In comparison with existing codes for structural concrete new design aspects have to be added. Light, large span, elegant and material saving structures in UHPC are for instance only possible if reliable rules for control of fatigue behavior are available. Other aspects of significance in design are crack width control and the possible use of steel fibers as shear reinforcement.

There are design guidelines that provide the necessary information to fully design and calculate in UHPC. These are:

- French AFGC/SETRA Recommendations provisoires, 2002
- German DAfStb Sachstandsbericht UHFB, 2008
- Japanese JSCE Recommendations UFC, 2006

#### French Recommendation

The first French recommendations for Ultra-High Performance Fiber Reinforced Concretes (UHPFRC) were published in 2002 [AFGC/SETRA 2002]. These recommendations integrate feedback from experience with the first industrial applications and experimental structures, as well as more than 10 years of laboratory research. They are intended to constitute a reference document serving as a basis for use of this material in civil engineering applications.

These recommendations are divided in three parts: 1) Characterization of UHPC, 2) Design and analysis of UHPC structures and 3) Durability of UHPC.

#### German Recommendation

The German Committee for Structural Concrete (DAfStb: Deutscher Ausschuss für Stahlbeton) published a state of the art report with design parameters and approaches [DAfStb 2008]. It is essentially based on the design specification for high strength concrete in German Code DIN 1045-1. Furthermore, the draft "Guideline on Steel Fiber Reinforced Concrete (Richtlinie



Stahlfaserbeton)”, published by DAfStb, was cited in the recommendation and was filled with [AFGC/SETRA 2002] for another important source.

The state of the art report of [DAfStb 2008] deals with the following aspects:

- examples of application
- raw materials (cement, additions, admixtures, aggregates)
- fresh and young concrete characteristic
- hardened concrete properties (strength, deformation behavior, durability, etc.)
- design and construction
- research activities

### Japanese Recommendation

The Concrete Committee of Japan Society of Civil Engineers has published the research report as “*Recommendations for Design and Construction of Ultra High Strength Fiber Reinforced Concrete Structures*”-Draft [JSCE 2006]. The recommendations prescribe a procedure for examining safety and serviceability performance, which differs from conventional reinforced concrete, in consideration of the resistance to tensile stresses of UHPC without applying any reinforcing bars. The recommendations concluded that the standard lifespan is 100 years under normal environmental conditions and that examinations of many items regarding durability are not necessary.

#### 2.4.2 Design values for compressive strength

The design compressive strength for UHPC of the three recommendations can be defined by equation 2.1 in the same way.

$$f_{cd} = 0.85 \cdot \frac{f_{ck}}{\gamma_{c,UHPC}} \quad (2.1)$$

Table 2.5: The safety factors ( $\gamma_{c,UHPC}$ ) of the recommendations for design compressive strength

AFGC/SETRA 2002	DAfStb 2008	JSCE 2006
$\gamma_{c,UHPC} = \theta \cdot \gamma_b$	$\gamma_{c,UHPC} = \gamma_c \cdot \gamma'_c$	$\gamma_{c,UHPC} = 1.3$
$\gamma_b$ = Partial safety factor · 1.5 for normal cases · 1.3 for special cases $\theta$ = Coefficient representing the period of load action · $\theta = 1.0$ (> 24h) · $\theta = 0.9$ (1h~ 24h) · $\theta = 0.85$ (< 1h)	$\gamma_c = 1.5$ for in-situ concrete $1.35$ for precast concrete with fibers: $\gamma'_c = 1.25$ for in-situ UHPC $\gamma'_c = 1.11$ for precast UHPC without fibers: $\gamma'_c = 1.25$ for in-situ UHPC $\gamma'_c = 1.11$ for precast UHPC	

Table 2.4 shows the various safety factors ( $\gamma_{c,UHPC}$ ) for a design compressive strength of the recommendations. Because of the partial safety factor ( $\gamma'_c$ ) based on DIN-1045-1 for HSC, German safety factor ( $\gamma_c \cdot \gamma'_c$ ) is higher than the values given in the French and Japanese recommendation.

### 2.4.3 Design values for tensile strength

The design tensile strength of UHPC derived from [fib-Recommendation 1996] and [AFGC/SETRA2002] is shown as follows.

$$f_{cta} = 0.85 \cdot \frac{f_{ctk}}{\gamma_{ct} \gamma_f} \quad (2.2)$$

- where:  $f_{ctk}$  = 5% Quantile of the tensile strength (maximum value of the  $\sigma$ - $\varepsilon$  curve)  
 $\gamma_{ct}$  = Partial safety factor for the tensile strength of fiber reinforced concrete  
(1.3 for Ultimate limit stages, 1.0 for serviceability limit states)  
 $\gamma_f$  = Partial safety factor taking into account irregularities in fiber orientation  
(1.25 in general, except for local effects, 1.75 when taking local deficiencies into account)

The coefficient of 0.85 considers the strength reduction due to permanent loading. It is the same as that used for HSC. The characteristic tensile strength,  $f_{ctk}$ , should generally be determined by tests on specimens.

### 2.4.4 Other design values for UHPC

#### Modulus of elasticity

For a preliminary design of UHPC structure, in general, an E-modulus of 50 – 55 GPa can be considered for the UHPC. Because there is no available formula for design,  $E_c = 50$  GPa by [DAfStb 2008] and [JSCE 2006], and  $E_c = 55$  GPa by [AFGC/SETRA 2002] are recommended respectively.

The modulus of elasticity of UHPC is influenced by a number of factors just as it is the case of normal strength concrete. As UHPC members are generally thin and thus susceptible to deformation, the modulus of elasticity should be determined by testing on a case-to-case basis.

#### Poisson's ratio

Poisson's ratio can be taken as equal to 0.2 in the elastic region.

#### Coefficient of thermal expansion

The coefficient of thermal expansion,  $\alpha_T$ , can be taken as equal to  $1.1 \cdot 10^{-5}/K$  unless more exact values are available.

## Shrinkage and creep

Autogenous and drying shrinkage must both be taken into account when designing UHPC members. As for drying shrinkage, a value of  $\varepsilon_{csd} = 250 \mu\text{m/m}$  can generally be taken for members which have not been heat cured while a value of  $0 \mu\text{m/m}$  can be taken for UHPC after heat curing. According to [AFGC/SETRA 2002], the creep coefficient can be taken as follows:

- $\varphi_{\infty} = 0.8$  without heat curing
- $\varphi_{\infty} = 0.2$  with heat curing

These values only apply to UHPC subjected to loading at an age of 28 days. If loading starts earlier than 28 days, higher values must be expected for non-heat-cured members.

## 2.5 Applications of UHPC in bridges

### 2.5.1 Examples in Germany

#### Precast UHPC footbridges

In 2004, the applications for UHPC-bridge were started in Niestetal at Kassel [Schmidt et al. 2006]. The first UHPC-bridge, which has a span length of 12 m and width of 3 m, consist of a monolithic precast member with U-shaped cross-section (see Figure 2.9 (a)). In longitudinal direction the structure is prestressed by tendons SUSPA 150, 6-7, which are arranged in the webs. The other UHPC bridges, built in 2004, have 7 m and 9 m span lengths (see Figure 2.9 (b)).

The UHPC bridge series include 165 MPa characteristic compressive strength and 1.0 vol. % steel fibers.

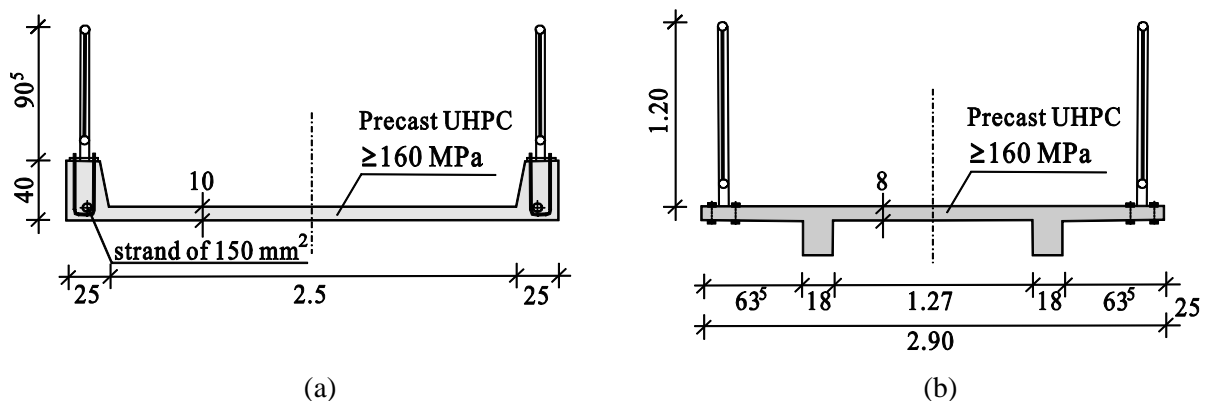


Figure 2.9: Cross-sections of footbridges made of UHPC in Germany [Schmidt et al. 2006]

### Hybrid UHPC-Steel Bridge: Gärtnerplatz Bridge in Kassel

The Gärtnerplatz Bridge in Kassel is a hybrid multi-span bridge, which has a length of 132 m with six spans built across the river Fulda in 2007 (see Figure 2.10). UHPC offers supreme durability characteristics and, hence, has been selected for the replacement of an existing, damaged timber structure. The bridge consists of a hybrid steel-UHPC truss structure and precast prestressed UHPC plates for the bridge deck. These deck plates are glued to the upper chords of the truss structure. For the transfer of shear forces from the truss diagonals (steel tubes) to the UHPC chords, prestressed bolted friction connections are used.

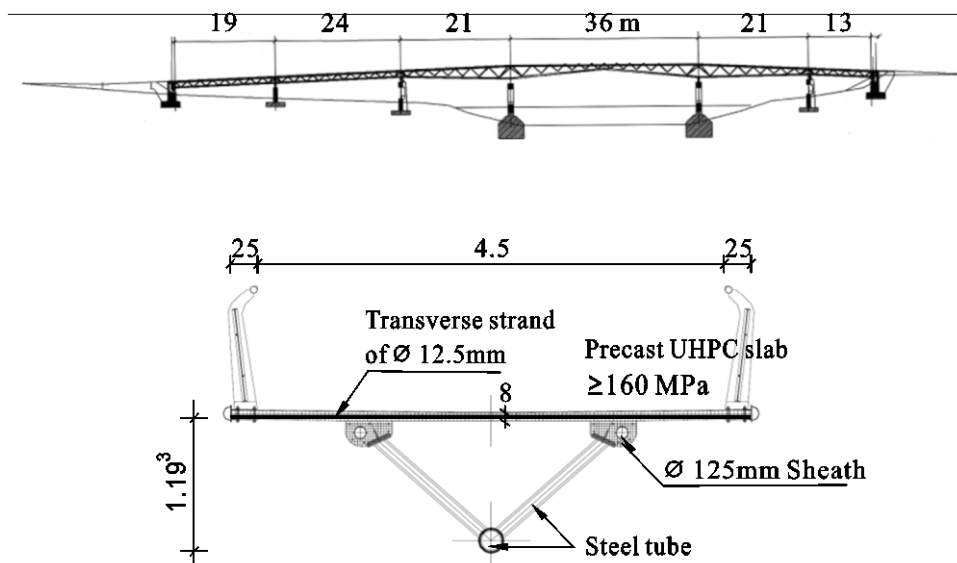


Figure 2.10: Cross-section of Gärtnerplatz Bridge in Kassel [Fehling et al. 2005]

### Research projects for structural UHPC members

60 shear tests on precast pretensioned UHPC girders with and without stirrups in the web opening have been investigated at Aachen University (RWTH). The research presents some parameters, which are the prestressing, the shear slenderness, the number and position of web openings, the opening diameter, additional shear reinforcement and beam size effect, with different amount of the steel fibers as shear reinforcement [Bertram 2012].

At the iBMB (Institut für Baustoffe, Massivbau und Brandschutz) of the Technical University of Braunschweig, experimental studies on monolithic and segmental UHPC girders with steel fibers under torsion were conducted. The experimental results are compared with conventional design for normal concrete girders [Empelmann, Oettel 2012].

### 2.5.2 Examples in other countries

The following four bridges may be regarded as early representatives of UHPC structures and are mentioned in detail: Sherbrooke footbridge in Canada, Bourg-les-Valence Bridge, Seonyu footbridge in South Korea (see Figure 3.17) and Sakata Mirai footbridge in Japan (see Figure 3.18).

### World's first UHPC Bridge in Canada

Sherbrooke footbridge, built in Quebec, is the world's first structure with UHPC. This precast bridge is a post-tensioned open-web space truss made with RPC (Reactive Powder Concrete). The main span is an assembly of six 10 m long pre-fabricated match-cast segments.

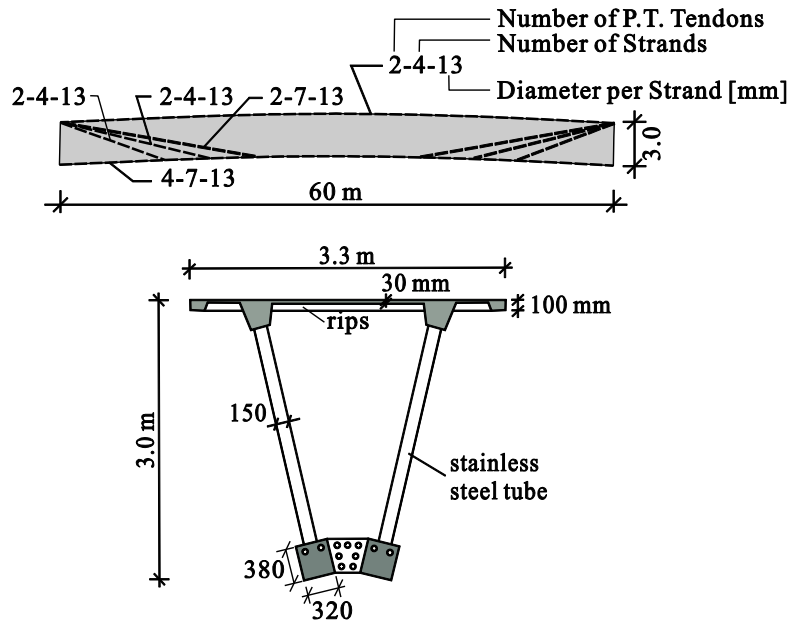


Figure 2.11: Sherbrooke Footbridge, Canada, 1997 [Blais, Couture 1999]

### First UHPC road bridge in France

As the world first UHPC road bridge, the Bourg-Les-Valence Bridge (Figure 2.12) has been built in France in 2001. The bridge consists of five  $\pi$ -shaped precast beams made of UHPFRC. The beams are longitudinally pre-tensioned with bonded strands (cast in place) in-situ UHPC.

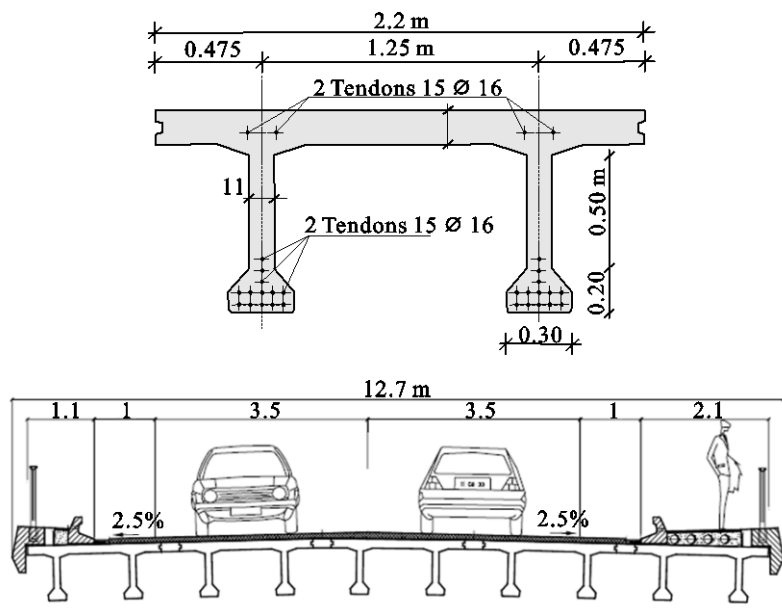


Figure 2.12: Cross-section of Bourg-Les-Valence Bridge [Hajar et al. 2004]

The used concrete compressive strength was greater than 170 MPa. A characteristic direct tensile strength of 8 MPa was achieved with a 3% of volume fiber incorporation. The beam dimensions are: 20.5 m and 22.5 m length, 0.9 m height, 2.4 m width, 11 cm web thickness, 37 tons weight.

### AASHTO type II-prestressed I-girder and 2<sup>nd</sup>Pi-girder in USA

The first UHPC-bridge in the United States, the Mars Hill Bridge in Wapello County Iowa, opened to traffic in 2006. The structure consists of 33 m long prestressed beams with 1.07 m depth. The girders have shallower top and bottom flanges and narrower webs more than the standard Iowa Bulb-Tee. In the U.S, specially, the cross-section for short spans of 20 – 35 m with UHPC (Ductal®) was optimized by the FHWA (Federal Highway Administration).

A full-scale prestressed I-girder (AASHTO type II) was investigated through the testing and FE analysis. These precast girders (max. 24.4 m long) contain 26 low relaxation prestressing strands (1,860 MPa) (Figure 2.13(a)). For this research program, the UHPC I-girder design was in three ways. First, the normal concrete was replaced with UHPC. Second, the I-girder contained no mild rebar. Third, to avoid damage in the end regions of the girders resulting from the large amount of prestressing forces on this small cross-section, the prestressing strands were only jacked to 55% of their ultimate strength [Graybeal 2008].

In 2008, the third UHPC-bridge in the United States was constructed in Buchanan County Iowa. This bridge has  $\pi$ -shaped cross-section called the Pi-girder (Figure 2.13(b)). This prototype girder with a deck of only 10.5 cm thickness has a maximum slenderness ratio of 30, and reduced weight of 30 % compared to conventional standard girders. Also, the girder with  $\pi$ -shaped cross-section allows rapid construction [Graybeal 2009], [Keierleber 2007].

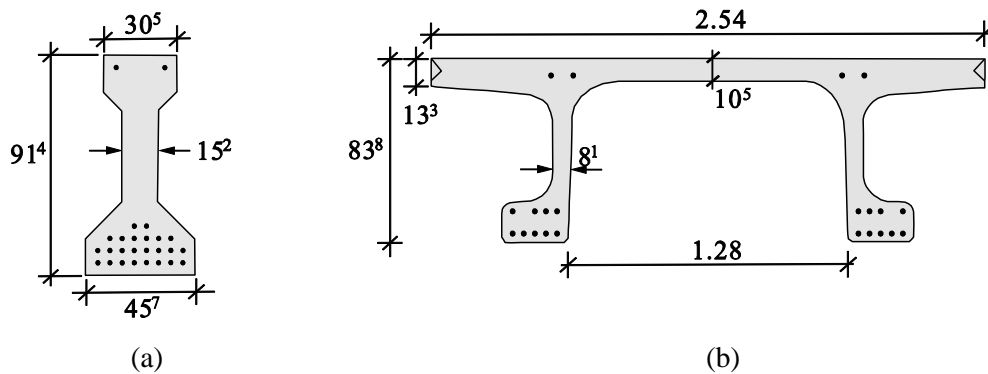


Figure 2.13: Cross-sections of precast pre-tensioned UHPC: (a) I-girder [Graybeal 2008] and (b) Pi-girder [Graybeal 2009]

## 3 Ultra High Performance Concrete Precast Segmental Bridge (UHPC-PSB)

In this chapter there will be a brief introduction for precast segmental bridges (PSB), the suitability for application of UHPC in segmental bridge construction and several examples of UHPC segmental bridges are given in section 3.3.

### 3.1 Precast concrete segmental bridge (PSB)

#### 3.1.1 Introduction

Segmental construction is defined as the method of assembling concrete structures from precast segments by means of post-tensioned tendons.

Precast segmental construction is a very fast construction method determined by the time required for the erection. The major part of the work is performed in the precasting yard, where it can be protected against inclement weather. Precasting can start simultaneously with the substructure and foundation work. The time-dependent deformations of the concrete become less important, as the concrete may have reached a higher age by the time the segments are placed in the structure. This method requires relatively important investments in precasting yard, molds, lifting gear, transportation, and erection equipment.

As the features of this construction method, the advantages and disadvantages are summarized as follows;

- Advantages:*
- very rapid and safe construction
  - high concrete quality and durability through prefabrication
  - application of high strength concrete
  - overlap of activities: casting during substructure works
  - construction independent of weather conditions
  - easy dismantling
- Disadvantages:*
- high initial cost for precasting yard, erection truss etc. and prestressing
  - lack of standard design

### 3.1.2 Casting of segments

There are two methods for segment casting. The first one is the long-line match cast method, where all segments of a span are cast in their correct position in a casting bed that reproduces the span. The second method, used most of the time, is the short-line match cast method, where all segments are cast in the same place in a stationary form against the previously cast segment. After casting and curing, the previously cast segment is removed for storage, and the fresh cast segment is moved into place (Figure 3.1).

The advantages and disadvantages of the two match cast methods are as follows:

#### The long-line match cast

*Advantages:* - easy to set up

- the geometry of the segments is easily controlled

*Disadvantages:* - after stripping of forms, it is not necessary to remove segments immediately

- substantial space is required for the casting bed. The minimum length of long line casting bed depends on the geometry of the structure and the degree of uniformity of the segments. It is often a little more than half the longest span. The weight of the segments must be supported by the foundation.

- the casting bed must be built on a firm foundation, which will not settle or deflect under the weight of the segments.

#### The short-line match cast

*Advantages:* - Space requirements are small in comparison to the long-line match cast method.

- The entire manufacturing process is centralized.

- Horizontal and vertical curves and cross-fall variations are obtained simply by adjusting the position of the matching segment.

*Disadvantages:* - To obtain the desired geometry of the structure, the matching segment must be accurately positioned. Detailed geometry control is required.

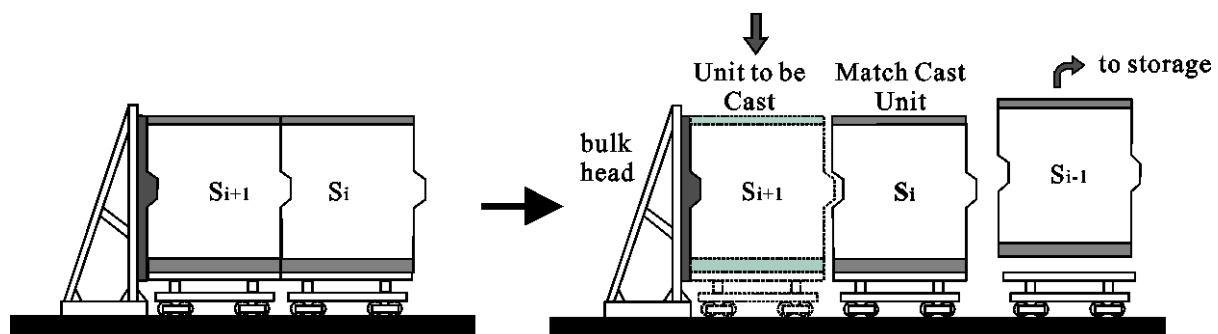


Figure 3.1: Short-line match cast [Combault 2008]



### 3.1.3 Erection methods

Segmental bridges can be classified by the various methods for construction. In cast-in-place segmental construction, segments are cast one after another in their final location in the structure. Special equipment is used for this purpose, such as travelers or formwork units. In precast segmental construction, on the other hand, segments are manufactured in a plant or near the construction site, and then transported to their final position for assembly.

Table 3.1: Range of application of concrete bridge types by span lengths

Bridge Types		Span [m]					
		30	60	90	150	200	300
Precast segmental	Balanced cantilever: constant depth						
	Balanced cantilever: variable depth						
	Span-by-span						
	Progressive placement						
Cast-in-place segmental	Balanced cantilever						
	Incremental launching						
	Progressive placement						
monolithic	I-type pretensioned girder						
	Post-tensioned box girder						
	Composite box girder						
	Composite beam girder						
Cable stayed with balanced cantilever segmental							

The span length of a prestressed concrete bridge is determined by the construction method considering cost-efficiency and environmental condition. With cable-stayed structures, the span length of a segmental bridge can be extended to 400 m, e.g. the Dames Point Bridge in Florida [Gimsing 1999]. Table 3.1 summarizes the range of application of various forms of construction by span lengths.

The types of segmental bridge construction are summarized as follows:

- *with precast segments*: balanced cantilever, span-by-span, progressive placement
- *with cast-in-place segments*: balanced cantilever, incremental launching

The three important precast segmental construction methods, which are balanced cantilever, span-by-span and progressive placement, are introduced in the following section.

#### Balanced cantilever construction

Since the Choisy-le-Roi Bridge near Paris (see FigureA.5), during the initial development of segmental bridge construction, this method has grown in popularity and is used throughout the world today. The three methods for a precast balanced cantilever construction are shown in Figure 3.2. The features of this method provide significant advantages over the cast-in-place method as follows:

- The bridge decks are mostly built without any contact with the ground, making it possible to build structures over rivers subject to severe flooding or above very deep and rugged valleys.
- This method can also be used to erect structures with very different geometries. Thus, in elevation, it is possible to design decks of a constant or variable depth.
- Rate of erection is usually 10 to 15 times the production achieved by the cast-in-place method. The time required for placing reinforcement and tendons and, most importantly, the waiting time for curing of the concrete is eliminated from the critical path.

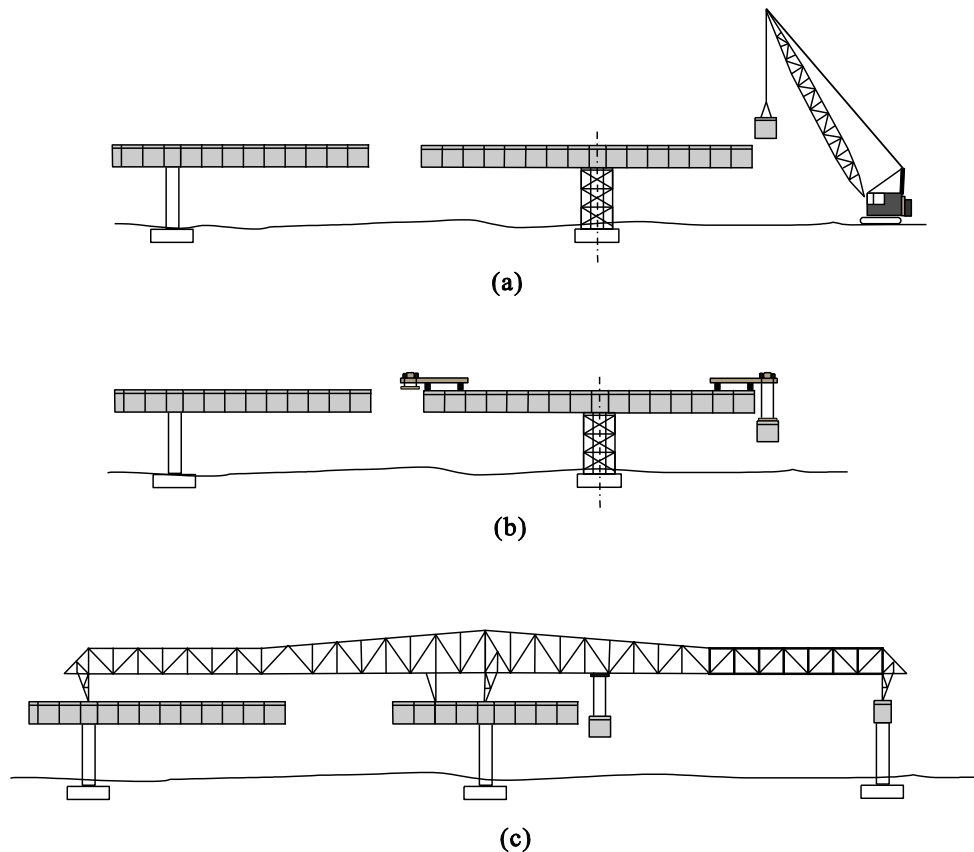


Figure 3.2: Typical precast balanced cantilever erection methods: (a) Crane placing, (b) Beam and winch method and (c) Launching gantries [Podolny, Muller 1983]

### Span-by-span construction

The balanced cantilever construction method was developed primarily for long spans, whereas the span-by-span construction method was developed for long viaduct structures with relatively shorter spans, where it is particularly advantageous.

The two typical methods for span-by-span construction are as follows:

**Overhead gantries**, as shown in Figure 3.3 (b), are supported off the piers or the completed deck. They move forward ‘stepping’ onto the next pier in front of the erection and by running along the top of the already completed section of the deck. The advantage of overhead gantries is to cope with a wide range of deck geometries and tight horizontal curves. However, this construction

method is generally more complex to design and assemble and also slower in erecting the segments compared to an underslung gantry.

**Underslung gantries**, as illustrated in Figure 3.3 (a), are positioned beneath the deck normally supporting the segments under their side cantilevers or soffit. The gantries are supported at the piers by brackets fixed to the column top or by props from the foundation. They move forward by launching themselves and stepping between the piers. The advantages of underslung gantries are that they are generally simpler to design, assemble and operate as well as being easier to erect the segments. However, they are used only with decks on a large horizontal radius and where headroom is not critical. The decks from The Bang Na Expressway in Bangkok were erected using an underslung gantry with a lifting arm at the front to position the segments [Rombach 2003].

With the segments supported by the gantry, temporary prestress is not needed other than to help position the segments. Span-by-span erection is used on both continuous decks and simply supported spans; the process of erecting the segments is the same for either arrangement. With the span-by-span placement method and with epoxy in the segment joints, a typical 40 m span is usually erected every 2 or 3 days. With an underslung gantry and a dry-jointed deck an erection rate of up to one span a day is achievable.

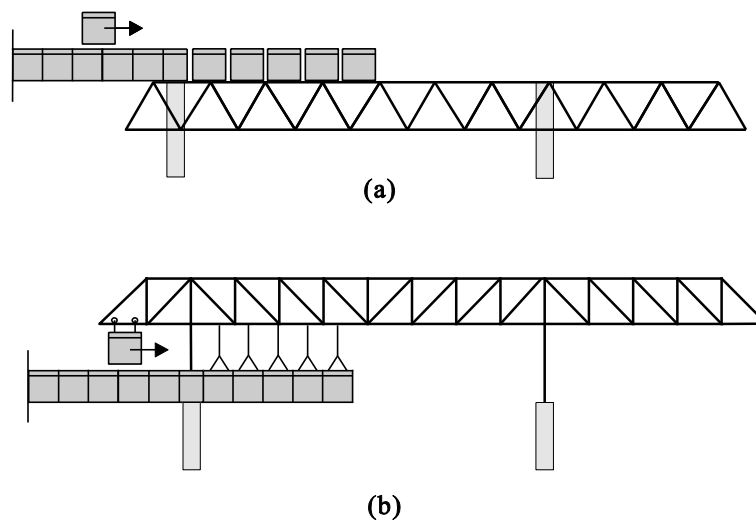


Figure 3.3: (a) Underslung gantry and (b) Overhead gantry for Span-by-Span construction [Rombach 2003]

### Progressive placement

As shown in Figure 3.4, for precast construction using a temporary support (or a temporary tower and a stay cable system), segments are transported over the erected portion of the bridge to the end of the completed portion. Using some type of lifting equipment, e.g. a swivel crane, the segment is placed in position and supported temporarily either by post-tensioning to the previous segment or by stays from a tower. The advantages and disadvantages of this method are:

- Advantages:*
- Operations are conducted at deck level.
  - Reactions on piers are vertical.
  - The method can easily accommodate variable horizontal curves.
- Disadvantages:*
- The first span is erected on falsework.
  - Forces in the superstructure during erection are different from those in the completed structure.
  - The piers are temporarily subjected to higher reactions from dead load than in the final structure because of the length of the cantilever erected. However, considering the other loads in the final structure, this case is not generally controlling the pier design.

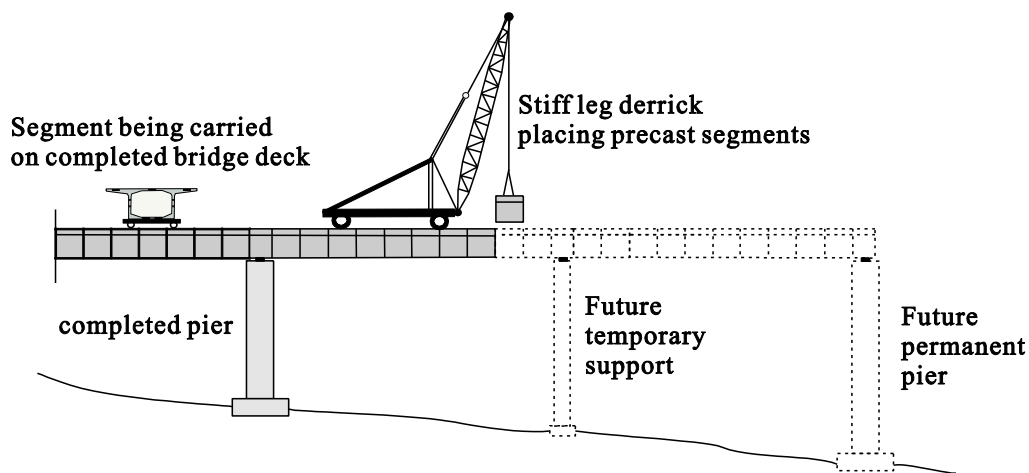


Figure 3.4: Erection scheme for progressive placement of the Linn Cove Viaduct [Podolny, Muller 1983]

### 3.1.4 Development of PSB

With the demand of the construction market, the techniques for PSB were changed compared with the early types. This chapter describes the important changes due to the development of PSBs

#### Shear-key

In early segmental bridges, a single large key was used in each web. The typical details are shown in Figure 3.5(a). Nowadays in a typical joint several, 10-20, small keys are distributed over the height of the web. The dimensions of these keys are much smaller than those used in single key joints, and they are usually not reinforced (Figure 3.5(b)). The small multiple shear-keys spread out down the webs are more efficient with respect to load transfer between segments than large single key or individual keys. The multi-keys have the added advantage of not needing to be reinforced [Koseki, Breen 1983].

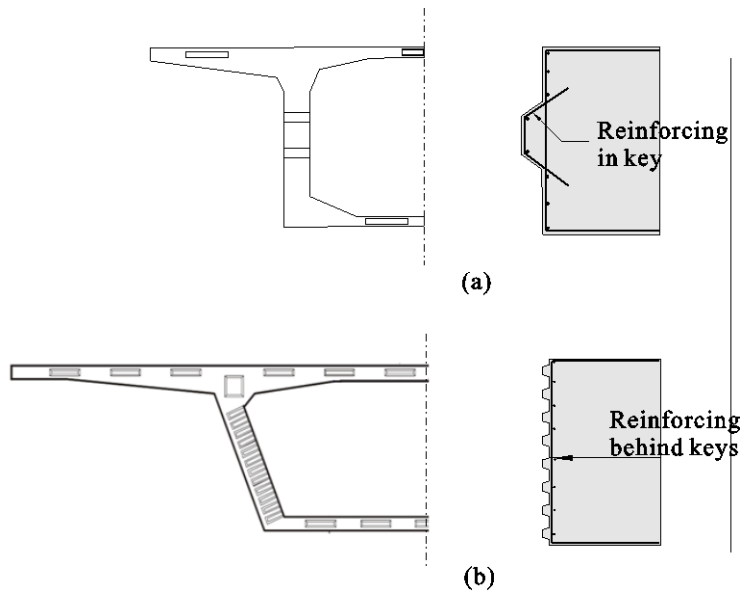


Figure 3.5: Joint comparison between (a) reinforced large single shear-key used on early projects and (b) unreinforced small multiple shear-keys used nowadays

### Joint

Figure 3.6 shows the width of the gap and types of joints between adjacent segments. Dry joints with multiple shear-keys and external tendons, which are protected by high density polyethylene ducts (HDPE) show several advantages in relation to epoxy or mortar joints. Without epoxy, the erection procedure is simplified and much quicker.

Dry-joints in a precast segmental box girder have been used on several long span bridges, especially in the USA and South East Asia. However, with this method of jointing, a watertight seal cannot be achieved at the segment joints. This would therefore reduce the corrosion protection of internal grouted tendons. For this reason dry jointing may only be used in segmental construction in association with external tendons and in regions without freezing. Epoxy joints may further be required when the required high accuracy of adjacent joint surfaces cannot be guaranteed.

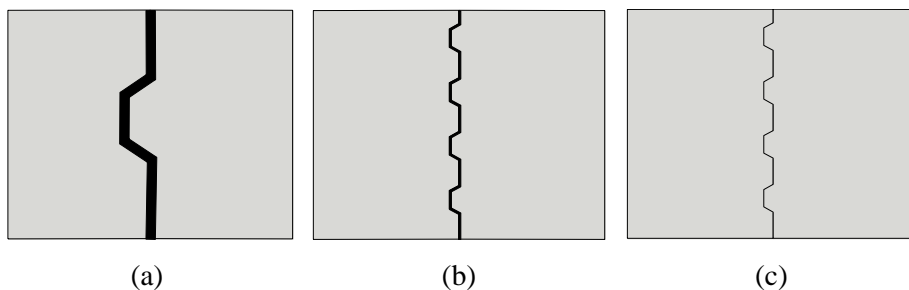


Figure 3.6: Types of joints used in PSBs: (a) mortar joint of 2 – 3 cm  
(b) epoxy joint of < 3 mm (c) dry joint of < 1 mm

## Concrete

Early prestressed concrete bridge designs were based on 20 MPa compressive strength concrete. To date, over 50 MPa strength concrete is generally applied to precast segments. Obviously, use of high strength concrete, external tendons and the variable constructions have permitted the design of longer spans, the increase of load bearing capacity and easy and fast construction.

In Appendix A, a historical overview and more information on precast segmental bridges are presented.

## 3.2 Considerations for UHPC segmental bridges

### 3.2.1 Concepts

With the use of UHPC and the application of segmental construction, durable and maintenance free bridge structures can be economically built.

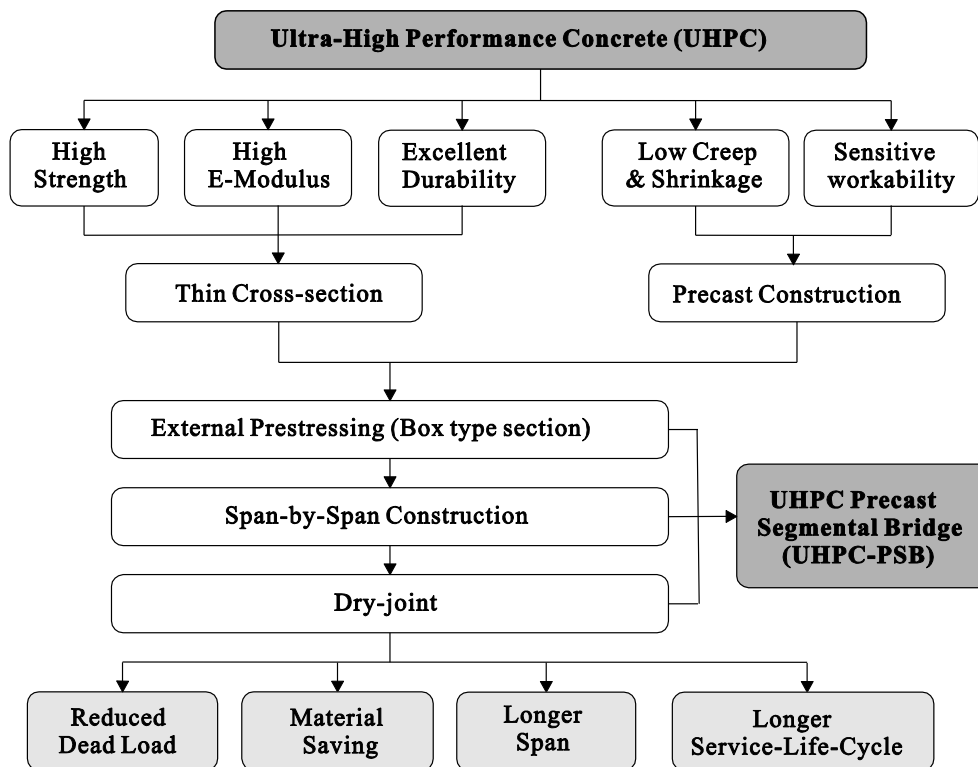


Figure 3.7: Combination effects of precast UHPC and segmental construction

Figure 3.7 shows the synergy effect of UHPC precast members and segmental construction method. UHPC has a very high compressive strength over 160 MPa, high elastic modulus over 50 GPa and a high durability due to a low porosity and improved homogeneity (see chapter 2). These great material properties can lead to reduction of cross-section. Also UHPC has very low creep coefficients and shrinkage strains. As a result of a lower water/cement ratio (0.20 - 0.25), it

requires very long mix time and hasn't a good workability. Thus it is most suitable for precast/prestressed concrete structures. In fact, because of the high demands made on the fabrication of UHPC, it is mostly used in precasting works.

The external prestressing with a box type section is most appropriate for thin cross-sections and precast-members. With external tendons, span-by-span construction and dry joints are mostly used. These are very significant components for a UHPC segmental bridge.

From the UHPC segmental bridges, many advantages originate, such as fast and easy construction. As the main advantage, the self-weight of the structure may be reduced by up to 60 %. The next section presents the advantages and problems of UHPC for structural applications, a brief introduction for external tendons, the span-by-span construction method and dry joints, as important components for UHPC segmental bridges, and some applications in the field.

### 3.2.2 Advantages and disadvantages of UHPC for structural application

The major advantages of Ultra High Performance Concrete (UHPC) are durability and strength. Thus, various possibilities for new developments in structural concrete arise. The enormous compressive strength allows slender and light building elements. This material is structurally more comparable to steel than conventional concrete.

The advantages of UHPC are similar to that of HPC. As it is a new material, however, the main characteristics of UHPC have superior properties than high performance concrete. With the significantly improved physical properties of UHPC, there are a number of advantages when compared to conventional concretes and steel for structural applications. The properties of UHPC can be optimized when used in conjunction with prestressing, which maximizes the use of the inherent tensile capabilities [Almansour et al. 2008], [Harris 2005]. With respect to the conceptual design for structures made of UHPC, the advantages are summarized in Table 3.2.

Table 3.2: Advantages of UHPC for structural application in bridge construction

advanced mechanical properties	advanced durability	constructability
<ul style="list-style-type: none"> <li>• higher strength</li> <li>• less material</li> <li>• fewer beams</li> <li>• lower depth/longer spans</li> <li>• Higher toughness</li> </ul>	<ul style="list-style-type: none"> <li>• very low shrinkage and creep</li> <li>• less permeability; higher chemical and freeze-thaw resistance</li> <li>• less abrasion, scaling</li> <li>• longer life cycle, less maintenance</li> </ul>	<ul style="list-style-type: none"> <li>• easier, faster and safer erection</li> <li>• less labor</li> </ul>

In spite of the many advantages of UHPC, some disadvantages of this material also exist. The biggest disadvantage of using UHPC in today's market is that it is considerably more expensive than standard classes of ready mix concrete and difficult to handle on a construction site.

With UHPC being relatively new to the industry, there have been only a limited number of applications. The cost is still significantly higher than that of conventional concrete. The producers expect that as UHPC becomes more commonly used in practice, the cost will decrease. Savings may be achieved over the life cycle when compared to conventional solutions. The costs may be offset by reduced girder cross-section, decreased traffic control and construction time, and longer lifetime with reduce maintenance.

Harri [2005] mentioned about structural application of UHPC as follows:

*Another difficulty with the use of UHPC in design is that it is more suited for use in a precasting facility rather than onsite applications. UHPC in standard bridge girder shapes does not allow for use of the material to its full potential; however, standard sections can be minimized (shorter sections, thinner flanges/webs, etc.) to make better use of the material properties.*

The main disadvantages of UHPC for structural application are:

- *Expensive initial cost:* It also has a very long mix time and requires high-energy mixers to properly mix. The design and use of the material has not yet been optimized.
- *Design for UHPC:* While the strength of UHPC allows for minimization of section properties, design with UHPC must still meet the stiffness requirements for serviceability. There is a limit as to how thin or small a member can be and still satisfy deflection and vibration criteria.
- *Formwork for UHPC:* formwork must be carefully designed and curing carefully monitored, because UHPC exhibits considerable early age shrinkage. The formwork must be designed so it can be released to allow the UHPC to shrink without restraint.

### **3.2.3 Construction techniques**

As mentioned previously, most for UHPC segmental bridge construction the three modern construction techniques are external tendons, dry-joint and span-by-span construction. The advantages have been demonstrated on the projects in Bangkok and in Florida [Hewson 1992]. These construction techniques are briefly described in this chapter.

#### **External prestressing**

One of the main advantages of external prestressing is the possibility of decreasing the web thickness. It is the most appropriate for the UHPC members with thin cross-section. The main disadvantages of external prestressing, such as short lever-arm and reduced bearing capacity compared to internal prestressing, can be partly compensated by the UHPC material properties.

The following is a list of advantages associated with the use of external prestressing.

- Facilities for inspection, monitoring and re-stressing or replacing of tendons can easily be done.
- The lack of ducts within concrete when using external prestressing makes steel fixing easier and facilitates the use of thinner webs, thereby resulting in a reduction in dead load (it means reducing of the section) and concreting of new structures is improved.



- External tendons afford simpler cable layouts.
- Prestress losses due to both friction and creep is lower.
- Flexural failures will always be preceded by extensive cracking and excessive deflection, thus giving prior warning of collapse.

Also, the various disadvantages of external prestressing are described as below:

- Only straight tendon profile is possible.
- External tendons are more sensitive to fire and vandalism.
- The prestressing force disappears over the overall length of the tendon once a section of steel is broken.
- External tendons are protected by High Density Polyethylene Ducts (HDPE) which are fully cement grouted or wax filled which result in a higher initial material cost for the prestress system.
- Under ultimate bending conditions external prestressed structures require more prestressing to generate the same moment of resistance as the tensile strength of PT is not reached in the ultimate limit state.
- Anchorage points and deviators are subjected to high concentrations of forces which need to be properly tied into the structure
- The actual eccentricities of external tendons are generally smaller compared to internal tendons.

In general, there is no fundamental difference between girders with bonded or unbonded tendons below the decompression moment. The cross-section with unbonded tendons has usually a larger initial prestressing force and, therefore, a higher decompression moment than the section with bonded tendons. With regard to the fatigue behaviour, in unbonded tendons negligible stress variations occur in the prestressing steel under live loads.

The increase of the tendon force under loads depends primarily on the geometry and the overall deformation of the structure as well as the tendons profile. For long tendons and slender structures, this increase will be relatively small, even for large overall deformations of the system ( $\Delta\sigma_p \approx 300$  MPa in the BBB project in Thailand [Fischer et al. 1998]).

Experiments and full-scale tests showed that a concrete box girder with external tendons fail in a flexural mode where concrete crush in the compression zone. Thus, the high compressive strength of UHPC gives an increase of flexural resistance capacity in segmental bridges at the ultimate limit states. The behaviour of a PSB with external tendons is independent on the joint type (dry or epoxy). Usually, the ultimate bending capacity of external tendon girders will be reduced by 10 – 20 % compared with that of internal tendon girder (see Figure 3.8) due to a smaller stress increase in the tendons.

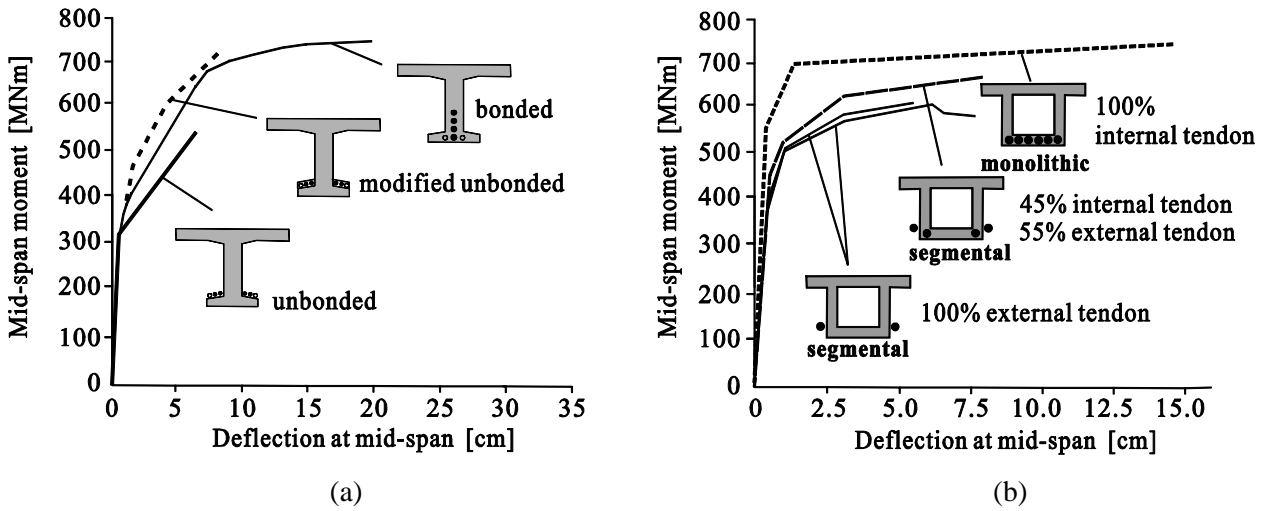


Figure 3.8: Comparisons of load bearing capacity for different tendon types; the experiments were carried out by (a) [Rabbat et al. 1987] and (b) [Foure et al. 1991] (conducted by the CEBTP)

### Dry joint

Joints between segments in precast concrete segmental bridges require special attention in design and construction. These joints introduce discontinuity in the bridge; meanwhile they must transmit compressive and shear stresses. The shear keys at dry joints provide the mechanism for transferring shear forces across the joints at all stages of the structure's life. Tests carried out by Koseki & Breen [1983] and Buyukozturk et al. [1990] have shown that dry joints with multiple small shear keys spread out down the webs are more efficient than large individual keys (see Fig. 3.9). Nowadays multi-small sized shear-keys without reinforcement are used.

The ultimate shear capacity of a web is made up of two components; the resistance of the keys plus the frictional resistance on the web area. In the following some further information of the joint behaviour are mentioned.

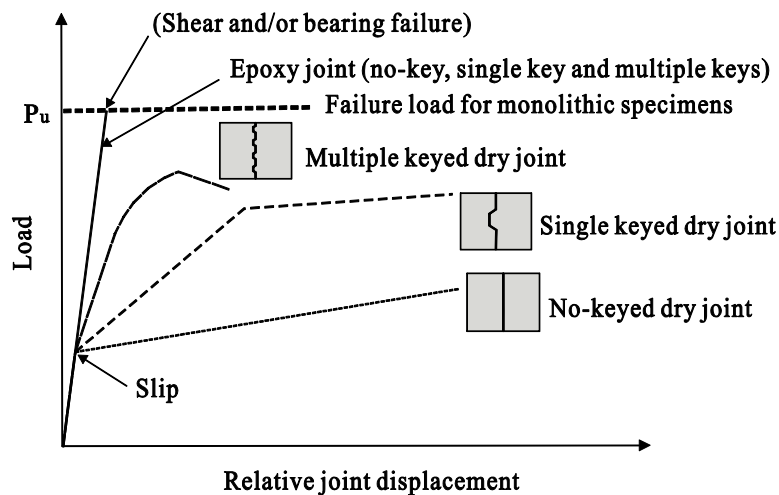


Figure 3.9: Comparison of behaviour of joints [Koseki, Breen et al. 1983]

If the friction between the mating surfaces is exceeded slippage will occur until the shear keys are fully engaged. Increased shear is then resisted until either the bearing capacity or the frictional capacity of the keys is reached, at which stage the keys will either fail by crushing or by shearing off. The shear capacity of a dry joint is less than for an epoxy joint or monolithic structure, with up to 30 – 40 % reduction being observed in tests [Hewson 2003].

Tests were carried out to assess the shear strength and deformation behavior of precast segmental bridge joints, e.g. [Koseki, Breen et al. 1983]. The parameters studied included flat and keyed joints, without epoxy (dry) and with glue, the level of prestressing, and the epoxy thickness. It was found that the strength of epoxy joints is consistently higher than that of dry joints. A comparison of the shear behaviour of various types of joints is presented in Figure 3.9. The three specimens with epoxied joints had almost the same load bearing capacity and relative displacement at failure. However, the failure of the epoxied joints was found to be very sudden and brittle.

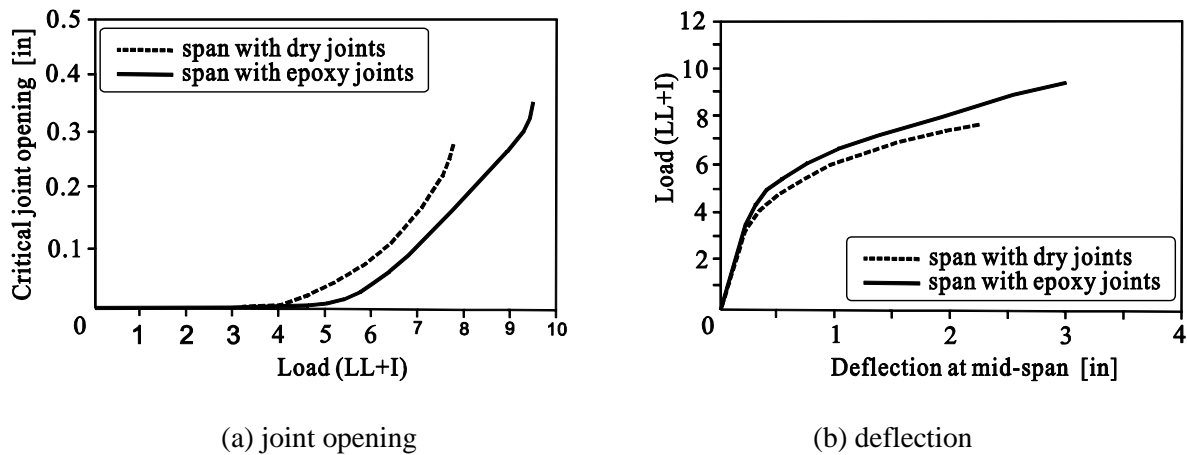


Figure 3.10: Comparison of behaviour from ultimate flexural test by Hindi, MacGregor et al. [1995]

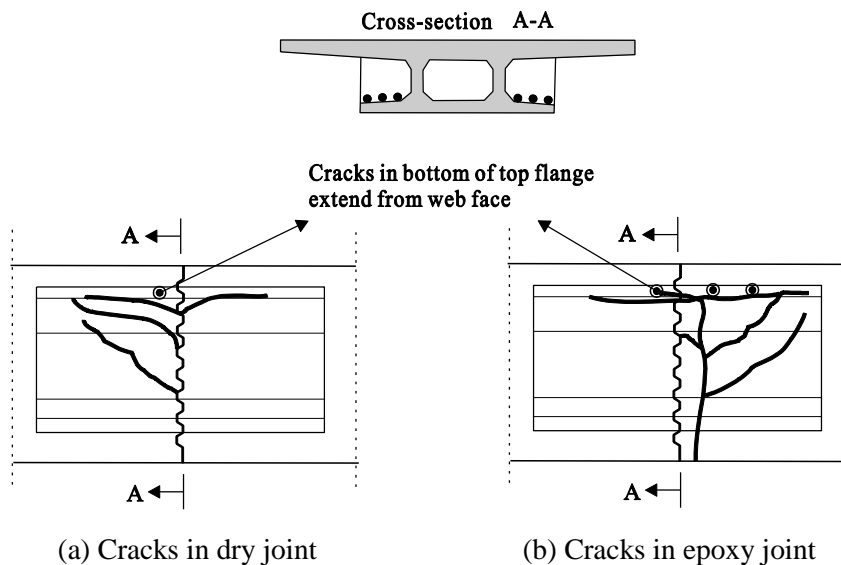


Figure 3.11: Comparison of crack pattern from ultimate flexural test by Hindi, MacGregor et al. [1995]

Among the shear key tests, the experiment by Breen 1995 [Hindi, MacGregor et al. 1995] shows the real difference of shear key capacities, including the joint opening, the deflection and failure pattern, due to different joints types (see Figure 3.10 and Figure 3.11). The dry joint girder shows a bigger joint opening and a lower failure load, whereas the load-deflection curves of both joint types are quite similar. A vertical crack can be seen for the glued specimens.

Several formulas are being proposed for assessing the shear strength of joints of precast concrete segmental bridges. These formulas will be introduced in chapter 5.

### Span-by-span construction

The prestressing layout and tendon profile is dependent on the method of construction. In general, for span lengths of less than 50 m, a common erection method is to place the segments span-by-span. With this technique a gantry, either overhead or underslung, is used to support a complete span of segments which are pulled together by installing either temporary prestress or the permanent tendons. For span above 50 m erection gantries become very heavy and tend to be uneconomic when compared to the balanced cantilever erection method. The extreme low self-weight of UHPC material can expand the range of application of span-by-span construction with a longer gantry. In addition, the light precast elements can be simply lifted by a crane after longitudinal post-tensioning on the ground (see chap. 3.3.2). Next larger segments can be used which reduces the time for assembling the segments.

### 3.2.4 Structural concepts for UHPC segmental bridge

For precast concrete segmental bridges, the box type cross-sections are widely used. In the US, the cross-sections of segmental bridges are standardized for conventional concrete, according to construction methods and span lengths, e.g. AASHTO-PCI-ASBI Segmental Box Girder Standard [AASHTO 2002]. Also, the cross-sections of monolithic girders for higher performance concrete material were optimized by the studies of the  $\pi$ -girder that was designed by MIT (Massachusetts Institute of Technology). However, a standard cross-section for higher strength concrete, such as high performance or ultra high performance concrete does not yet exist.

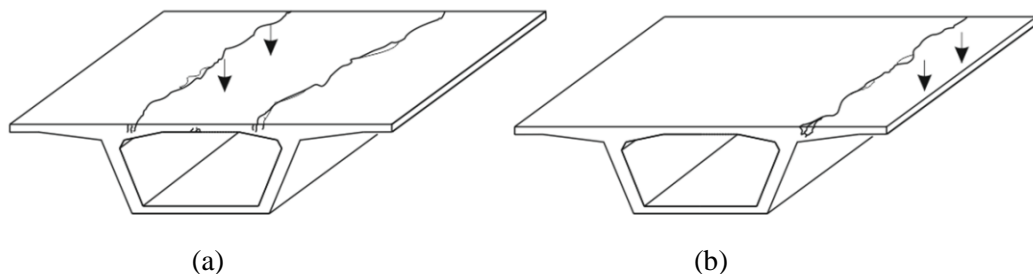


Figure 3.12: Cracking in the tensile zone (a) between webs and (b) in cantilever

As the typical cross-section for PSBs, in general, single hollow box girders are used as shown in the various recommendations for segmental bridges. The main advantage of this cross-section is the high resistance for torsion and the applicability for positive (field) and negative (support)

bending moments. Also, the box type cross-section is very suitable for external tendon layout. On the other hand, this type has a greater depth of cross-section than I-girders or T-girders.

When a single hollow box cross-section is used for UHPC bridges, the behaviour in the tensile zone of the top slab must be considered. Because UHPC structures have very thin slabs and webs for material saving (reduction of dead load), the damages of thin slabs without reinforcing steel bar should be considered as shown in Figure 3.12.

As the method for providing efficient transverse bending resistance in a deck slab, the box girder with stiffener or strutted wing slab can be applied for UHPC segmental bridges (see Figure 3.13). The width of the deck slab of a single box girder can be easily widened by these types. Also, for the additional deck slab, transverse reinforcement or external prestressing can be used. The span of the long cantilever is supported by the compression struts or stiffener. Recently, segmental bridges with compression struts were built by using higher performance materials [Saito, K. et al. 2001], [JCI 2002] and [Mutsuyoshi et al. 2010] etc.

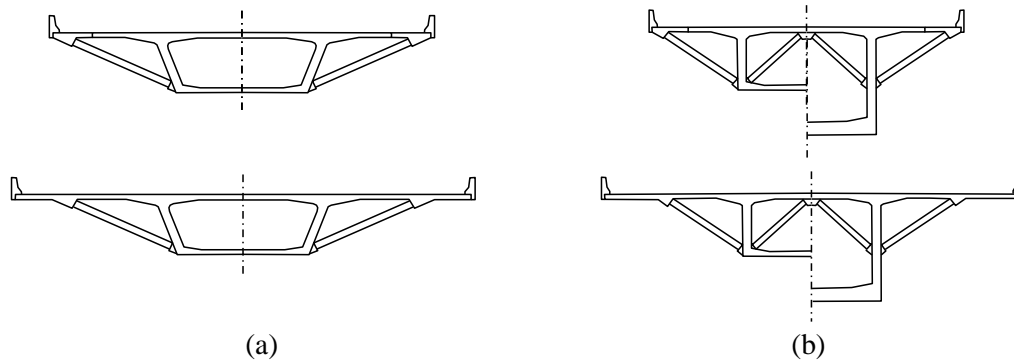


Figure 3.13: Cross-section widening of box girder with strutted wing slab (a) constant depth bridge [Shushkewich 2006] and (b) variable depth bridge [Shushkewich 2003]

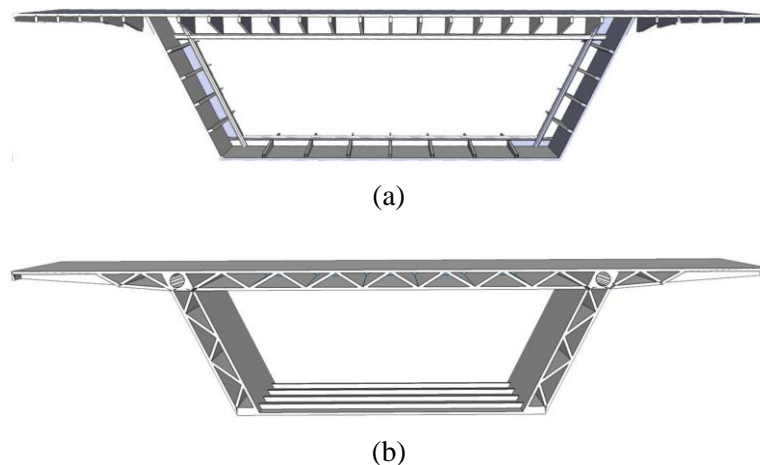


Figure 3.14: UHPC concept segment designed by [Reichel 2010]: (a) Precast segment with rib and stiffener (b) Precast segment with truss structure and stiffener

For the span-by-span construction method, in general, a constant cross-section height is applied. The constant depth cross-section doesn't need the interior transverse compression struts because the inner compression struts are required for the balance of the exterior compression struts in the

variable depth cross-section. On the other hand, when a constant depth cross-section has a relatively shorter cantilever and a longer span between the webs, interior compression struts are required.

Structural studies for UHPC bridges with thin members had been performed at TU Graz in Austria. Reichel proposed a cross-section shown in Fig. 3.14 (a) based on a steel box girder. He conducted FE analysis to estimate the load bearing capacity of such a UHPC segmental bridge, having external tendons and dry joints [Reichel 2010]. These sections have complex structure for prefabrication. In spite of many stiffener and ribs, pretension strands in very thin-walls was excessively used. This may cause durability problems.

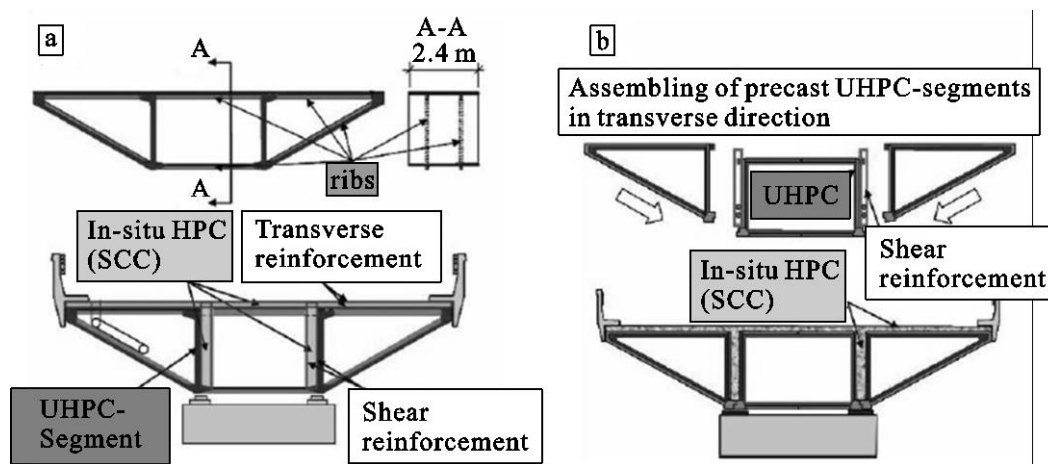


Figure 3.15: Cross-section of UHPC segmental bridge [Reichel 2008]

The superstructure of the UHPC segmental bridge can also be made by several segments joined in transverse direction (see Fig. 3.15). The cross-section of the superstructure consists of three or more segments with in-situ concrete. The slenderness of the construction does not much differ from the depth of conventional superstructures. But the benefits of the UHPC segmental can be found in a light, thin-walled and sufficiently stiff structure [Reichel 2008] and a lack of formwork on site.

### 3.2.5 Ultimate failure pattern

At the serviceability limit state (SLS), there is no difference in the structural behaviour between monolithic, epoxy jointed and dry jointed segmental girders. However, after decompression, segmental bridges show relatively fast decreasing of load bearing capacity due to opening of joints. A girder with external tendons and dry joints has 10 % or 20 % lower load bearing capacity compared to internal tendons and epoxy joint (Fig. 3.10).

Figure 3.16 shows the ultimate failure behaviour of these girder types. In a simply supported segmental bridge with external tendons and dry joints, there are two important issues. First one has to analyze the longitudinal stress distribution across flanges. As shown in Figure 3.16, the failure occurs in the upper part of the web and in the top slab due to concrete crushing at joints.

Thus, the compressive stresses in this area have to be checked. Furthermore the transmission of shear forces in the joint must be analyzed. In dry jointed girders, the shear-keys will transfer most of the vertical force. For this reason, the shear-key performance of UHPC is very important.

Therefore, the following two topics will be analyzed in detail in this thesis:

- Longitudinal bending moment resistance (see chapter 4)
- Shear force resistance (see chapter 5)

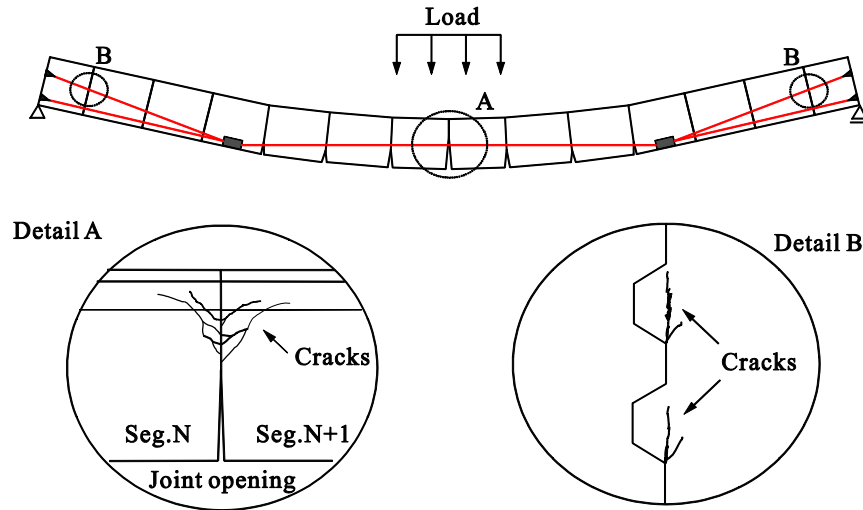


Figure 3.16: Ultimate failure pattern of segmental bridges with external tendons and dry-joints

### 3.3 Applications of UHPC segmental bridges

Precast segments made of UHPC will be applied in various fields of concrete structures exceeding the limit of the present concrete constructions. The many benefits as high strength and durability of UHPC have increased performances when it is used with the segmental construction method. The segment production in a factory ensures the high quality for concrete strength. Furthermore, it allows for a high prestressing force. The smaller cross-section reduce the dead load and simplifies transport and erection.

Currently, in spite of the higher cost of UHPC, the application of UHPC in the field of bridges is steadily increasing world-wide. In the following, some bridges are presented.

#### 3.3.1 Footbridges

As the early UHPC-bridges, the Seonyu footbridge (Figure 3.17) and Sakata Mirai footbridge (Figure 3.18) built in the year 2002 must be mentioned [Behloul et al. 2003]. The arch of Seonyu footbridge has a  $\pi$ -shaped cross-section of 1.3 m depth and has been assembled by six 20 m prefabricated segments. The upper flange is a ribbed slab of only 3 cm thickness prestressed in transverse direction with monostrands.

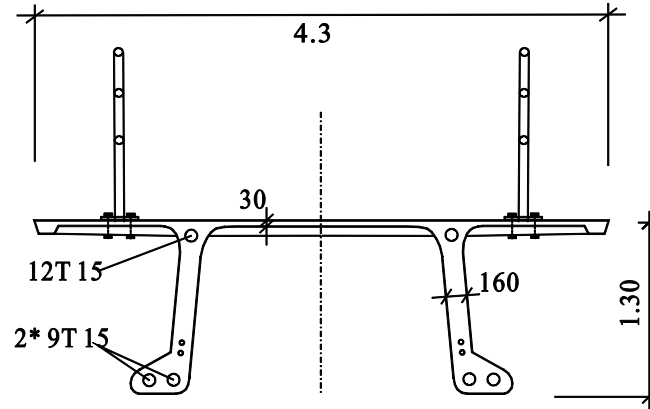


Figure 3.17: Cross-section of Seonyu footbridge, South Korea, 2002 [Behloul et al. 2003]

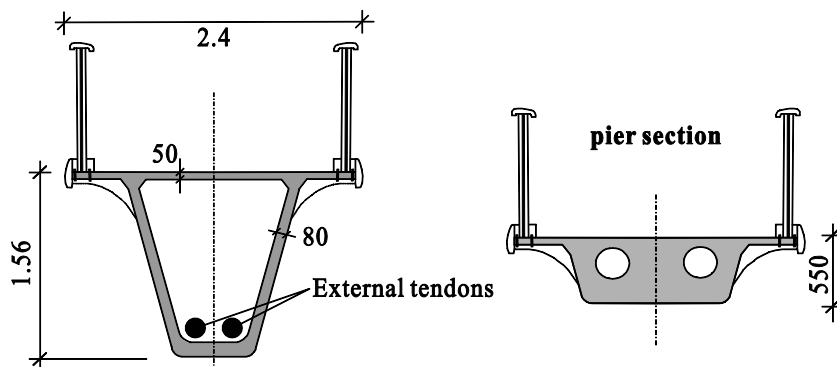


Figure 3.18: Cross-section of Sakata Mirai footbridge (left: mid-span section, right: at the pier), Japan, 2002 [Acker 2004]

Also, as one of the early UHPC-bridge made of Ductal®, Sakata Mirai footbridge with a span of 50 m was built in Japan in 2002. The deck is a simple beam 2.4 m wide with circular holes at the pier section. The structure is longitudinally prestressed with external tendons and has passive reinforcement. From 2000 to 2008, a total of 8 UHPC footbridges had been built in Japan [Acker, 2004].

### ***Toyota city gymnasium footbridge in Japan***

This footbridge, completed in 2007, is a two-span continuous two-box girder with a span length of 27.96 m, a width of 4.72 m and a height of 0.55 m ( $l/h = 51$ ) (Figure 3.19). The top and bottom slab has a thickness of 60 mm only. The web thickness is 70 mm. A precast segment construction method has been adopted, accounting for a newly developed dry joint method. The whole structure was divided longitudinally into 12 precast segments with a length of 1.9 – 2.5 m. A 1 % parabolic curve was required in the longitudinal direction. The prestressing consists of four sets of 19 @ 15.2 mm external tendons.



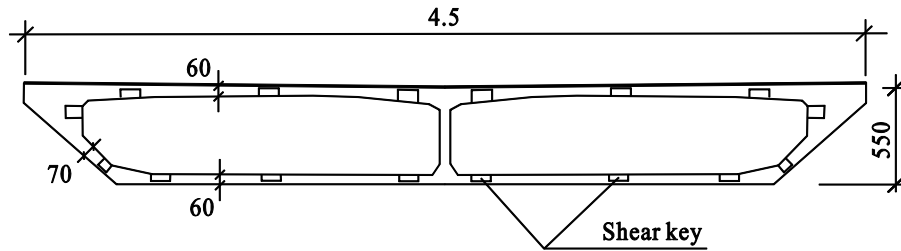


Figure 3.19: Match cast section and shear keys at the dry joint [Tanaka et al. 2007]

### 3.3.2 Road bridges

#### *PS34 Bridge in France*

In France, the PS34 Bridge (no. 4 Overpass) over the highway A51 was built in the year 2005. This overpass was made of a precast prestressed box girder with a single span of 47.4 m in length, a road width of 3 m and a constant height of 1.63 m ( $l/h = 29$ ). The deck slab has a thickness of 14 cm; and thickness of the webs and the bottom slab are 12 cm.

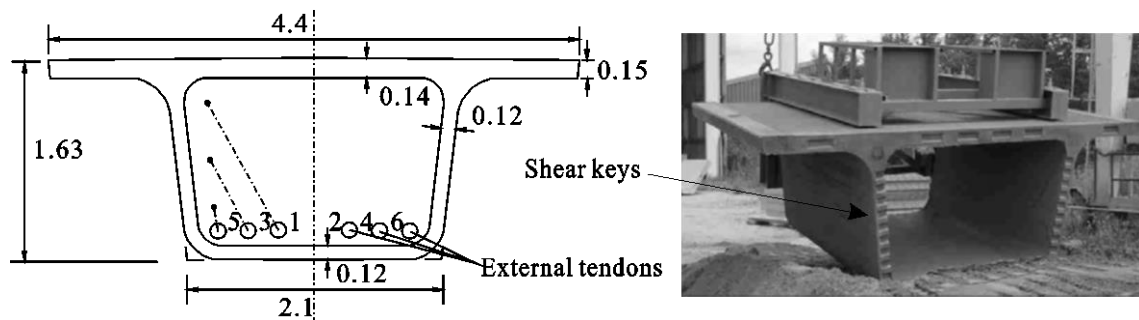


Fig.3.20: Cross-section and shear-keys of the PS34 Bridge [Resplendino, Bouteille 2006] [Resplendino 2008]

The superstructure consist of 22 match-cast prefabricated segments made of UHPFRC (BCV<sup>®</sup>), 18 typical segments with a length of 2.44 m, two deviators with a length of 0.5 m (segments no. 8 and segments no. 15) and two segments on the abutments with a length of 2.04 m. The structure is prestressed by six 19T15S external tendons (Figure 3.20).

The main physical and mechanical characteristics of the concrete BCV<sup>®</sup> are summarized in Table 3.3. The concrete used for PS34 has a 2 % volume fiber content (no polymer fibers have been used).

The PS34 Bridge was designed for normal traffic loads according to the rules provided by [AFGC/SETRA 2002]. To avoid any opening of joints at serviceability limit state (SLS), full compression is required. The structure has average concrete compression stresses of 25 MPa with a maximum value of 55 MPa through tensioning. Due to local concentrated loads (wheel loads), tensile stresses in the top slab of the box girder occur. Thus the tensile strength of the BCV<sup>®</sup> must be high enough to resist the transverse bending forces. In order to ensure a sufficient shear capacity,

the PS34 Bridge has a small decompression at the ultimate limit state (ULS). The shear capacity is always ensured by the compressed residual part of the cross-section.

Table 3.3: Physical and mechanical characteristics of BCV® [Toutlemonde, Resplendino 2011]

Properties	BCV®
Density	2.480 kg/m <sup>3</sup>
Compressive strength (24 hours, 28days)	50 MPa, 130 – 150 MPa
Tensile strength (28 days)	8 MPa
Flexural strength	30 MPa
Static modulus of elasticity	44 GPa

The segments were joined together using epoxy-type glue. The deck was placed within around 20 minutes using an 800 tonne-capacity crane directly on its final bearings. The deck was lifted up with four slings.

Table 3.4: Comparison of construction period of a classical bridge and PS34 Bridge [Toutlemonde 2011]

PS34 bridge	Month 1	Month 2	Month 3	Month 4	Month 5	Month 6
Segments prefabrication						
Bridge abutment						
Segments assembly						

Classic bridge	Month 1	Month 2	Month 3	Month 4	Month 5	Month 6
Bridge abutment						
Pier erection						
Shoring of deck						
Deck erection						
Fittings						

This pilot project presents important material quantities as compared to conventional concrete bridges; 80 m<sup>3</sup> of UHPFRC instead of 200 m<sup>3</sup> C35/45 concrete. Table 3.4 presents a comparison of the construction period between PS34 Bridge and a conventional concrete bridge. With assembly of segments, this type of bridge can be finished very rapidly. Also, from the economical point of view, the initial cost for formwork will be reduced by industrialization of this type of concrete structure [Resplendino 2008].

### **Wild Bridge in Austria**

The arch bridge has a total length of 157 m and consists of two arches made of precast segments. The polygonal cross-sections of the UHPC-segmental-arch, made of UHPFRC C165/185, have 6 cm thin walls. The very light precast UHPC-segmental-box-girders are stressed by 24 external tendons. For the columns connection and for the anchorages and deviations of the external tendons, so called “knee-elements”, special segments for the arch are used (see Figure 3.21).

The Institute for Structural Concrete at Graz University of Technology (TU Graz) mentioned that the slenderness of UHPC bridges may not be reduced because of the resistance against vibration and deflection. Nevertheless, UHPC-segmental bridges will have economic benefits such as faster construction, less maintenance cost and longer life-time.

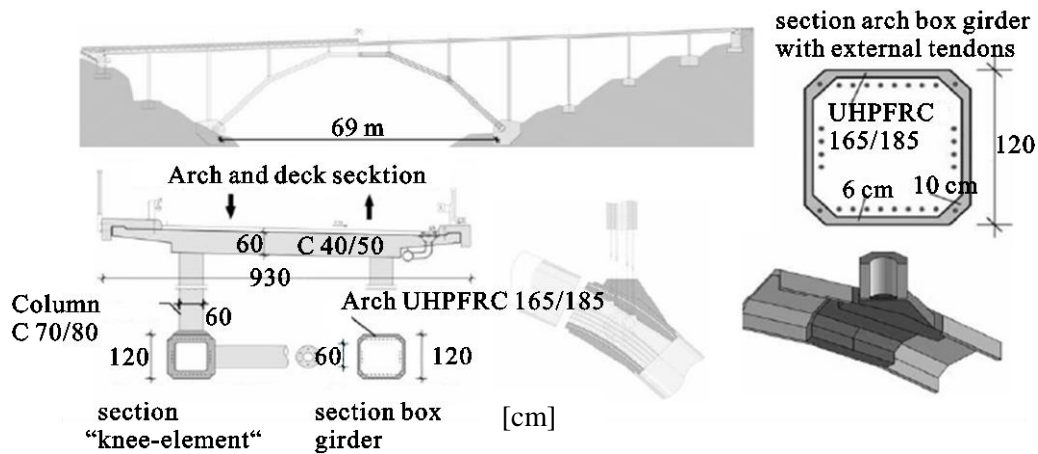


Figure 3.21: Construction details of Wild bridge [Reichel et al. 2008], [Freytag et al. 2009]

### Ground Support Equipment (GSE) Bridge in Japan

A single-span GSE Bridge (see Fig. 3.22) was constructed in 2008 over the road connecting the south and north apron of the extension of the Tokyo International Airport Airline project. This structure has a span of 46 m and a width of 16.2 m. The main live load of the bridge is the heavy towing tractor that weights a total of 500 kN. It is used for pulling an aircraft. The wheel load is 125 kN/wheel, which is heavier than an ordinary truck wheel load [Watanabe et al. 2007].

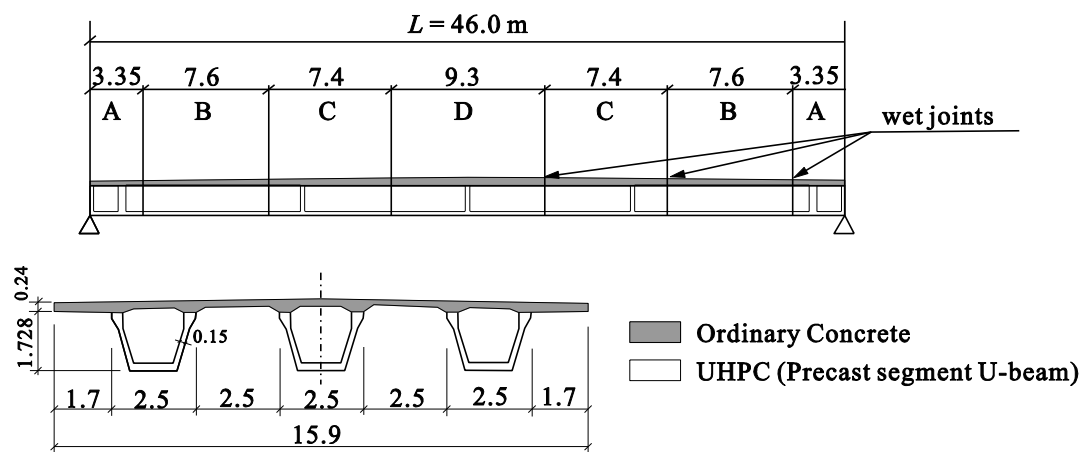


Figure 3.22: Construction details and cross-section of the GSE Bridge [Watanabe et al. 2007]

Meeting the need for a low height and light dead weight, the end girder height of the bridge was 1.86 m (girder height to span ratio is 1/25) and the dead weight was reduced by 40 % compared to an ordinary concrete bridge. The major structural features are:

- three box girders composed of U-shaped UHPC precast segments

- the main deck slab was made of cast-in-situ conventional concrete ( $f_{ck} = 40$  MPa)
- one box U-shaped girder was divided into seven precast segments, connected together by wet joints. (UHPC girders with large shear keys for precast segment joints were developed based on full-scale model experiments. This test for UHPC shear key will be presented in Chapter 5)
- the deck slab and the girders were jointed together by Perfobond Strip shear connector

Most UHPC bridges in Japan were prestressed by external tendons. However, the internal tendons system was adopted for this project. The width of the wet joints between the U-shaped precast segments was set up at 15 cm to join the internal tendon sheaths.

### *Tokyo monorail girder in Japan*

In 2007, the Tokyo Monorail and Taisei corporations completed their corporative technical development of a 40 m long monorail girder made of UHPC. Due to length restrictions in the case of a 40 m long monorail girder, three reversed U-shaped girder (rU girder) segments and three bottom slab segments were separately manufactured in a factory, conveyed to the construction site and jointed together by wet and dry joints. Three rU girder segments were connected by dry joint. It should be noted that the dry joints of the rU girders are located in the inner side of the span, as shown in Fig. 3.23.

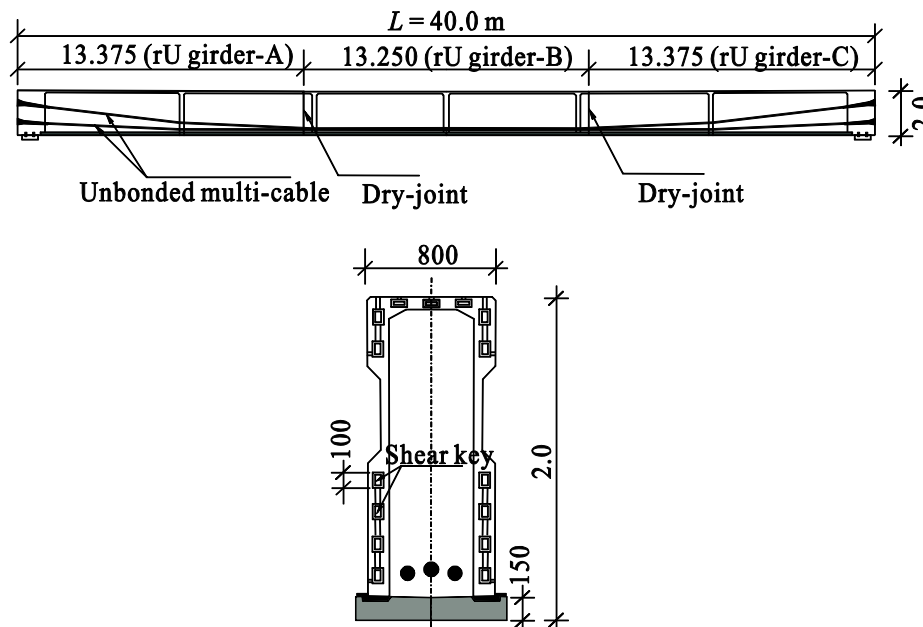


Figure 3.23: Structural composition of precast segments and shear keys in the dry joint [Tanaka et al. 2011]

## 4 Flexural Behaviour of Ultra High Performance Concrete Precast Segmental bridges (UHPC-PSB)

The behavior of UHPC-PSB with external tendons and dry joints is different from ordinary PSBs due to high concrete strength and thin sections. Thus this chapter deals with the flexural behaviour of UHPC-PSB. First, a nonlinear Finite-Element model is developed. The full-scale test results from the S.E.S project in Bangkok are used to verify it [Takebayashi 1994]. Then parameter studies with the most relevant factors like E-Modulus, concrete strength, member thickness, prestressing force etc. were conducted. Based on these studies, a UHPC-PSB, which has very thin sections, is proposed and the behaviour is analyzed by a FE-model. This numerical study focused on the change of normal stresses at mid-span and the joint opening.

### 4.1 Behaviour of PSB

The behaviour of a PSB is different from a monolithic structure due to the dry joints. Figure 4.1(a) shows the typical load-deflection relationship of a monolithic girder. Ideally, the load-deflection response is characterized by three stages: (a) linear elastic un-cracked stage; (b) linear elastic cracked (post cracking) stage; and (c) nonlinear cracked (post serviceability cracking) stage.

In a segmental bridge with external tendons and dry joints, however, there are two stages only. Before the joints open, the structure behaves linear-elastic as in a monolithic structure shown in Figure 4.1(b). Tests carried out by Macgregor et al. [1989] and Rabbat & Sowlat [1987] etc. demonstrated that dry-jointed segmental girders behave in a similar manner to a monolithic or epoxy-jointed structure up to the point when longitudinal bending stresses give rise to decompression of the joints. Hewson [2003] mentioned that the joints of segmental construction should always kept in compression under service conditions, and the longitudinal stress check and other serviceability checks are carried out as if the deck is monolithic.

As the load increases, more joints along the span open up and the crack openings extend over a greater part of the segment's depth. As the ultimate moment capacity is approached, the girder deflection rapidly increases and final failure occurs on the compression side by crushing of the concrete due to excessive strain. Thus, a segmental bridge with dry joint and external tendons after service limit state shows a different behaviour compared with monolithic or epoxy-jointed structure.

In principle, the analysis of externally prestressed beams is the same as that of internally prestressed members with unbonded tendons. However, there is an additional point to be

considered in the structure of external tendons, namely the variation of tendon eccentricity due to the deformation of the structure.

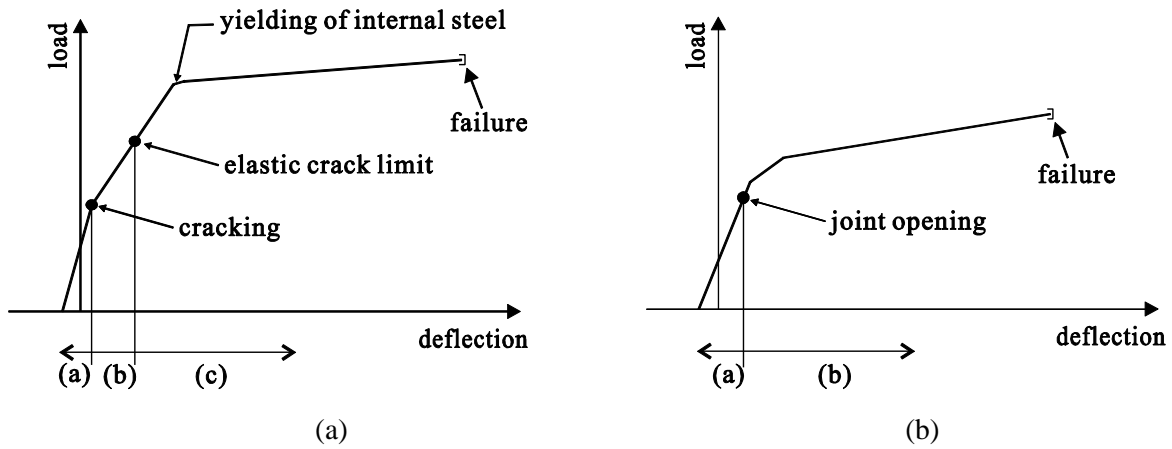


Figure 4.1: Typical load-deflection relationship of an externally prestressed concrete beam:  
(a) monolithic and (b) segmental

As an early nonlinear analysis of a segmental bridge, Virlogeux [1988] presented the important factors involved in the analysis of externally prestressed concrete structures, and proposed a plastic hinge concept for predicting tendon elongation at the ULS. Virlogeux proposed a very simple model for evidencing the different behaviour of bonded and internal unbounded tendons. The model consists of two rigid bodies (an isostatic span) linked by a hinge at mid-span (see Figure 4.2).

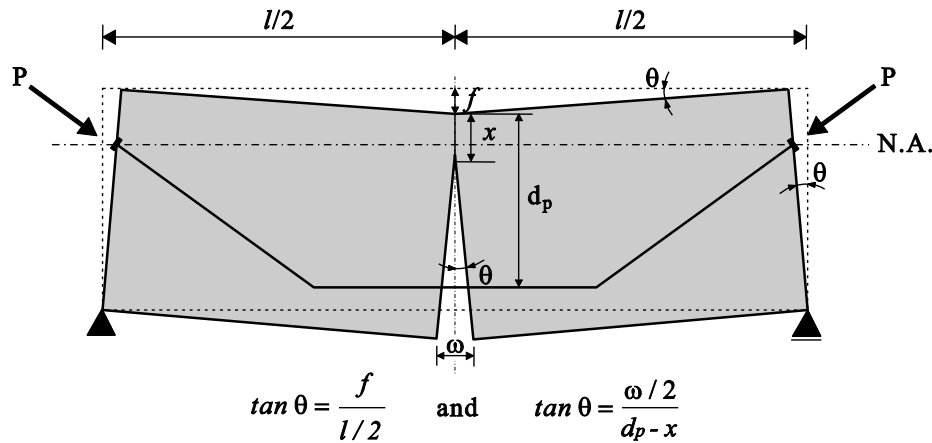


Figure 4.2: Simple model for the analysis of a segmental beam in the ultimate limit state  
[Virlogeux 1988]

Using the geometry of Figure 4.2 the following equation can be derived to determine the tendon length variation ( $\Delta l_p$ ) from the displacement on each side of the opened central section.

$$\Delta l_p \approx \omega = \frac{4 f (d_p - x)}{l} \quad (2.1)$$

where:  $\omega$  width of the opened joint  
 $l$  span length  
 $f$  deflection at mid-span  
 $d_p$  distance from the top flange to the tendon  
 $x$  depth of compression zone

Thus, the change in tendon strain  $\Delta\varepsilon_p$  is as follows:

$$\Delta\varepsilon_p = \Delta l_p / l_p \quad (2.2)$$

Because the external tendons between the anchorages or deviators with applied load remains straight as shown in Figure 4.3, the distance between the neutral axis and the tendons is reduced. The eccentricity variation is most commonly referred to as second-order effects. The loss of eccentricity between two deviators (Figure 4.3 (b)) is smaller than that without deviators (Figure 4.3 (a)). So, a prestressed beam with straight type external tendons leads to a lower load bearing capacity. In a segmental structure with dry joints, therefore, these effects will be more significant because the joints cannot resist tensile forces. Even though these effects may not be so important at SLS, the loss of tendon eccentricity can have considerable effect at ULS depending on the span-to-depth ratio, tendon profile and position, and the spacing of deviators.

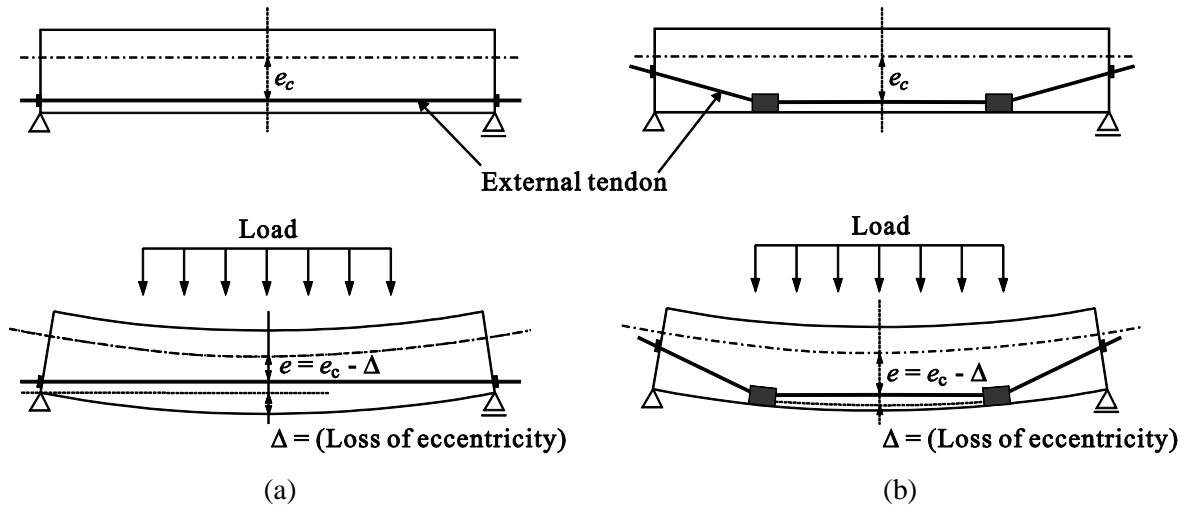


Figure 4.3: Deflection and loss of eccentricity in an externally prestressed concrete beam  
(a) straight tendon and (b) draped tendon

To evaluate the behaviour of a bridge made of precast segments at ULS, the structural deformations cannot easily be assessed because joints are opened in critical zones. Thus, simplified methods must then be derived in order to evaluate the stress distribution and deformation on either side of opened joints.

## 4.2 Finite-Element-Model of PSB

A significant number of precast segmental bridges with external tendons and dry joints have already been constructed. With development of structural FE-programs, some numerical investigations were also conducted to accurately predict the behavior of precast segmental bridges.

As an early study, Adel-Halim [1982] presented a general approach for nonlinear analysis of segmental bridges. The general approach accounts for concrete cracking with a tension stiffening effect and for multi-axial behaviour and strength properties of concrete (three-dimensional finite elements). Then, the finite element analyses were compared to the results obtained from the test. Also Muller and Gauthier [1990] provided a computer program with 3-dimensional elements, which includes only elastic material properties, for precast segmental box girders. The opening of dry joints between segments was considered by the program. A nonlinear finite element analysis of a PSB with external post-tensioning tendons and dry joints was conducted by Kreger et al. [1990]. Their objective was to examine the effect of dry joints on the strength and ductility of a box girder construction. Ramos and Aparicio [2006] also developed a FE-model to analyze externally prestressed concrete bridges, compared with a monolithic structure, up to failure. The model considered the material nonlinearity, the effect of eccentricity variations of the external tendon with applied loads, and joint opening.

FE-analyses of segmental bridges with external tendons and dry joints can also be found at the Universities of Technology in Karlsruhe Huang [1994] and Hamburg Rombach & Specker [2000] in Germany. Huang [1994] studied a segmental box girder model with plane shell elements under combined actions of bending, shear and torsion. Rombach & Specker [2000] used volume elements to model the indentation of the surfaces of the segments due to shear-keys to investigate the effect of joint behaviour under shear and torsion in detail. In addition, various subjects, like different tendon types [Kasic 2002], the bowing effect of match-casting [Abendeh 2006] and the torsion behaviour [Möller 2006], were modeled with FE-methods.

After SLS, an exact prediction of the behaviour of a PSB with dry joints is extremely difficult because of joint opening and second-order effects. A rigorous analysis of stress and displacement is required for all ranges of loads up to failure. Therefore, the load bearing behavior of UHPC-PSB, as a new type structure, has to be studied before its construction proceeds.

A segmental bridge model with external tendons and dry joints consists of three types of finite elements: plane shell elements for segments, a contact element that transmits compressive and shear forces through the joints between segments, and a tendon element connected to the segments by rigid diaphragms and deviators.



### 4.2.1 Second Stage Expressway System (SES)

For the verification of the developed FE-model the experimental outcomes from a full-scale test of a typical span of the Second Stage Expressway (SES) segmental bridge reported by Takebayashi et al. [1994] were used.

The SES in Bangkok consists of approximately 1130 spans ranging in length from 24.9 m to 48.7 m with a typical span length of 45 m. A full-scale test of a 45 m long span, a prototype of the segmental decks in the SES, was carried out in the year 1991. Figure 4.4 shows the bridge dimensions and the tendon layout of a simply supported standard span. The segments used had a width of 10.2 m and a length of 3.4 m ( $w/L = 3.0$ ). The external longitudinal tendons were deviated at the three locations within a span. Dry joints were used in this project. A span consists of 9 standard segments, 3 deviator segments and 2 pier segments. The material parameters for concrete ( $f_{ck} = 55$  MPa and  $E_C = 43$  GPa) and tendon properties used in the numerical model for the verification are identical to that of the real structure.

More details of the segments and the shear keys can be found in Appendix A (see Figure A. 12).

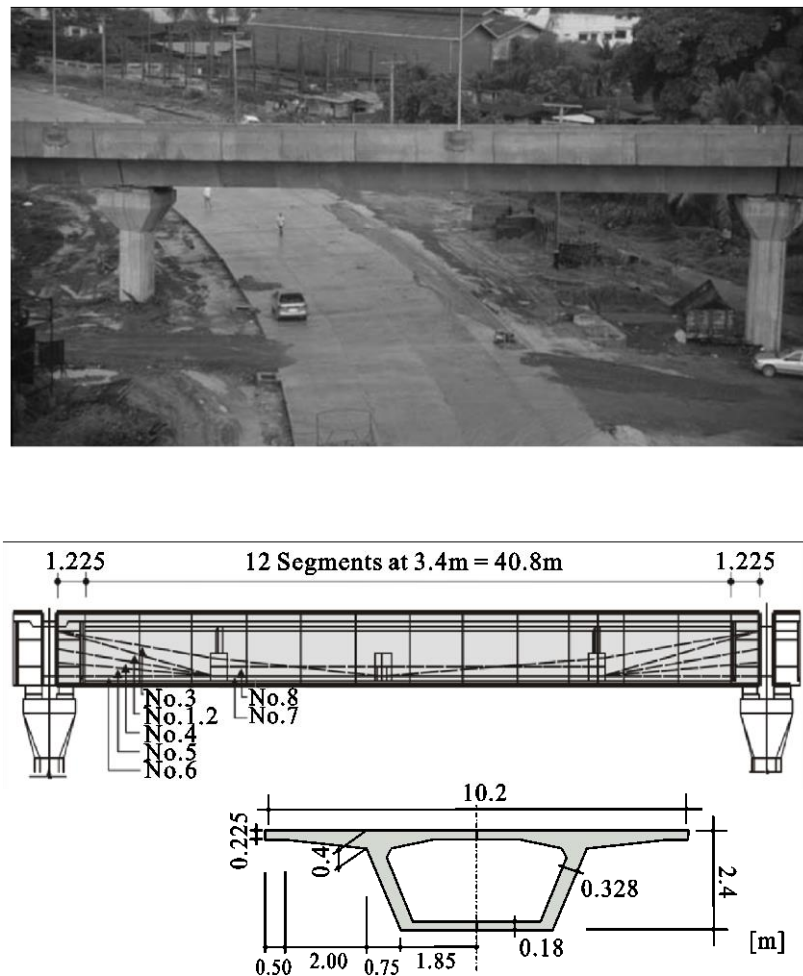


Figure 4.4: Tendon layout and cross-section of a standard span of the Second Stage Expressway System (SES) in Bangkok [Rombach 2004], [Rombach 2002]

### Loading used in the FE Model

The test span was loaded by steel billets up to failure. Figure 4.5 shows the arrangement of the live loads (billets) on the deck. As shown in Table 4.1, after prestressing the loading operations are carried out in three loading phases until failure load of the test span at 1.3 ULS mid-span moment.

Table 4.1: Loading phases

Load stage	No. of billets and load [kN]	Applied mid-span moment [kNm]
Design service load ( $M^{SLS}$ )	1080 (3,676.4)	24,600
Design ultimate load ( $M^{ULS}$ )	1980 (6,740.1)	44,600
Failure load ( $1.3M^{ULS}$ )	2620 (8,918.7)	58,200

\* 1 Billet = 347 kg

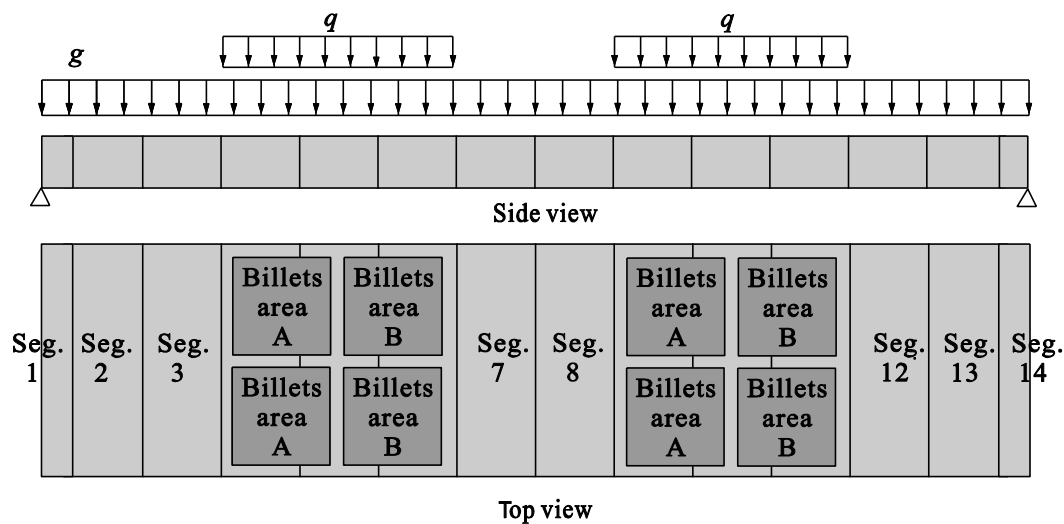


Figure 4.5: Load arrangement of the full-scale test [Takebayashi et al. 1994]

### 4.2.2 Material properties used in the FE model

#### Ultra High Performance Concrete (UHPC)

The properties for UHPC may be significantly different from normal strength concrete (NSC) and must be carefully applied based on experimental results and recommendations. The properties of UHPC are listed in Table 4.2. As the behaviour of a PSB is dominated by the joint opening, a simple elastic stress-strain relationship is assumed for the concrete (Fig. 4.6 (a))

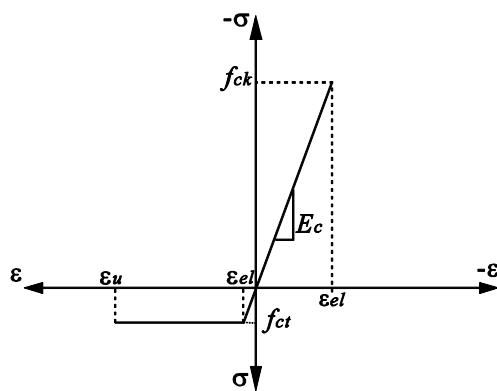
### External tendons

The bridge was prestressed by external tendons only, which were formed from 12K15 and 19K15 ( $P_o = 2440$  kN and  $P_o = 3864$  kN) protected by high density polyethylene ducts (HDPE) and cement grout. The prestressing tendons (straight and draped types) used in the model include material nonlinearity according to [Eurocode 2] (Figure 4.6 (b)).

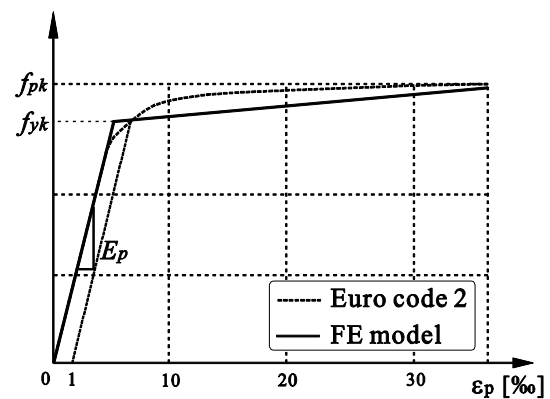
There is a friction between the external tendons and the deviators. The real value of the friction coefficients depends on many factors. It can only be determined by experimental investigations. For the numerical analysis, the friction coefficients at the deviators were assumed to have a certain value ( $\mu = 0.15 - 2.0$ ) taken from the literatures [Radloff et al. 1991], [Aeberhard et al. 1992].

Table 4.2: Material properties used in the numerical model

Material	Characterization-item	Value
UHPC	Compressive strength ( $f_c$ )	180 MPa
	Tensile strength ( $f_{ct}$ )	9 MPa
	Limited strain in tension ( $\varepsilon_u$ )	3 ‰
	Modulus of elasticity ( $E_c$ )	55 GPa
	Poisson's ratio ( $\nu$ )	0.19
Tendons	Yield strength ( $f_{yk}$ )	1,530 MPa
	Breaking strength ( $f_{pk}$ )	1,920 MPa
	Modulus of elasticity ( $E_p$ )	193 GPa



(a)



(b)

Figure 4.6: Assumed stress-strain curves for (a) UHPC and (b) prestressing steel used in the FE model

### Dry joints: Contact elements

Contact elements can be defined as coupling springs between two nodes. Figure 4.7 shows a spring in normal direction and a lateral spring between two nodes. The shear keys are not modeled in detail, as the flexural behaviour of the structure is in the focus of this research and not the shear capacity. In the flexural behavior of girders, the vertical displacements at joints are insignificant. Therefore, shear-keys were neglected in the model. The springs can transfer compression and friction forces across the joints only.

In reality the shear keys hinder the differential deformation in the joints. No or very little relative vertical deformation between two adjacent segments in the joint is possible due to the shear keys. Thus, it is not necessary to include a vertical contact element. As a flat joint without shear keys, however, lateral springs are needed for assembly of adjacent segments.

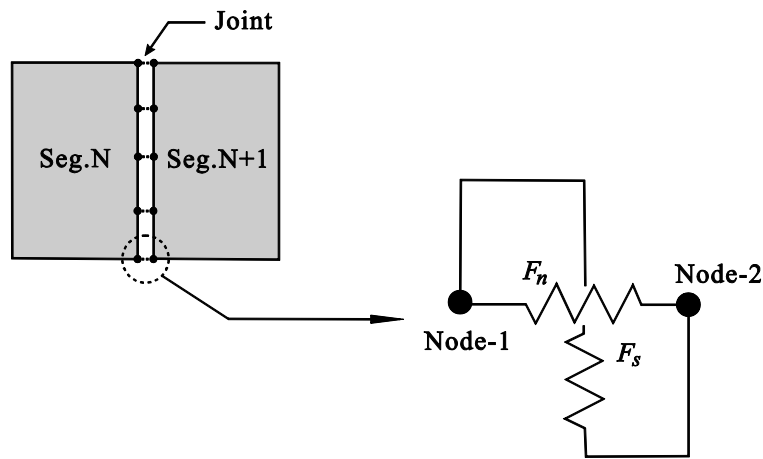


Figure 4.7: Contact element by springs between two nodes

The force-displacement relationships of the springs are shown in Figure 4.8. The force-displacement relationship of normal springs is the same as that of the UHPC compressive stress-strain relationship used in the model.

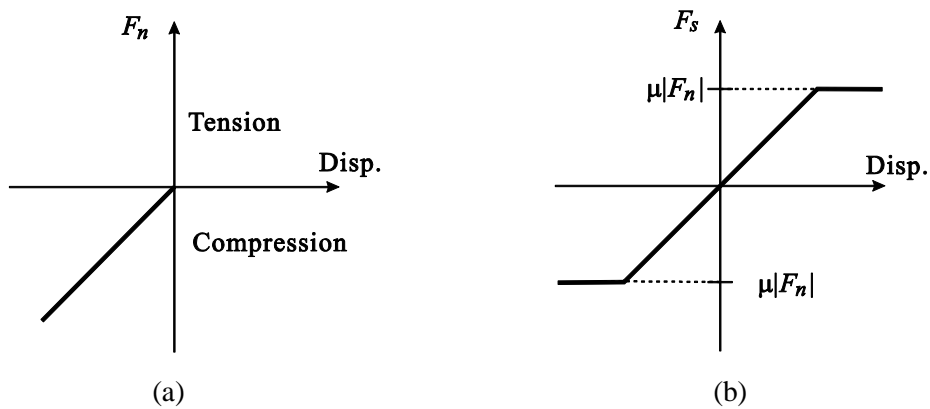


Figure 4.8: Force-displacement curves of contact element: (a) normal force, (b) shear force

### 4.2.3 Verification

The FE-analyses can be used for SLS verifications when sections are fully compressed, but also allow verifications of ULS when joints open. The SES standard box girder model, consisting of plane shell elements, shown in Figure 4.9 (a) is analyzed. The FE-software “SOFiSTiK 2010” is used for the analysis. Figure 4.9 (b) shows the deformation with joint opening and the compressive stresses in the joint at mid-span of the SES segmental bridge at ULS (the failure load:  $1.3M^{ULS} = 58.2 \text{ MNm}$ , see Table 4.1).

First, the bridge deformed upwards due to the high prestressing forces (dead + p.t. only, without live load). Then the live load (billets) was increased on the structure (see Figure 4.5). The bridge behaved elastically until the first joint close to mid-span opened. After ULS, especially, the stiffness of the model is significantly reduced.

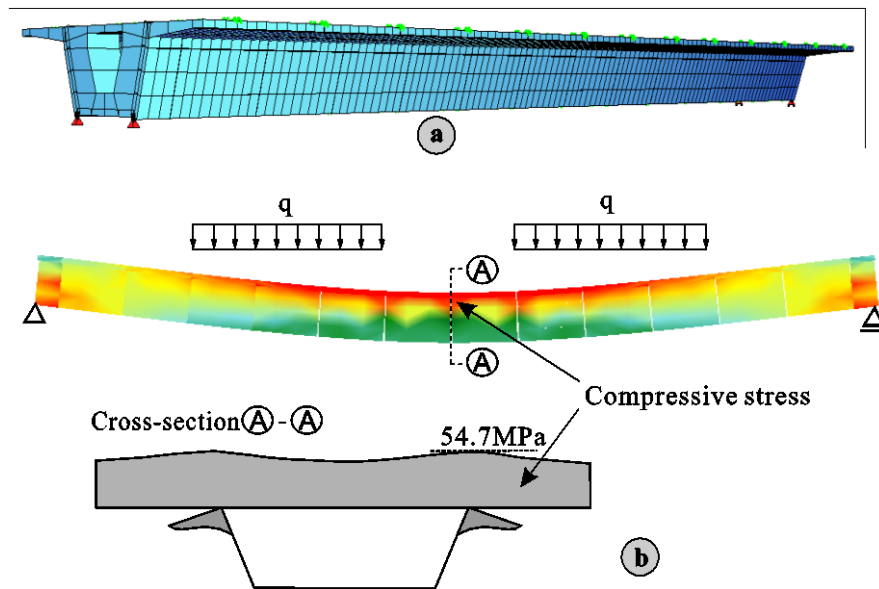


Figure 4.9: SES precast segmental box girder: (a) Finite element model and (b) Longitudinal and transverse stress distribution at mid-span at failure load

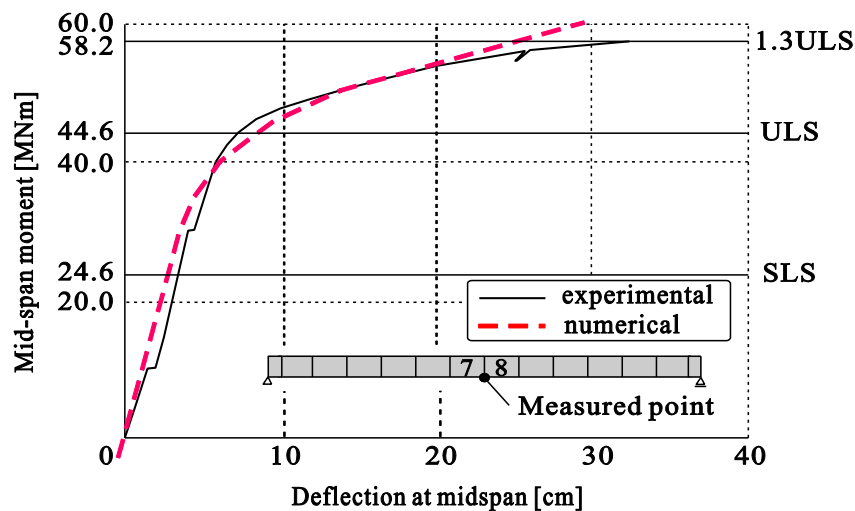


Figure 4.10: Comparison of the mid-span deflection between numerical simulation and test by Takebayashi et al. [1994]

The load-deflection responses from the experimental results obtained by Takebayashi et al. [1994] and from the numerical analysis are given in Figure 4.10. A good agreement between the FE-results and the experimental values can be observed. This demonstrates that the numerical model can simulate the behaviour of the real bridge.

The failure load of the bridge cannot be calculated by the FE-model due to the assumed linear-elastic behavior of the shell elements. The FE-model behaves fully elastic until the joint between segment no. 7 and segment no. 8 starts to open. However, after ULS, the maximum deflection occurred at the joint between segment no.8 and segment no. 9 due to segment no. 7 with the center deviator (the asymmetric arrangement of the deviators). The phenomenon can be also explained by the test results of Takebayashi et al. [1994].

The measured value of the joint opening after applying a live load bending moment of  $M_q = 58.2$  MNm was about 35 mm, whereas the numerical analysis gives about 27 mm ( $\Delta = 30\%$ ). The difference is caused by the elastic material behavior used in the FE-model. The comparison of the joint opening between both the numerical and measured results is plotted in Figure 4.11.

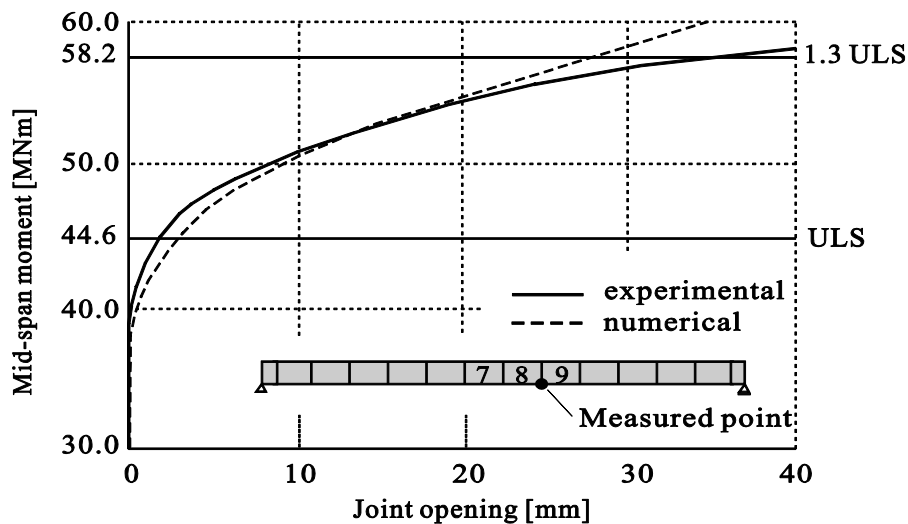


Figure 4.11: Comparison of joint opening between test by [Takebayashi 1994] and numerical simulation

The behaviour of external tendons is characterized by a linear and nonlinear portion, with departure from linear at a loading slightly above  $M_q = 40$  MNm. The strain of the tendon T1 (draped tendon of the test) is similar to that of the numerical model (see Fig.4.12). The behaviour of the tendon T1 is represented by a large increase in strain levels in the mid-span portion of the tendon, compared to smaller increase in strain at the end span portion between deviator and anchorage due to high friction forces at the deviators. The measured value of tendon strain at mid-span when applying the failure load (equal to  $M_q = 58.2$  MNm), was about  $\epsilon_p = 0.0016$ , whereas the numerical value was about  $\epsilon_p = 0.0014$ .

The typical failure mechanism of a precast segmental box girder with external tendons and dry joints was presented by the full-scale test of Takebayashi et al. [1994]. The major cracks, as a crushing in the compressive zones, were observed at the webs of segments no. 6-9. The cracks

were detected first at a load level of the design ultimate moment ( $M^{ULS}$ ). These cracks were the result of very high compressive stresses at the upper region of the webs at the joints, which is similar to the results of the FE-model as shown in Figure 4.9 (b). The real cracks were found on both the inside and outside of the box in the test span (see Figure 4.13).

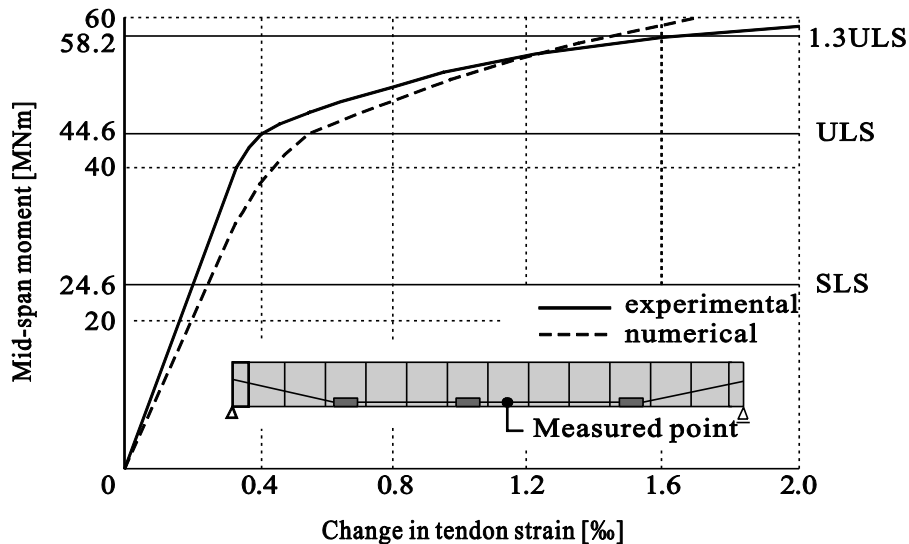


Figure 4.12: Comparison of change in tendon strains between the test results by [Takebayashi et al. 1994] and the numerical simulation (tendon no. T1)

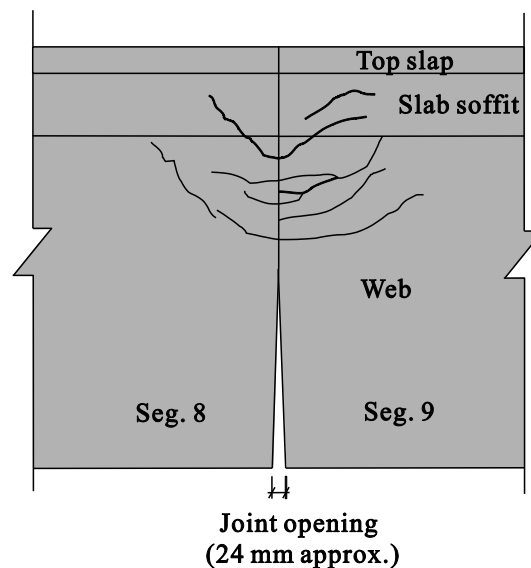


Figure 4.13: Typical cracks and the joint opening between two segments at mid-span before failure [Takebayashi et al. 1994]

The finite element analysis shown in the sections demonstrated that the behaviour of a real PSB can be simulated by means of the developed numerical model. Next parametric studies will be conducted to study the behaviour of a UHPC-PSB.

### 4.3 Parameter studies

One of the most important advantages of high strength concrete is the reduction of self-weight. Figure 4.14 shows a typical box type cross-section with external tendons and the area ratio. As illustrated in this figure, the top slab is approximately 60 % of the total cross-section area. For a reduction of the total section area, the reduction of the top slab thickness is necessary. UHPC members without rebar or very little rebar can be built with very small thicknesses.

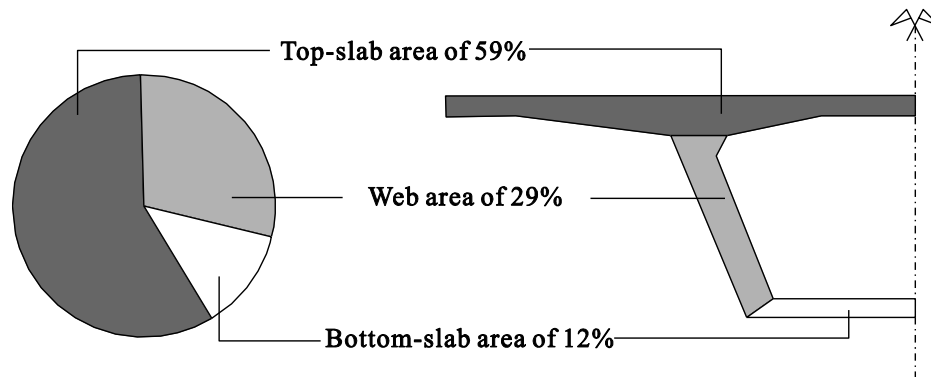


Figure 4.14: Area ratio of cross-section components of a typical hollow box girder with external tendons (from the cross-section of the SES)

Because of the different material properties of UHPC in comparison to NSC, thin cross-sections, and complex behaviour of PSBs with external tendons and dry joints, various parameter studies are inevitable for an application using UHPC material.

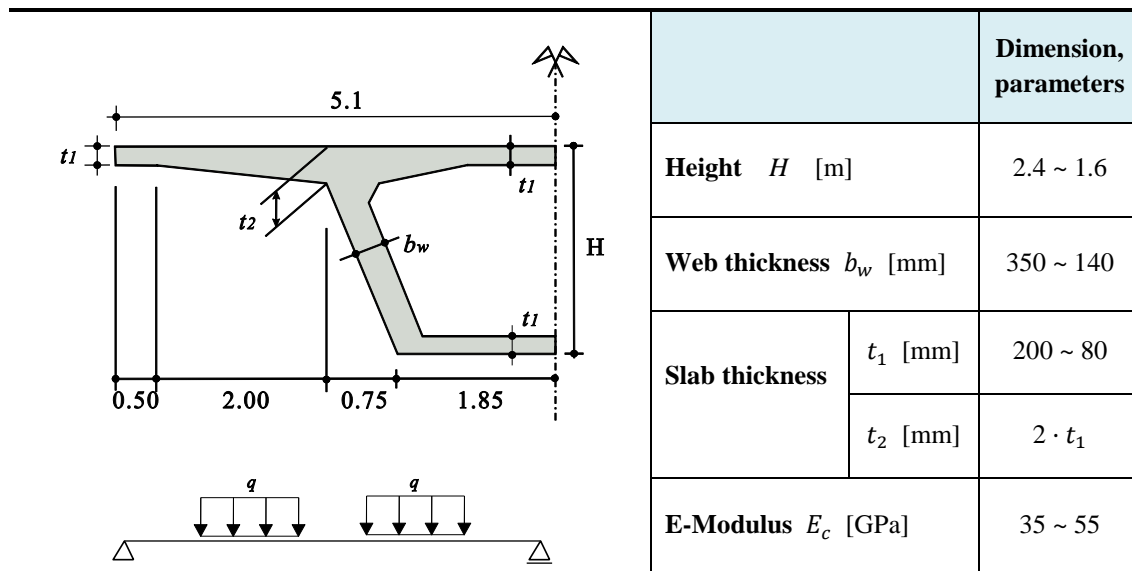


Figure 4.15: Variation of member thicknesses and E-modulus based on the SES test span

Thus, starting with the SES standard segment, different member thicknesses and the following parameters are considered (Figure 4.15):

- effect of concrete E-modulus ( $E_c$ )



- member thickness-concrete strength relationship
- span-to-depth ratio ( $l/h$ )
- stress change in tendon ( $\Delta\sigma_p$ )
- comparison with various concrete classes and sections

The loading and prestressing used in these parameter studies are the identical to those of the SES test span.

### 4.3.1 Effect of E-modulus

Normal Strength Concrete (NSC) is a nonlinear inelastic material. Its initial tangent modulus, which is the slope of the tangent to the curve at the origin, is not considered in the design because it applies only to small stresses and strains. Therefore, the secant modulus, which is equal to the slope of the secant between the origin and a point on the stress-strain curve are used in the design of concrete structures. These values are usually determined at 40% of compressive strength. On the other hand, UHPC has a high modulus of elasticity ( $E_c = 50 \sim 55$  GPa) and, as shown in Fig. 2.4 and Fig. 2.5, the compressive stress-strain curve is linear up to approximately  $0.8f_c$ .

As previously described in Section 4.1, the flexural stiffness ( $EI$ ) of a segmental girder with dry joints, as well as monolithic girders, can be estimated using  $E$ -modulus ( $E_c$ ) of concrete and the moment of inertia of the cross-section without joint opening. The behaviour of a concrete girder with higher  $E$ -modulus will provide some merits to ensure serviceability on deflections of a bridge.

To study the influence of the  $E$ -modulus of concrete on the behaviour of PSB with dry joints, the numerical model of the SES was analyzed with 3 different values (35 GPa, 45 GPa for NSC and HSC, respectively, and 55 GPa for UHPC, same p.t. as SES)

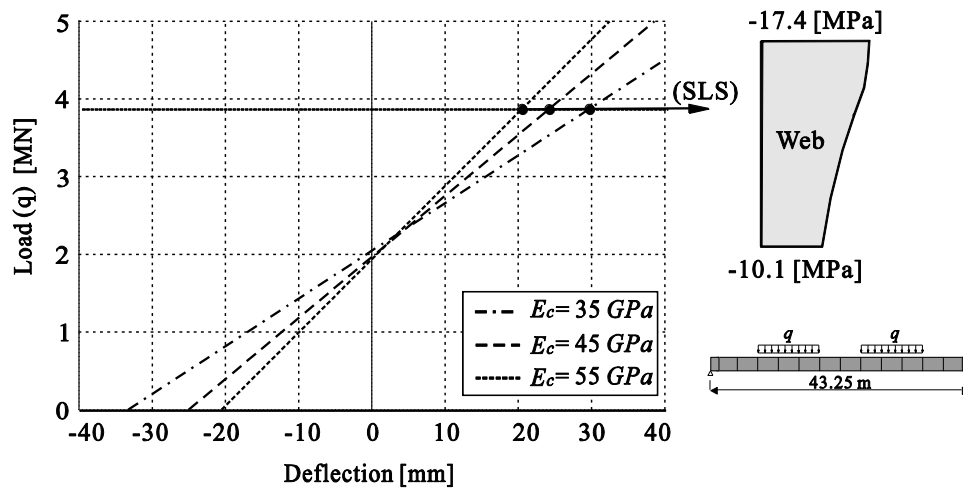


Figure 4.16: Deflections at mid-span and compressive stress distribution in the web at the SLS due to different concrete  $E$ -modulus (elastic analysis)

Figure 4.16 presents the deflections at mid-span, from the cambers (after prestressing without live load) to the SLS and the compressive stress distribution in the webs at mid-spans. The load-deflection curve of this range has essentially a straight line defining full elastic behaviour without joint opening such as a monolithic member. In comparison to the model with an  $E$ -modulus of 35 GPa, the deflection and the camber of the model with  $E$ -modulus of 55 GPa was relatively small. At SLS, the deflection of the model with  $E_c = 55$  GPa only presented about 72% to that of the model with  $E_c = 43$  GPa.

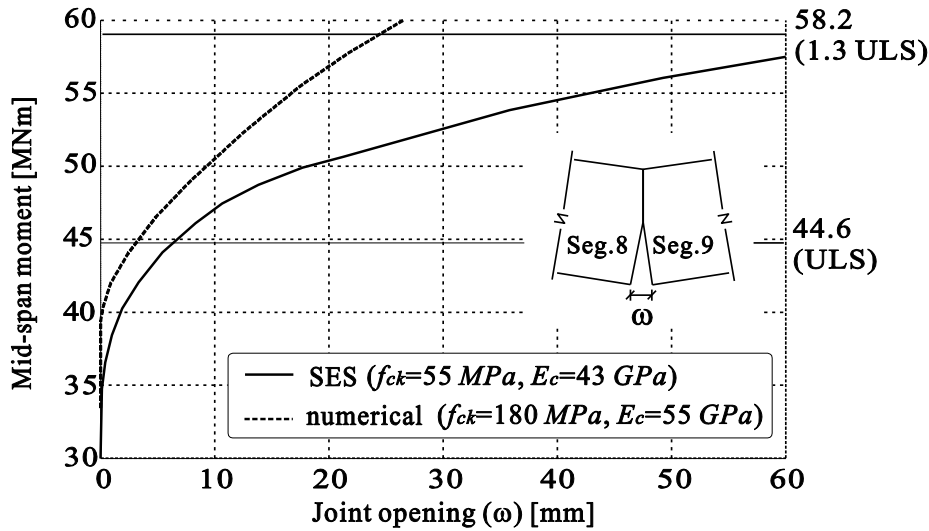


Figure 4.17: Joint opening of the UHPC model ( $E_c = 55$  GPa) and the SES test results ( $E_c = 43$  GPa)

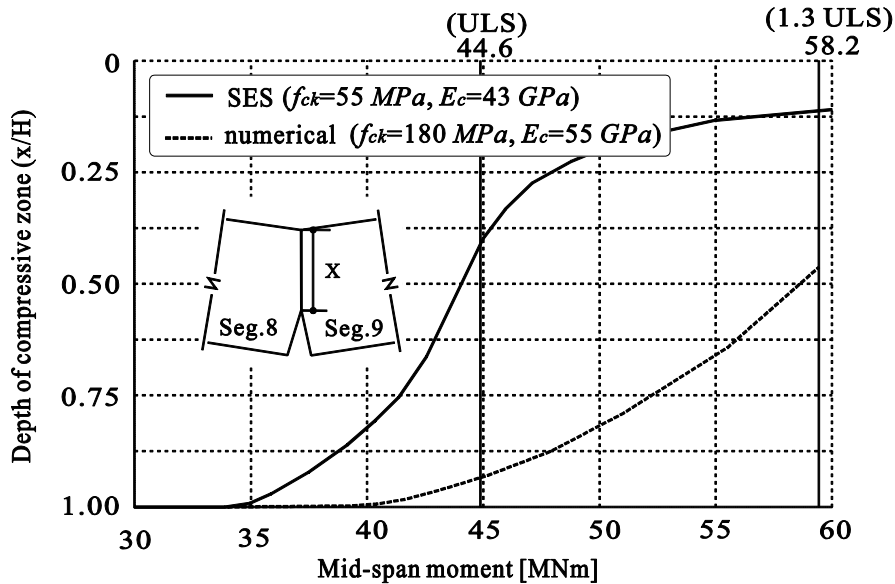


Figure 4.18: Depth of the compressive zone ( $x$ ) of the UHPC model ( $E_c = 55$  GPa) and the SES test results ( $E_c = 43$  GPa)

Figure 4.17 and Figure 4.18 illustrate the changes of the width ( $\omega$ ) of joint opening and the depth ( $x$ ) of the compression zone between NSC and UHPC. Compared to the SES test results, UHPC-

PSB model shows a smaller joint opening and a slower progress due to smaller deflections (same p.t. as SES). In contrast to the sudden deflection increase of NSC after SLS (from the SES test results), the deflection and the joint openings of UHPC-PSB model were proceeding more slowly.

Considering the material properties of UHPC, especially its elastic characteristic in the compressive stress-strain relationship, after SLS higher  $E$ -modulus will lead to small deflections in a concrete girder. In general, the deflection of segmental bridges with dry joints is larger than that of an epoxy joint or monolithic structure. Therefore, high  $E$ -modulus in PSBs is clearly advantageous.

### 4.3.2 Relationship between member thickness and compressive stresses

When considering the failure pattern of an externally prestressed simply supported beam (see Chapter 3.2.5), the stresses in joint regions, including joint openings, at mid-span must be checked. The load bearing capacity of a prestressed concrete beam is associated with its member thicknesses, the concrete compressive strength and the prestressing force under same loading. A high strength concrete in PSB can obviously lead to a thinner section and higher load carrying capacity. So this section presents the relationship between member thicknesses and the compressive stresses from PSB models using UHPC material.

The top slab thicknesses of 20 cm, 16 cm, 12 cm and 8 cm, and the web thicknesses of 35 cm, 24.5 cm and 14 cm are used in these computations. For the comparison with the load carrying capacity of NSC segmental girders, the sections at mid-span of all models are tested until the failure load ( $1.3M^{ULS} = 58.2 \text{ MNm}$ ) of the SES test. Figure 4.19 illustrate the longitudinal stress distributions in the top slabs at 1.3 ULS load level, and the deflections including the joint openings. The maximum compressive concrete stresses increases when member thicknesses are reduced.

In all FE analysis, the models with thinner sections deflected less than the UHPC-PSB with thicker sections until ULS due to the reduction of dead load and the bigger camber. After ULS, the models with thinner sections show a rapid stiffness reduction, like a segmental girder made of NSC. However, the deflections of all models were significantly smaller than those in the SES test span. Until ULS the load-deflection curves were almost straight lines due to the linear compressive stress-strain curve and the high  $E$ -modulus of UHPC. Also, the joint opening of all models occurred just before ULS load level because of smaller deflections and the longer linear behaviour compared to the results of the SES test span.

Due to the shear lag effect, the maximum compressive stresses are observed in the top slab areas above the webs. These maximum stresses are more clearly shown in the models with thin member thickness. In comparison to the failure load level (1.3 ULS) of the SES test span, the model of the thinnest member (top slab of 8 cm and web of 14 cm) presented the maximum compressive stress of  $\sigma_{c,max} = 165 \text{ MPa}$  (Figure 4.19(c)). However, the deflection of this model was 6.7 cm only in spite of similar load carrying capacities between the two models. The behaviour is affected by the excessive normal force, so a comparative study with different prestressing forces is conducted in the next section.

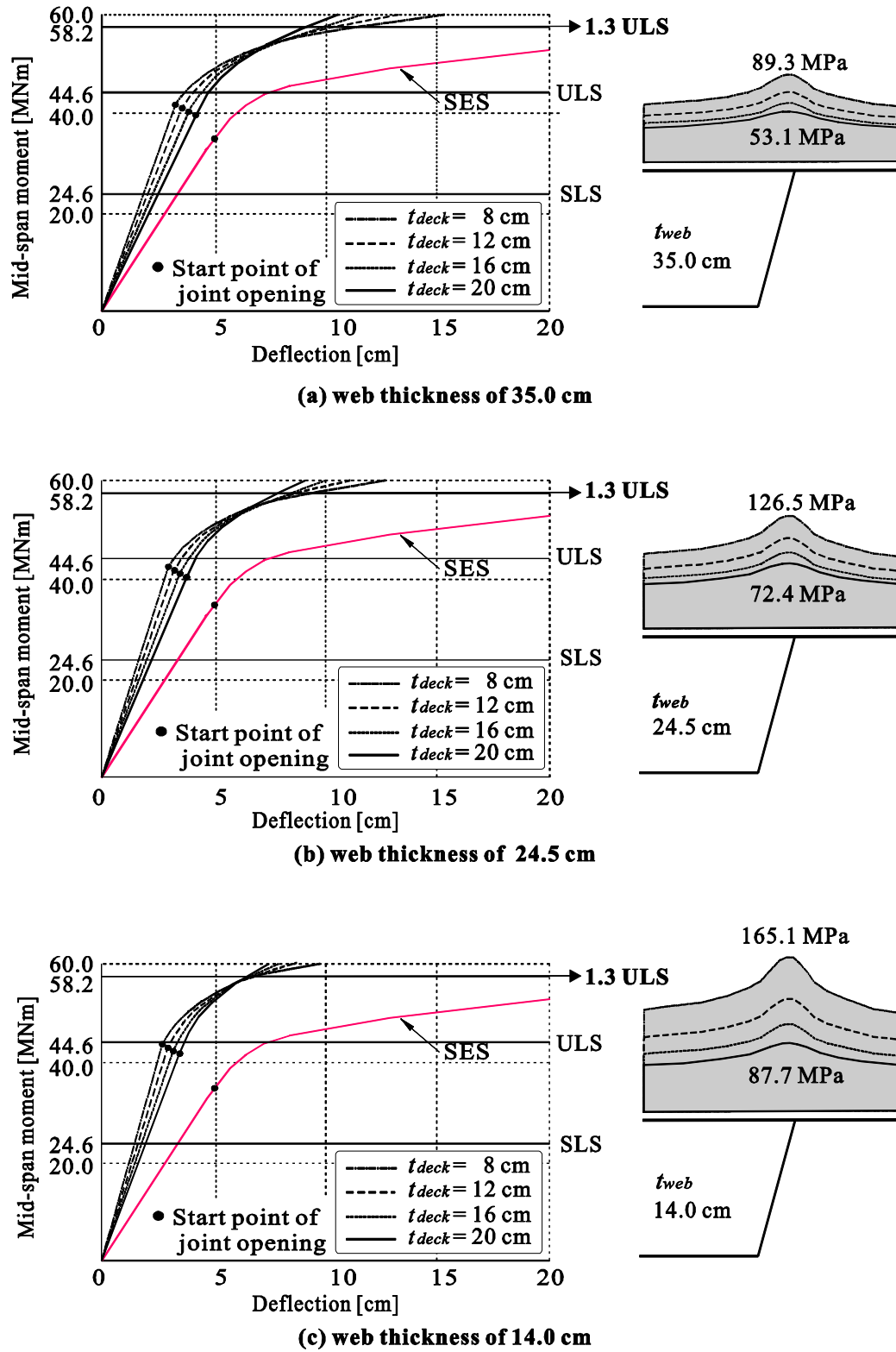


Figure 4.19: Compressive stress distributions in the top-slab and deflections due to different top-slab thicknesses: (a) web of 30.5 cm , (b) web of 24.5 cm and (c) web of 14.0 cm

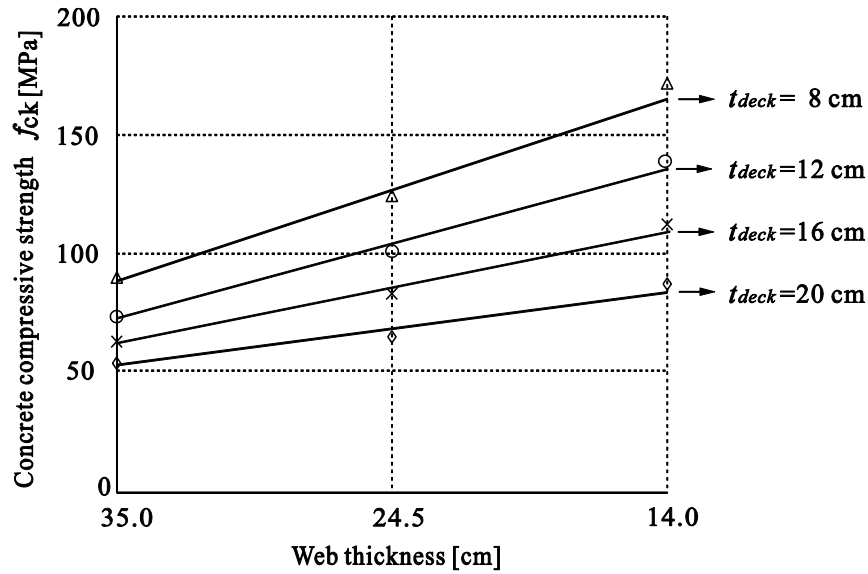


Figure 4.20: Max. concrete compressive stresses versus web thickness for different deck slab thicknesses for UHPC in PSB

From this parameter study, the relationship between deck/web thickness and the required compressive strength of UHPC is shown in Figure 4.20, compared to the load carrying capacity of the SES test span. When considering the compressive strength ( $f_{ck} \geq 160$  MPa) of UHPC, the UHPC-PSB model with a very thin section, such as a web thickness of 14 cm and a top slab thickness of 8 cm in the Figure 4.20, can reduce about 60 % of the self-weight under the same prestressing force. The sections with thinner members may not be used in UHPC-PSB construction.

### 4.3.3 Prestressing force

At SLS, the tendons strain variation between two deviators (at mid-span) are obtained from the displacement of the deviators by assuming that the beam has no joint opening and remains linearly elastic. In a segmental bridge with external tendons and dry joints, however, the stresses of concrete and tendons as well as the deflection increase insignificantly after joint opening. In general, the behaviour of tendons is characterized by a linear and nonlinear portion such as shown in Figure 4.12. External tendons in PSB are only tensile members. In particular, the variations of a tendon strain at the critical section, as well as the increase of concrete stresses in the compressive zone, are very important.

Based on section 4.3.2, the thin cross-section (top slab of 8 cm and web of 14 cm) was used in the parameter study of this section. In comparison with the quantity of external tendons in the SES test span, three tendon quantities (100 %, 82 % and 64 %) were evaluated with the thin cross-section.

Figure 4.21 presents the load-deflection relationships between the test result of the SES and three UHPC-PSB models with different tendon quantities. The deflection of the UHPC model with  $A_p = 100$  % is relatively small due to the excessive prestressing force. Therefore, it generates a

large camber and is ineffective. On the other hand, the UHPC model with  $A_p = 82\%$  shows smaller deflections than that in the SES test through all the load levels. The joint opening in this model starts similar to that of the SES test span. Also the UHPC model with  $A_p = 64\%$  shows very similar behaviour to the SES full-scale test. Although the joint opening starts earlier than the SES test result, this model deflected less than that in the SES test. After SLS the joint also opened. The reduction of dead load can lead to savings of tendon quantity. However, the maximum compressive stress of the model with  $A_p = 64\%$  was 176 MPa. With a relatively low tendon quantity, the concrete compressive stresses in the critical section must be checked.

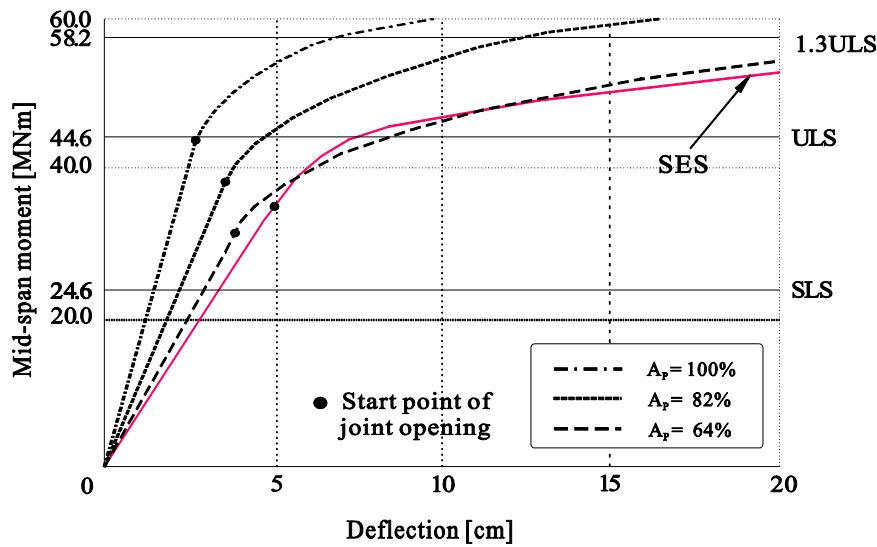


Figure 4.21: Load- deflections relationship due to different quantities of tendon (with 8 cm top slab and 14 cm web)

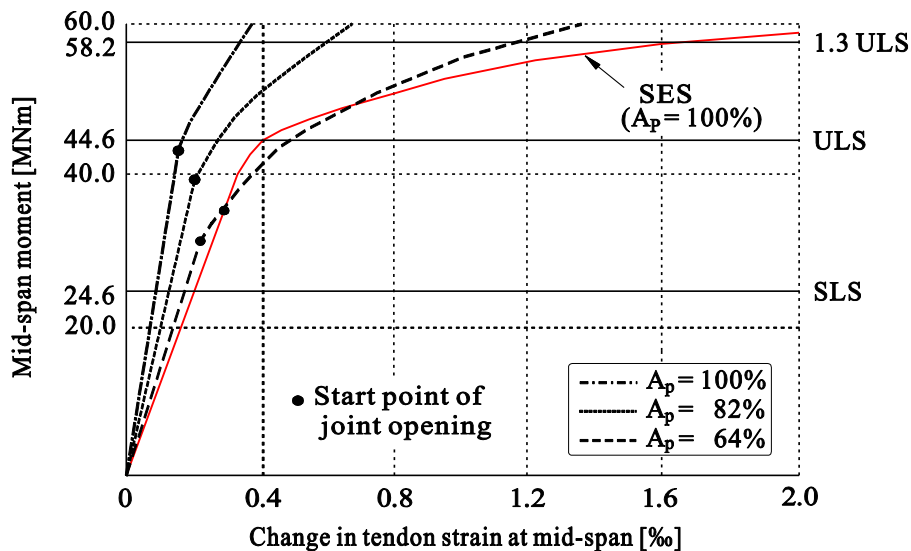


Figure 4.22: Change in draped tendon strain at mid-span due to different tendon quantities (with 8 cm top slab and 14 cm web)

As mentioned before, the maximum strain of external tendons occurs between deviators at mid-span. So Figure 4.22 shows the strain changes of external tendons for three UHPC models. After

joint opening the increase of tendon strain in all models were nonlinear. However, the changes show a slow grade compared to the SES. Until 1.3 ULS, which is the failure load of the SES test span, the strains of all models are smaller than in the full-scale test.

#### 4.3.4 Span-to-depth ratio

Span-to-depth ratio ( $\lambda$ ) is a very significant parameter for bridge design. Based on experience values of the past constructions, in general, the ratios are determined by optimization within an iterative process between span length and girder depth to evaluate cost-efficiency, aesthetics and load-bearing capacity of the structure. Particularly, the girder bridges are directly affected by  $\lambda$ , because a superstructure with high  $l/h$  ratio is a lighter structure and has a smaller moment of inertia, which reduces concrete consumption and increases the amount or size of prestressing tendons.

The maximum span length for span-by-span construction in precast segmental bridges is commonly limited by 50 m due to the increasing cost for the girder. One of the major advantages of a higher performance concrete girder bridge in relation to normal-class concrete is a decrease in dead load due to small sized cross-section. It also means that HPC structures enable material-saving and longer spans. Thus, the optimum span-to-depth ratio ( $l/h$ ) and the cross-section dimensions are significant parameters for a superstructure design. The AASHTO-PCI-ASBI recommends ratios from 12.7 to 25.4 with various segment depths (1.8 m, 2.1 m and 2.4 m) for span-by-span construction [AASHTO 2002]. These ratios are lower than the one of cast-in-place box girder bridges because external tendons have lower eccentricity ( $z_p$ ) compared to internal tendons of cast-in-place construction. In spite of thinner sections and higher span-to-depth ratios, however, higher performance concrete structures greatly enhanced by their excellent properties are able to resist the same loads.

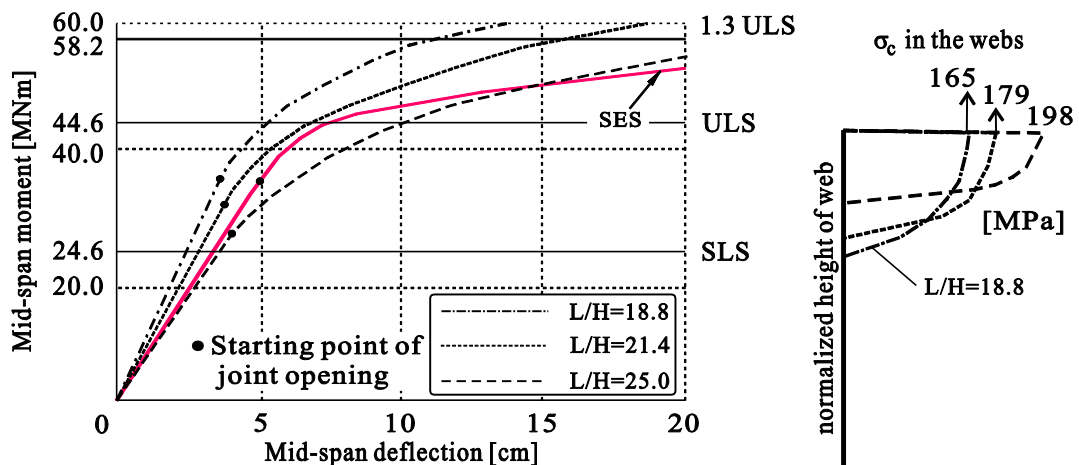


Figure 4.23: Deflections and compressive stress distributions in the web at the 1.3 ULS due to different span to depth ratios (thickness of top-slab of 8 cm,  $b_w = 14$  cm and 71 % of prestressing force of SES)

In comparison with SES segmental bridge ( $l/h = 45$  m/2.4 m = 18.8), the three UHPC segmental box girder models, which have  $H = 1.8$  m ( $l/h = 25.0$ ), 2.1 m ( $l/h = 21.4$ ) and 2.4 m ( $l/h = 18.8$ )

girder height, respectively, were evaluated with thin cross-section (thickness of top-slab: 8 cm; web: 14 cm) and 71 % of prestressing forces of SES. Figure 4.23 presents the load-deflection relationship due to different span-to-depth ratio. The models with the span-to-depth ratio of 21.4 and 18.8 show sufficient load carrying capacities until 1.3 ULS. On the other hand, the joint opening of the model with  $l/h = 25.0$  started immediately at SLS because of the fast loss of tendon's eccentricity due to the low height of the girder.

### 4.3.5 Comparison of various concrete classes

This section presents a comparative study on the structural behaviour of externally prestressed monolithic box girders made of conventional concrete, high performance concrete (HPC) and ultra high performance concrete (UHPC) under the serviceability limit state, where the structure behaves elastic. Thus, the following study aims to verify the relative benefits of concrete girders with higher performance concrete as an evaluation of the structural efficiency.

#### Materials

For precast segmental bridge construction, in general, high strength concrete of more than C40/50 is used as high compressive stresses occur due to full-prestressing, the tendons can be stressed earlier due to higher early-age strength of concrete and thus construction speed is increased.

In the Eurocode 2, concrete strength of more than C100/115 is not mentioned. So, the properties of various concrete classes offered by SOFiSTiK 2010 are used in this analysis as shown in Table. 4.3.

Table 4.3: Concrete properties used in the numerical analysis

Concrete class	Compressive Strength $f_{ck}$ [MPa]	Tensile Strength $f_{ctm}$ [MPa]	Modulus of Elasticity $E_c$ [MPa]
C55/67	55	4.21	35,653
C80/95	80	4.48	42,256
C120/145	120	5.56	47,877
C180/217	180	18.0	54,422



## Modeling

The cross-sections and the dimensions of a simply supported box girders, which are modeled by beam elements, are shown in Figure 4.15. In particular, the cross-section of test model C55/67, which has the typical value of slenderness ratio ( $l/h = 18.8$ ) for precast span-by-span construction with constant-depth, is identical to the standard segment (D2-Type) in the SES bridge project.

Also, the cross-sections of bridge models with higher concrete strength have smaller thicknesses of the box girder webs, bottom and top slabs. Concrete grades C55/67, C80/95, C120/145 and C180/217 are used. The FE-models C180/217-H18 and C180/217-H24 have a height of 1.8 m and 2.4 m respectively.

The model C180/217-H18 has the smallest cross-section, moment of inertia and tendon eccentricity due to the largest span-to-depth ratio of 25.0. On the other hand, the model C180/217-H24 has very thin web and slab thicknesses like C180/217-H18 but has the highest tendon eccentricity because of the cross-section height of 2.4 m.

Table 4.4: Dimensions and section properties used in the numerical analysis

		C55/67	C80/95	C120/145	C180/217-H18	C180/217-H24
<b>Height</b>	$H$ [m]	2.4	2.2	2.0	1.8	2.4
<b>Web thickness</b>	$b_w$ [cm]	35	28	22	15	15
<b>Slab thickness</b> [cm]	$t_1$	20.0	18.0	16.0	12.0	12.0
	$t_2$	40.0	36.0	32.0	24.0	24.0
<b>Area</b>	$A_c$ [m <sup>2</sup> ]	4.89	4.18	3.58	3.06	3.32
<b>Area decrease</b>	$\Delta A$ [%]	-	14.5	26.8	37.4	32.1
<b>Moment of inertia</b>	$I_y$ [m <sup>4</sup> ]	3.582	2.668	1.900	1.328	2.661
<b>Distance from top to centroid axis</b>	$z_s$ [m]	0.781	0.707	0.612	0.524	0.724
<b>Tendon eccentricity</b>	$z_p$ [m]	1.57	1.46	1.33	1.24	1.65
<b>Span to depth ratio</b>	$L/H$	18.8	20.5	22.5	25.0	18.8
<b>No. of tendons</b>		12	12	12	12	10

External tendons inside a box girder of a segmental bridge were arranged by straight and draped types as shown in Figure 4.4 The models have 12 tendons whereby each tendon consists of 19 strands with 15.7 mm diameter ( $A_p = 342 \text{ cm}^2$ ). Model C180/217-H24 has 10 tendons only because its self-weight decreasing ratio is 32% less compared with the model C55/65 as a prototype.

Generally, “full” prestressing is required for a segmental bridge because tensile stresses in concrete and opening of joints respectively are not allowed under service loads. Therefore, the same posttensioning quantity as in a segmental bridge was used.

## Results

The FE analysis focused on the comparison of the structural behaviour and the efficiency between conventional and higher strength concrete girders. Generally, the compressive strength of concrete produced in precast industry has higher grade than C60/75 [Toutlemonde 2007]. The model with concrete C55/67 should represent a standard precast segmental box girder as a basis of comparison for the other models.

The maximum moments and deflections at midspan due to same prestressing force (amount of tendons, see Table 4.4) are shown in Table 4.5. The FEM results indicate that a reduction of self-weight can lead to smaller total bending moments and shear forces in the girder. Especially, in the long span bridges, the reduction of dead load is very important because the load bearing capacity rely heavily on the dead load.

Table 4.5: Bending moments and concrete stresses for different PSB models

	Max. $M_{gk}$ [MNm]	Max. $M_{(g+q)k}$ [MNm]	Max. $M_{pk}$ [MNm]	Max. $V_{(g+q+p)k}$ [MN]	Tendon quantity $A_p$ [cm <sup>2</sup> ]	Max. concrete compr. stress [MPa]	Allowable concrete stress * $0.45f_{ck}$ [MPa]
<b>C55/67</b>	37.49	57.64	- 55.3	2.14	342	- 16.6	- 24.7
<b>C80/95</b>	33.01	53.16	- 49.8	1.98	342	- 19.4	- 36.0
<b>C120/145</b>	29.18	49.32	- 46.47	1.84	342	- 24.3	- 54.0
<b>c180/217-H18</b>	25.92	46.06	- 42.59	1.73	342	- 29.6	- 81.0
<b>C180/217-H24</b>	27.58	47.73	- 49.26	1.78	285	- 24.0	- 81.0

\* The allowable concrete compressive stress at SLS according to EC2-1

Due to the higher strength of concrete, the models from C55/67 to C180/217-H18 with the same tendon quantity  $A_p = 342 \text{ cm}^2$  show a gradual reduction of cross-section area, cross-section height and thus an increase of span to depth ratio. (see Table 4.4). Model C55/67 and C180/217-H24 with the same cross-section height show a reduction of tendon quantity. This means that with higher strength concrete one can realize bridges with longer spans than with conventional concrete.

Table 4.6: Deflections at mid-span for different loads

Deflection to be considered	C55/67	C80/95	C120/145	C180/217-H18	C180/217-H24
Due to the dead load +prestressing (G+P) [mm]	- 40.3	- 42.3	- 52.9	- 62.3	- 40.8
Due to the dead load +prestressing + live load (G+P+q+Q) [mm]	17.6	19.6	19.9	20.2	13.8

downward deflection : (+) sign, upward deflection : (-) sign

Table 4.7: Concrete stress distributions at mid-span [MPa]

	$\sigma_g$	$\sigma_{g+q}$	$\sigma_p$	$\sigma_{g+q+p}$	$\sigma_{g+p}$
<b>C55/67</b> H = 2.4 m 0,45 $f_{ck}$ = 24.7 MPa					
<b>C80/95</b> H = 2.2 m 0,45 $f_{ck}$ = 36.0 MPa					
<b>C120/145</b> H = 2.0 m 0,45 $f_{ck}$ = 54.0 MPa					
<b>C180/217-H18</b> H = 1.8 m 0,45 $f_{ck}$ = 81.0 MPa					
<b>C180/217-H24</b> H = 2.4 m 0,45 $f_{ck}$ = 81.0 MPa					

The maximum concrete compressive stresses at the bottom side of mid-span appears when the girder deflects upward due to the prestressing force without live load. These stresses have not exceeded the permissible concrete compressive stresses ( $0.45f_{ck}$ ) at SLS. The same is true for the structure loaded with  $g+p+q$ .

Table 4.6 presents the concrete stress distributions at mid-span of the girders for different phases under serviceability limit state. In spite of the smaller cross-section area, the models with lower height show larger stresses for the all loading conditions due to smaller moment of inertia ( $I_y$ ).

Also, the mid-span deflections increase with the reduction of girder height. The model C180/217-H18 with the smallest cross-section height ( $H = 1.8$  m) presents several problems like the largest deflections at mid-span as well as a significant increase of the concrete stresses. The model C180/217-H24, on the other hand, shows the efficient results like the smallest deflection, the minimum prestressing tendon area and a decrease of dead load.

## **4.4 Numerical analysis of UHPC-PSB in longitudinal direction**

### **4.4.1 Proposed model for numerical analysis**

#### **4.4.1.1 Numerical model**

##### **Proposed cross-section**

As a reasonable cross-section for UHPC segmental bridges, thin-walled multi-cell box girders can be considered. There are generally two types for such structures. The first one has independent cells which are only connected by their deck slabs. The other one consists of cells which are connected both at the deck and bottom slabs. In the structural point of view, the second type is usually recommended to adopt. In general, the flanges (deck slab) of the first type are heavily stressed in the transverse direction compared to the second type section.

Multi-cell box girders have various advantages, e.g. high torsion resistance, as a box girder. Also, bridges with higher span-depth-ratio than with a single cell box girder can be built. Next, the span lengths of cantilever and interior slab between webs are shorter. Considering a thin cross-section for the UHPC material, therefore, the multi-cell box girder types seem to be the best choice.

When the depth of girder is smaller than  $1/6$  of the width of the bridge deck, multi-cell box sections are usually recommended. In the case of single cell box segmental girders, the span-to-depth ratios are generally adopted between 18 and 20. On the other hand, precast multi-cell box girders may have a ratio in the range of 25 to 30. However, the cross-sections with four and more cells are not efficient because of the abilities of the load distribution in transverse direction and the torsion rigidity, such as I- or T-girders, decrease significantly. So, the number of cells should be minimized

Based on the before mentioned investigations, a two-cell box cross-section with stiffeners for an UHPC segmental bridge as shown in Figure 4.24 is proposed. The stiffeners should avoid the need of transverse prestressing. A segment length of 2.40 m is used like in the SES project. For numerical analysis, this cross-section will be used in the following study.

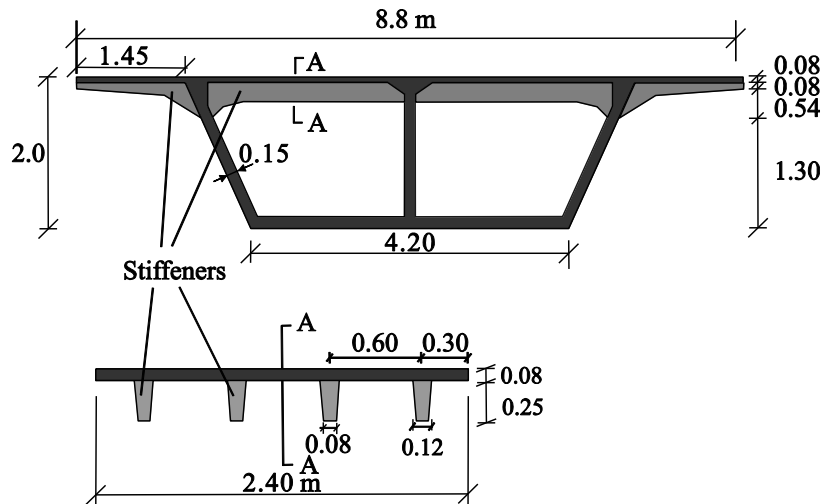


Figure 4.24: Proposed two-cell box girder cross-section for UHPC-PSB

### Section properties

The cross-sectional properties of the proposed model are listed in Table 4.7. The FE-analysis were based on the properties of the concrete cross-section.

Table 4.7: Cross-sectional properties of UHPC girder

Cross-section area of the girder ( $A_c$ )	$2.22 \text{ m}^2$
Distance from the concrete centroid to the top surface ( $C_1$ )	$0.92 \text{ m}$
Distance from the concrete centroid to the bottom surface ( $C_2$ )	$1.08 \text{ m}$
Moment of inertia about y-y axis ( $I_y$ )	$1.45 \text{ m}^4$
Self-weight per unit length of the girder ( $g_k$ )	$55.4 \text{ kN/m}$

### FE model

For the finite element analysis, the software “SOFiSTiK” is used to investigate the behaviour of UHPC segmental bridges. The multi-cell box girder is modeled by thin shell elements, which have various thicknesses for top-slabs, webs, bottom-slabs and stiffeners. The superstructure consists of 17 standard segments with a uniform length of 2.4 m and 2 pier segments with a length of 1.8 m. This gives a span length of 44.4 m. The dry-joints between adjacent segments are modeled by “contact” elements, which consist of two nonlinear spring elements. Fig. 4.25 shows the finite element model.

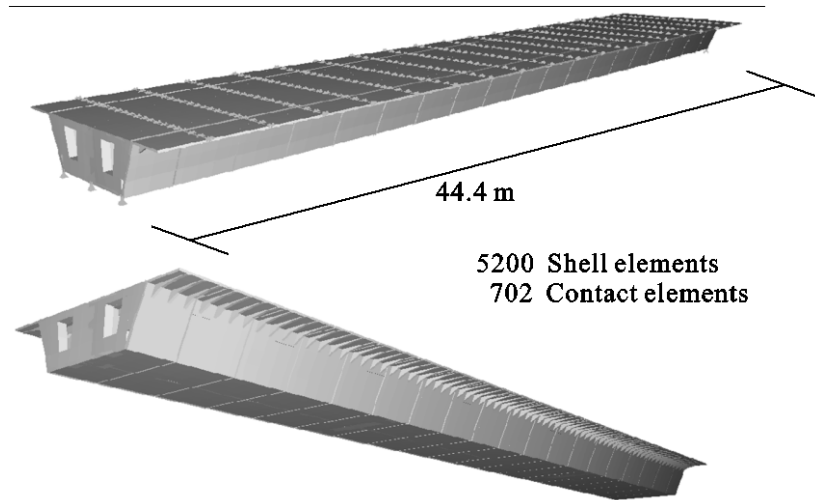


Figure 4.25: Finite element model used in the analysis

#### 4.4.1.2 Loads and prestressing

##### Load arrangement

In SLS the quasi-permanent load combination is used for long term, whereas the rare load combination is used for short term. In this study, only load combination for the short term in SLS was used with a live load factor of  $\gamma_q = 1.0$  for the comparison of deflections as well as stresses.

For the short term loading, the load combination on the girder models was used as follows.

$$\text{rare combination : } \Sigma G_k + P_k + \alpha_{Qi} \cdot Q_{ik} + \alpha_{qi} \cdot q_{ik}$$

Table 4.8: Values of live loads for the load model 1 according to [DIN-FB 101]

Position	Double axle			Uniform distributed load $\alpha_{qi} \cdot q_{ik}$ [KN/m <sup>2</sup> ]
	$Q_{ik}$ [KN]	$\alpha_{Qi}$	$\alpha_{Qi} \cdot Q_{ik}$ [KN]	
Lane 1	300	0.8	240	9.0
Lane 2	200	0.8	160	2.5
Lane 3	0	-	0	2.5
Another lane	0	-	0	2.5
Remaining area	0	-	0	2.5

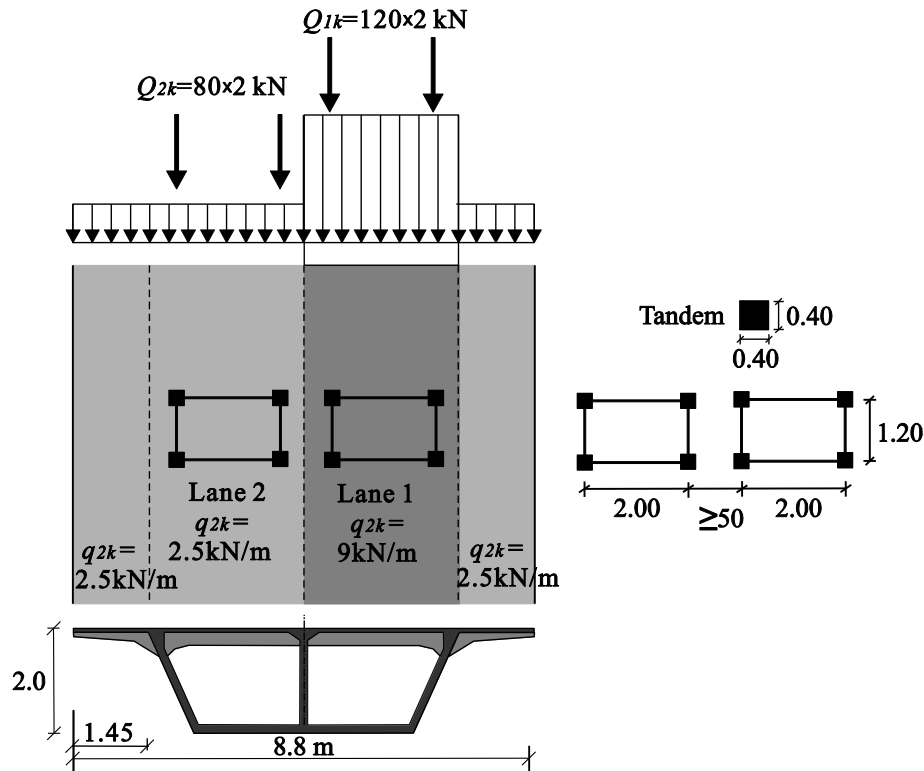


Figure 4.26: The live load arrangement according to [DIN-FB 101]

For the dead loads ( $G_k$ ), concrete unit weight of  $25 \text{ kN/m}^3$  and superimposed loads of  $g_{k,2} = 19 \text{ kN/m}$  were applied. The weights of the anchor blocks, tendons and deviator were ignored. Live loads were taken from German Report ‘DIN-Fachbericht 101’ as shown in Figure 4.26 and Table 4.8. The behavior of the bridge due to bending is in the focus of the following investigations. Thus the live load arrangement in transverse direction is not relevant.

### Prestressing

The external tendons inside the box girder were arranged by straight and draped types as shown in Figure 4.27. 12 total tendons, each consisting of 19 strands with 15.7 mm diameter ( $A_p = 342 \text{ cm}^2$ ) are used.

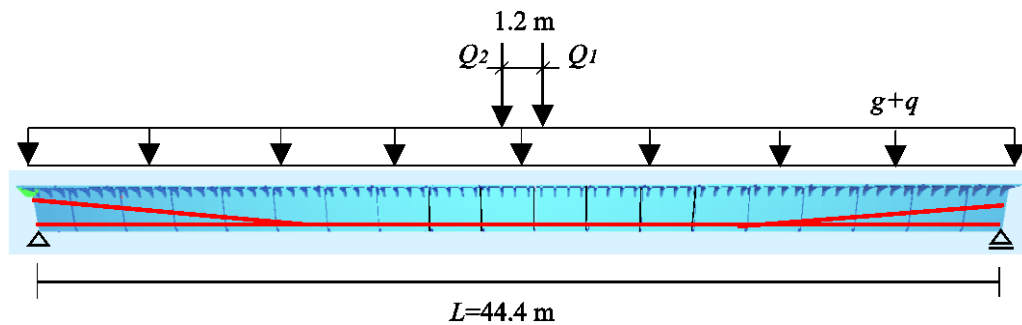


Figure 4.27: The load arrangement and tendon layout

#### 4.4.1.3 Loading step

According to the German Recommendation for precast segmental bridges with external prestressing [DBV 99], the general load combination in the service limit states (SLS) is

$$G_k + \Delta G_k + Q_k + P$$

whereas the general load combination in the ultimate limit states (ULS) is

$$1.5G_k + 1.75\Delta G_k + 1.75Q_k + 1.0P$$

The same global safety concept is used for the numerical analysis. The load on the structure is increased incrementally by a load factor “ $\phi$ ”.

$$\phi(G_k + \Delta G_k + Q_k) + 1.0P$$

The load factor varies from 0 to 2.0. For  $\phi = 0$  the prestressing forces are applied only.  $\phi = 1$  is a state of serviceability limit.

#### 4.4.2 Single span girder

In a simply supported segmental bridge with external tendons and dry joints, there are two important considerations. First, one has to analyze the longitudinal stress distribution across flanges. It is known from the full-scale tests of box girders with external prestressing that the failure occurs in the web-top slab-joint due to concrete crushing. Thus, investigation of the compressive stresses in this area is important as it is relevant for the load bearing capacity of such structures. Another important aspect is the transmission of shear forces not only at the pier but at mid-span. In spite of the relatively small shear force at mid-span, the load bearing part of the cross-section is limited to the compressive zone. The shear stresses at mid-span as well as at the piers must be checked.

##### 4.4.2.1 Deflection and joint opening

Figure 4.28 shows the longitudinal stress distributions in the web and in the deck slab of the single span due to two loading steps: (a) serviceability limit state ( $\phi = 1$ ) and (b) before the failure ( $\phi = 1.83$ ). Maximum compressive stresses of 176 MPa and strains of 0.0033 had been calculated at ULS (see Figure 4.28). High tensile stresses were estimated on both sides at the anchorages of tendons. These stresses are not relevant as this study was focused on the behaviour and longitudinal stresses at mid-span.

The deflection-curve of the UHPC-PSB single span model has a linear range until  $\phi = 1.125$ , and then progresses in a non-linear shape as shown in Figure 4.29. Just after loading step 1 (SLS), the joint at mid-span starts to open. The neutral axis at the central segment (No. 10) ascended to the compressed zone of the deck slab. The joints 9-10 and 10-11 have the same deflections throughout the whole loading step because the girder and the loading is symmetrical. Before the failure state, a maximum deflection at mid-span of 240 mm was estimated.



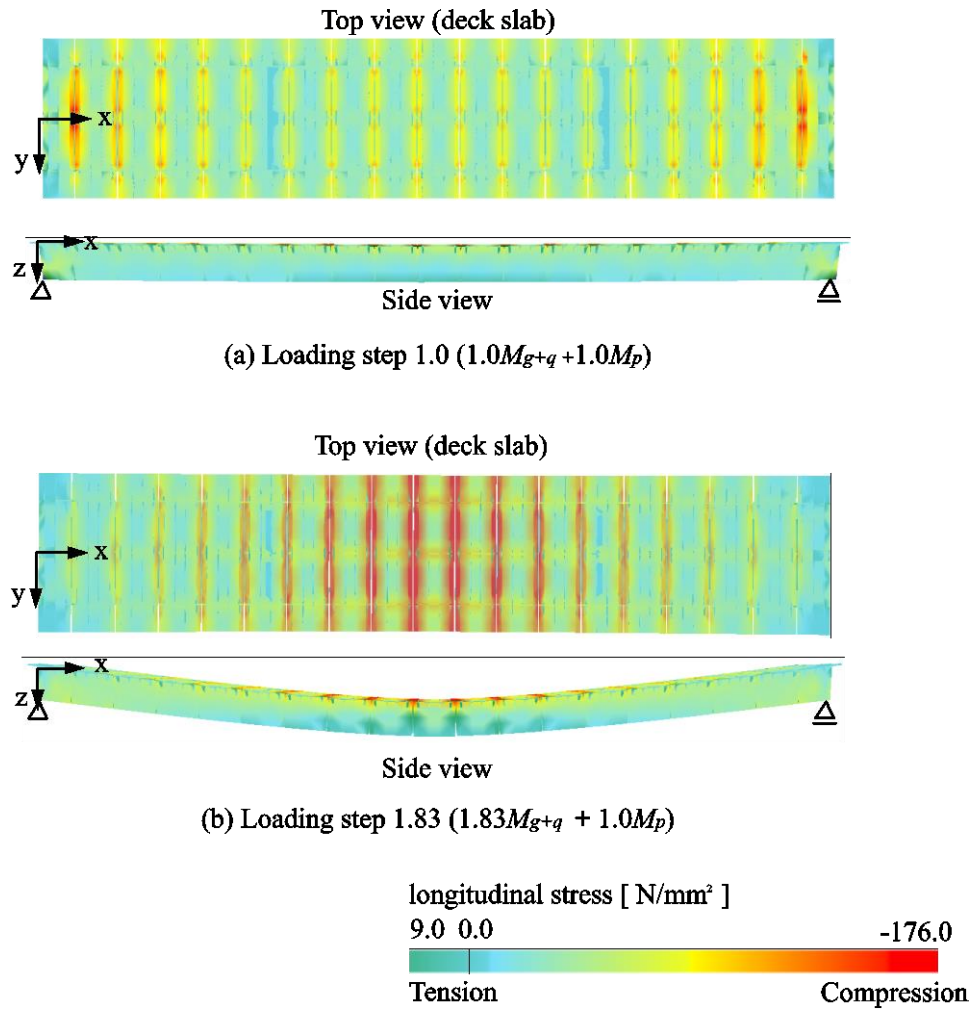


Figure 4.28: Longitudinal stress distribution ( $\sigma_x$ ) in the single span girder under loading steps (a) 1.0 (SLS) and (b) 1.83 (before the failure)

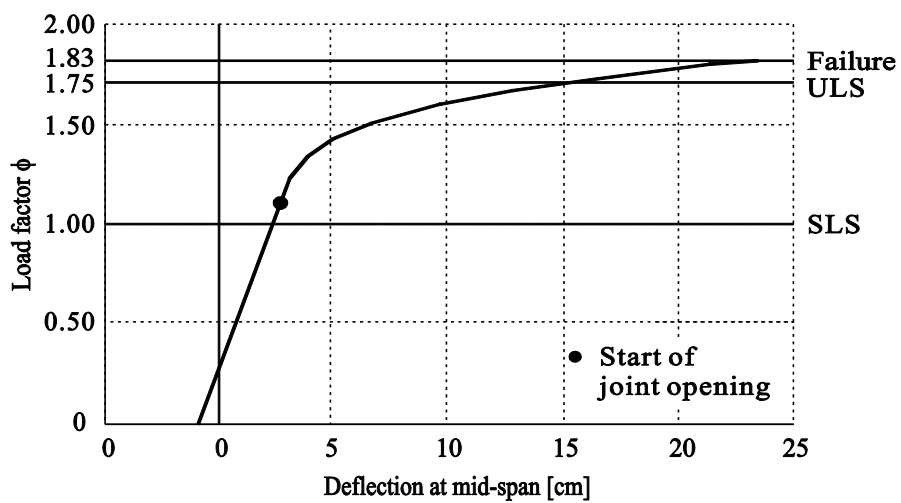


Figure 4.29: Deflection at mid-span due to increasing load

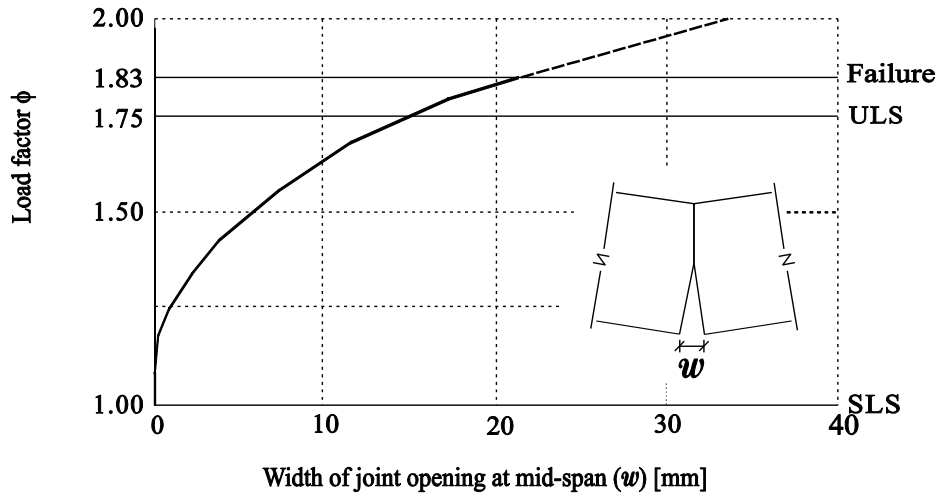


Figure 4.30: Width of joint opening due to increasing load

The joint opening can be taken from the extension of the contact elements (normal springs). When the compressive stresses due to prestressing are changed into the tensile stresses due to the live loads, the joint at mid-span starts to open. Figure 4.30 shows the increase of joint opening at mid-span due to increasing loads. As mentioned above, joint 9-10 and 10-11 have also the same width of the joint opening. For simply supported girders, the maximum joint opening corresponds to the location of the greatest deflection (in case of equal number of segments). Before the failure, the maximum joint opening was 21.7 mm.

After the initial frictional resistance of the concrete contact surfaces at the joints, slippage is expected. However, this results in very small displacements. The full scale test carried out by Takebayashi et al. [1994], reports a maximum value of joint slippage of about 0.03 mm only. Thus, in the numerical model the joint slippage was ignored.

#### 4.4.2.2 Longitudinal stress distributions

The development of the openings at each joint and the compressive stresses distribution of the section at mid-span and pier are shown in Figure 4.31. It can be seen that the maximum joint opening concentrates at joint 9-10 and 10-11 because the arrangement of the loading and external tendons layout are symmetrical about the center of the girder. The wheel loads for the truck were concentrated on the segment No.10 (at mid-span). The maximum joint opening corresponds to the location where the maximum deflection is observed (joint 9-10 and 10-11). In general, all joint openings take place between the two deviators.

For the compressive stress distribution at the pier (joint 1-2), there are certain patterns that almost never change. On the other hand, the compressive stress distributions at mid-span with increased loads show that an ascent of the neutral axis results in a growth of width and depth in joint opening and decreasing compressive zone. The compressive stresses at the top slab above the webs are larger than that at the cantilever and at the mid-section of the top slab between webs (shear lag effect).

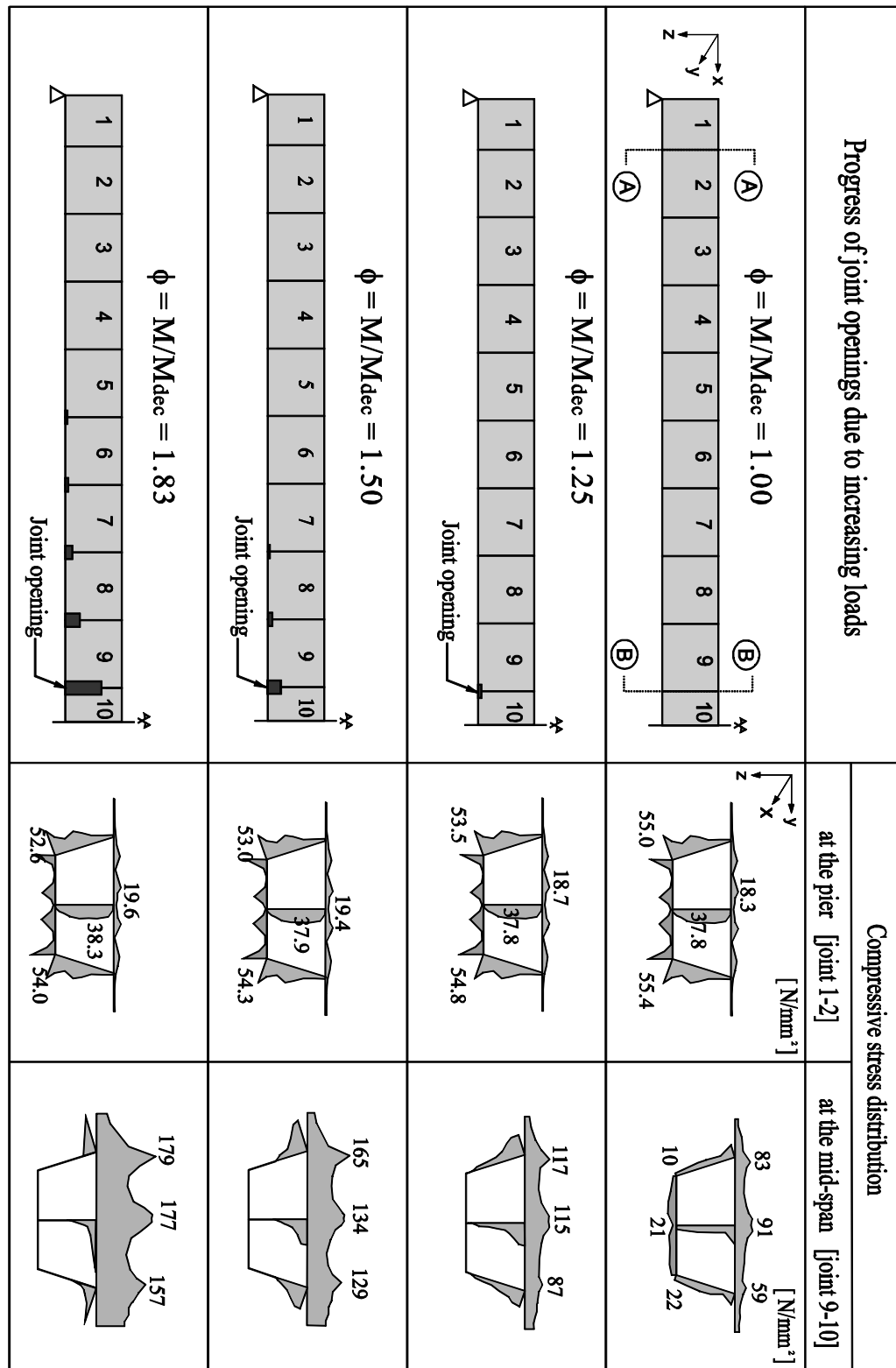
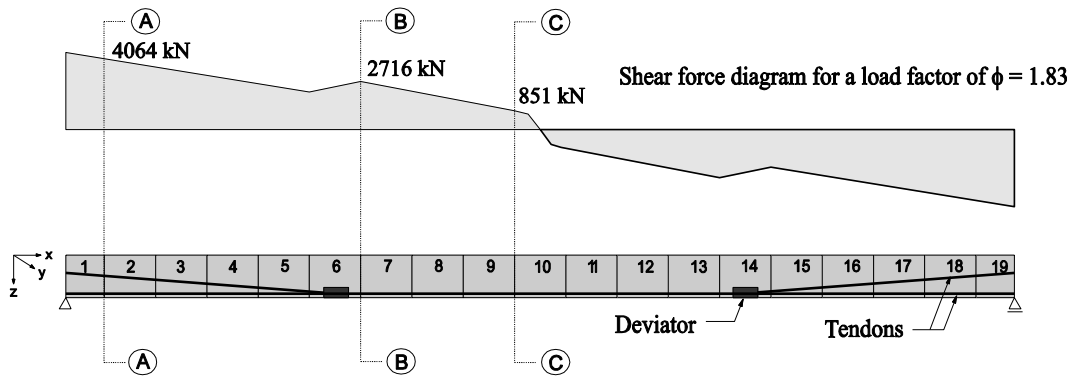


Figure 4.31: Compressive stress distribution at mid-span and pier due to increasing loads

#### 4.4.2.3 Shear stress and rotation

Figure 4.32 shows the shear stress distributions at the different sections (pier, deviator mid-span). The upward force of tendon due to change of inclination at the deviators increases the shear force. In spite of the small shear forces at mid-span, the deep opening of joint may decrease the capacity of shear transfer. As shown Fig. 4.32, the shear stresses at mid-span, such as at the pier, are higher because of the smaller contact surface.

Figure 4.33 shows the change of the angle of rotation at mid-span for two loading steps. As with the deflection at mid-span, the rotation is also influenced by a joint-opening. After decompression at the loading step  $\phi = 1.125$ , the angle of rotation at mid-span increases rapidly. As compared with a torsion moment of a general monolithic box girder, however, these values present similar pattern, if the shear keys are not be considered in the analysis.



M/M <sub>dec</sub>	Shear stress distributions [N/mm <sup>2</sup> ]		
	at the pier (joint 1-2)	at the deviator (joint 6-7)	at the mid-span (joint 9-10)
1.0			
1.83			

Figure 4.32: Shear stress distributions for two loading steps

An unsymmetrical distribution of live loads in the transverse direction tends to warp the box girders and causes shear stresses. The rotation is determined by means of the vertical displacements of the four edges.

For a rotation angle of top slab:  $\theta_{t1} = \tan^{-1} \left( \frac{|w_{t1}|}{0.5B_t} \right)$  or  $\theta_{t2} = \tan^{-1} \left( \frac{|w_{t2}|}{0.5B_t} \right)$

And for a rotation angle of bottom slab:  $\theta_{b1} = \tan^{-1} \left( \frac{|w_{b1}|}{0.5B_b} \right)$  or  $\theta_{b2} = \tan^{-1} \left( \frac{|w_{b2}|}{0.5B_b} \right)$

Where :  $\theta_{t1}, \theta_{t2}, \theta_{b1}, \theta_{b2}$  angle of rotation of the four edges from the centre in the top slab and bottom slab  
 $w_{t1}, w_{t2}, w_{b1}, w_{b2}$  vertical displacements at the edges in the top slab and bottom slab  
 $B_t, B_b$  width of the top slab and the bottom slab

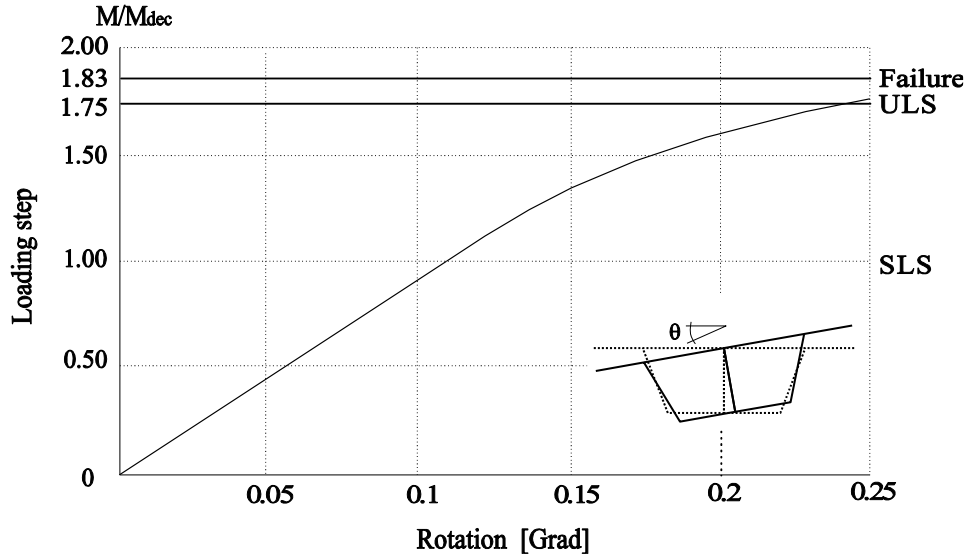


Figure 4.33: Rotation due to loading steps

#### 4.4.2.4 Normal force variation in webs

Figures 4.34 – 4.36 show the changes of horizontal forces ( $F_x$ ) on the joint surface at mid-span. The nodal forces of adjacent elements are shown at the three different locations (nodes) of the web. The nodes T1, T2 and T3 (see Figure 4.34), where the top slab and the webs are jointed, show a linear increase of horizontal forces and then a rapid increase after loading step  $\phi = 1.25$ . Especially, the force at point T2 on the inner web is always bigger than the value of the outside webs. Torsion moments caused by asymmetric loads give different forces at the nodes (T1, T3, W1, W3 and B1, B3) of the outside webs.

The compressive forces (T1, T2 and T3) in the top slab increase with ascending loading. It has linear range until loading step  $\phi = 1.25$ . With the onset of the decompression or joint opening (no further reduction in compressive stress at the bottom of box section), the curves (Figure 4.34) start a rapid rise from linearity.

The nodes W1, W2 and W3 located at half the height of the section show a constant compressive force until the neutral axis starts to ascend (loading step  $\phi = 1.25$  for W3 and loading step  $\phi = 1.5$  for W1, W2). After loading step  $\phi = 1.6$ , the neutral axis passed the nodes W1 to W3 and thus the stresses are reduced to zero (see Figure 4.35).

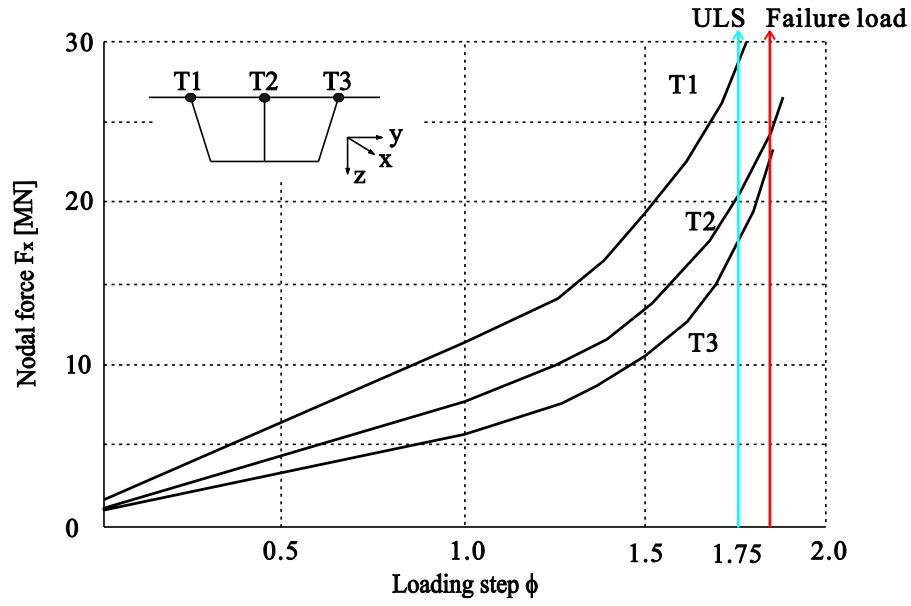


Figure 4.34: Forces in the top-slab at mid-span due to increasing loads

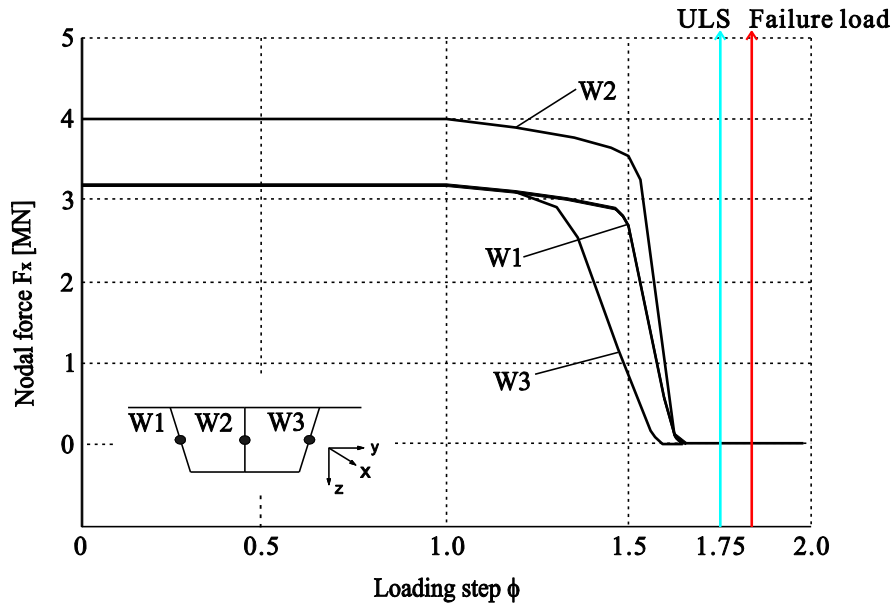


Figure 4.35: Forces in the webs (0.5H) at mid-span due to increasing loads

From the post-tensioning (without live loads) to the loading step  $\phi = 1.125$  with additional loads, the forces (B1, B2 and B3) to the bottom slab show a linear decrease corresponding to a reduction in the initial compressive stresses (see Figure 4.36).

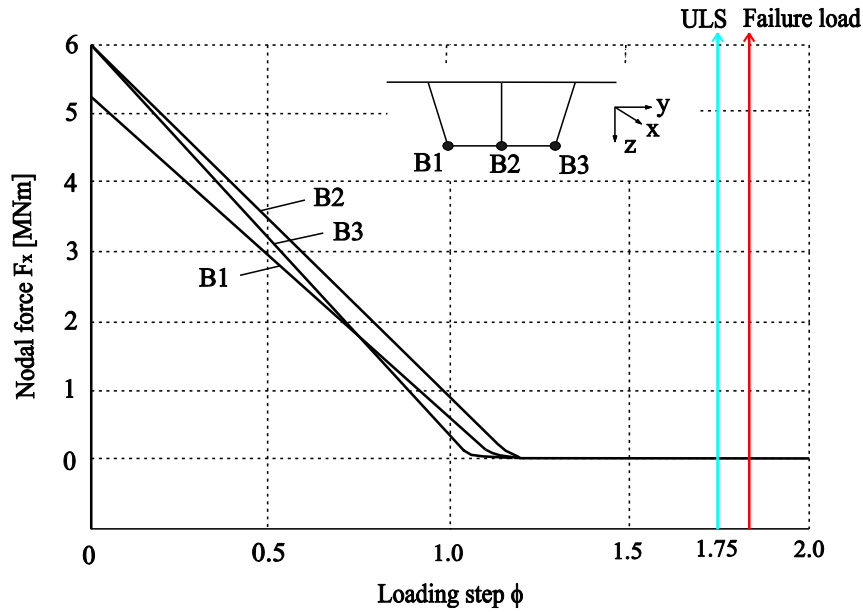


Figure 4.36: Forces in the bottom-slab at mid-span due to increasing loads

#### 4.4.2.5 Change of tendon stress

External tendons which have two different layouts, straight and draped, like in the real bridge were used in the FE model. The tendon stresses at four locations, two at mid-span between deviators and the other two between the deviator and the diaphragm, were observed as shown in Figure 4.37. The tendon stresses up to loading step 1.125 are uniformly increasing as the joints are closed. Then after loading step 1.25 a non-linear rapid increase can be observed.

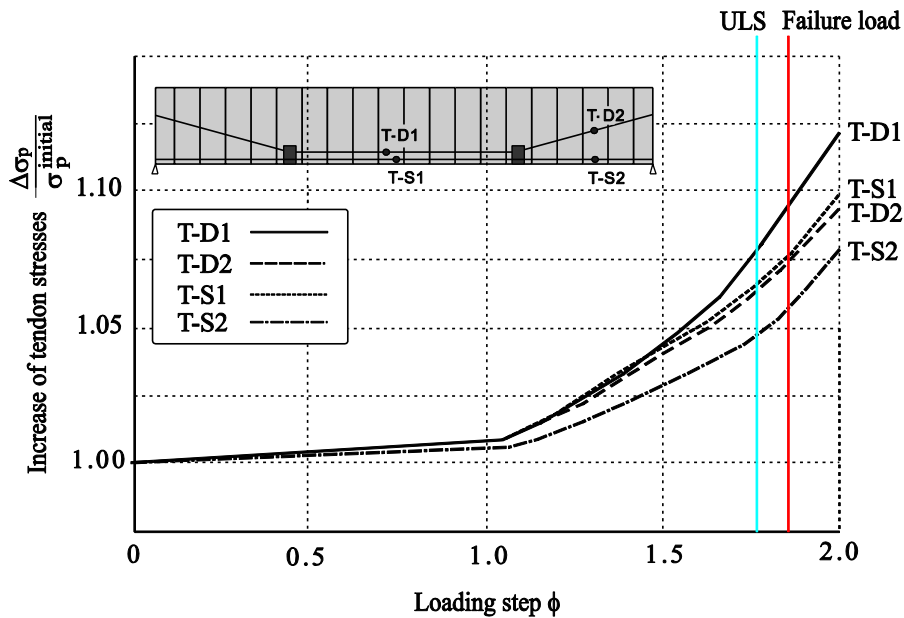


Figure 4.37: Increase of tendon stresses due to increasing loads

The behaviour of draped tendons is different from the straight ones. The mid-span sections of draped tendons display a larger strain than the section between the deviator and the diaphragm.

This different behavior results from the large frictional force arising from the big deviation angle in draped tendon. Experiments have shown, that the tendons are fixed for live load if the deviation angle is bigger than 6 degrees [Rombach 2000]. Straight or smaller deviated tendons have evenly distributed strains along the whole length of the tendon.

A friction coefficient  $\mu = 0.15$  for strands inside plastic tube running over the saddle at the deviators was assumed. However, the FE analysis does not consider temperature effects.

#### **4.4.3 Multi-span girder**

##### **4.4.3.1 Deflection and joint opening**

The study for simply supported girders was focused on the behaviour and longitudinal stresses at mid-span. Thus the same live load arrangement as for the simple supported FE-model was used. For a continuous girder the behaviour at the pier must be checked. In a continuous span, high compressive stresses in the bottom slab at the pier occur as well as in top slab at mid-span. In the following an end span is analyzed only, whereby a full restraint at the inner support is assumed. The tendon layout is adopted for the structure.

Figure 4.38 shows the longitudinal stress distributions in the web and in the deck slab of the single span due to two loading steps: (a) serviceability limit state and (b) before the failure (loading step  $\phi = 1.95$ ).

In particular, Figure 4.38 (b) illustrates the joint opening and high compressive stresses in the bottom slab before failure. At loading step  $\phi = 1.95$ , the UHPC segments have compressive stresses up to 178 MPa and maximum concrete strains of 0.0035. Once the maximum compressive stress reached the UHPC capacity, failure was assumed to have occurred in the same manner as the single span girder.

The load-deflection relationship of the end span model shows a linear range until loading step  $\phi = 1.20$ , and then progresses a non-linear behavior as shown in Figure 4.39. After the loading step 1 (SLS), the joint at the mid span and at the pier immediately starts to open. The neutral axis at the central segment (No. 10) ascended to the compressed zone of the deck slab. Joint 10-11 has the greatest deflection throughout the whole loading steps because the girder has a longitudinally asymmetrical system for the loading and prestressing. Before the failure, a maximum deflection of 183 mm was estimated.

When the compressive stresses due to prestressing changed into the tensile stresses due to increase of the live load, the joint at mid-span and at the pier start to open. Figure 4.40 shows the joint opening at mid-span and at the pier due to increased loading. As mentioned above, joint 9-10 and 10-11 do not have the same width of the joint opening due to the asymmetric structure. The first joint opening occurred at the pier between segments 1 and 2. The maximum joint opening corresponds to the location where the maximum deflection is observed. However, the joint opening (joint 1-2) pattern at the pier due to negative moment is similar to the pattern of joint opening at



mid-span (see Figure 4.40). Before the failure, the maximum joint opening was 16.3 mm at mid-span and 12.6 mm at the pier, respectively.

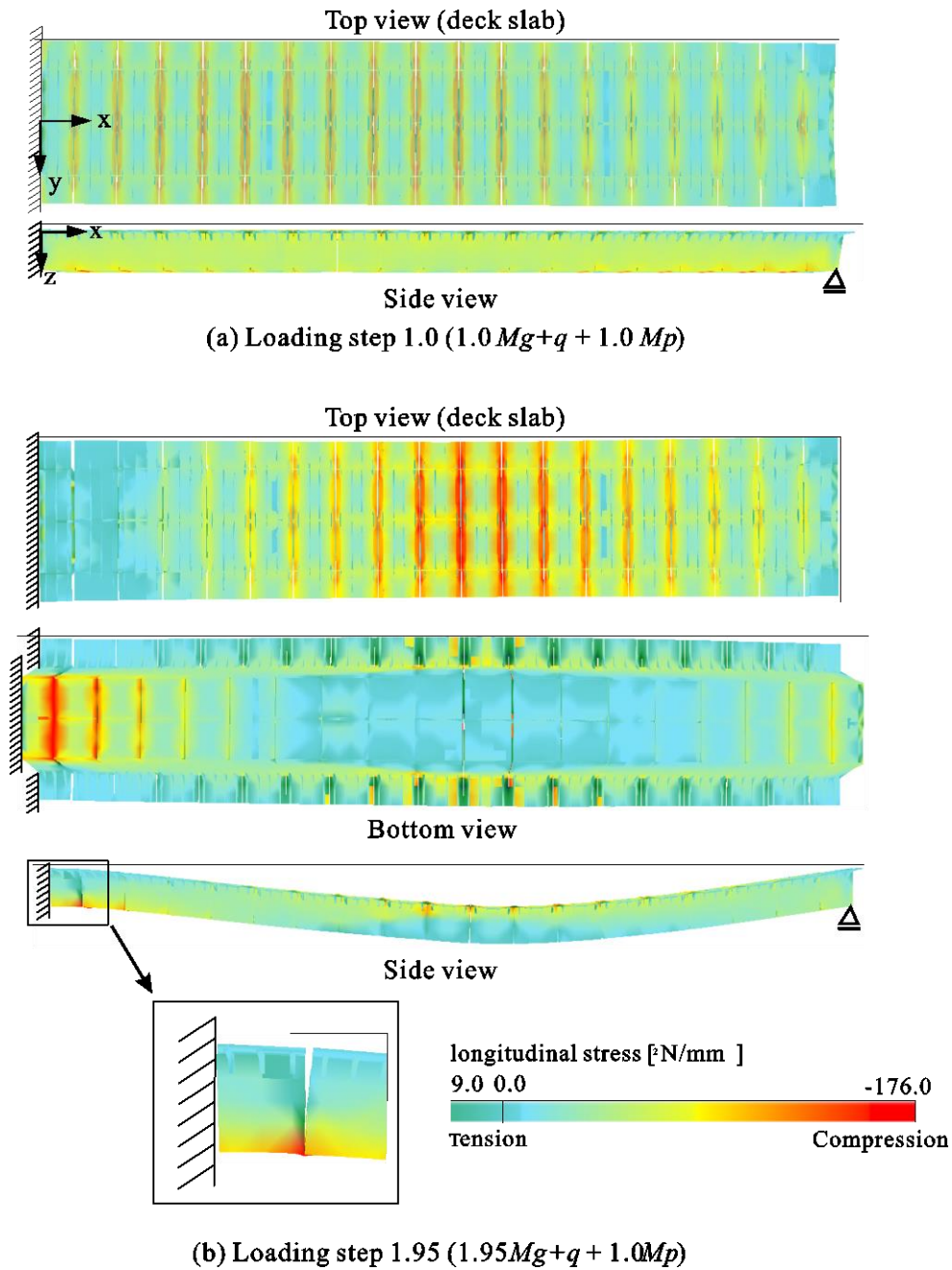


Figure 4.38: Longitudinal stress distributions ( $\sigma_x$ ) in the single span girder under increasing loads (a) 1.0 (SLS) and (b) 1.95 (before the failure)

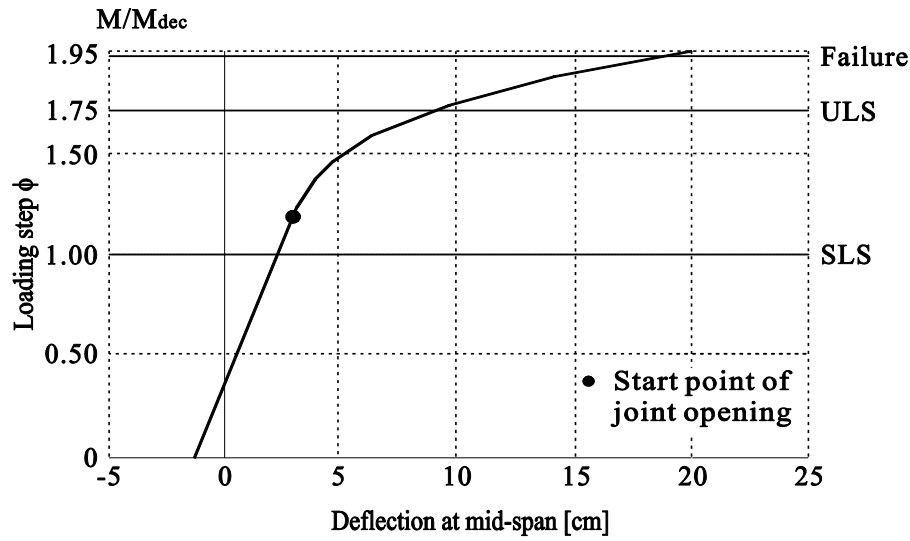


Figure 4.39: Deflection at mid-span due to increasing loads

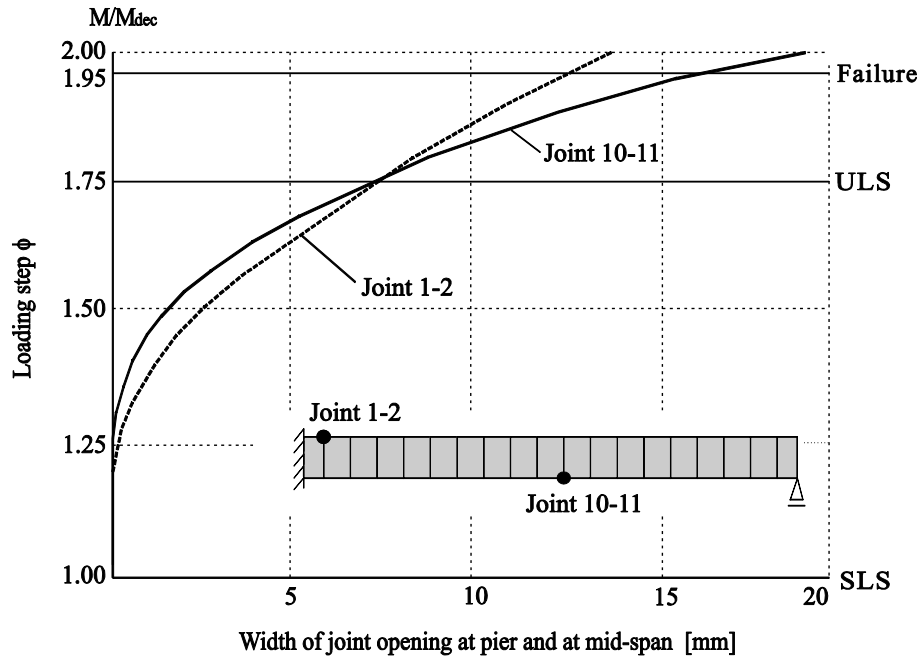


Figure 4.40: Widths of joint opening due to increasing loads

#### 4.4.3.2 Longitudinal stress distributions

The joint openings and compressive stress distributions of the section at mid-span and pier are shown in Figures 4.41. The maximum joint opening occurs between segment 10 and 11 because the external tendons are located asymmetrical to the center of the girder. It corresponds to the location where the maximum deflection is observed. The first deviator was located in segment 8 (see Figure 4.43). In general, all openings of joints were concentrated at the pier and between deviators.

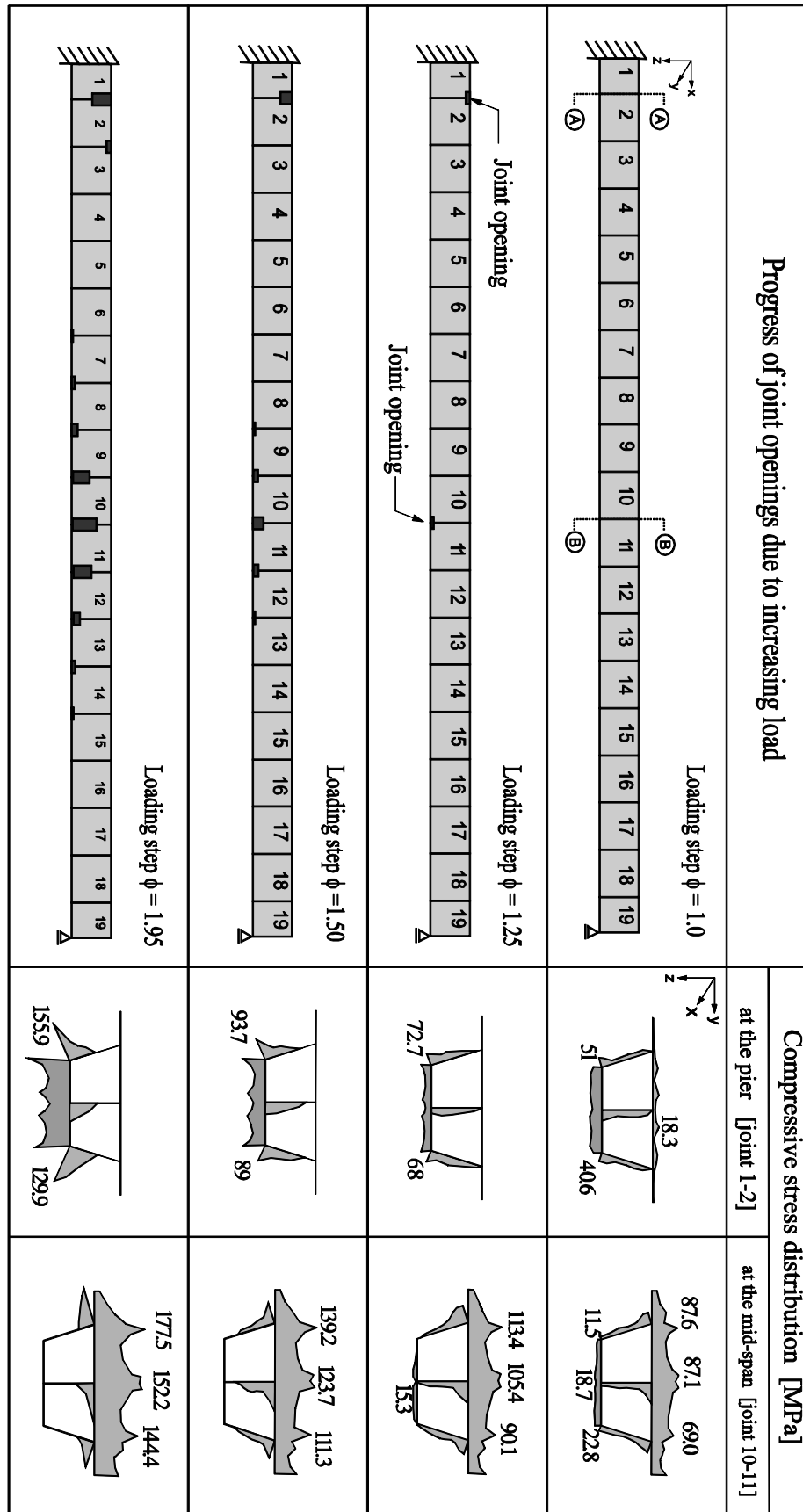


Figure 4.41: Compressive stresses distribution at mid-span and pier due to increasing loads

The compressive stress distribution at mid-span (joint 10-11) is similar to that of a simply supported girder. However, the compressive stress distributions at the pier with increasing loads show that a descent of neutral axis results in a growth of width and depth in joint opening and a decreasing compressive zone in the opposite direction to mid-span. The compressive stresses at the top slab above the webs are larger than those at the cantilever and at mid-section of the top slab between webs such as for simply supported girders.

#### 4.4.3.3 Shear stress and rotation

Figure 4.42 shows the angle of rotation at mid-span due to increasing load. As with the deflection at mid-span, the rotation is also influenced by a joint-opening. After decompression (at the loading step  $\phi = 1.125$ ), the angle of rotation at mid-span increases rapidly. In comparison with a torsion moment of a general monolithic box girder, however, these values present a similar pattern. The rotation of the continuous segmental girder model was significantly smaller than that of the simply supported model. It should be noted that the shear keys are not modeled in the FE-model. Thus the angle of rotation in the real structure will be much less than in the numerical simulation.

An unsymmetrical distribution of live loads in the transverse direction results in a wrapping of the box girders and causes shear stresses. The rotation was determined by vertical displacements of the four edges as mentioned previously.

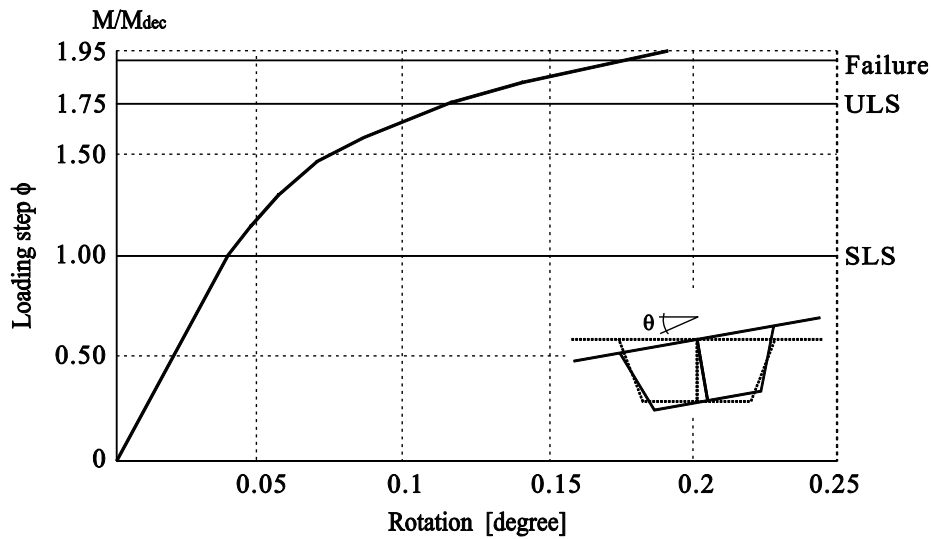
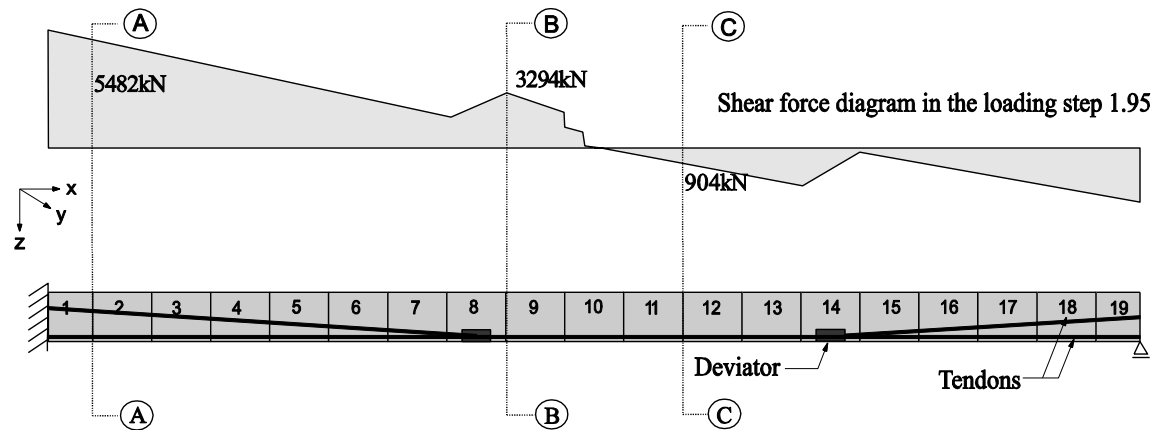


Figure 4.42: Rotation due to increasing loads

Figure 4.43 shows the shear stress distributions at the three sections, at the pier, at the deviator and at mid-span. The upward tendon force at the deviators increases the shear force. The shear stresses at the pier (joint 1-2) were higher than other joints because of the shorter contact surface, which is a similar behavior as for the single span PSB model.



Loading step $\phi$	Shear stress distributions		
	at the pier [joint 1-2]	at the deviator [joint 8-9]	at the mid-span [joint 11-12]
1.0			
1.95			

Figure 4.43: Shear stress distributions due for loading step 1.0 and 1.95

#### 4.4.3.4 Normal force variation in webs

Figure 4.44 and Figure 4.45 show the changes of the horizontal forces ( $F_x$ ) on the surface of joint 1-2 at the pier. The forces were observed at the three points (nodes), located on different levels of web. The same load bearing behaviour as for a single span bridge can be observed. Joint opening starts at loading step 1.125.

The compressive forces (B1, B2 and B3) in the top slab increase with ascending loading. It has linear range until loading step 1.35. Then the curves start a rapid rise from linearity.

From the post-tensioning (without live loads) to the loading step  $\phi = 1.125$  with additional loads, the forces (T1, T2 and T3) on the top slab at the pier show a linear decrease corresponding to a reduction in the initial compressive forces (see Figure 4.45).

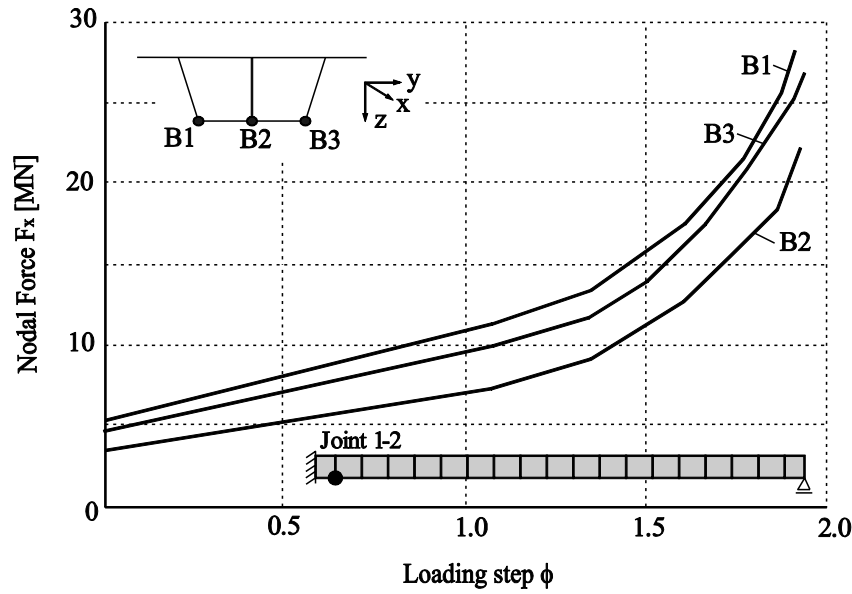


Figure 4.44: Forces in the bottom-slab at the pier due to increasing loads

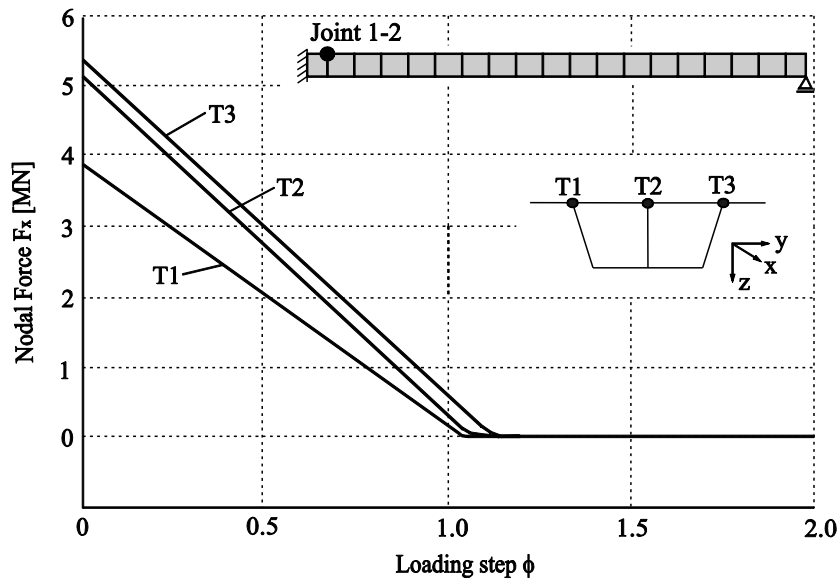


Figure 4.45: Forces in the top-slab at the pier due to increasing loads

#### 4.4.3.5 Change of tendon stress

The change of tendons stresses is similar to that of a single span bridge. As with simply supported girders, the mid-span sections of draped tendons show a larger strain than the section between the deviator and diaphragm. However, the draped profile tendon (T2) between the deviator and fixed diaphragm shows a higher stress increase than straight profile tendon. As the angle of the tendon at the deviator is bigger than for the simple span girder, this leads to higher strains in the whole tendon.

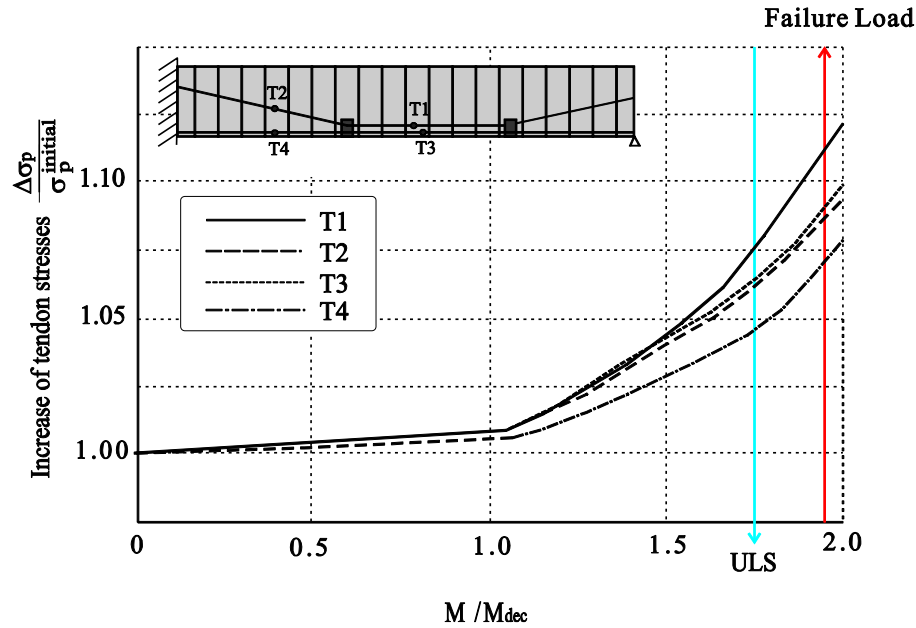


Figure 4.46: Increase of tendon stresses due to increasing loads

## 4.5 Conclusions

Chapter 4 focused on the flexural behaviour of UHPC-PSBs analysed by the Finite Element models. As reasons for the usage of UHPC in PSBs, some significant results can be taken from the studies in this chapter.

First, the SES full-scale test results were used in this research to verify the numerical model. The good agreement between the deflections, stresses and joint openings of the FE-analysis and the test demonstrate that the numerical model can be used to simulate the behaviour of a real segmental bridge with dry joints and external prestressing.

The study shows that UHPC-PSB made of thin elements can be used for road bridges. In comparison with the behaviour and the load bearing capacity of the SES test span (NSC-PSB), the efficiency and the applicability of UHPC-PSB models were presented by some parameter studies:

- The linear compressive stress-strain curve and the high E-modulus of UHPC lead to smaller deflections and a more linear behaviour.
- A reduction of the cross-section area of about 60 % and of the tendon quantity of about 36 % are possible.
- Also, with 60 % less cross-section area and 18 % less tendon quantity, a span-to-depth ratio of up to  $l/h = 25$  can be built. However, such slender structures show large deflections and early joint openings. This may cause problems in serviceability state and an increase of tendon quantity may be required.

- When the depth and length of spans are not altered as the same size of conventional concrete girders, the relative efficient of thin sections results in smaller deflections, smaller tendon quantity and a reduction of dead load. For higher span-to-depth ratios more tendon quantity is required. However, this leads to large camber due to the excessive prestressing force.

Based on parameter studies a special cross-section for a UHPC-PSB was proposed. The behaviour of the Finite Element model of this structure was investigated under increasing loads. Over the ULS, a sufficient stiffness and bending resistance are assured by the post-tensioning. After decompression beyond the SLS, some joints start to open. The deflection and the joint opening of the UHPC-PSB model slowly increased in contrast with NSC-PSBs. Next, the behaviour of a multispan bridge had been studied and compared with that of a simply supported structure. This continuous model presents higher ultimate moment capacity and smaller deflections and rotations than a simply supported bridge. However, high increase of the tendon strains and joint openings at the pier should be considered in a continuous NSC-PSBs. The high compressive strength of a UHPC member requires higher stresses in the tendons.



## 5 Shear Design of UHPC Joint

As shown in chapter 3.3, the strength of precast concrete members is increasing with the application of HSC or UHPC. In the design of UHPC precast structures, the joints between segments are of critical importance for the safety of a bridge. In the match-cast construction method, dry joints without any bonding material are often used in the contact surfaces between adjacent segments.

The objectives of this chapter are to evaluate the relationship of concrete compressive strength and shear strength of keyed dry joints for the UHPC-PSBs and to propose a new design formula for practical applications.

In this chapter, the experimental and numerical works are presented, which had been conducted to assess the shear strength and deformation behaviour of precast segmental bridge joints. The studies included flat joints (without shear-keys) to estimate the friction coefficient of UHPC and keyed joints with different levels of normal stresses. From the tests, therefore, the shear capacity, structural behaviour and crack patterns of dry joints in UHPC precast members were investigated. The results obtained in these tests are compared with existing formulae and a new approach for design of dry joints is proposed.

### 5.1 Literature review

The early bridges, constructed using precast segmental construction method, were built with *in-situ* concrete or mortar joints. More recently the segments were joined with a thin layer of epoxy (see chap. 3.1.4). Recently, projects in the USA and Southeast Asia were presented as precast segmental bridges without any epoxy in the joints, a technique known as ‘dry-joint’. With development of precast segmental construction, the dry joint studies were actively conducted since the 1980’s (e.g. [Koseki, Breen 1983], [Buyukozturk, Bakhoun 1990], [Fouré, Bouafia 1993] and [Specker 2001] etc.). In the following sections, the state of the art, existing design models, tests for UHPC joints and effect of SFRC on shear key behaviour will be introduced.

#### 5.1.1 Shear design models for dry joint

The existence of shear keys clearly increases the shear capacity of a joint. To predict the capacity of a joint between precast segments, there are several design formulae available. When considering the current situation of segmental bridges that are widely used in construction, the various formulae present very different values for the ultimate shear capacity of joints.

The existing formulae for keyed joints between concrete segments are introduced in this section.

### Eurocode 2

Eurocode 2-1:2004 (in the following EC2) is applicable for design of buildings and not for bridges. The formula gives the shear capacity at interfaces cast at different times. It's applicability to PSB joints is doubtful. Nevertheless, this approach will be presented in the following. EC2 approach is valid for concrete strength up to  $f_{ck} = 90$  MPa (cylinder).

The shear capacity of a joint without reinforcement depends on adhesion ( $c \cdot f_{ctd}$ ) and friction ( $\mu \cdot \sigma_n$ ). EC2 provides detailed surface information, which is classified as very smooth, smooth, rough and indented joint surface. For indented joints, the factors, such as cohesion  $c$ , friction  $\mu$  and strength reduction factor  $\nu$ , are given higher values than other surface conditions. In particular, the coefficient of friction ( $\mu$ ) in the indented joint has a very high value of 0.9. Almost all codes and recommendations for shear-key design include the concrete compressive strength ( $f_{ck}$ ) in their formulas. However, EC2 suggests the function of design tensile strength of concrete ( $f_{ctd}$ ), and its maximum value is restricted by strength reduction factors and design compressive strength of concrete ( $f_{cd}$ ). Figure 5.1 illustrates the details of shear key according to Eurocode 2-1-1.

The design shear resistance at the interface between concrete cast at different times can be determined as follows:

$$v_{Rdi} = c \cdot f_{ctd} + \mu \cdot \sigma_n \leq 0.5 \cdot \nu \cdot f_{cd} \quad (\text{DIN EN 1992-1-1:2011}) \quad (5.1)$$

- Where :
- $v_{Rdi}$  is the design shear resistance at the interface [MPa]
  - $c$  is a factor depending on the roughness of the interface;  $c = 0.5$  for indented surfaces
  - $\mu$  is the coefficient of friction depending on the surface;  $\mu = 0.9$  for indented surfaces
  - $\sigma_n$  is the normal stress across the joints (compression) [MPa]
  - $f_{ctd}$  is the design tensile strength of concrete ( $f_{ctd} = \alpha_{ct} \cdot f_{ctk;0.05} / \gamma_c$ ) [MPa]
  - $\nu$  is a strength reduction factor;  $\nu = 0.7$  for indented surfaces
  - $\nu_2 = 1.1 - f_{ck}/200$  additional reduction factor for  $f_{ck} \geq 55$  MPa
  - $f_{cd}$  is the design compressive strength of concrete [MPa]

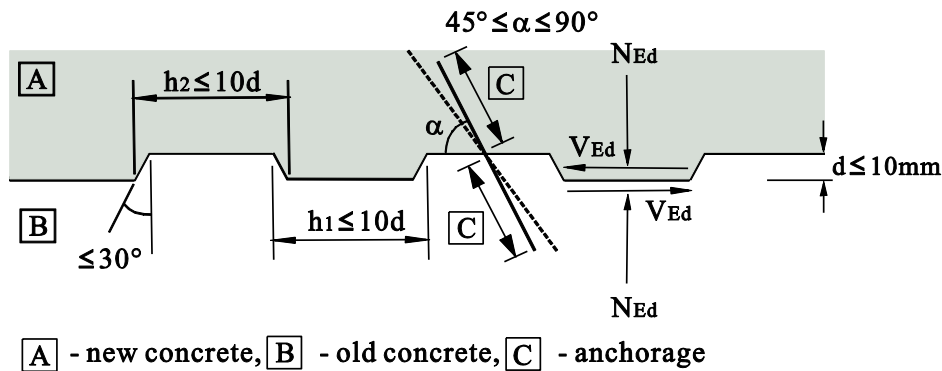


Figure 5.1: Details of keyed joint according to Eurocode 2 [DIN EN 1992-1-1:2011]

### AASHTO Guide Specification

The AASHTO Guide Specification [AASHTO 1999], which was theoretically proposed by Robert and Breen [Robert, Breen et al. 1993] and compared with the test results by [Koseki, Breen 1983] and [Buyukozturk et al. 1990], is widely used for design of dry joints. This formula includes a shear resistance by the key area ( $A_k$ ) and a friction resistance by the flat area ( $A_{sm}$ ) of joints. The coefficient of friction in this formula is  $\mu = 0.6$  for concrete to concrete surface, according to [ACI-318-05]. A strength reduction factor ( $\phi$ ) of 0.75 for dry joint capacity is recommended.

For precast concrete segmental bridge design and construction of joints, the AASHTO Guide Specification offers various details. In particular, the area of shear keys is recommended as 0.75 times the depth of the section and 0.75 width of the web. It also proposes that the longitudinal compressive stresses of a segmental bridge with dry joints and external tendons shall exceed 0.69 MPa (100 psi) in the serviceability limit state.

$$V_{nj} = A_k \sqrt{6.792 \cdot 10^{-3} \cdot f_{ck}} (12 + 2.466 \cdot \sigma_n) + 0.6 \cdot A_{sm} \cdot \sigma_n \quad (5.2)$$

Where :  $V_{nj}$  shear strength of the dry joint [MN]  
 $A_k$  area of the base of all keys in the failure plane [ $m^2$ ]  
 $f_{ck}$  compressive strength of concrete [MPa]  
 $\sigma_n$  compressive stress in concrete after allowance for all prestress losses [MPa]  
 $A_{sm}$  area of contact between smooth surfaces on the failure plane [ $m^2$ ]

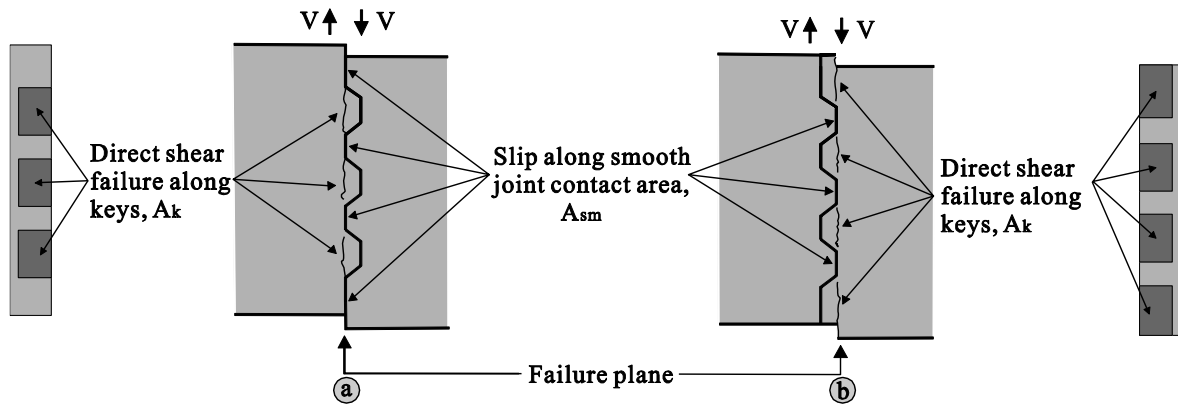


Figure 5.2: Joint shear failure plane [AASHTO 1999]

Figure 5.2 shows a typical failure plane of a keyed joint. The critical failure plane means the greatest area of slip and the least area of key breakage as the greatest ratio of  $A_{sm}$  to  $A_k$ . For the same joint configuration, the failure plane in Figure 5.2 (a) is most critical because it contains a larger smooth contact surface and a smaller area of key breakage.

**DBV (Recommendation for design of segmental bridges)**

According to German recommendation for design of segmental bridges [DBV 1999], the resistance of shear keys is not considered in the design of segmental bridges because only epoxy joints can be used in this country, where a smooth failure surface is expected. Thus, the effective shear area and the friction forces were mentioned as shown in the following formula (5.3). Figure 5.3 illustrates the effective area for shear resistance at a joint defined by [DBV 1999]

$$V_j = \mu \cdot \sigma_n \cdot A_T \quad (5.3)$$

Where:  $A_T$  Effective shear area (part of compression zone)  
 $\mu = 0.7$  Coefficient of friction (concrete-concrete)  
 $x_i$  Neutral axis depth

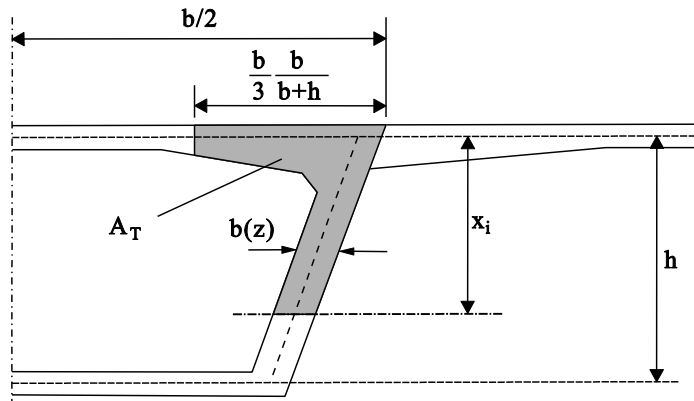


Figure 5.3: Effective area ( $A_T$ ) for shear resistance [DBV 1999]

**Design model proposed by Rombach and Specker**

Considering a combination of frictional and shear areas, that include shape and number of shear keys, the shear capacity of a dry joint was proposed by Rombach and Specker at Hamburg University of Technology (TUHH) as shown in Figure 5.4 and equation 5.4 [Specker 2001], [Rombach 2004]. This formula has a relatively high safety factor of 2.0 to take imperfections and the brittle failure of the joints into account.

$$V_{j,d} = \frac{1}{\gamma_F} \cdot [\mu \cdot \sigma_n \cdot A_{joint} + f \cdot f_{ck} \cdot A_k] \quad (5.4)$$

Where :  $V_{j,d}$  design shear strength of the dry joint [MN]  
 $\mu = 0.65$  coefficient of friction (concrete-concrete)  
 $\sigma_n$  average compressive stress across the joints [MPa]  
 $A_{joint}$  total area of the compressive zone [ $m^2$ ] ( $= b \cdot h$ )  
 $f = 0.14$  factor for the indentation of the joint  
 $f_{ck}$  compressive strength of concrete [MPa]  
 $A_k$  area of the base of all keys in the failure plane [ $m^2$ ]  
 $\gamma_F = 2.0$  safety coefficient

For epoxy joints:  $V_j = \mu \cdot \sigma_n \cdot A_{joint}$

The friction area ( $A_{joint}$ ) is equal to the total area of the web and not the smooth areas ( $A_{sm}$ ) only like in the AASHTO formula.

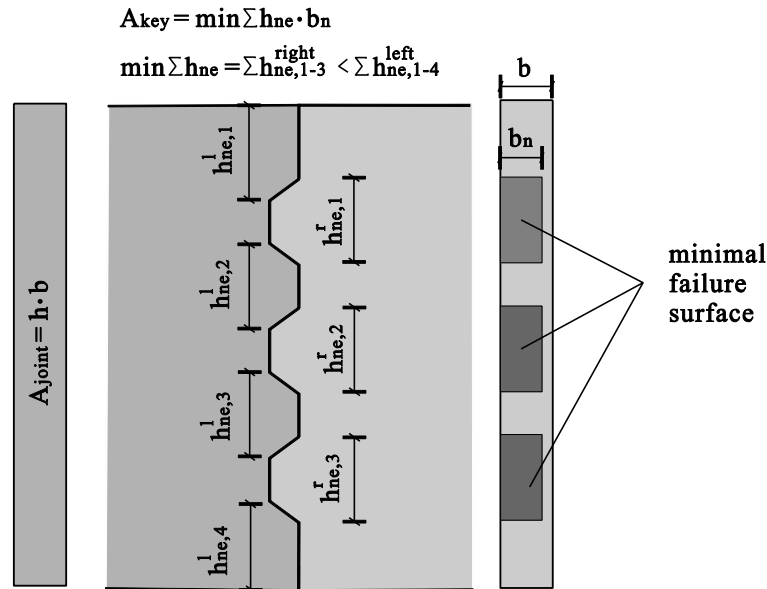


Figure 5.4: Definition of a joint surface with shear keys [Rombach 2002]

### JSCE (Japan Society of Civil Engineer) UHPC guideline

As the most up-to-date design for UHPC-joints, a guideline [JSCE 2006] of Japan Society of Civil Engineers presents the formula considering the types of joints and the characteristics of UHPC. The equation 5.5 has a very similar concept to the approach of Rombach and Specker. However, it involves a relatively low friction coefficient of  $\mu = 0.45$  and a factor for shear keys of 0.1. This formula offers a factor,  $b$ , for different joint types such as wet and epoxy joint. JSCE UHPC guideline does not mention dry joints.

$$V_{cwd} = \mu \cdot f_{cd}^b \cdot \sigma_{nd}^{(1-b)} \cdot A_{cc} + 0.1 \cdot A_k \cdot f_{cd} \quad [\text{kN}] \quad (5.5)$$

Where :	$V_{cwd}$	design shear strength of UHPC joint [N]
	$\mu = 0.45$	average coefficient of friction due to contact with the solid body
	$f_{cd}$	design compressive strength of UHPC [MPa]
	$\sigma_{nd}$	average compressive stress acting perpendicular to the shear plane [MPa]
	$b$	exponent representing the shape of the plane (0 ~ 1.0 ; 0.4 for wet joint, 0.5 for epoxy resin )
	$A_{cc}$	area of the shear plane on the compression side [ $\text{mm}^2$ ]

### Comparison of different models for joint design

Figure 5.5 shows the relationship between shear and normal stress according to five different design models. It should be noted that the approach proposed by JSCE is the only one which has been developed for application of UHPC. The five typical design models present the shear capacity due to different concrete compressive strengths from NSC ( $f_{ck} = 40 \text{ N/mm}^2$ ) to UHPC ( $f_{ck} = 180 \text{ N/mm}^2$ ). All the diagrams are based on the standard segment of the SES in Bangkok (see Fig. A. 12).

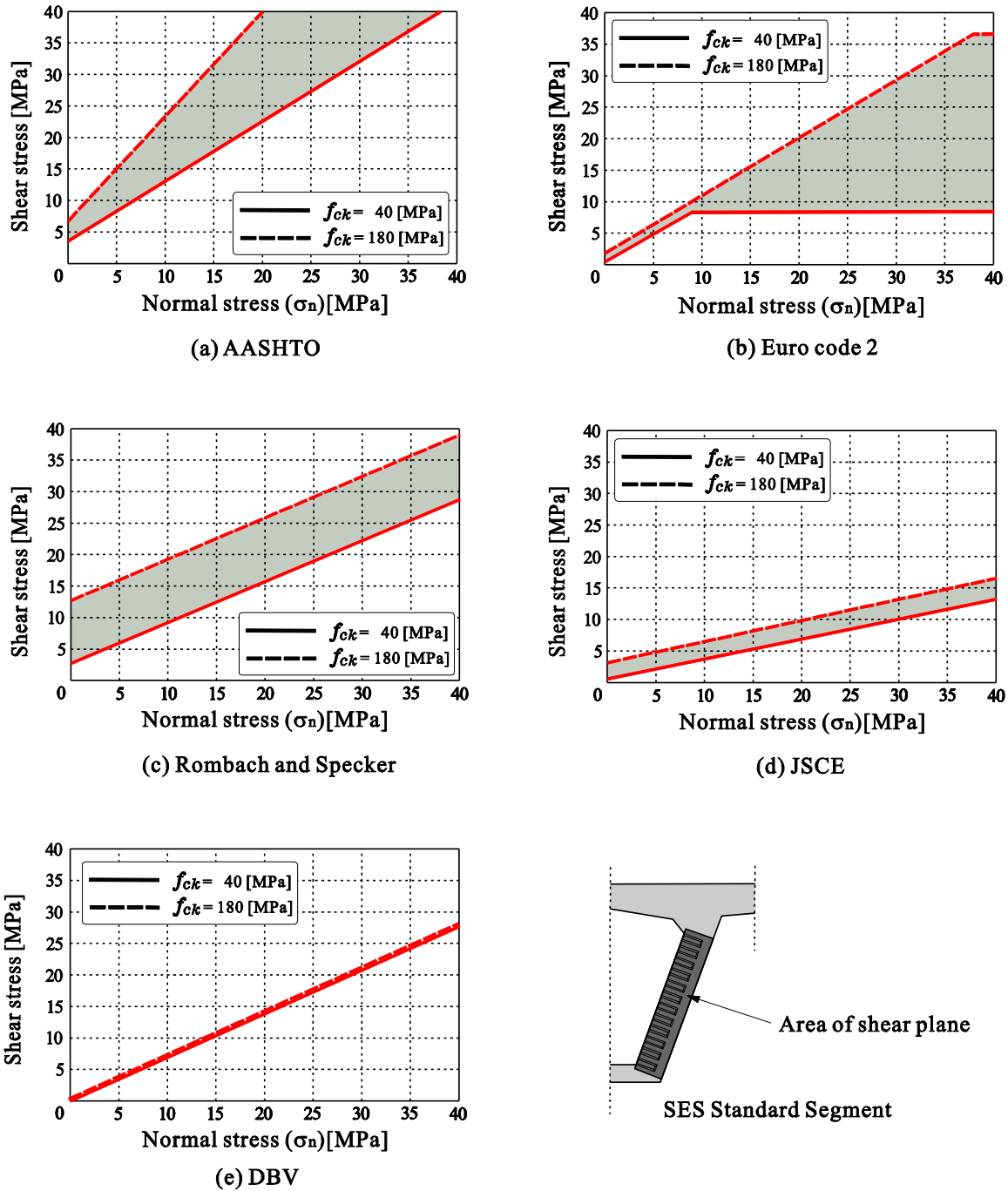


Figure 5.5: Design shear capacity of dry joint from NSC ( $f_{ck} = 40 \text{ MPa}$ ) to UHPC ( $f_{ck} = 180 \text{ MPa}$ ) (based on SES standard segment, see Fig. A.12)

As can be seen in Figure 5.5(a), AASHTO specification has a relatively large increase of shear capacity with increasing concrete strengths for NSC and even more for HSC and UHPC. The shear capacity of pure shear keys, without frictional resistance ( $\sigma_n = 0$ ), for UHPC is only about two times higher than that of NSC acc. to eq. 5.2 ( $V_{nj} \sim f_{ck}^{0.5}$ ). Especially considering the compressive strength of UHPC, the difference is very small. To apply HSC or UHPC, therefore, the AASHTO model seems to overestimate the shear capacity of a joint.

In the formula of Eurocode 2, the shear capacity is limited by the strength reduction factor  $\nu$ , the safety factor of 0.5 and the design compressive strength of concrete,  $f_{cd}$ , as shown in Figure 5.5(b). It means that the effect of normal pressure for shear capacity is restricted to very low values of  $\sigma_n$ . In essence, under 10 MPa of normal compressive stress, there is little difference between NSC and UHPC. The restricted maximum shear stress value of NSC seems to be conservative and highly inefficient.

On the other hand, the design model proposed by Rombach and Specker (see Figure 5.5(c)) presents two parallel lines (UHPC and NSC). The magnitude of the distance is the difference of shear capacity due to the compressive strength of concrete. The pure shear strength of UHPC is about four times higher than that of NSC. The slope and the initial shear strength values in this formula are very reasonable compared to other design models.

The JSCE model (Figure 5.5(d)) is similar to that of Rombach and Specker, however, because of low friction coefficient and low shear key factor (see Equation 5.5), this formula seems to be very conservative. Thus, the shear strength for HSC or UHPC joints can be underestimated.

The DBV (German recommendation) illustrates the great difference compared to other design models. First of all, this approach is valid for epoxy joints only, as dry joints are not allowed in segmental bridge construction in Germany. In this formula, the compressive strength of concrete is not considered. As seen in Figure 5.5(e), the shear strength of UHPC and NSC are the same. Therefore, the formula of DBV will not be used further in this research.

Figure 5.6 shows a comparison of the various design models for UHPC ( $f_{ck} = 180$  MPa) until normal stress reaches 90 MPa, as one-half of compressive strength of concrete. As mentioned above, each design model gives significantly different results. AASHTO specification seems to overestimate the shear capacity of a joint in comparison with the other design models. On the other hand, JSCE seems to underestimate the shear strength with increasing normal stresses.

The significant points for the application of the various models to UHPC segments are the shear strength of pure shear keys ( $\sigma_n = 0$ ), the initial shear stress in Figure 5.6, and the steady increase of shear strength due to a frictional resistance. Through experiments and extensive FE-analysis,

these two load bearing mechanisms will be investigated to develop a more reliable new design model.

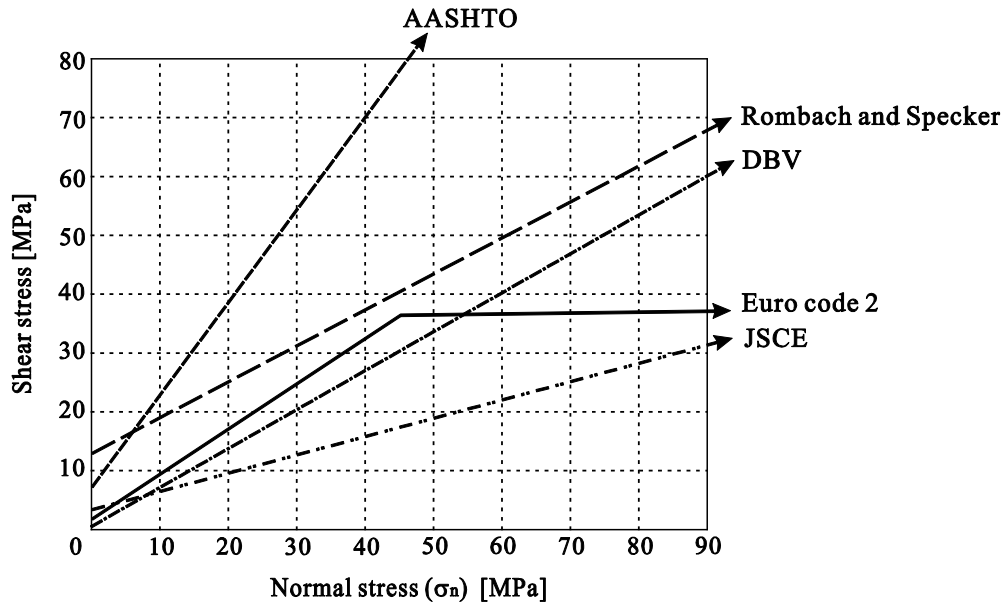


Figure 5.6: Shear strength of dry joints according to existing design models for UHPC ( $f_{ck} = 180$  MPa) (based on SES standard segment, see Fig. A.12) [Watanabe et al. 2007]

### 5.1.2 Tests on UHPC joint

UHPC bridges with hollow or T-cross-section will be built with very thin webs. Thus the joint capacity is becoming more important.

In recent years, joint tests of UHPC elements have been conducted. This section presents the results of the UHPC joint tests taken from literature and own experimental investigations.

#### Tests of wet joints

To verify the shear transfer capacity of a UHPC wet joint in the U-shaped webs of the GSE bridge (see chap. 3.3.2), which was made of Ductal with a characteristic compressive strength of 180 MPa, full-scale tests were conducted in Japan. The average design compressive stress, a confining pressure of 10 MPa, was used in the tests. Figure 5.7 shows the test results as well as the two different types of test specimens (with shear key and without). With all test specimens, cracks developed under loads of 1.6 to 1.7 MN.

Type 1 test specimen showed a diagonal compression failure mode without slippage at the interface. The number of cracks increased under loads exceeding 2.0 MN. Cracks of type 2 test specimen developed from the corner of shear key under a load of 2.4 MN. The number of cracks increased sharply near the maximum load. The design shear capacity was based on the formula (Eq. 5.5) by [JSCE 2006] described in the previous section.

The maximum loads of all tests (two types) were more than the design shear capacity  $P_{ud} = 1621$  kN [Watanabe et al. 23007]. The test shows that UHPC wet joint without shear keys



has a higher shear resistance than the value according to the design shear capacity and that shear keys increases the shear capacity.

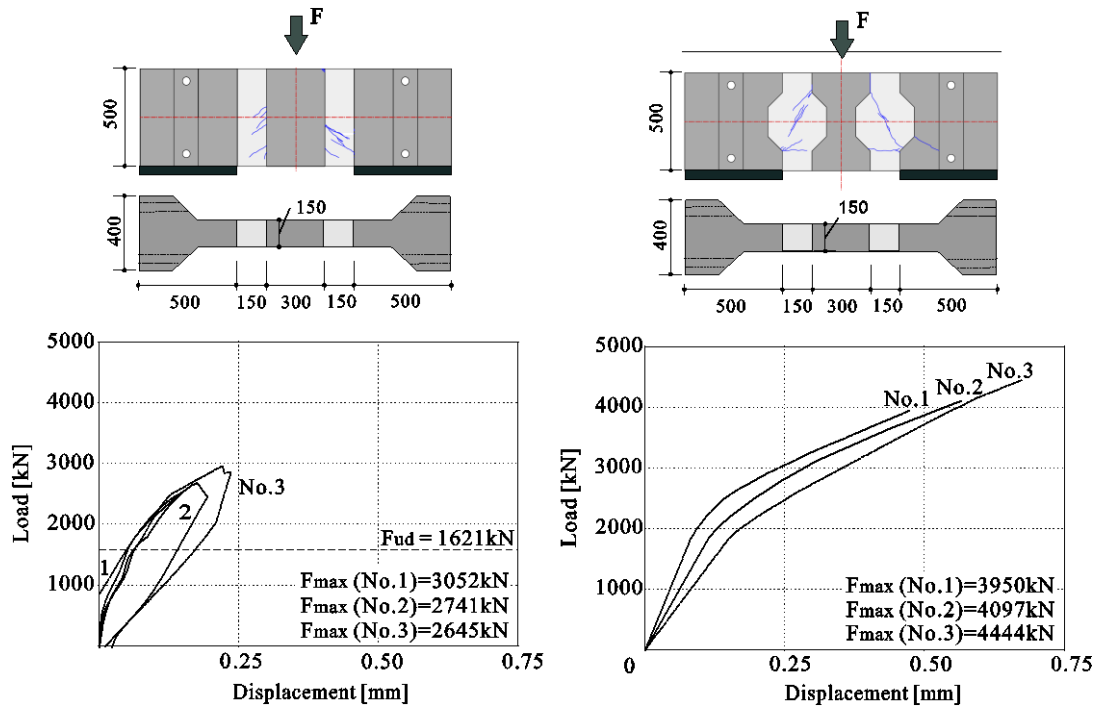


Figure 5.7: UHPC wet joint tests without shear key (type1) and with shear key (type 2) [Watanabe et al. 2007]

### Tests of flat dry joint and friction coefficient

The coefficient of friction  $\mu$  of UHPC can be found in the tests by Hense [2009]. The tests were carried out with different surface conditions, which were treated by sand-blasting and formwork-smooth. The experimental investigations showed that the coefficients of friction ranged between  $\mu = 0.6$  and  $\mu = 0.8$ . In particular, the coefficient of friction for formwork-smooth surfaces ranged from  $\mu = 0.7$  to  $0.8$ .

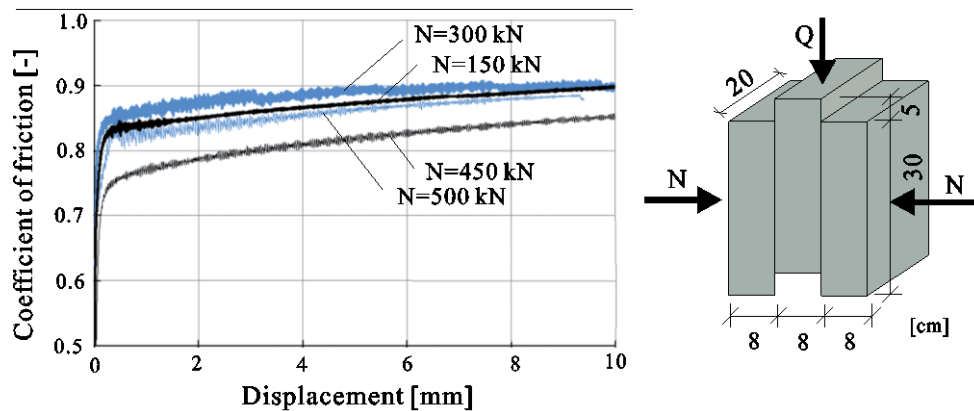


Figure 5.8: Coefficient of friction for flat dry joints (formwork smooth surface) with different confinement levels [Tue, Winkler et al. 2011]

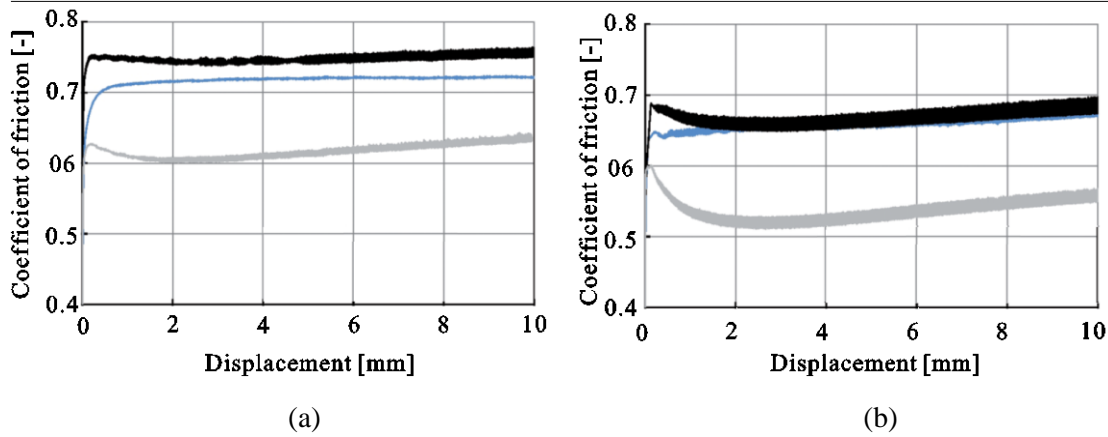


Figure 5.9: Coefficient of friction for flat dry joint with (a) and without (b) fibers [Schoening et al. 2013]

More recently, experimental studies within the research project “Sustainable Construction with UHPC” funded by the German Research Foundation (DFG) have been conducted by the Institute for Structural Concrete at RWTH Aachen in Germany [Schoening et al. 2013] and at TU Graz in Austria [Tue, Winkler et al. 2011]. In these studies, the connections for precast UHPC elements, such as the compression/compression-, tension/tension- and compression/shear forces, are studied by tests.

The results of UHPC dry joint tests with different normal forces present a coefficient of friction between 0.75 and 0.9, as shown in Figure 5.8. In the flat joint tests, the comparison of friction coefficient for the grinded dry joints with and without fibers is also presented in Figure 5.9. It shows that the friction coefficient at surfaces with fibers is higher than that of surfaces without fibers. In comparison with Figure 5.8 and Figure 5.9, the friction coefficient at plane surfaces, such as formwork smooth surface, is higher than that at grinded surfaces. [Tue, Winkler et al. 2011] and [Schoening et al. 2013] also presented the frictional coefficient, which has values between 0.85 and 0.9, for indented dry joints, and the different frictional behaviours in original and repeated tests.

### Test of keyed dry joint

The iBMB (Institut für Baustoffe, Massivbau und Brandschutz) at the TU Braunschweig, Germany, conducted an experimental study on indented dry joints made of UHPC [Oettler and Empelmann, 2013]. The experimental program was based on test setup by Kupfer et al. [1982]. The joint has a very fine indentation (Fig. 5.10). The UHPC specimens were produced with concrete mixture M3Q-2.5, with 2.5 vol.-% steel fibers, and contain different joint-inclination ( $f_{c,cyl,u} = 161 \div 176$  MPa). Figure 5.10 shows the set-up, the dimensions of the test specimens and test results. Based on the obtained test results, a slightly modified formula from Rombach and Specker [2002] has been proposed as shown in Equation (5.6).

$$v_{Ri} = 0.65 \cdot \sigma_n \cdot + 0.19 \cdot f_c \cdot \frac{A_{key}}{A_{joint}} \quad (5.6)$$

In this formula, a shear strength factor,  $f_c$ , of 0.19, with  $A_{\text{key}}/A_{\text{joint}} = 0.75$ , was proposed for UHPC dry keyed joints. The report also recommended that the ratio of shear key height/width shall be applied as  $h_{\text{ne}} \leq 6 \cdot b_n$  (see Fig. 5.4).

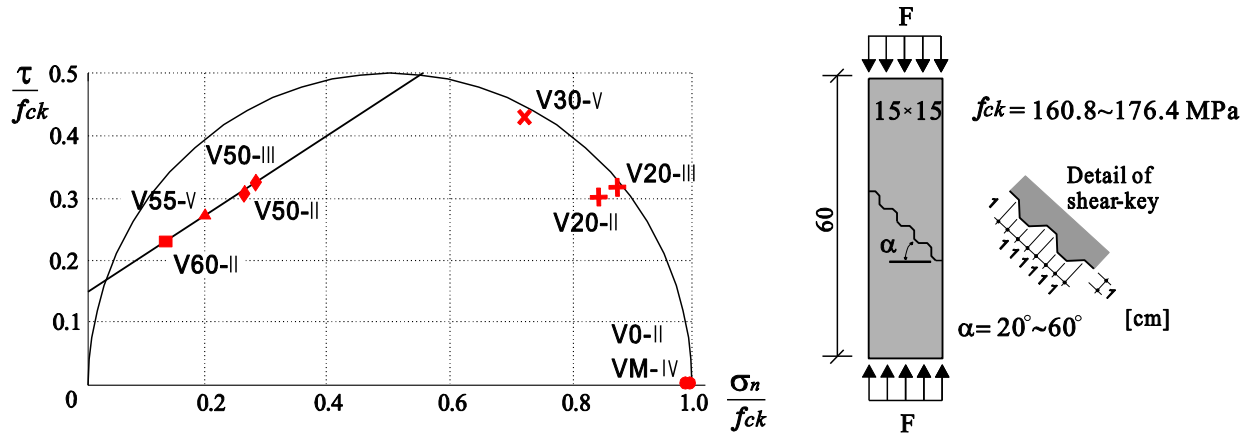


Figure 5.10: Test results in a shear-pressure diagram of [Oettel, Empelmann 2013]

### 5.1.3 Effect of SFRC (steel fiber reinforcement concrete) in joints

This section gives a brief overview of the potential benefits of fibers used in precast segments. In general, failure of the joints in segmental bridges occurred though shearing-off of the shear keys. It was also observed that failure of dry and epoxy joints are very sudden and brittle, and accompanied by a large drop at the shear keys. To improve the shear behaviour of joints, steel fiber reinforcement can be considered. Steel fibers can delay the sudden failure of shear keys (see Fig. 5.11).

The steel fibers resist tensile stress perpendicularly to the joint failure plane (cracks). This results in a higher shear strength, ductility and fatigue resistance of keyed joints.

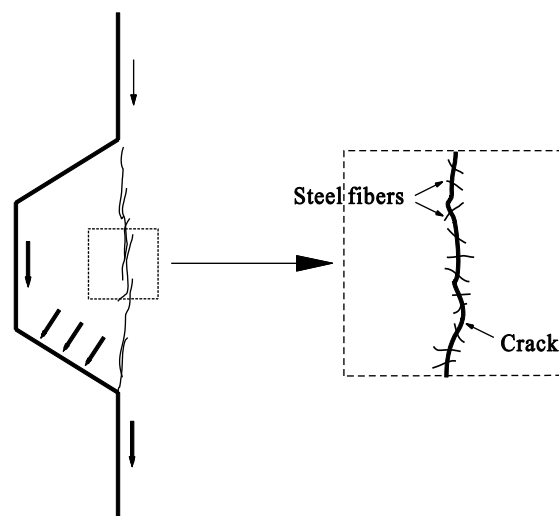


Figure 5.11: The effect of steel fibers in segmental joints

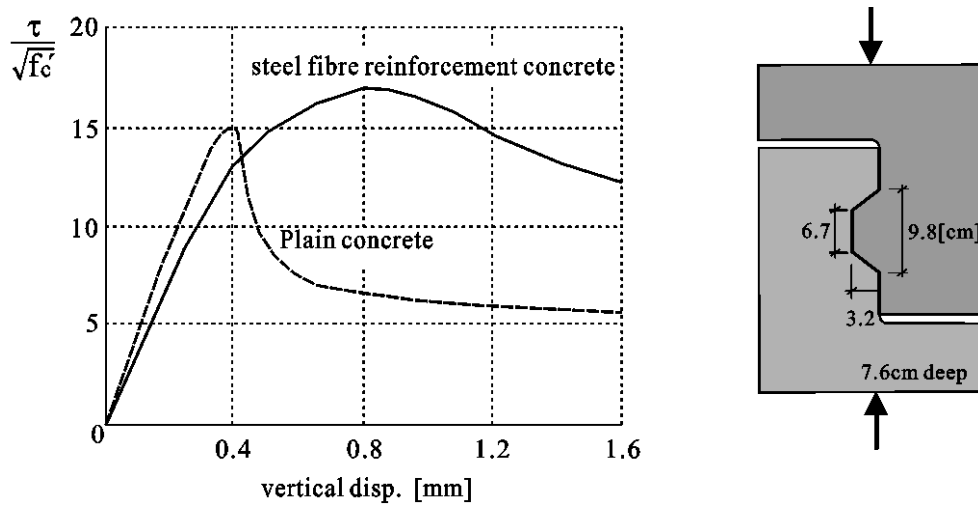


Figure 5.12: Effect of fibers on strength and ductility of joints [Beattie 1989]

Figure 5.12 shows the comparison of the shear stress to vertical displacement of shear keys made with plain concrete and SFRC with 2 % fibers. According to Bakhoun [1991], the use of fibers resulted in a ductility increase and a 20 % increase of the joint shear strength. Moreover, with use of fibers, giving some warning before failure, a less brittle behavior and smaller drop in the load-vertical displacement relationship after peak load were observed.

Turmo et al. [2006(b)] also showed that the shear capacity using SFRC in dry joints does not increase significantly. However, when multi-cracks in all the keys arise, the joints consistently resisted the loads. In comparison with the failure pattern from Beattie [1989], the similar results of both tests show the effects of joints using SFRC.

## 5.2 Experimental program

The load bearing behaviour of PSCBs will heavily depend on the shear capacity of the joints. In PSCB with dry joints, in particular, the shear strength depends only on the performance of shear keys and the level of forces across joints. Many parameter studies of a shear key, e.g. configuration and geometry of shear key, effect of multiple shear keys, and comparison of dry and epoxy joints etc. were already carried out. Therefore, all the tests were conducted with fixed factors such as same dimension of shear key and dry joint.

The main objectives of this experimental study were:

- to obtain the friction coefficient of UHPC joints for different normal stresses.
- to obtain experimental data to verify a FE-model of the test specimens.
- to evaluate the differences in shear strength, behaviour and failure mode between NSC and UHPC.

- to propose a new formula for design of dry joints with high strength concrete including UHPC.

### 5.2.1 Test specimens

#### Specimen details

The experimental program was conducted with 10 specimens made of UHPC. Figure 5.13 shows the two different specimens which consisted of 3 UHPC parts with thickness of 20 cm. Vertical loads and normal pressures apply at the top surface of the inner part and on both sides, respectively. Tests with flat joints (Figure 5.13 (a)) and the keyed joints (Figure 5.13 (b)) were conducted.

In order to compare the relative shear capacity between NSC and UHPC, the dimensions (shear key configuration and thickness) of the specimens are the same as that of the test specimen used by Specker [2001]. In all specimens, no reinforcement was provided.

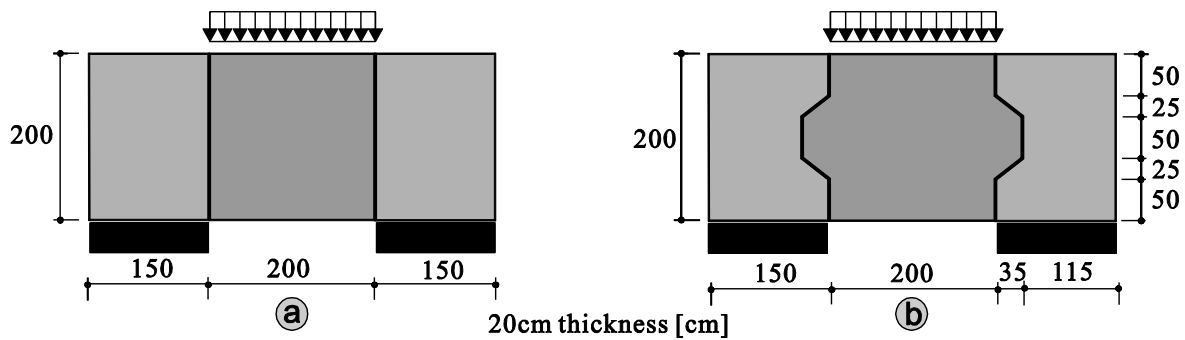


Figure 5.13: Specimen dimensions for flat joint (a) and keyed joint (b)

#### Material properties

The test specimens were made with M3Q mixture, which include 1 % steel fibers (details see Appendix B.1). The concreting work was carried out in the Institute for Structural Materials at the University of Kassel, Germany.

The compressive strength of the UHPC cylinder ( $\phi 150/300$  mm) after 28 days ranged from 176.2 MPa to 193.0 MPa. The average concrete compressive strength was 184.8 MPa. The tensile strength by split cylinder test was 12.90 MPa. More details about the material properties and information of test specimens can be found in Appendix B.2.

#### Fabrication

Because the use of a dry joint requires a perfect fit between the ends of adjacent segments, a match-casting method was used where each segment is cast against the end face of the preceding one. Thus, the middle parts of the specimens were prefabricated after the hardening of both sides, left and right parts, through a match-cast method.

As to avoid bonding between segments cast at different times and to maintain the friction of a joint's contact surface, a thin foil was used on the joint surfaces. UHPC was compacted externally with a vibrator. The fabrication process of the test specimens is shown in Appendix B.3.

### 5.2.2 Test procedure

The original purpose of the tests was to present the relationship of concrete compressive strength and shear key capacity at a dry keyed joint through the tests of UHPC specimens. In order to compare the normal concrete tests Specker [2001], therefore, the fixed conditions and parameters of the tests are as follows:

*Fixed conditions:* dry single keyed joint (no epoxy resin), shear key geometry

*Parameters:* different levels of normal force (0 to 1000 kN).

### Test specimens

The test specimens were divided into two types, flat joint tests to estimate the frictional coefficient  $\mu$  of UHPC and keyed joint tests with increasing confining forces, as shown in Table 5.1. The horizontal confining pressure of the flat joint test was 25 MPa. In the case of FJ-25-I, however, first a confining pressure of 1 MPa was applied up to vertical displacement of 2.5 mm, and then the confining pressure was increased up to 25 MPa.

Table 5.1: Parameters for UHPC dry joint tests

Test specimens	Type of joint	Horizontal force [kN]	Horizontal stress [MPa]	Concrete compressive strength ( $f_{ck}$ ) [MPa]	E-modulus ( $E_c$ ) [GPa]
FJ-25-I	flat joint	40~1000	1~25	183.3	50.273
FJ-25-II		1000	25	183.3	50.273
KJ-0-I	keyed joint	0	0	193.0	51.140
KJ-0-II		0	0	193.0	51.140
KJ -1-I		40	1	182.4	50.000
KJ -4-I		160	4	182.2	50.000
KJ -8-I		320	8	176.2	49.068
KJ-16-I		640	16	176.2	49.068
KJ-25-I		1000	25	188.9	50.759
KJ-25-II		1000	25	188.9	50.759

The horizontal confining pressure levels of keyed joint tests were 0, 1, 4, 8, 16 and 25 MPa, respectively. These confining pressures were applied before the vertical loading. In the specimens

with flat surfaces, KJ-0-I and KJ-0-II actual initial confining forces were 0.7 kN and 1.1 kN, respectively to avoid a movement of the specimens.

### Test set-up

The vertical actuator (max. 5.0 MN) and the horizontal actuator (max. 1.0 MN) were used in the test as shown in Figure 5.14. The vertical actuator, which has a constant stroke rate of 0.005 mm/s, was adopted for the load-displacement control of all tests. All the segmental specimens were tested under uniform loading which was applied directly on top of the middle segments after the application of the horizontal confining force. During the test, the changes of normal forces were measured and corrected if required.

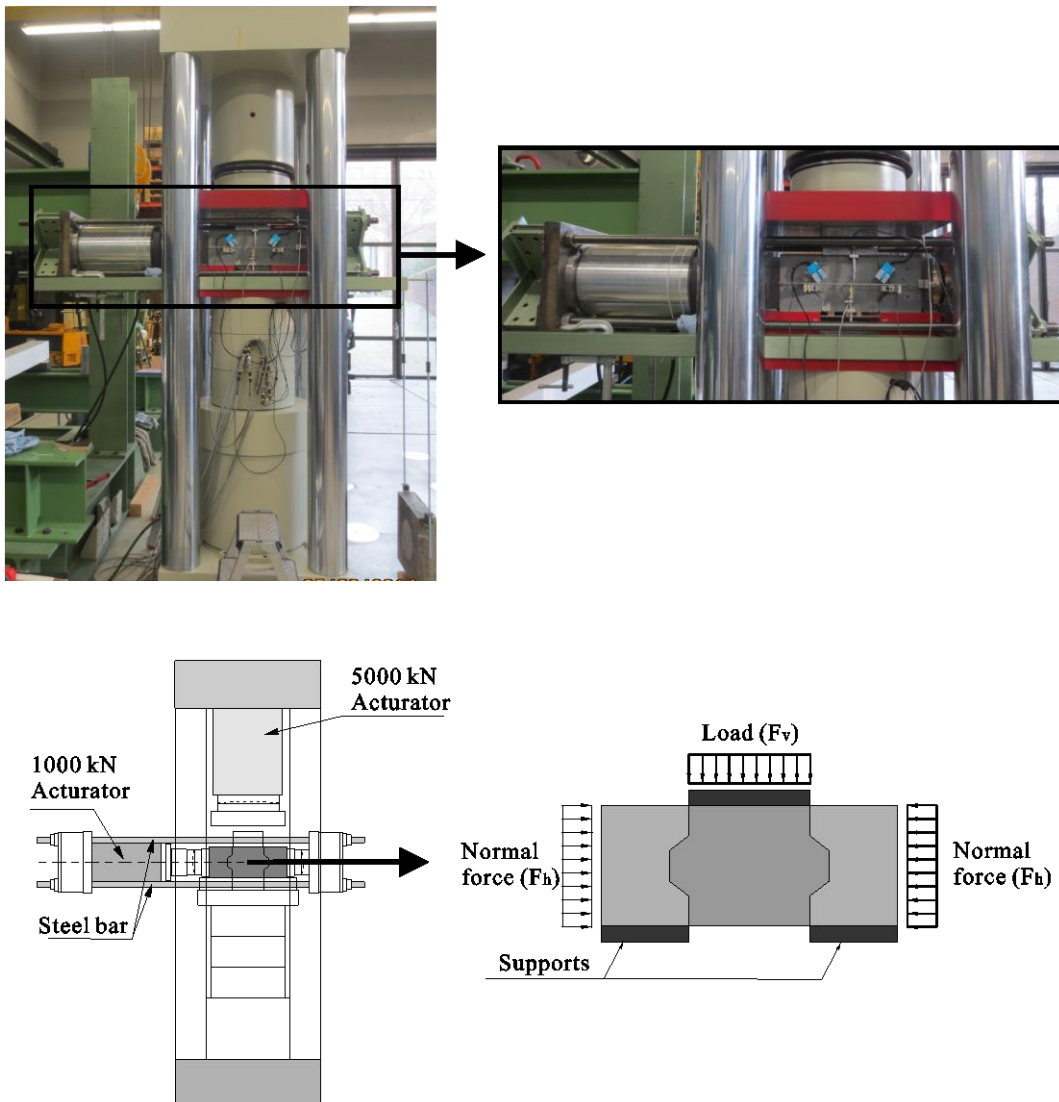


Figure 5.14: Test set-up and basic concept of loading

## Instrumentation

The crack displacement transducers were set across joints between two concrete segments to measure the displacement of openings. As shown in Figure 5.15, the transducers were located at the upper face and at the plane face (or back) of key areas between the middle segment and the side segment. More details regarding instrumentation are given in Appendix B.4.2.

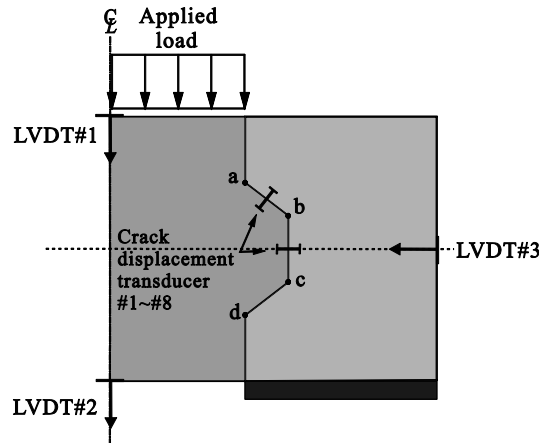


Figure 5.15: Instrumentation of keyed test specimens

## 5.2.3 Test results

### 5.2.3.1 Tests on flat joints

The coefficient of friction can be defined from equation (5.7) by the relationship between the vertical force ( $F_v$ ) and applied normal forces ( $F_h$ ).

$$\mu = \frac{F_v}{2 F_h} \quad (5.7)$$

The coefficients of friction,  $\mu$ , from the results of two flat joint tests were calculated by equation (5.7) (see Figure 5.16 and Table 5.2). The tests give a  $\mu$ -value of 0.78 and 0.81 with surfaces of a segment manufactured by the match-cast method. The coefficients of friction (or the maximum vertical forces) of the tests were constant with increasing deformations.

Table 5.2: Results of UHPC flat joint test ( $A_j = 400 \text{ cm}^2$ )

Specimens	Horizontal force ( $F_{h,test}$ ) [kN]	Vertical force ( $F_{v,test}$ ) [kN]	Coefficient of friction ( $\mu$ )
FJ-25-I	38.4	60.3	0.785
	1000.7	1616.2	0.808
FJ-25-II	1000.4	1573.2	0.786



These frictional coefficients show similarity with existing test results, such as [Hense 2009], [Schoening et al. 2013] and [Tue, Winkler et al. 2011]. Moreover, when considering that  $\mu$  depends on the surface conditions, the frictional coefficients of match-casted joint surfaces throughout the test results were similar to these of the formwork-smooth surfaces of the existing tests.

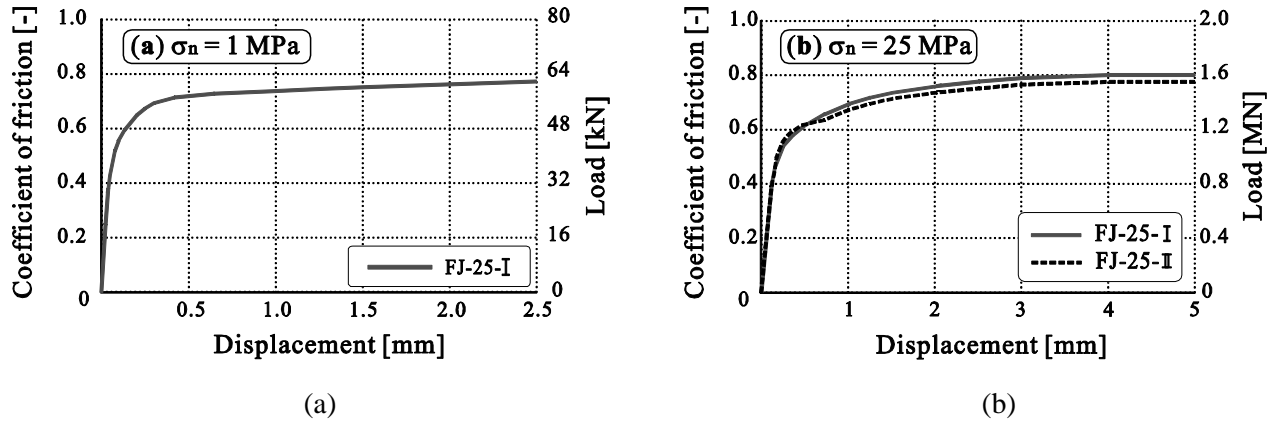


Figure 5.16: Coefficient of friction for flat joints with confining pressure of (a) 40 kN ( $\sigma_n = 1 \text{ MPa}$ ) and (b) 1000kN ( $\sigma_n = 25 \text{ MPa}$ )

In the casting of dry joints, the contact of joint surfaces for the function of inter-locking, is essential. After testing, the contact surfaces, which were damaged through normal force and slippage, are presented in Figure 5.17. The contact areas were spread throughout all contact surfaces. No cracks were observed in these specimens.

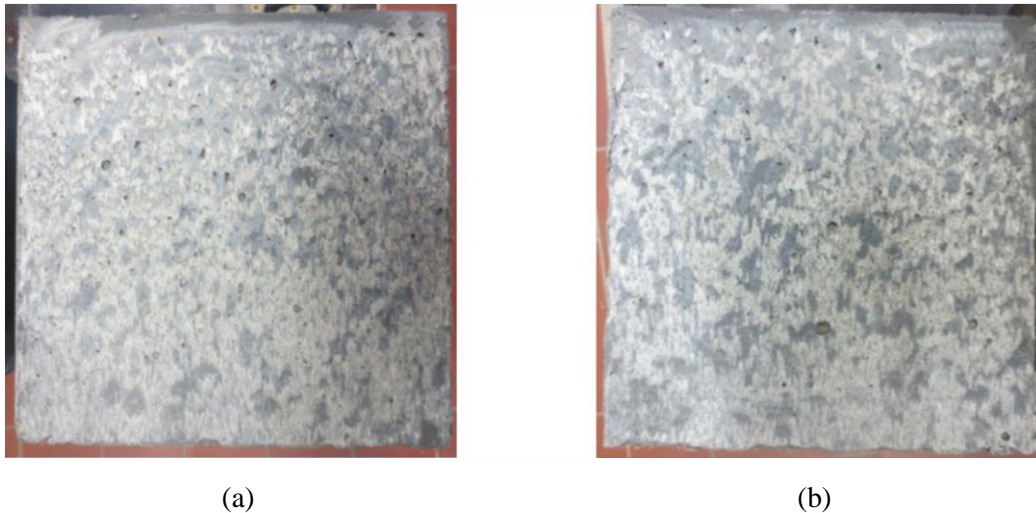


Figure 5.17: Contact surfaces after the flat joint test of (a) FJ-25-I and (b) FJ-25-II

### 5.2.3.2 Tests on keyed joints

#### Load-displacement relationship

The results of keyed joint tests are presented in Table 5.3. The maximum shear load, the displacement at failure (at top and bottom of the middle segment) and the changes of normal forces are given.

The maximum shear capacity of test specimens increased gradually with increasing normal force. In comparison with the flat joint test, effects of shear key for shear resistance are remarkably high. The specimens KJ-0-I and KJ-0-II, in particular, represent the shear capacity of pure shear key without initial normal force. The maximum vertical load of pure shear key were above 1200 kN.

The vertical displacements of failure of all specimens ranged between 1.0 mm and 1.3 mm. In all test specimens, the displacement at the top of the center segment was slightly higher than that of the bottom due to the compression strut that acted between top surface, where the load is applied, and lower surfaces at the shear key.

The numbers of specimen names indicate the initial normal confining pressure before the application of the vertical load. As the vertical load increases, the normal force, as a horizontal component of a vertical load, across the joint at lower surface of shear key also increases. When the friction force on the inclined surface is smaller than the components of the vertical and horizontal force, the sliding occurs (see section 5.3.4).

Table 5.3: Results of UHPC dry keyed joint test

Specimens	Maximum Load ( $F_{h,test}$ ) [kN]	Displacement at failure [mm]		Horizontal force [kN]	
		top of the centre	bottom of the centre	before vertical load ( $F_{v,test}$ )	at failure
KJ-0-I	1218.1	1.295	1.222	0.7	90.0
KJ-0-II	1213.1	1.238	1.112	1.2	82.0
KJ -1-I	1421.0	1.072	1.014	39.6	137.6
KJ -4-I	1722.4	1.005	0.976	160.3	239.5
KJ -8-I	2146.8	1.202	1.165	320.1	386.7
KJ-16-I	2808.9	1.144	1.137	636.1	665.3
KJ-25-I	3218.2	1.305	1.237	999.2	1005.2
KJ-25-II	3319.1	1.259	1.189	999.8	1009.3

Similar behaviours of all tests were observed. Compared to NSC shear keys, the load-displacement curves of all the tests presented almost linear increases up to the maximum load. In particular, the vertical displacements of the specimens KJ-0-I, KJ-0-II and KJ-1-I were very linear up to the maximum shear force. The specimens KJ-0-I and KJ-0-II, where the initial confining force was almost zero, after sliding on the sloping face, because of very low horizontal forces, the shear forces increased together with the horizontal forces.

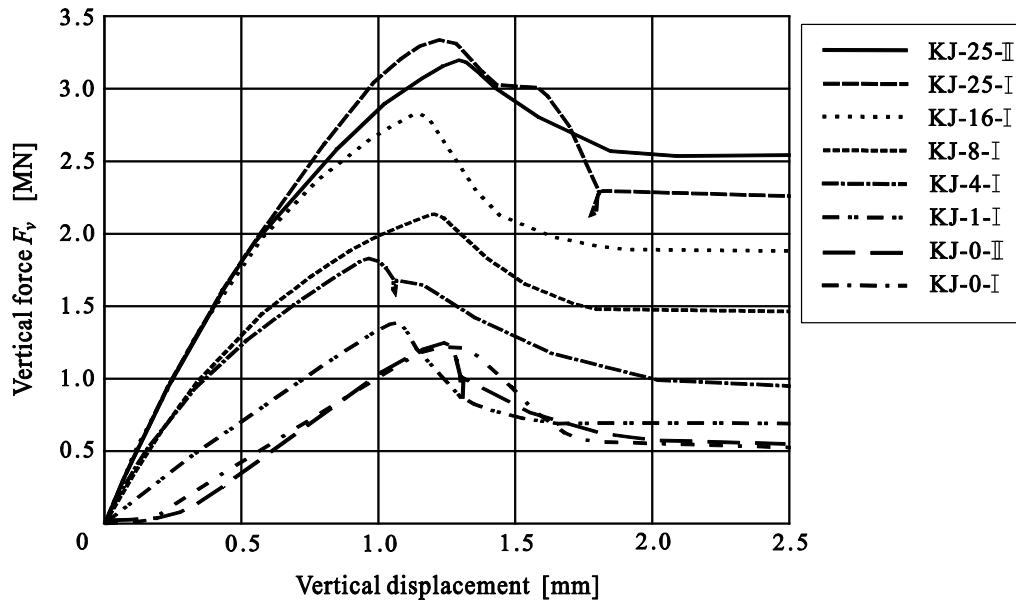


Figure 5.18: Comparison of load-displacement at different normal forces

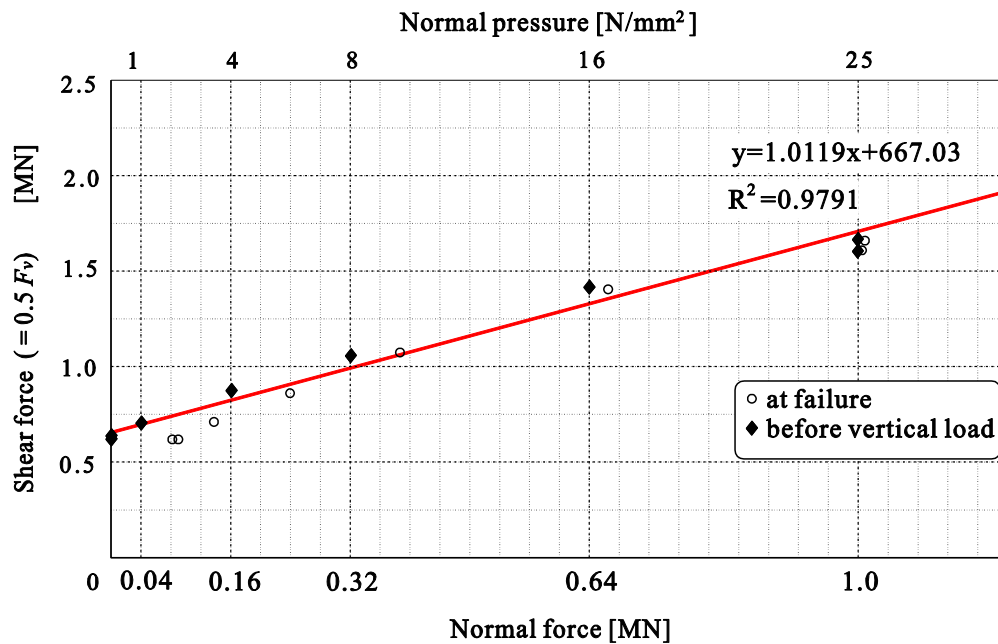


Figure 5.19: Maximum shear forces due to increasing normal forces

After peak load, a ductile behaviour can be seen in Figure 5.18. A reduction of the maximum shear force and a residual shear force were observed in all the tests. As mentioned in section 5.1.3, avoiding brittle failure, the residual shear force is maintained by the tensile strength of steel fibers and proportional to the normal confining forces as shown in Figure 5.19. This increase in shear capacity is directly proportional to the magnitude of confining force and stress respectively. When the level of normal stress increases by 1 MPa ( $F = 40\text{kN}$ ), the ultimate shear resistance of the dry keyed joint was increased approximately by 40.5 kN. This indicates that a high prestress force is very effective to the shear strength in UHPC keyed joints.

### Variation of normal stress

With increasing the vertical force, however, the normal force also increases because of the horizontal force component on the sloping surface, which is the lower face at key area in all specimens, increases gradually (see Table 5.3). The horizontal forces push out the neighbor segments with female keys. This behavior generates the increase of normal pressure and the sliding on the sloping surface, when the joints don't have enough restraint by the initial normal force.

Figure 5.20 shows the variation of normal stress due to increase of vertical load. The initial normal force is close to zero. The increasing amounts of normal forces were in inverse proportion to the magnitude of the initial normal forces.

In the specimen KJ-0-I, KJ-0-II and KJ-1-I, the biggest increments of normal force were observed. The specimens KJ-25-I and KJ-25-II showed a small change in the normal force. At the peak load, a small increase of the normal pressures had been observed.

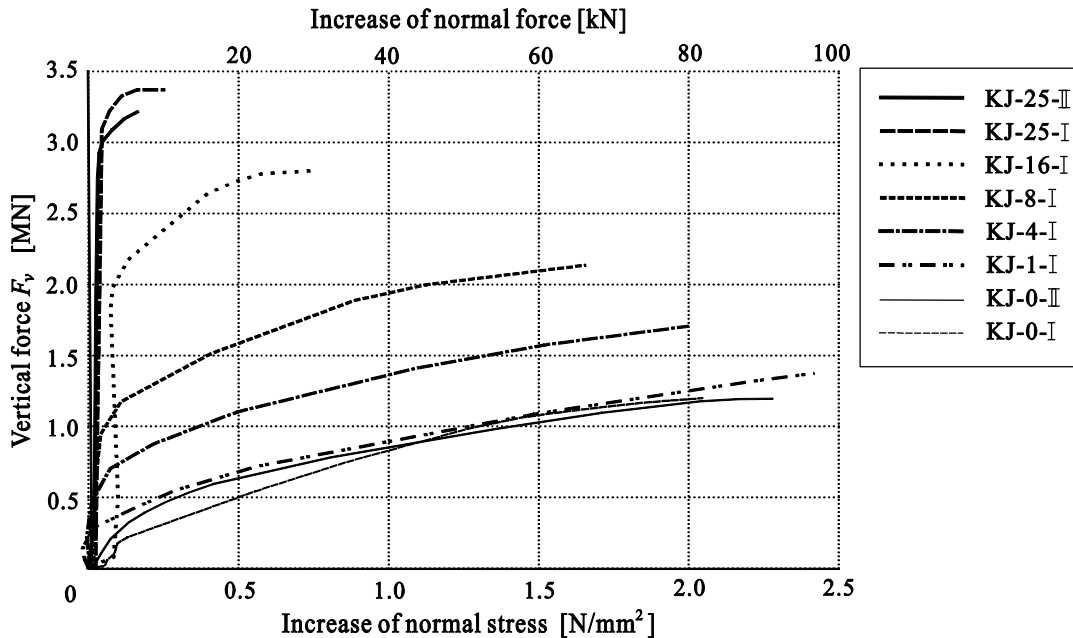


Figure 5.20: Normal stress versus shear force

### Variation of contact surfaces at key area

Figure 5.21 and Figure 5.22 illustrate a local joint opening at the shear key area measured by the crack displacement transducers. The horizontal axis of the diagrams presents the condition of contact (presence [-] or not [+]) at the surface. Negative displacements mean contact produced by the initial confining forces. Figure 5.21 shows a joint opening of the upper face of the key area. As shear load increases, the key areas are vertically constricted by the compressive stresses derived from the shear load. All specimens, excluding KJ-0-I and KJ-0-II, which have little initial confining pressure, had compressive stresses at the contact surfaces by the initial confining pressure before the loading. However, joints of these specimens opened with an increase of shear load. This means that the upper face at the key area cannot act as a contact surface with friction.

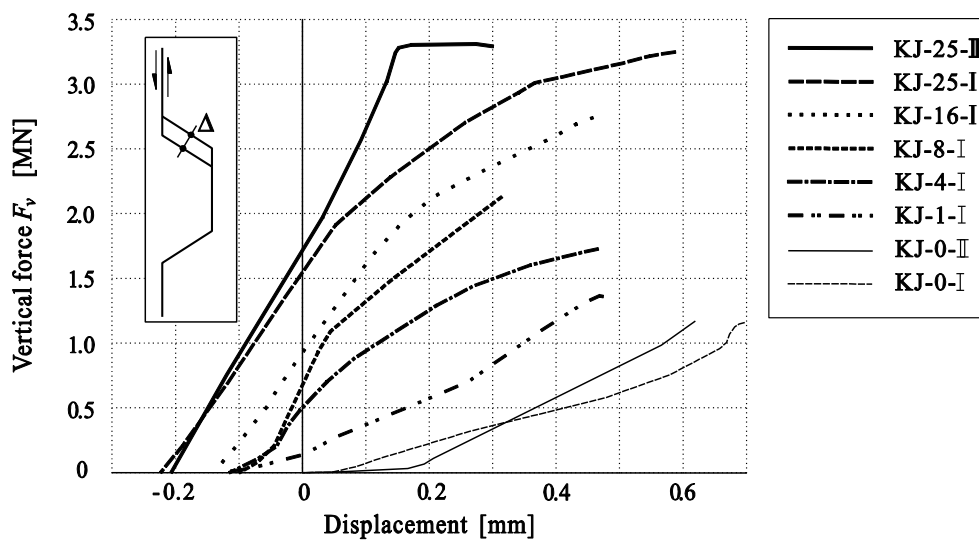


Figure 5.21: Joint opening at upper inclined face of key due to increasing load

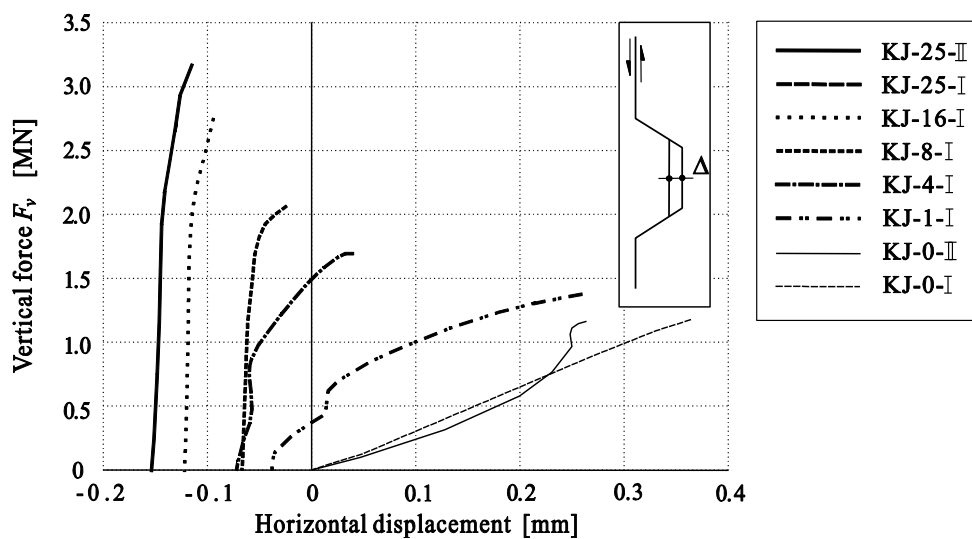


Figure 5.22: Joint opening at plane (vertical) face of key due to increasing load

Figure 5.22 shows that the joint opening of the upper face of the key area occurs due to the sliding of the key on the sloping surface (lower face of the key area). As described above, this joint opening is caused by relatively small confining stresses of the four specimens KJ-0-I, KJ-0-II, KJ-1-I and KJ-4-I in the tests. To prevent the sliding at key areas, therefore, it needs to determine the minimum compressive stress in PSB. A new approach will be introduced in Section 5.3.4 to predict the sliding, as a joint opening. In addition, the behaviour on the sloping surface in the tests will be compared to an analytical formula.

### 5.2.3.3 Crack pattern and failure mode

The crack development of dry keyed specimens is divided into three phases, as shown in Figure 5.23.

- Phase I* : no cracks
- Phase II* : development of diagonal cracks
- Phase III* : shear-off failure

The initial cracks, as diagonal cracks, always started at the lower face (surface c-d, see Figure 5.23) of the male key. The cracks developed with an upward angle of about  $45^\circ$ . At the maximum load, the width of the diagonal cracks increased. After maximum load, the typical shear-off failure of the keys occurred by a sudden slip of the middle part (see Figure 5.18).

Shear forces at a dry joint are transferred by means of two principal mechanisms: These are the friction between joint surfaces and a combination of shear and compressive stresses. Frictional forces are present along all surfaces of joints except upper surfaces of the key areas. The magnitude of the frictional force depends on the confinement level.

As mentioned in Section 5.1.1, the steel fibers at the shear cracks could easily be observed due to the great width of the cracks (see Figure 5.24). Almost all of the steel fibers were perpendicular to the crack growth direction in order to resist the tensile stresses.

After ultimate shear loads, all test specimens present continuous shear resistance as shown in phase (III). In particular, the specimens without normal force, KJ-0-I and KJ-0-II, carried the vertical load by the shear keys only without friction forces. In the specimens without or with little normal force, slippage occurred simultaneously with introduction of vertical load. Therefore, the effect of steel fibers has been demonstrated to improve the performance of shear stress transmission. The test specimens don't show a brittle failure.

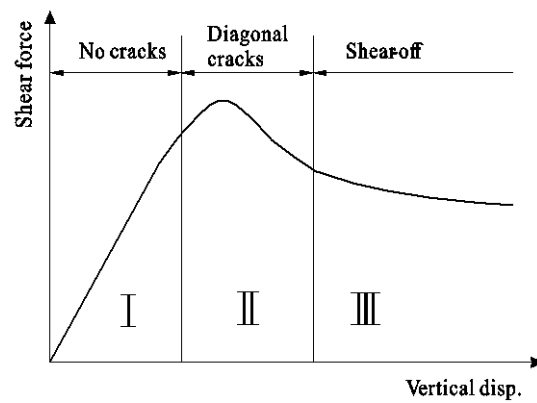
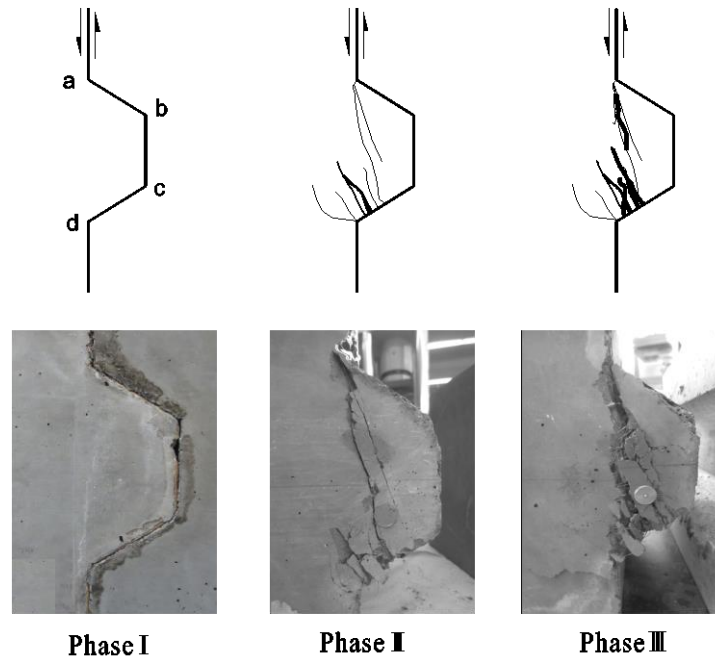


Figure 5.23: Cracking sequence with increasing shear load

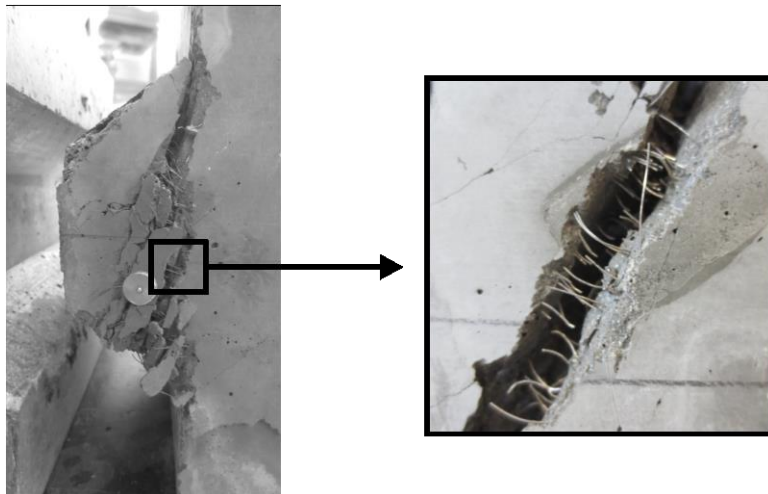


Figure 5.24: Steel fibers at cracks at maximum load

### 5.2.3.4 Comparison with test results and design models

The measured shear strengths of the tests had been compared with the various design models as shown in Figure 5.25. No safety factors are included in the analysis. The dimensions of the test specimen shown in Fig. 5.13 ( $A_k = 400 \text{ mm}^2$ ,  $A_{\text{joint}} = 200 \text{ mm}^2$ ) and  $f_{ck} = 185 \text{ MPa}$  are used. All design approaches presented relatively low shear force values compared to the test results. However, AASHTO specification overestimates the shear capacity when normal pressure increases over 30 MPa ( $f_{ck}/\sigma_n = 0.22$ ). This means that AASHTO formula is not appropriate for HSC or UHPC members.

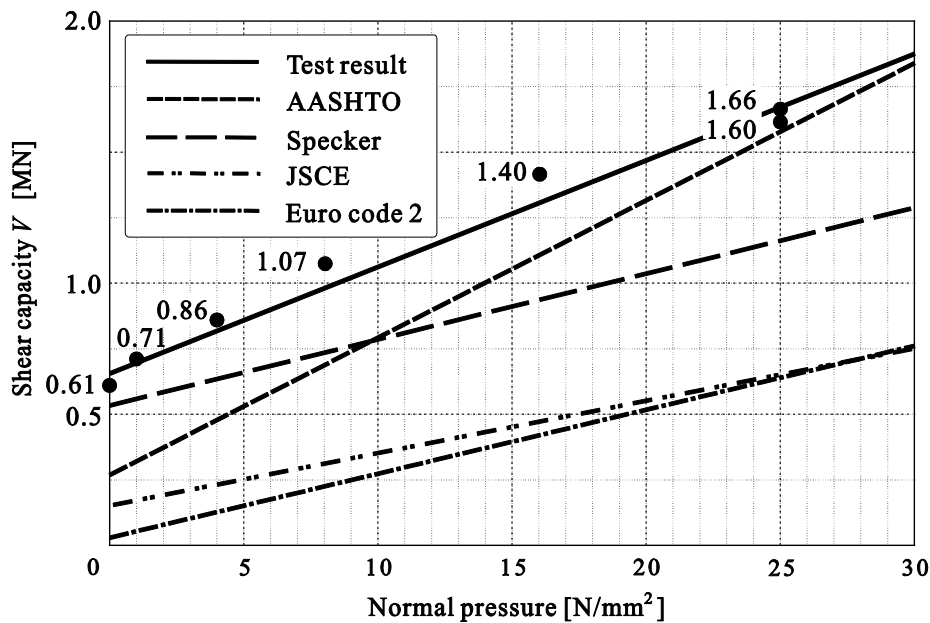


Figure 5.25: Comparison of shear capacity between test results and design models depending on the confining stress

On the other hand, JSCE and Eurocode 2 present low shear strengths compared to the test results. In particular, the shear strength of pure shear keys without normal pressure showed very low values compared to the experimental values and other design models.

The formula by Rombach and Specker shows a good agreement with the tests on the safe side. The different inclination of the two lines, formula and test result, are caused by different coefficient of friction (approx. 0.8 in tests and 0.65 according to analytical formula). Due to the low  $\mu$ -value of 0.65, the approach of Rombach and Specker was always conservative compared to the ultimate shear capacity of tests as the normal pressure increases.

Therefore, the formula suggested by Rombach and Specker is confirmed by the test results and is very appropriate for HSC and UHPC as well as NSC.



## 5.3 Finite element analysis of UHPC shear key tests

Following the tests, which presented failure mechanisms and behaviour of UHPC shear keys, a finite element analysis was performed with ABAQUS software [SIMULIA 2010] to investigate stress distributions during loading and to study the joint behaviour in more detail.

The 3D-FE-models of the UHPC test specimens are based on complex concrete models, which are described in the next Section. After that, the validation of the material models for NSC, HSC as well as UHPC, is discussed. Finally, in order to propose the new design formula, the pure performances of a shear-key due to concrete compressive strength are investigated.

### 5.3.1 Constitutive models for concrete

In the last decade, the number of numerical analyses of UHPC structures using FEM is increasing with researches of UHPC structural components. The FE program ABAQUS/STANDRD offers a general capability for modeling concrete in all types of structures including beams, trusses, shells and solids. Two different constitutive models for the analysis of concrete are used in this study: the concrete smeared crack (CSC) model and the concrete damaged plasticity (CDP) model. Both models can be applied to plain and reinforced concrete with rebar. They are based on two different failure mechanisms, which are tensile cracking and compressive crushing of the concrete material.

#### Concrete smeared crack (CSC) model

The CSC model has been designed for application of concrete which is subjected to monotonic straining at low confining pressures. It uses damaged elasticity concepts (smeared cracking) to present the response of concrete after cracking failure. Cracking is assumed to be the most important aspect of concrete behaviour, which occurs when the stress reaches a failure surface. The cracking, compressive and tensile responses of concrete in the CSC model are illustrated by the uniaxial behaviour of a material shown in Figure 5.26. Under low stresses, the material shows an elastic response. As the load is increased, inelastic straining occurs. After the material loses strength until it can no longer carry any higher loads, the material reaches an ultimate stress level. If the load is removed after inelastic straining has occurred, the ‘linear’ elasticity has been damaged.

The values of tension stiffening of reinforced concrete members are significant in the finite element analysis because more tension stiffening improve the speed of convergence of the analysis and make it easier to obtain numerical solutions.

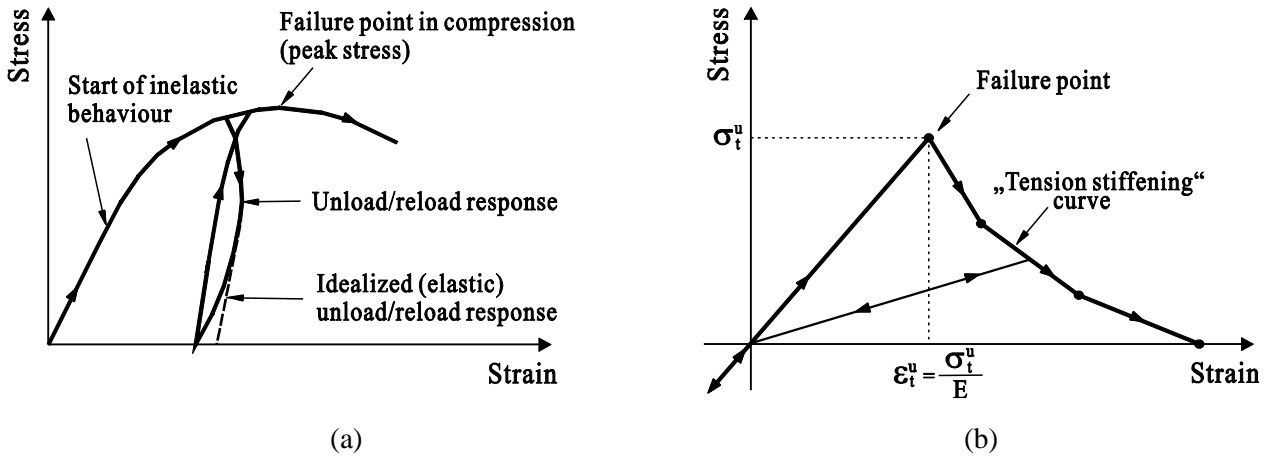


Figure 5.26: (a) uniaxial behaviour in compression and (b) tension stiffening for CSC model [SIMULIA 2010]

### Concrete damaged plasticity (CDP) model

In general, the CDP model can be considered for basic concrete materials in the FE simulations. The concepts of damaged elasticity and isotropic compressive plasticity are used in this material model. It can also be used for static and dynamic analyses, and accounts for stiffness recovery effects under cyclic loading.

Under low confining pressures, the main failure mechanisms of concrete are cracking in tension and crushing in compression. The compressive stress-strain relation of CDP model is shown in the Figure 5.27. The compressive behaviour is elastic until initial yield and then it is characterized by stress hardening after the ultimate stress. Similar to the CSC model, post-cracking behaviour of the CDP model can be accounted for by specifying a post stress-strain relation.

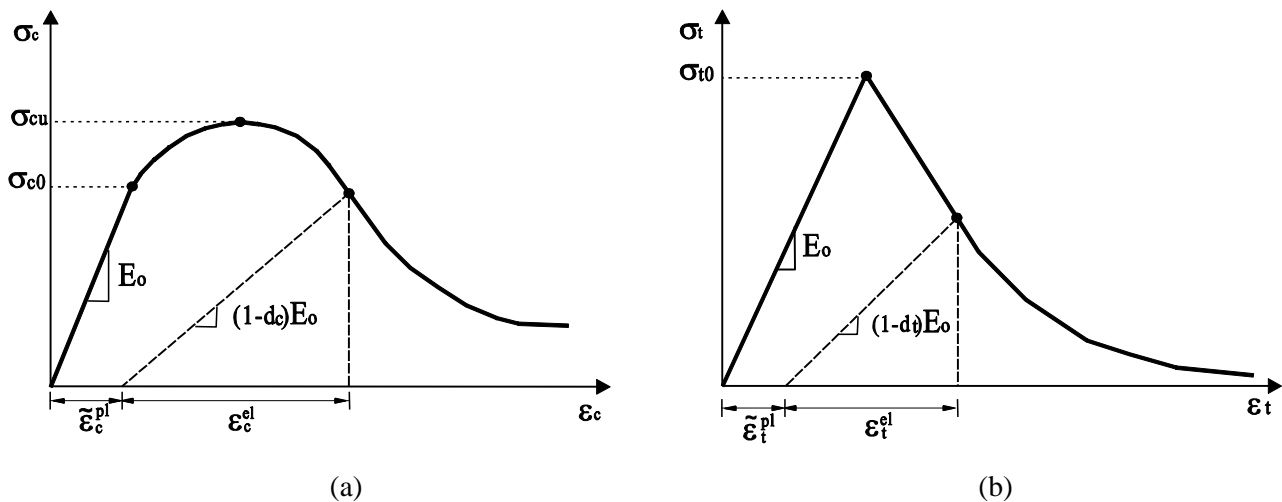


Figure 5.27: Uniaxial behaviour in compression (a) and in tension (b) for CDP model [SIMULIA 2010]

### 5.3.2 Nonlinear-FE model of UHPC shear keys

#### 5.3.2.1 Material model of UHPC

##### The nonlinear behaviour of UHPC

To represent the inelastic behaviour, the isotropic compressive plasticity and damaged elasticity material models are used in ABAQUS. Based on the idealized stress-strain curves of SFRC proposed by existing reports [Mansur et al. 1991], [Lim et al. 1987], the assumed nonlinear behavior of the UHPC is given in Figure 5.28. The uniaxial compression and tension curves of UHPC are used with the same input values for CSC and CDP models.

The compressive stress-strain relation used in the analysis is based on work by Mansur et al. [1991] for SFRC (see Figure 5.28 (a)). It consists of four stages which are an initial straight (elastic) portion, parabolic portion up to the maximum stress, straight descending portion up to  $\varepsilon_{co} = \varepsilon_{cu}$  and the residual stress level which remains constant with increasing strain. Thus, the curve can be described by the following equations:

$$\sigma_c = E_c \cdot \varepsilon_c \quad \text{for } \varepsilon_c \leq \varepsilon_c^{el} \quad (5.8)$$

$$\sigma_c = f_c \left[ \frac{2 \cdot \varepsilon_c}{\varepsilon_{co}} - \left( \frac{\varepsilon_c}{\varepsilon_{co}} \right)^2 \right] \quad \text{for } \varepsilon_c^{el} < \varepsilon_c \leq \varepsilon_{co} \quad (5.9)$$

$$\sigma_c = k' \cdot f_c + \frac{f_c (1 - k') (\varepsilon_{cu} - \varepsilon_c)}{(\varepsilon_{cu} - \varepsilon_{co})} \quad \text{for } \varepsilon_{co} < \varepsilon_c \leq \varepsilon_{cu} \quad (5.10)$$

$$\sigma_c = k' \cdot f_c \quad \text{for } \varepsilon_{cu} \leq \varepsilon_c \quad (5.11)$$

$$\text{where } k' = 0.38 V_f \frac{l_f}{\phi_f}$$

$$\varepsilon_{cu} = \varepsilon_{co} + \frac{0.041 - \varepsilon_{co} \cdot f_c}{f_c - 6.896}$$

In which  $l_f$ ,  $\phi_f$  and  $V_f$  are the length, equivalent diameter and volume fraction of fibers, respectively. The coefficient  $k'$  accounts for the effect of discrete fibres.

The behaviour of post-failure depends on the TENSION STIFFENING model in ABAQUS. The option can be defined as the strain-softening behaviour for cracked concrete. Similar to the curve in compression, the stress-strain relation in tension has been modified from that of SFRC suggested by Lim et al. [1987]. It consists of three stages, as shown in Figure 5.28 (b). The ascending stage is expressed as

$$\sigma_t = E_c \cdot \varepsilon_t \quad \text{for } \varepsilon_t \leq \varepsilon_{cr} \quad (5.12)$$

In the elastic portion, the maximum tensile stress terminates when the strain reaches  $\varepsilon_{cr}$ . The post-cracking stress is described by both the fracture energy and the residual tensile stress maintained by the bonding of fibers. The magnitude of the post-cracking stress,  $f_{tu}$ , is given in Eq. (5.13).

$$\sigma_t = f_{tu} \quad \text{for } \varepsilon_t > \varepsilon_{cr} \quad (5.13)$$

$$\text{where: } f_{tu} = 2 \eta_l \eta_o \tau_{uf} V_f \frac{l_f}{\phi_f}$$

In which  $\eta_l$ ,  $\eta_o$  and  $\tau_{uf}$  are the length efficiency factor for fibers, fiber orientation factor and ultimate bond strength of fibers. The values used in the FE model (TENSION STIFFENING in ABAQUS) are  $\eta_l = 0.5$ ,  $\eta_o = 0.33$  and  $\tau_{uf} = 4.12$  MPa, respectively.

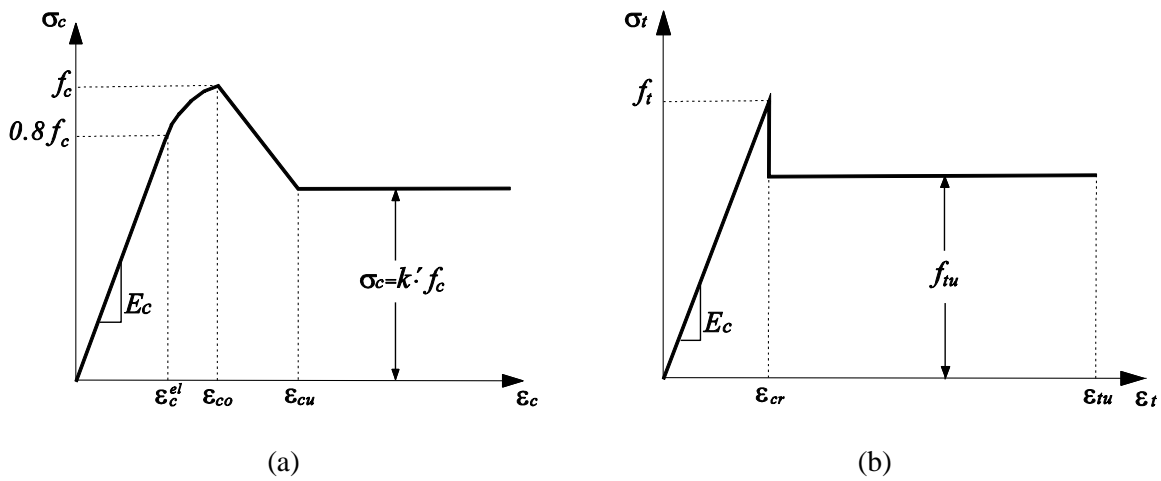


Figure 5.28: Constitutive models for UHPC with steel fibers in (a) uniaxial compression [Mansur et al. 1991] and (b) uniaxial tension based on [Lim et al. 1987]

### The parameters for nonlinear behaviour

Table 5.4 presents the material parameters, which are based on UHPC cylinder tests (see Appendix B.2) and the biaxial UHPC compressive strength tests by Curbach and Speck [2007], used for nonlinear analyses with CDP and CSC models.

In CSC model, the failure surface is defined by ‘FAILURE RATIOS’ and ‘SHEAR RETENTION’. Four failure ratios are as follows:

- The ratio 1: the ratio of the ultimate compressive stress in biaxial to the ultimate compressive stress in uniaxial.
- The ratio 2: the absolute value of the ratio of the ultimate tensile stress in uniaxial to the ultimate compressive stress in uniaxial.
- The ratio 3: the ratio of the magnitude of a principal component of the ultimate compressive plastic strain in biaxial to the ultimate compressive plastic strain in uniaxial.

- The ratio 4: the ratio of the tensile principal stress at cracking, when the other principal stress is at the ultimate compressive value, to the tensile cracking stress in uniaxial.

The shear stiffness in the cracked concrete is decreased. It is defined by specifying the reduction in the shear modulus as a function of the opening strain across the crack. The shear stiffness of open cracks reduces linearly to zero as the width of cracks increases. The assumption of the shear retention model in ABAQUS is as follows: The modulus for shearing of cracks:  $\varrho \cdot G$

Where  $G$ : the elastic shear modulus of the uncracked concrete  
 $\varrho$ : a multiplying factor.

$$\begin{aligned} \varrho &= (1 - \varepsilon/\varepsilon^{max}) & \text{for } \varepsilon < \varepsilon^{max} \\ \varrho &= 0 & \text{for } \varepsilon \geq \varepsilon^{max} \end{aligned}$$

Where  $\varepsilon$  is the direct strain across the crack and  $\varepsilon^{max}$  is a user-specified value. The model also assumes that cracks that subsequently close have a reduced shear modulus:

$$\varrho = \varrho^{close} \quad \text{for } \varepsilon < 0$$

$\varrho^{close}$  and  $\varepsilon^{max}$  can be defined with an optional dependency on temperature and/or predefined field variables.

Table 5.4: Material parameters of CDP and CSC models for the UHPC with steel fibers used in the FEA

Density [kg/m <sup>2</sup> ]		2.383
<b>Concrete elasticity</b>		
E-module[GPa]		50.0
Poisson's ratio (v)		0.19
<b>The parameters of CDP model</b>		
Dilation angle ( $\psi$ )		15°
Eccentricity ( $\epsilon$ )		0.1
$\sigma_{bo} / \sigma_{co}$		1.0
$K_c$		0.667
Viscosity ( $\mu$ )		0
<b>The parameters of CSC model</b>		
Failure ratio	Ratio 1	1.0
	Ratio 2	0.07
	Ratio 3	1.28
	Ratio 4	0.333
Shear retention	Rho_close	1.0
	Eps_max	0.1

As for plasticity parameters, the CDP model requires the following five parameters:

- Dilation angle ( $\psi$ )
- Flow potential eccentricity ( $\epsilon$ )
- The ratio of initial equibiaxial compressive yield stress to initial uniaxial compressive yield stress  $\sigma_{bo} / \sigma_{co}$
- The ratio of the second stress invariant on the tensile meridian to that on the compressive meridian ( $K_c$ ). It must satisfy the range  $0.5 < K_c < 1.0$
- Viscosity ( $\mu$ ) used for the visco-plastic regularization of the concrete. The default value is 0.0

Considering the characteristic of UHPC as concrete, the defaults of the above parameters were defined as shown in Table 5.4.

Details about the material models can be found in ABAQUS Analysis user's Manual.

### 5.3.2.2 Modeling of the shear-key specimens

In all FE-models the half of the specimen with proper boundary conditions is taken into account because of symmetry to reduce computation time. 3D hexahedral (brick) elements with quadratic approximation of displacements are used. The width of the inner section had been increased to 150 mm (instead of 100 mm in the real test specimen, see Fig. 5.13) to get a more uniform normal stress distribution in the joint area. The behaviour of the joint is not affected.

To apply the confining pressure in the model, the horizontal displacement values (without vertical load) measured from tests were utilized to define an equivalent displacement load in ABAQUS. In the contact surfaces of vertical load and confining pressure, the rigid body option instead of the steel plates used in the tests were applied in all models (see Figure 5.29).

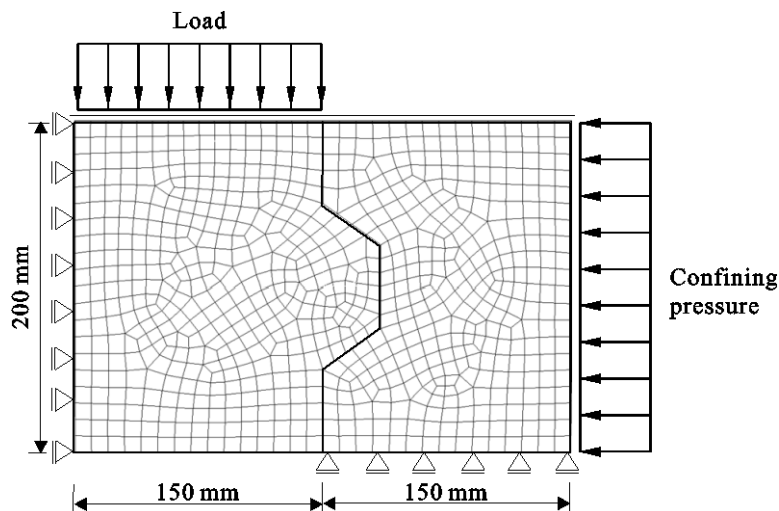


Figure 5.29: Finite element mesh, boundary conditions and loading system in the FE models

As surface-to-surface contact, the interactions between UHPC parts were defined as follows:

- *friction coefficient  $\mu$* : 0.8 (measured from the flat joint tests)
- *tangential behaviour*: friction formulation → penalty  
friction directionality → isotropic
- *normal behaviour*: pressure-overclosure → “Hard” contact  
allowed separation after contact

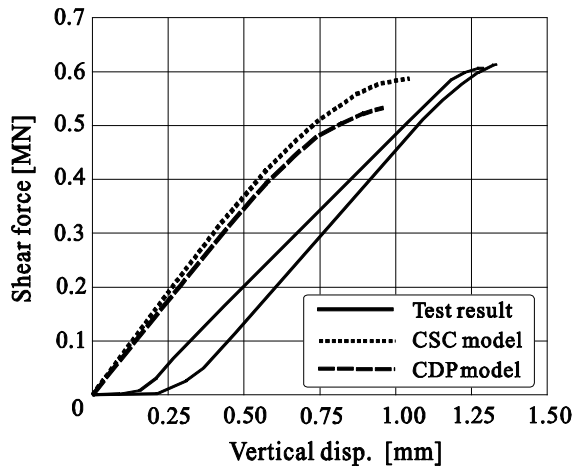
### 5.3.3 Verification of FE models

The FE analyses had been conducted to study the behaviour of UHPC shear keys. The numerical model takes the global joint opening as the sliding on the sloping surface and local joint opening of the upper face at key areas into account. The stress distribution before failure due to the relative magnitude of normal and shear forces is calculated. In the analysis, the failure of shear key specimens was considered when the compressive stress reaches the ultimate value (or the load decreases).

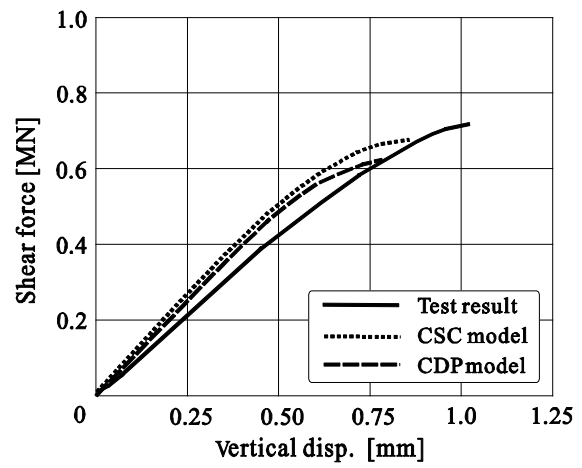
The nonlinear FE models were verified by comparing the numerical with test results as illustrated in Figure 5.30. The load-vertical displacement curves show a good agreement. The two FE-models (CSC and CDP), which show quite similar results, give a lower shear capacity and smaller displacements. Also, the models with low confining pressure (or not) presented slightly lower stiffness than the test results. It is guessed that the difference is due to the movement of both side parts with female-key when the vertical loads are applied in the tests. In test KJ-0 with minor confining pressure a vertical movement of around 0.25 mm was needed to get the shear keys in full contact. This slippage is not considered in the numerical analysis.

These FE-analysis also provide the behaviour and the stress distributions, which are in the middle Section of the specimen's thickness, in all the tests. It has to be noted, that the FE-model assumes a constant stress over the thickness of the element (plane strain condition) whereas the stresses in the real test specimen may decrease to the outer surfaces. Figure 5.31 shows the stresses in the CSC and CDP models of the test specimens with 1 MPa and 25 MPa normal pressures, respectively. As normal pressure increased from 0 to 25 MPa, the maximum compressive stress zones on the root of the keys, which are associated with shear-off failure of the keys, increased. In the tests with low normal pressure (KJ-0 and KJ-1), as concrete crushing, the diagonal cracks (see Appendix B.5) developed more than in the other specimens, which are under high normal pressures. The FE models also show sliding of the specimens on the inclined surfaces (see Figure 5.31 (a) and (b)).

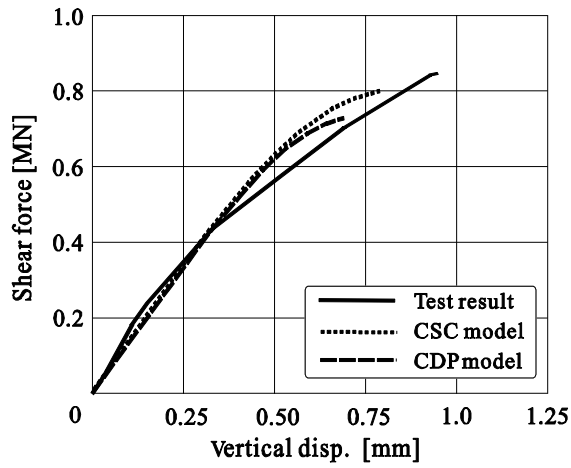
The shear capacity of six tested keyed dry joint specimens are shown in Figure 5.32 in relation to the confining pressure. The two FE-models give slightly smaller values compared to the test results. However, the shear to normal force relation of both numerical models is very similar to that of the tests. Thus, it means that the FE models are reliable and conservative in predicting the shear capacity of keyed dry joints, especially, CSC approach gives slightly more accurate values than CDP models compared to the test results.



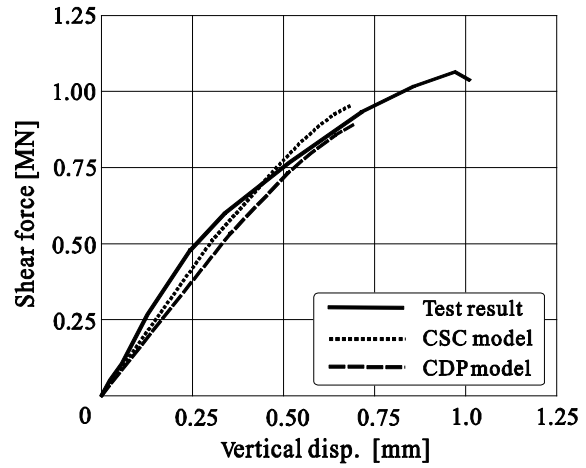
(a) KJ-O



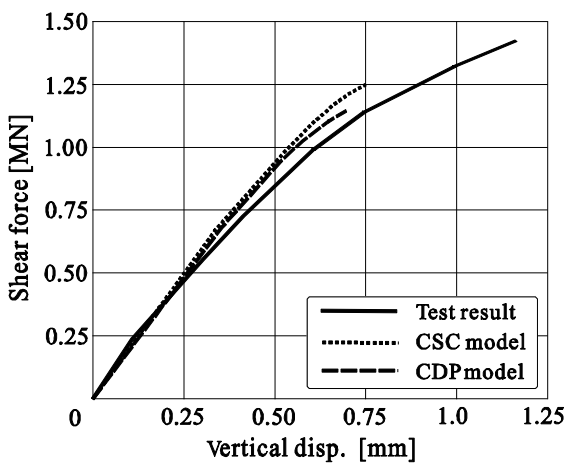
(b) KJ-1



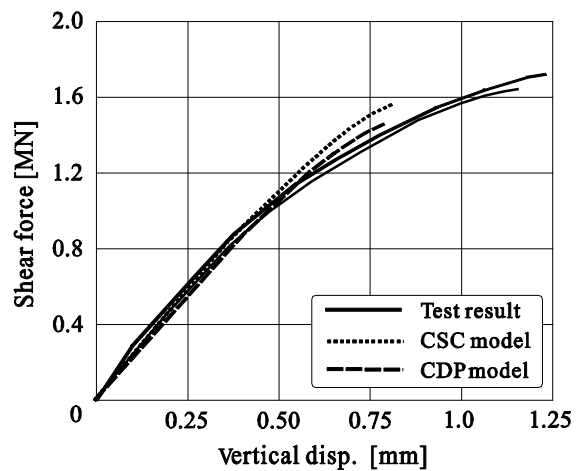
(c) KJ-4



(d) KJ-8



(e) KJ-16



(f) KJ-25

Figure 5.30: Comparison of load-deflection curves between the test results and the FE models



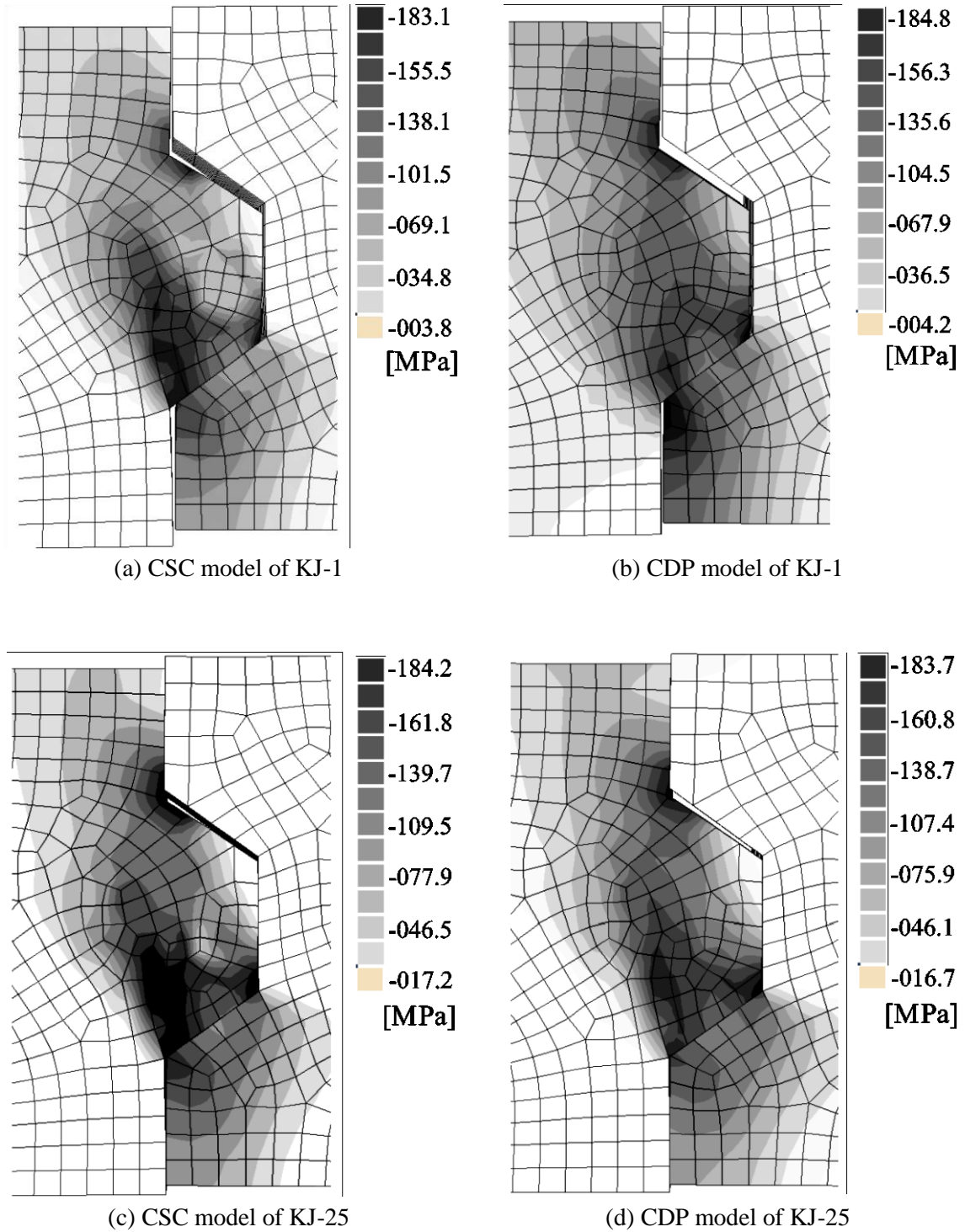


Figure 5.31: Deformations and principal compressive stress distributions at the peak load of FE models

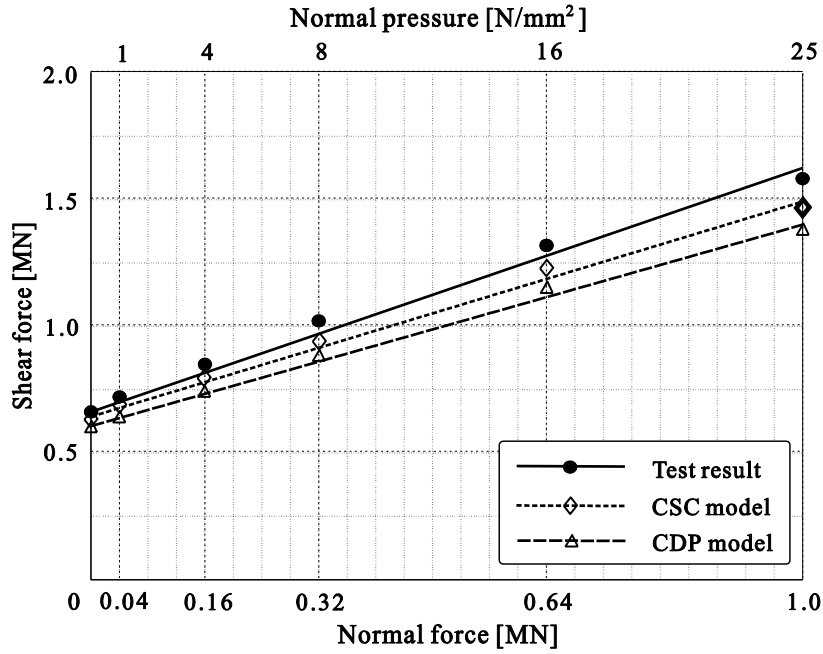


Figure 5.32: Comparison of the test results and FE analysis

### 5.3.4 Sliding on inclined contact surface at a key area

In the FE analysis and the tests, the sliding on the inclined contact surface has been observed as a joint opening (see Figure 5.21 and Figure 5.31). This Section provides the analytic formulation for the sliding, and comparisons with the results of the FE analysis and the tests.

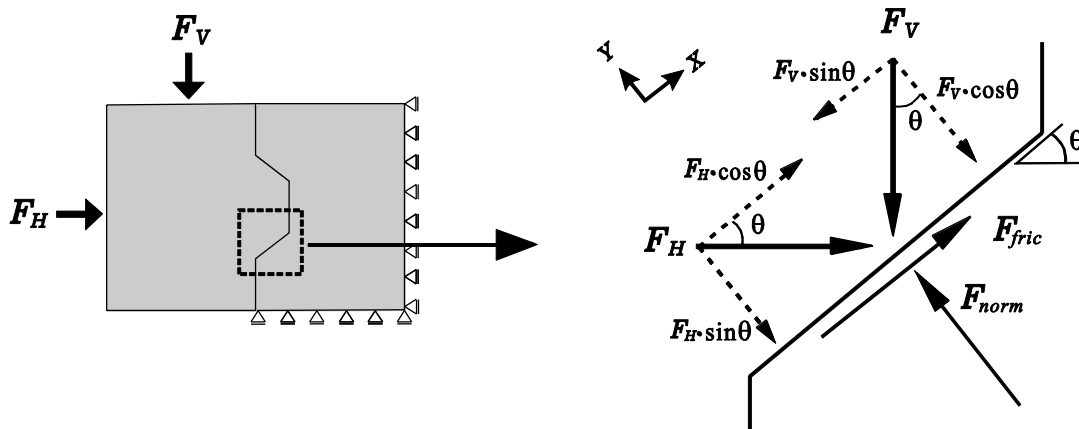


Figure 5.33: Force components on an inclined surface at shear key area for downward slippage

Figure 5.33 presents the force components, which consist of a vertical force,  $F_V$ , horizontal force,  $F_H$ , and frictional force,  $F_{fric}$ , on an inclined surface at the shear key area. Force transfer through the other parts of the specimen (e.g. vertical surfaces) are neglected.

When  $F_H > 0$ , as shown in Figure 5.33, then the horizontal and vertical forces on an inclined surface are as follows:

$$\Sigma F_x = 0 ; \quad F_{fric} + F_H \cos \theta \leq F_V \sin \theta + \quad \rightarrow \quad \text{sliding downwards}$$

$$\Sigma F_y = 0 ; \quad F_{norm} = F_V \cos \theta + F_H \sin \theta$$

$$\text{with:} \quad F_{fric} \leq \mu F_{norm} \quad \rightarrow \quad F_{fric} \leq \mu (F_V \cos \theta + F_H \sin \theta)$$

Where  $F_{fric}$  Frictional force  
 $\mu$  Coefficient of friction

Taking the sum of forces, the relative ratio of horizontal force ( $F_H$ ) and vertical force ( $F_V$ ) is as follows:

$$\frac{F_V}{F_H} = \frac{\cos \theta + \mu \sin \theta}{\sin \theta - \mu \cos \theta} \quad (5.14)$$

For  $\theta = 90^\circ$  (flat joints without shear keys) the ratio is equal to  $F_V/F_H = \mu$ . Without normal force ( $F_H = 0$ ), the frictional coefficient ( $\mu$ ) is  $\tan 34.5^\circ \approx 0.7$ . When  $\mu < 0.7$  and Eq. (5.14) has positive values, the sliding on the inclined surface occurs due to the self-weight of specimens without confining pressure. In the flat joint tests, the sliding actually started at  $\mu = 0.6$  (see Fig. 5.16 and Fig. B.9). With a frictional coefficient  $\mu = 0.6$  and the inclination angle ( $\theta$ ) of  $34.5^\circ$ , therefore, the ratio is as follows:

$$F_V/F_H = 16$$

When the ratio is higher than 16 the sliding begins. Table 5.5 presents the ratio of maximum shear loads and normal forces in all the specimens, and the presence, or lack thereof, of the sliding on the sloping surface in the tests and FE models. The sliding formulation with the ratio of  $F_V/F_H$  predicts a sliding of specimens KJ-0-I, KJ-0-II and KJ-1-I. This is in good agreement with the experimental and numerical results. In the specimen KJ-4-I, the sliding occurred only slightly before the failure.

Table 5.5: Comparison with sliding progress between the formulation, test result and FEA

Test specimens	Maximum shear load ( $F_{v,test}/2$ ) [kN]	Initial normal force ( $F_{h,test}$ ) [kN]	$F_{v,test} / 2 F_{h,test}$	Sliding progress	
				in test	in FEA
KJ -0- I	609.1	0.7	870.14	O	O
KJ -0- II	606.6	1.2	505.50	O	O
KJ -1- I	710.5	39.6	17.94	O	O
KJ -4- I	861.2	160.3	5.37	O	X
KJ -8- I	1073.4	320.1	3.35	X	X
KJ-16- I	1404.5	636.1	2.21	X	X
KJ-25- I	1609.1	999.2	1.61	X	X
KJ-25- II	1659.6	999.8	1.66	X	X

As shown in Figure 5.31 (a) and (b), the FE models of test specimens KJ-0-I, KJ-0-II and KJ-1-I presented the sliding on the lower faces (sloping surfaces) at the key areas. In the FE model of specimen KJ-4-I, however, no sliding (any joint opening) was observed in both models. Because the maximum shear load,  $F_V$ , is smaller than that of the test results and no movement of sides parts due to the displacement loads in the FE models, it is estimated that the ratios,  $F_V / F_H$ , of the tests are larger than that of the FE models.

Considering the global joint opening due to the sliding on sloping surfaces (upper face or lower face at shear key area), the minimum required compressive stress across the joints in PSB must be determined in accordance with the sliding formulation.

### 5.3.5 Shear strength of shear key without confining pressure

Shear strength of a shear key without confining pressure depends on the concrete compressive strength. The first crack occurs when concrete crushes and diagonal cracking starts at a key area. However, the ultimate shear capacity is not directly proportional to concrete compressive strength. Figure 5.34 presents a comparison of shear capacity of UHPC and NSC keys, which had the same configuration as the test specimens tested by Specker [2001]. Despite the compressive strength of UHPC is 4.7 times higher than that of NSC, the ultimate shear load of the UHPC member presented a difference of about 3.2 times. This means that the existing formula cannot be used for HSC or UHPC. Thus, a modification factor for various concrete compressive strengths is required for dry keyed joint design.

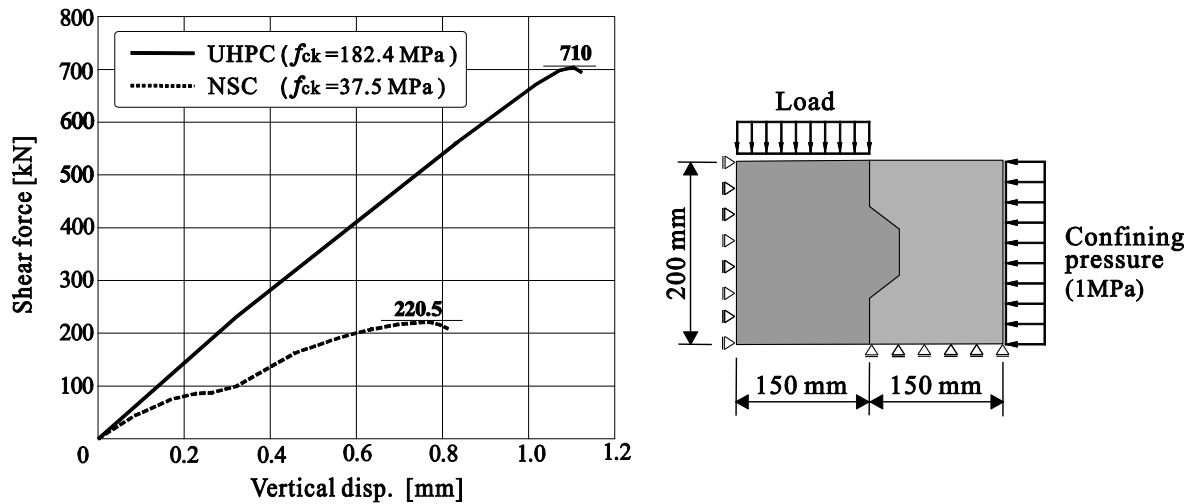


Figure 5.34: Comparison of shear strength between NSC [Specker 2001] and UHPC shear key (KJ-1-I)

A FE-study of shear capacity with NSC, HSC and UHPC shear keys was also conducted in terms of the load-vertical displacement relation.

The test results for biaxial compressive strength, which include NSC, HSC and UHPC, obtained from [Curbach, Speck 2003] and [Curbach, Speck 2007], have been used in the CSC material

models as shown in Figure 5.35. The uniaxial compressive strengths were defined according to Eurocode 2.

To define the strain-softening behaviour for cracked concrete, the post-failure *stress-displacement response* was modeled with the tension stiffening of displacement type ( $u_0 = 0.1$  mm), determined primarily by the opening at the cracks, in CSC material models as given in Figure 5.36. In situations with none reinforcement, the tension stiffening can be characterized by a simple linear stress-displacement response. The displacement referred to here is the crack width.

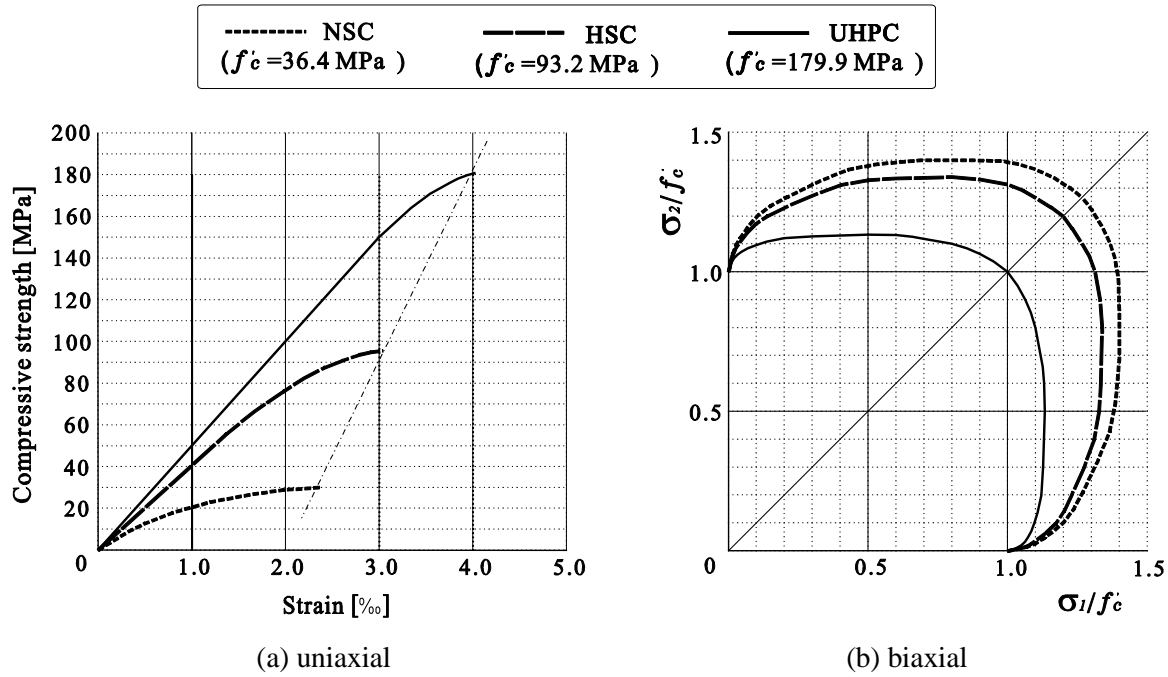


Figure 5.35: Compressive strengths of NSC, HSC and UHPC [Curbach 2007] used in FE investigation

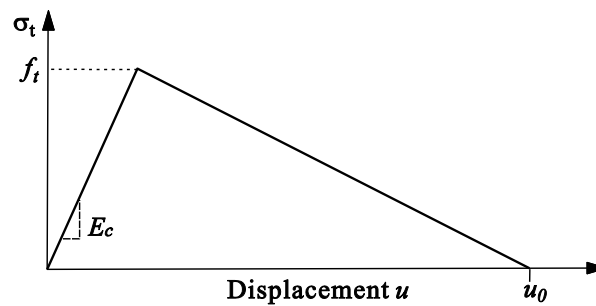


Figure 5.36: Post failure behaviour for tension stiffening in ABAQUS

The mean concrete tensile strength,  $f_{cm}$ , according to [EC2] was used in the FE analysis. The secant modulus of elasticity,  $E_{cm}$ , is taken from [DIN 1045-1]. For different concrete classes, the tensile strength and modulus of elasticity of concrete were given by:

$$f_{ctm} = 0.3f_{ck}^{2/3} \leq C50/60 \quad (5.15)$$

$$f_{ctm} = 2.12 \ln\left(1 + \frac{f_{cm}}{10}\right) > C50/60 \quad (5.16)$$

Where:  $f_{ctm}$  is the mean value of axial tensile strength of concrete

$$E_{cm} = 9500(f_{ck} + 8)^{1/3} \quad (5.17)$$

Figure 5.37 shows the computed shear capacity of dry keyed joint without confining pressure due to different levels of concrete compressive strength. The three curves show similarity with those of uniaxial compressive stress-strain curves. Higher strength concrete models presented larger vertical displacement (at the maximum shear load) and larger elastic region than lower strength concrete models. This demonstrates that the shear resistance of dry keyed joints greatly depends on the concrete compressive strength.

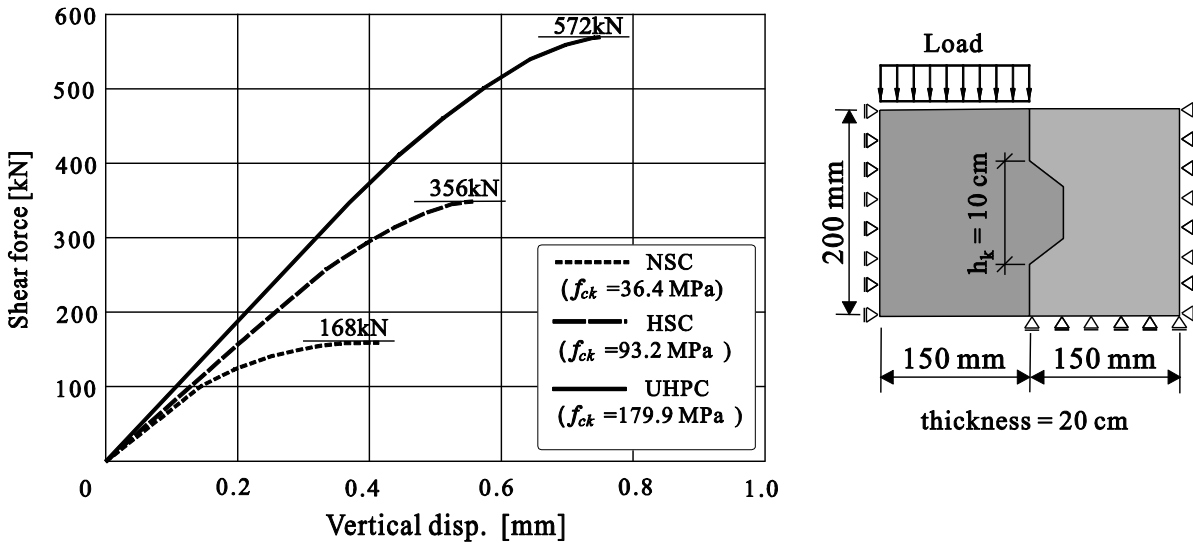


Figure 5.37: Shear capacity of dry keyed joint due to different levels of concrete compressive strength (FE-analysis)

From the results of nonlinear FE analysis, the relationship between shear capacity and concrete compressive strength can be represented as a linear function (see Fig. 5.38):

$$\tau_{\max} = F_v/A_k = 0.14 f_{ck} + 3.82 \quad [\text{MN}, \text{m}^2, \text{MPa}] \quad (5.18)$$

The results will be used for a new design formula, which will be explained in the next Section.

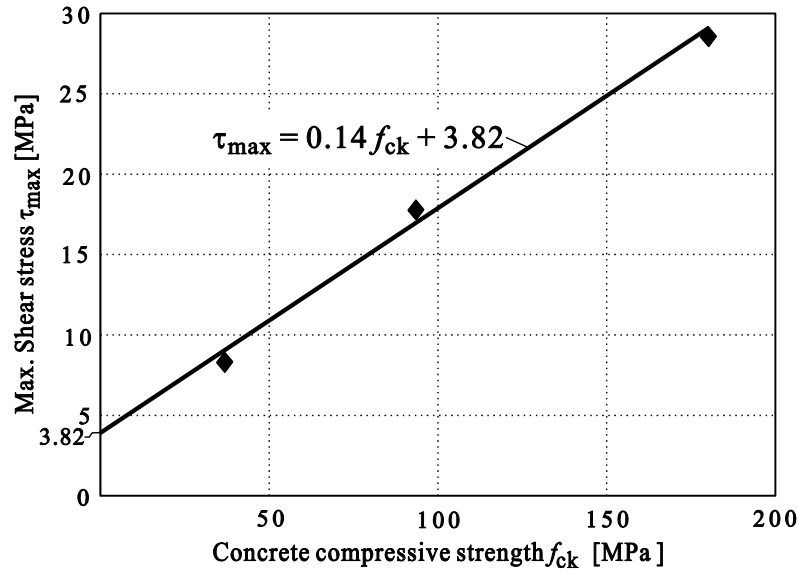


Figure 5.38: Relationship between shear capacity and concrete compressive strength of a shear key

## 5.4 New model for shear key design

Indented dry joints are one of the most important techniques in segmental construction method. Nevertheless, the existing methods present big differences as has been shown in Section 5.1.1. A more reliable and safe design model is needed.

Based on the results obtained from the tests, numerical simulations and the formula by Rombach and Specker (see equation 5.4), a new formula, which can be applied for HSC or UHPC joints, is introduced in this Section.

### 5.4.1 Shear strength of pure shear key

#### Shear strength of shear key

As expected, indented surfaces are very important for the capacity of dry joints. The shear keys act as an interlocking mechanism. Under the same level of normal stress, the presence of shear keys in the joint greatly increases the shear resistance in comparison to a plain joint (without shear keys). A shear key constantly carries vertical loads regardless of normal pressure as shown in Figure 5.39. After the sliding on the sloping surface (Figure 5.39 (a)), the shear load is mainly transferred through the contact of the sloping surface at the key area, as the formation of a compression strut (as shown in Figures 5.31 (a) and (b)). Without the sliding on the sloping surface (Figure 5.39 (b)), shear keys resist vertical loads with frictional forces on the contact surfaces

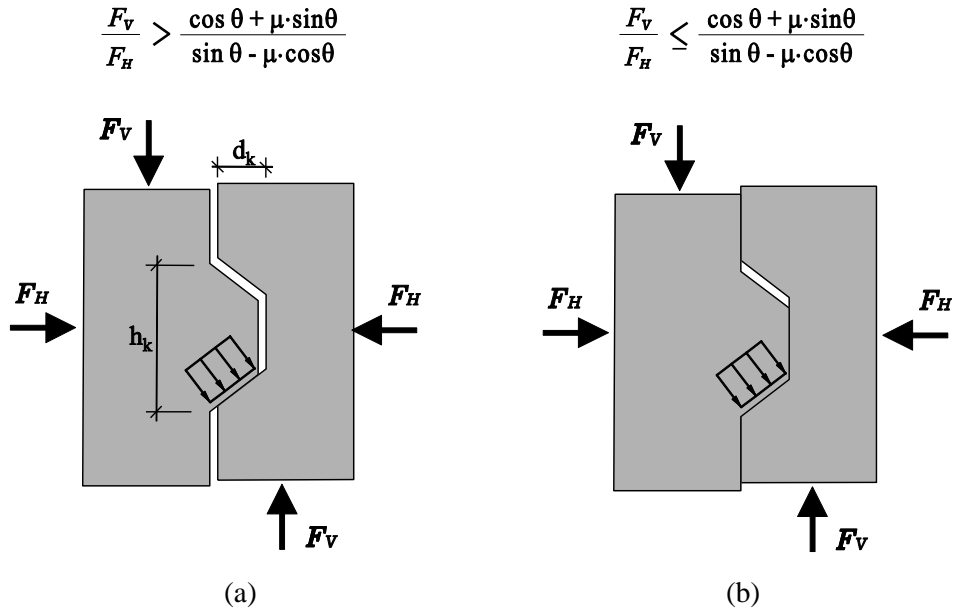


Figure 5.39: Shear resistance of shear key due to the compression strut:  
 (a) with joint opening by sliding (b) without joint opening

The shear capacity of a shear key without confining force depends on the area of shear keys and the concrete compressive strength. Therefore, the shear strength of pure shear key can be simply considered as follows:

$$V_k = f \cdot A_k \cdot f_{ck} \quad (5.19)$$

Where  $V_k$  is the shear capacity of pure shear key, as the resistance of the compression strut mechanism, and  $f$  is the shear key factor defined by the maximum shear stress of a shear key and the concrete compressive strength. The shear key area,  $A_k$ , is the same as mentioned in the previous Section (see Figure 5.43).

### Relation between concrete compressive strength and shear strength of a shear key

In keyed dry joints, the shear capacity depends on the normal force, the concrete compressive and the concrete tensile strength, the configuration of shear key and the area of shear key,  $A_k$ .

As mentioned in the previous Section, higher concrete compressive strength increases the shear capacity. However, the behaviour is not directly proportional to the concrete compressive strength. Thus, a modification factor for a shear key of different concrete classes is required. The shear key factor can be presented as a linear function, which is calculated by means of the FE analysis (see Figure 5.38), for different concrete compressive strengths. Figure 5.40 shows the values of factor  $f$  from conventional concrete ( $f_{ck} = 30$  MPa) to UHPC ( $f_{ck} = 200$  MPa).



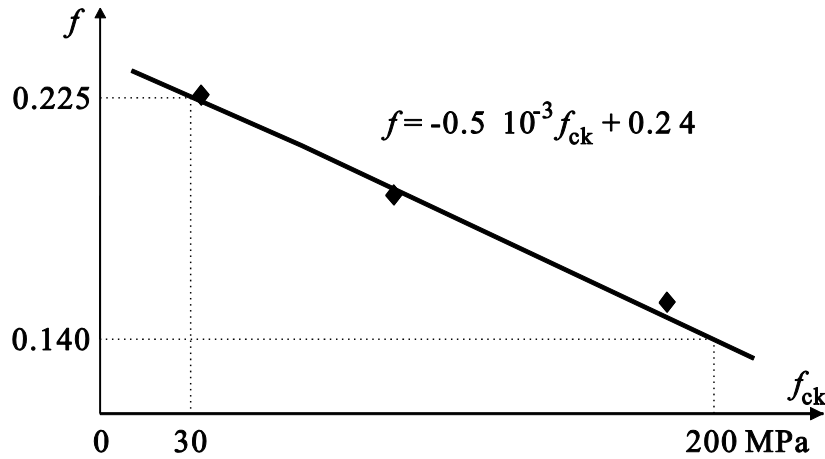


Figure 5.40: Relationship between factor  $f$  and concrete compressive strength

The shear key factor  $f$  is restricted to the general shear key geometry from SES standard segment, which has an inclination angle  $\theta = 35.54^\circ$ . If the value of  $\theta$  is different, the factor  $f$  must be slightly changed to suitable values. In the early studies, e.g. [Bakhoun 1991], [Specker 2001] etc., it was demonstrated that the inclination angle is not an important parameter for the load bearing capacity of shear keys. The shear resistance of dry keyed joints depends greatly on concrete compressive strength,  $f_{ck}$ , and normal pressure,  $\sigma_n$ .

#### 5.4.2 Frictional resistance between contact surfaces

The shear strength of the joint,  $V_f$ , depends on the coefficient of friction,  $\mu$ , the normal stress,  $\sigma_n$ , and the cross-sectional area of the joint,  $A_j$ . It can be described by the following equation:

$$V_f = \mu \cdot \sigma_n \cdot A_j \quad (5.20)$$

When the sliding on the sloping surface occurs (see Figure 5.39 (a)), however, the joint opening between the segments starts which means that the frictional resistance (against slipping along the failure plane) at contact surfaces is lost. Thus, frictional resistance can be maintained when the plain surfaces are in contact and compressed. If the horizontal force is kept constant, like in a real bridge, the friction force is independent of any joint openings as  $F_V = \mu \cdot F_H$  as long as the friction coefficient does not change.

Figure 5.41 presents the friction behaviour which includes the joint opening at the upper face of the key area when the vertical load,  $F_V$ , is applied. This separation of two parts has been demonstrated in the experiments (see Figure 5.21) and in the FE analyses (see Figure 5.31). The area of the upper inclined face of the key should be eliminated in the total joint area. Considering the actual contact surfaces, the cross-sectional area of the compressive zone at the joint can be defined as follows:

$$A_j = A_c - d_k \cdot b_k \cdot \tan\theta \quad (5.21)$$

Where  $A_c$  is cross-section of the joint,  $d_k$  and  $b_k$  are the depth and the thickness of shear keys respectively and  $\theta$  is the inclination of shear keys to horizontal. Based on test results (see Section 5.2.3.1) and the previous FE-studies (see Section 5.1.2) for the friction coefficient of concrete, a value  $\mu = 0.65$  is recommended.

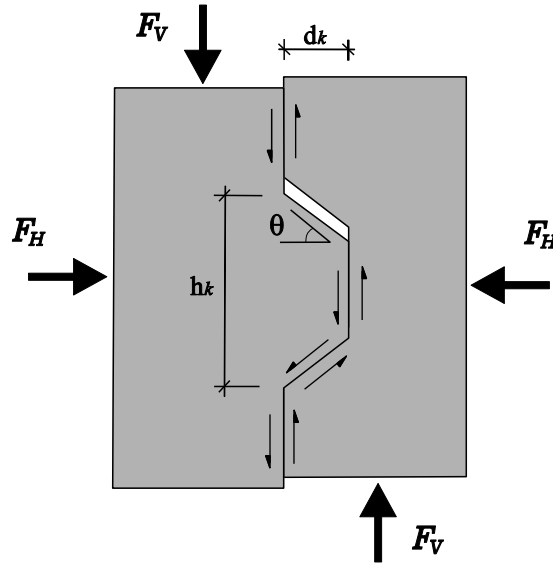


Figure 5.41: Friction behaviour at the contact surfaces

### 5.4.3 New proposal

#### Concept for new design model

The tests and the corresponding FE-simulations have demonstrated that the shear capacity of keyed dry joints only relies on two components:

- Shear resistance,  $V_c$ , of compression strut mechanism on sloping contact surfaces (upper face or lower face) at key area
- Frictional resistance,  $V_f$ , along the plain surfaces of the joints (concrete to concrete contact)

Therefore, the maximum shear force,  $V_j$ , for keyed dry joints can be defined in terms of the above two components as follows:

$$V_j = V_c + V_f \quad (5.22)$$

The relation between these two components on Mohr's circle is shown in Figure 5.42. In the simple equation, the magnitude of the initial shear stress ( $\sigma_n = 0$ ) greatly depends on the shear key factor  $f$  and the inclination depends on the coefficient of friction ( $\mu$ ). This results in a constant increase of shear stress with increasing normal pressure.

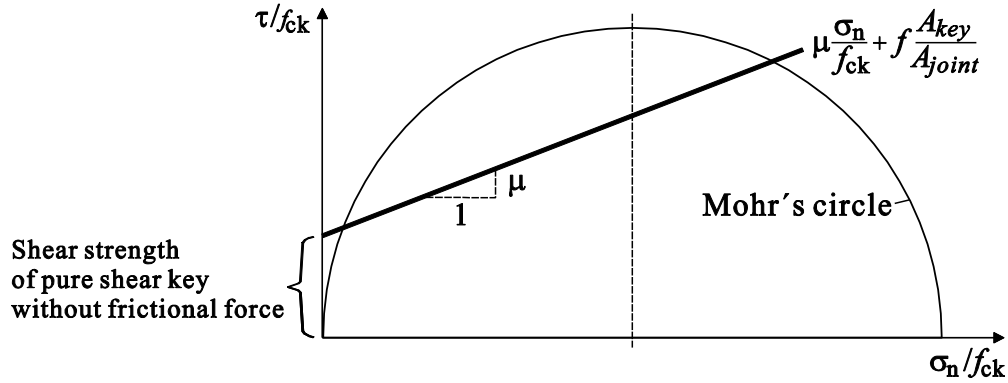


Figure 5.42: Concept for new proposal design on Mohr's circle

### Proposed new design model

As mentioned above, the shear capacity of a keyed dry joint,  $V_j$ , is a combination of a shear resistance of the key area,  $A_k$ , and frictional resistance on contact surfaces,  $A_j$ . Thus, a new proposed design for keyed dry joints, including HSC and UHPC as well as NSC, can be expressed as follows [Specker 2001, Rombach 2004]:

$$V_j = \mu \cdot \sigma_n \cdot A_{joint} + f \cdot f_{ck} \cdot A_k \quad (5.23)$$

Where :	$V_j$	shear strength of the dry joint [MN]
	$\mu = 0.6$	coefficient of friction (concrete to concrete)
	$\sigma_n$	average compressive stress across the joint ( $= F_h/A_{joint}$ ) [MPa]
	$A_{joint}$	the cross-sectional area of the compressive zone at the joint ( $= b_w \cdot h$ )
	$d_k$	depth of shear key
	$b_k$	width of shear key ( $b_k = (b_{k1} + b_{k2})/2$ )
	$f$	factor for the indentation of the joint ( $f = -0.5 \cdot 10^{-3} f_{ck} + 0.24$ )
	$f_{ck}$	compressive strength of concrete [MPa]
	$A_k$	area of the base of all keys in the failure plane [m <sup>2</sup> ] $A_k = \min \Sigma h_k \cdot b_k$ ( $h_k$ : height of shear keys) $\min \Sigma h_k = \Sigma h_{k,1-4}^l > \Sigma h_{k,1-3}^r$

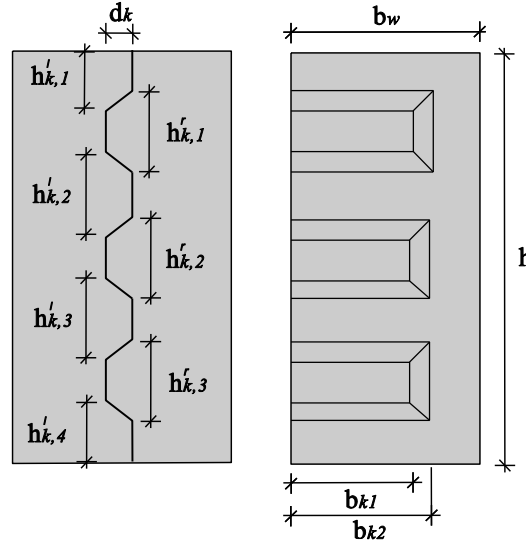


Figure 5.43: Definitions of a keyed joint for the proposed design model

In addition to the formula proposed by Rombach and Specker, the new design formula contains the practical contact surfaces at joints and the shear key factor for various concrete classes.

The shear key area,  $A_k$ , as the failure plane, is relatively small between the right and left failure planes. According to [AASHTO 1999] and [DBV 1999], the shear key area,  $A_k$ , is recommended to  $0.75b_w \cdot 0.75h \approx 0.55A_{\text{joint}}$ . Therefore, the failure plane can actually be defined on the joint surface with male keys.

In general, the average shear stress decreases as the number of keys increases, due to the sequentially failure of the keys caused by imperfection at the joints [Rombach 2004], [Zhou et al. 2005] and [Turmo et al. 2012] etc.

Due to brittle failure and imperfections at joints, the design value of the shear capacity at joints was recommended with relatively high safety coefficient,  $\gamma_F$ , of 2.0 by Rombach and Specker.

$$V_{j,d} = \frac{V_j}{\gamma_F} \quad (5.24)$$

The value for safety coefficient is appropriate for NSC or HSC as a plain concrete. Considering the material characteristics of UHPC with steel fibers, e.g. the residual stress after peak load, ductile fracture behaviour, larger maximum compressive and tensile strains compared to NSC, this safety coefficient is conservative. Thus, the safety coefficient,  $\gamma_F$ , is recommended as follows:

- $\gamma_F = 2.0$  for plain concrete
- $\gamma_F = 1.7$  for fiber reinforced concrete ( $f_{ck} \geq 160\text{MPa}$ )

Figure 5.44 presents the difference between the shear strength capacity,  $V_j$ , and its design values,  $V_{j,d}$ , for keyed dry joints on Mohr's circle from NSC ( $f_{ck} = 30$  MPa) to UHPC ( $f_{ck} = 200$  MPa). With the relatively lower shear key factor for UHPC, the initial  $\tau/f_{ck}$  value ( $\sigma_n = 0$ ) with the safety coefficient of 1.7 is very similar in comparison to that of the safety coefficient of 2.0 for NSC. It means that the safety coefficient of 1.7 for UHPC is very reasonable with the safety coefficient of 2.0 for NSC when considering the shear capacity of pure shear keys without frictional force.

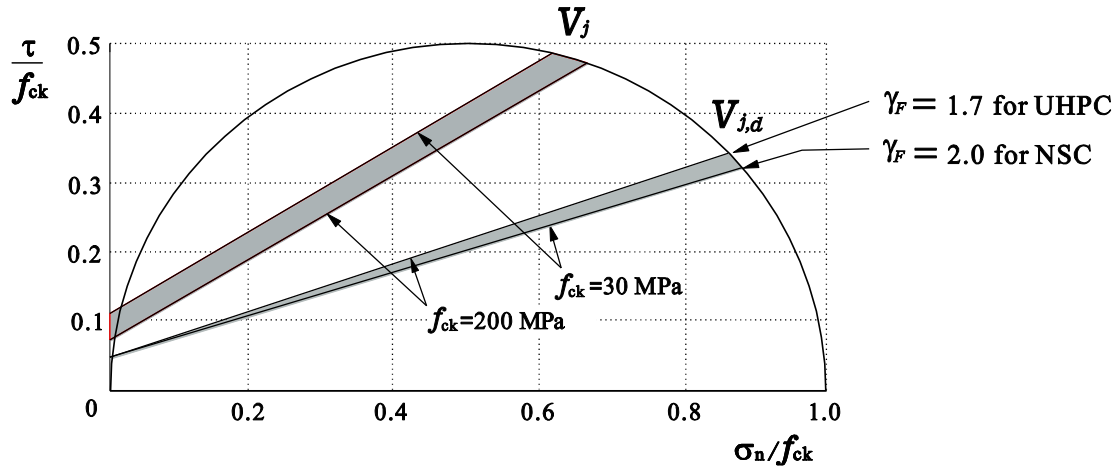


Figure 5.44: the shear strength capacity,  $V_j$ , and the design values,  $V_{j,d}$ , for keyed dry joints on Mohr's circle for NSC ( $f_{ck} = 30$  MPa) and UHPC ( $f_{ck} = 200$  MPa);  $A_k = 5400 \text{ mm}^2$ ,  $A_{\text{point}} = 200 \text{ mm}^2$

### Comparison with proposed and existing models

The measured results of UHPC dry joint tests, new proposed formula and the other formulae are compared with a Mohr's circle as shown in Figure 5.45.

AASHTO specification always greatly overestimates the shear capacity of keyed dry joints. This formula shows that the initial shear stress value without normal pressure is relatively very small in comparison with the other formulas. This means that AASHTO specification largely underestimates the shear strength capacity of pure shear keys. On the other hands, its inclination is extremely higher than those of the other design models. With a very low normal pressure ( $\sigma_n/f_{ck} < 0.05$ ), this formula can be used for the design of NSC segmental bridges. However, this formula is not appropriate for the design of HSC or UHPC segmental bridges with high compressive stresses caused by small sized members (or thin cross-section). This was already pointed out by Rombach [2004] and Zhou [2005] by means of experiments with NSC specimens. In the case of UHPC, the AASHTO specification overestimates the capacity like for NSC.

Eurocode 2 [EC2] has a very high slope area, because of high frictional coefficient of  $\mu = 0.9$ , and is restricted by maximum permissible shear stress. In the slope area, the difference between NSC and UHPC is very small as shown in figure 5.5. The area,  $\sigma_n/f_{ck} > 0.3$  in Figure 5.45, presents the constant shear stress value without increasing as a normal pressure increases. This also means that Eurocode 2 is very conservative for high normal stresses.

The formula by Rombach and Specker and the proposed model are closer to the test results than other models. The new proposed model is slightly conservative compared to the formula by Rombach and Specker and the test results.

JSCE shows that the shear strength capacity is more conservative due to the relatively low frictional coefficient and design compressive strength of UHPC in the formula. The equation recommended by JSCE is very similar to the proposed design formula with safety coefficient of  $\gamma_F = 1.7$  as shown in Figure 5.44.

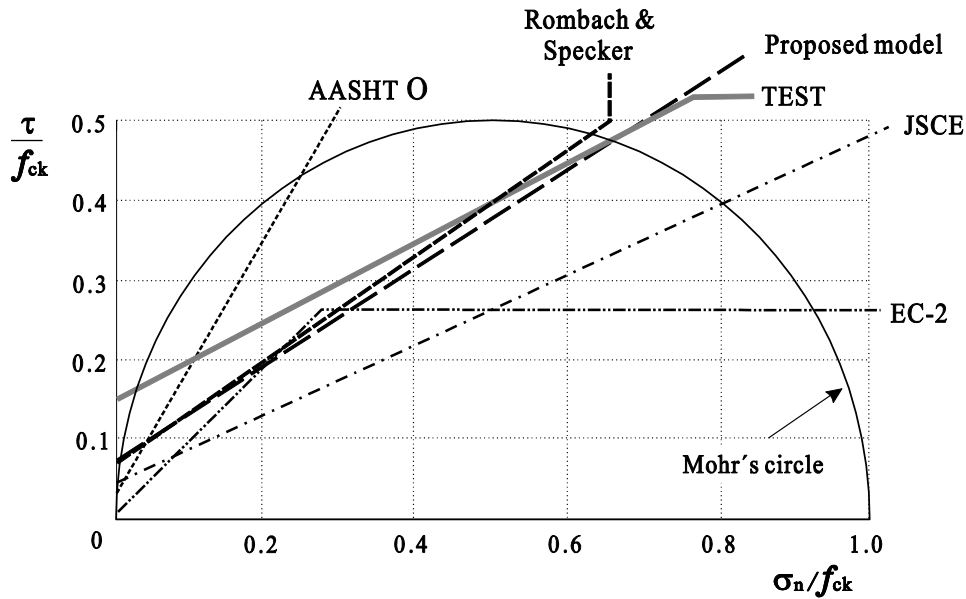


Figure 5.45: Comparison of various design approaches, including the new proposed model, and test results on Mohr's circle

## 5.5 Conclusions

To study the shear strength and behaviour of the joints in UHPC PSB, tests and FE analysis were conducted. Ten specimens, including two flat dry joints, were tested under static shear loading conditions to investigate the limit states of UHPC keyed dry joints. Numerical models were also developed to predict the shear capacity of shear keys with various values of normal pressure.

Based on the results of the experimental and numerical investigations reported in this thesis, the following conclusions are drawn:

- The ultimate shear strength of keyed dry joint depends on the concrete compressive strength. However, it is not proportional to  $f_{ck}$ .
- An increase of normal pressure increases the shear capacity of the joint with the rate of frictional coefficient and contact surfaces.

- Comparison with NSC, UHPC keyed dry joints with steel fibers presented large vertical displacement (over 1 mm), which are very linear, due to the large ultimate compressive strain. After peak load the residual stresses were observed due to the tensile resistance of steel fibers.

The first cracks, that are diagonal cracks on the lower faces at the key area, occur before the maximum load is reached. After the maximum load, the cracks propagated as shear-off along the failure plane at the key area, and then a sudden brittle slip was not accompanied.

- In order to prevent joint opening caused by sliding on inclined surfaces at key area, a sufficient confining pressure is required. As the compressive stress across joints in PSB, the confining pressure can be determined by the sliding formulation Eq. (5.14) which depends on the coefficient of friction,  $\mu$ , and inclination angle,  $\theta$ , of shear keys. In the test case, confining pressure of above 4 MPa was required.

Opened keyed joints due to the sliding on inclined surfaces at key area lose frictional forces on all surfaces (without contact) except the inclined surfaces (lower or upper faces) at key area. In this case, the shear strength capacity of joints greatly depends on a concrete compressive strength. Therefore, an increase of concrete compressive strength is recommended for application of PSBs.

- The verification of FE analysis is confirmed by comparing the analytical results with the experimental results. It is found that the FE analysis can provide good agreement with the test results. The influence of the concrete compressive strength on the shear bearing capacity of shear keys is also investigated by using nonlinear FEM analysis. In particular, the shear strength of pure shear keys and the behaviour, including the sliding on the inclined surfaces, of shear keys between the analytical and experimental results were very similar.
- The experimental and analytical results have been compared with the existing approaches for a joint design. The formula by Rombach and Specker demonstrated higher accuracy compared to the other formulas. Based on the formula, a modified design model has been proposed where the effects of concrete compressive strength and practical contact surfaces have been taken into account.

The shear bearing capacity of the proposed model has provided better accuracy in comparison with the existing formulas for segmental bridges.

## 6 Conclusion and Future Research

UHPC is a new type of concrete, which shows properties of very high strength, durability, long-term stability, and a viable substitute for NSC and HSC in bridge construction. The objective of this study was to evaluate the application of UHPC, as modular construction elements, in PSB construction. As previously described in Chap. 3, UHPC material and precast segmental bridge construction can be used in combination with great synergy. Thus, these studies contribute to better understand structural behavior of UHPC-PSB with very thin section.

### 6.1 Conclusion

The research focuses primarily on flexural behaviour analysis and design of dry keyed joints in UHPC-PSB. To evaluate the flexural behaviour of UHPC-PSB, analytical and numerical models were developed to predict the response governed by joint opening. Also, the new design formula for UHPC shear key, as well as NSC and HSC, was achieved through experiments and FE models.

The conclusions of two main studies in this thesis are summarized as follows:

#### *Flexural behavior of UHPC-PSB*

- The linear compressive stress-strain curve and the high E-modulus of UHPC can lead to smaller deflections and more linear behaviour than that from NSC. The application of higher performance concrete in bridges reduces the self-weight (dead load) in girder and/or enables longer span with thin cross-section. When the depth of cross-section and the span length are not altered as the same size of conventional concrete girders, higher performance concrete girders have less tendon quantity. Also, more slender sections made of UHPC segments could be designed replacing ordinary reinforced concrete. In comparison with the NSC-PSB (the SES test span), the reduction of the section of about 60 % and the tendon quantity of about 36 % are possible and the span-to-depth ratio is also available up to 25.
- The depth of cross-section is an important factor for efficient decompression and for resistance of deflection. Generally, a higher strength concrete bridge has a higher slenderness ratio than conventional concrete bridges. However, in box girder bridges externally prestressed cross-sections have a smaller moment arm (lever arm) than internal ones usually. Therefore, the very short depth of cross-section requires more prestressing forces due to the very short moment arm and also presents a relatively large deflection.
- In general, an externally prestressed segmental bridge is not as strong and ductile as bridges without joints (monolithic) or internal tendons, and large prestressing forces are required to avoid joint openings under SLS. As the solution of these problems in PSBs, The properties of UHPC material can delay openings of critical joints because the behaviour of UHPC-



PSB results from material mechanical properties, such as a linear compressive stress-strain curve and a ductility in tension. After SLS, the proposed UHPC-PSB models presented that the deflection and the joint opening slowly increased in contrast with NSC-PSBs.

- Due to the shear lag effect, the maximum compressive stresses are observed in the top slab areas above the webs at mid-span. These maximum stresses are more clearly shown in the models with thin member thickness. To avoid the concentration of compressive stresses and to resist the shear forces of in transverse direction, an effective extension of these areas are required.

### *Design for UHPC keyed dry joints*

- The ultimate shear strength of keyed dry joints depends on the concrete compressive strength. However, it is not directly proportional to the concrete compressive strength.
- A high normal pressure increases the shear capacity of the joint and can restrain the sliding on inclined surfaces at key area. In PSBs, therefore, UHPC is appropriate for high prestressing forces.
- UHPC keyed dry joints with steel fibres present large vertical displacement compared to NSC keyed dry joints due to the large ultimate compressive strain. In addition, after peak load the residual stresses occur due to the tensile resistance of steel fibres. Thus, a sudden brittle slip is not accompanied.
- In order to prevent joint opening due to the sliding on inclined surfaces at key area, a sufficient confining pressure is required. As the compressive stress across joints in PSB, the confining pressure can be determined by the sliding formulation.

Also the shear capacity of opened joints, as pure shear keys without frictional forces, greatly depends on a concrete compressive strength. In this case, the shear strength capacity of keyed dry joints greatly depends on a concrete compressive strength.

- In comparison with the existing formulas for a joint, the validity of the formula by Rombach and Specker was demonstrated in the experimental and numerical analysis. Based on the formula, the modified model for application of UHPC has been proposed. In the proposal model, the effects of concrete compressive strengths and practical contact surfaces are also considered.

In terms of material saving, easy construction, high durability and aesthetic appeal etc., structural application of UHPC could be solutions of more efficient design for advanced bridges. An increase in concrete performance and a reduction in material volume and weight can offset the high material costs. In particular, long term service life can be maintained by the greatly improved durability, e.g. low permeability, increased resistance to abrasion and corrosion. In addition, very early

strength of concrete can reduce a construction period and an error range due to deformation such as creep and shrinkage.

The material properties of UHPC facilitate to create new shapes and new construction methods for bridge. Because UHPC reinforced by steel fibers simplifies the segment formwork preparation through the reduction or elimination of rebars, placing UHPC in a segmental formwork can be completed very rapidly.

Application of UHPC in bridge construction is still in the early stages of commercialization. However, it will offers solutions with advantages e.g. rapid construction time, longer life span and improved aesthetic etc. beyond existing bridge designs and constructions. In the next few years, much research for optimized solutions will be progressed.

## 6.2 Future research

To encourage an extension of UHPC-PSB studies on the basis of the results of this work, additionally some further researches might be considered for future work.

- Transverse analysis of thin cross-sections: to develop optimized bridge girders that take advantage of the material properties of UHPC, comparative analysis of various sections, such as strutted box girder, ribbed deck slab and pretensioned slab etc., are required.
- To resolve problems associated with casting of reinforced and/or pretensioned slender UHPC members, Experimental studies of UHPC segments, including thin slab without rebar, should be investigated
- Development of non-linear FE models of UHPC, with material behaviour in cracked UHPC, as a fiber reinforced concrete is required.
- Considering all costs associated with use of UHPC on projects, the cost effectiveness of UHPC in comparison with conventional concrete girders should be shown. The major issue in this field may be which is more important between the high initial cost or the long service-life-cycle (low maintenance cost due to excellent durability)

## **Appendix A**

### **Historical Overview of Segmental Bridges**

## A.1 Introduction

The concept of segmental bridge construction began in Europe. The first precast concrete segmental bridge, the Luzancy Bridge across the Marne River in France, was erected in 1946. It was designed and built by Eugène Freyssinet. Since then the concept of segmental bridge construction has spread from Europe to all parts of the world. The first major commercial application of segmental bridge construction was done in France (1962). This landmark was the Choisy-le-Roi Bridge over the seine River, south of Paris. Several other structures of the same type were built in France [Rombach 2003]. At the same time, the techniques of precasting segments and placing them in the structure were continually refined. As time went on, improvements were made in precasting methods and in gantry design to allow for larger segments and longer spans which curved in plan. The technique of segmental construction not only gained rapid acceptance in France but spread to other countries. For example, the Netherlands, Switzerland, and later Brazil and New Zealand adopted the method. Many other countries are today using the segmental technique for various applications. The technique of precast segmental construction was exported to North America in the 1970s. In 1973, the first U.S. precast segmental concrete bridge was built and opened to traffic in Corpus Christi, Texas. Since the 1960s, nearly 200 bridges have been built in the United States and Canada using segmental concrete construction [Muller 1975] and the precast segmental construction method has won widespread recognition and is used extensively throughout the world. Particularly, in North America the precast segmental construction rapidly grew into a popular construction method. Figure A.1 presents growth in the number of segmental bridge in North America.

With the first segmental concrete bridge in the world, this chapter provides the various and significant features of the existing segmental concrete bridges.

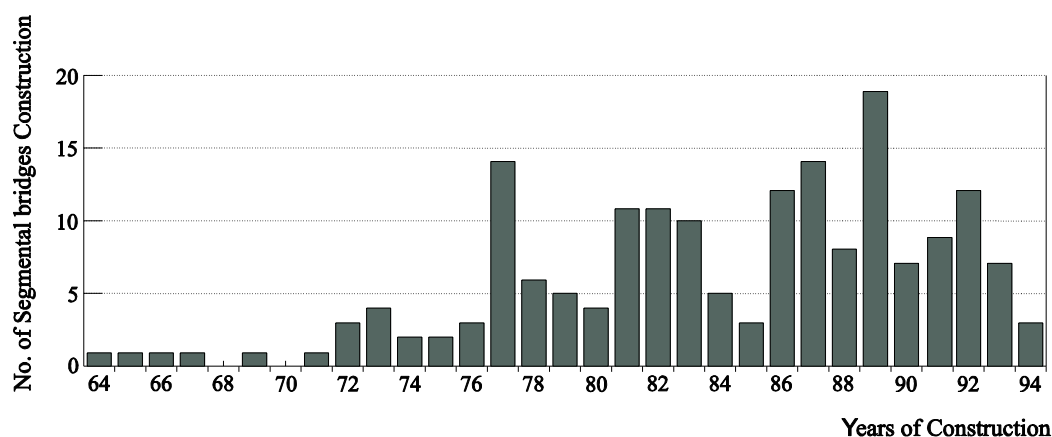


Figure A.1: Segmental concrete bridges constructed annually in North American (from 1964 to 1994) [Miller 1995]

## A. 2 Segmental bridges

### Luzancy-bridge - 1946, Paris, France

The first segmental concrete bridge had been built by Eugène Freyssinet over the Marne River in 1944-1946. All three of Freyssinet's inventions for prestressing (pre-tensioning, flat jacks, and post-tensioning) were used here. This bridge with about 55m span was jointed two frames of which the multiple hollow box cross-section is shown in Figure A.2. The girder height of 1.20 m at mid-span is a very slender construction in these days. The box girders show a segment length of 2.44 m and the joints between the segments were spilled with a mortar of 2 cm thickness.

The bridge has numerous innovative features. (1) It was the first bridge built using precast segments. This allowed better quality control of the concrete. (2) It was the first bridge to have trial compression. The segments were together held in longitudinal and transverse direction by internal stressing tendons. This allowed for exceptional concrete strength. (3) It was the first bridge to be erected without false work of temporary supports between the piers. This provided a very economical construction method while allow boat traffic to proceed [Xercavins 2008].

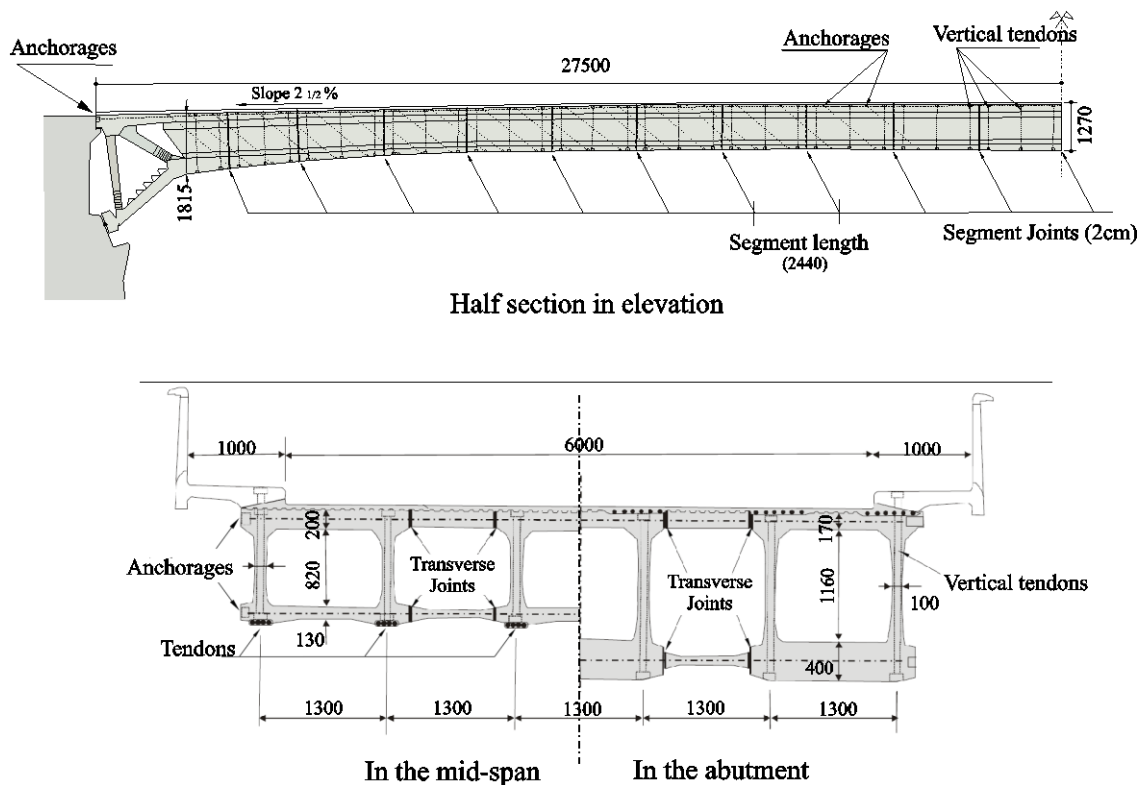


Figure A.2: the half section in elevation, and the cross-sections in the mid-span and in the Abutment of the Luzancy bridge over Marne River [Shushkewich 2012], [Rombach 2003]

### Hammer Flyover Viaduct - 1961, London, England

The Hammer Flyover Viaduct in London is a unique construction. The main girder elements consist of a three-cell hollow box, 7.9 m wide, cast in segments 2.6 m long. These alternate with 0.3 m (1 ft.) thick, precast cantilever “coast hanger” section 18.3 m wide. The sections are joined by 7.6 cm of cast-in-place concrete. Precast concrete slabs shape the deck of the bridge. The cantilever sections act as diaphragms for the box girder and also support the outer deck slab units (Figure A.3).

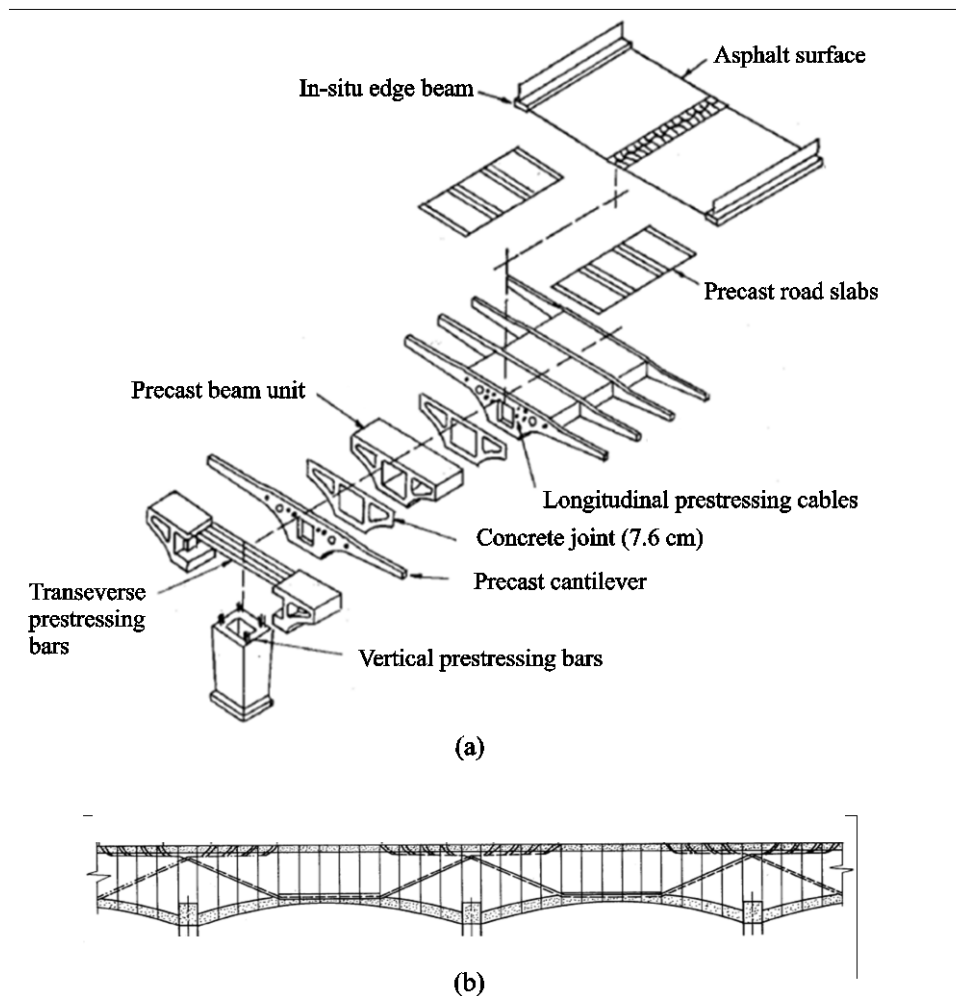


Figure A.3: (a) Superstructure (b) Typical cable profile of Hammersmith Flyover [Lacey et al. 1971]

Stranded cables, diameter of 2.86 cm, are arranged in four clusters of 16 each, one cluster on either side of each inner web of the girder. At mid-span, each cluster passes through a 25.4 cm diameter duct in the lower flange. The cables are arranged longitudinally in overlapping groups, each group passing through two successive spans and overlapping the next group by one span length. Both ends are anchored in the top flange of the box girder after passing over a column. The cables are kept in position by steel saddles over the columns and at points 7.6 m on either side of mid-span; cable profiles are linear between saddles (Figure A.3). The girder segments over the columns are

prestressed transversely through the top flange and are tied to the columns with vertical prestressing [Lacey et al. 1971].

**Choisy-le-Roi bridge (First precast prestressed segmental concrete bridge) - 1964, Paris, France**

As the significant prestressed precast segmental bridge, the constructed Choisy-le-Roi bridge in 1962-1964 is shown the existence with span lengths of 37.5, 55.0, 37.5 m by epoxy-joint. It was equally built in the cantilever construction such as the Oléron viaduct. The box girder section had the advantage of being more efficient than the I-beam section in terms of concrete quantities and structural properties (such as torsion and lateral stability) and lent itself to segmental construction, eliminating the need for a cast-in-place slab. The bridge segments were fabricated using the long line method. In other words, the segments were cast in their correct relative position on a casting bed that reproduced exactly the profile of the structure including camber to account for long-term deflections. Casting started with the pier segment, followed by the symmetrical segments on each side of the pier segment. As casting progressed, the initial segments cast could be removed from the bed and sent to storage. This method allowed for easy handling of the segments and control of deck geometry. After erection and longitudinal post-tensioning, the two girders are connected rigidly with a concrete joint and transverse post-tensioning.

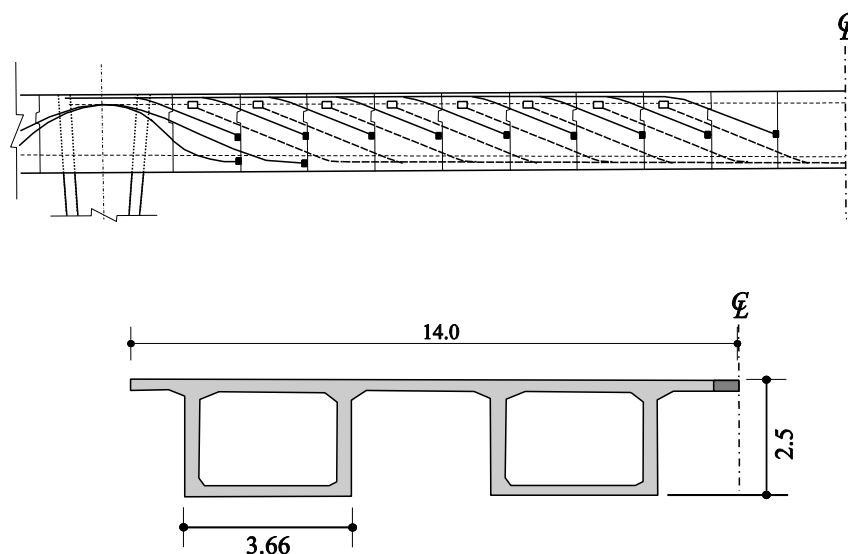


Figure A.4: Longitudinal cable profile and cross-section of the Choisy-le-Roi bridge [Lacey et al. 1971]

There are two sets of longitudinal prestressing cables (Figure A.4). The primary function of one set is to withstand the negative moments during construction (by the cantilever method). Some of these cables, of varying length, run horizontally in the deck slab; the remainder has draped profiles with anchorage in the girder web. The second set of cables is located in the lower slab for positive moment near mid-span with most of them draped and anchored in the deck slab. The structure was divided into two parallel bridges with two single-cell rectangular box girders each. It was erected in balanced cantilever with a floating crane [Tassin 2006].

**Oléron Viaduct - 1966, Oléron, France**

The Oléron Viaduct in France is a single cell box girder bridge, with the upper deck slab cantilevered out to a total width of 10.7 m (Figure A.5). The precast segments are 3.3 m long. The girders are prestressed in both the longitudinal and transverse directions and elastically fixed to each pier through four neoprene bearing pads.

The Oléron Viaduct provides a link between the west coast of France and the resort island of Oléron. The total bridge length is 2860 m, with span lengths up to 79 m. The bridge was decided to develop new construction methods to accelerate erection. Floating equipment could access the approach spans only at high tide, and crawler cranes could not be used at low tide for environmental reasons.

For the first time, a launching gantry was designed to erect the superstructure in balanced cantilever with segments delivered from the top of the previously built structure. The segments were fabricated by the long line method close to the bridge abutment. The gantry was capable of launching itself with a system of moveable supports. This method of construction was successful, and the bridge was designed and built in record time between 1964 and 1966 [Tassin 2006], [Lacey et al. 1971].

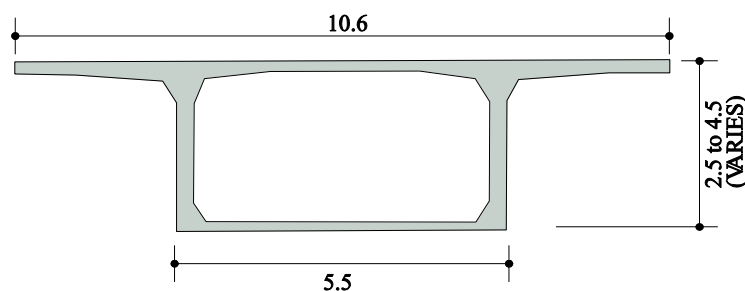


Figure A.5: The cross-section of the Oléron Viaduct [Lacey et al. 1971]

**Saint Lorenz bridge – 1968, Epfach, Germany**

The first segmental bridge in Germany, that is called the Saint Lorenz bridge (span lengths 31 + 68 + 45 m) (Figure A.6) over the river Lech at Epfach, followed in 1968 whereat the cantilever construction was also used. The segments were joined with a mortar-joint of approx. 3 cm width [Rombach 2003].

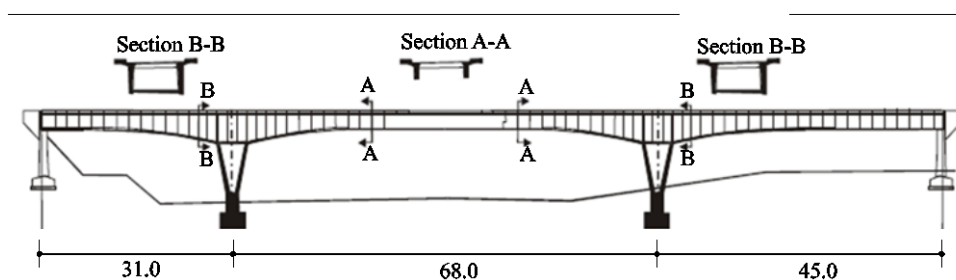


Figure A.6: Lorenz Bridge at Epfach in Germany [Rombach 2003]



### Brotonne Bridge – 1977, Caudebec-en-Caux, France

The Brotonne Bridge was designed to cross the River Seine downstream from Rouen, France. It was opened to traffic in 1977. It is composed of two approach viaducts and a cable-stayed structure with a 320-m-long central span. The deck consists of a prestressed concrete box girder 3.97 m deep and 19.20 m wide (Figure A.7). The stays and the pylon are placed in a single plane along the longitudinal axis of the bridge. The approaches and the main bridge were erected in the same way. In both cases a cantilever construction was used with success. The length of the segments was 3 m. The segments were cast in place except for the webs which were precast and prestressed. The erection of the deck-girder consisted of extending the bottom slab form of the traveling formwork carried by the previous completed segment, then placing the precast webs that formed the basic shape and acted as a guide for the remaining traveling formwork. The webs were transported and lifted by a tower crane. Concerning the main bridge, the stays were tensioned in every two segments and were anchored in the top slab axis [Muller 2000]. For the segments, two prestressed internal stiffeners were provided to transfer vertical loading generated by the stays. After the Brotonne bridge, as the forerunner of the box-section with two inclined internal stiffeners, many precast segmental concrete cable-stayed bridges have been built with the around the world [FHWA 2001].

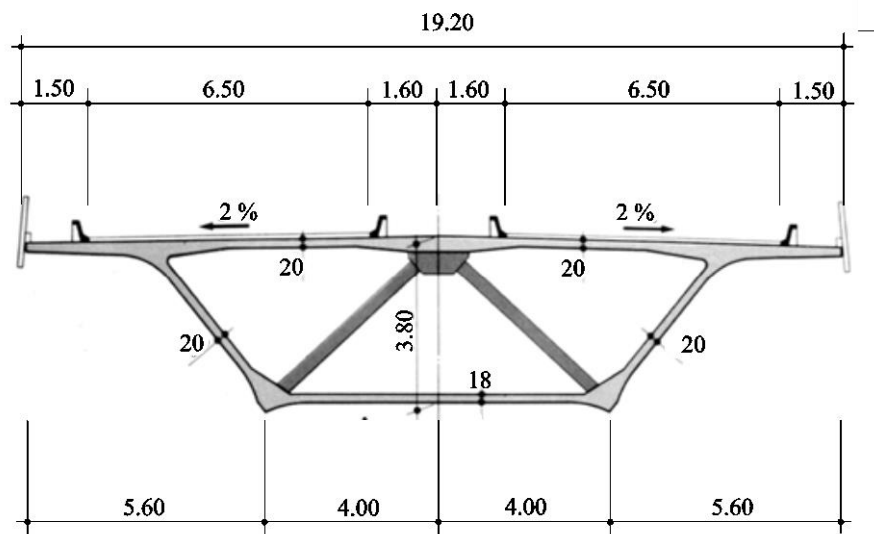


Figure A.7: Cross-section of the Brotonne Bridge [Leonhardt 1987]

### Linn Cove Viaduct – 1984, Carolina, USA

The Linn Cove Viaduct in the North Carolina Blue Ridge Parkway was completed in 1984. It was a complex structure with tight curves (76 m radii and variations of cross slopes of  $\pm 10\%$ ). In addition, the bridge alignment followed a steeply sloped mountainside with boulders and trees that could not be disturbed.

Several new construction techniques had to be developed for this project. Construction proceeded from the south abutment using the progressive cantilever method. The maximum span length was 55 m, and temporary supports were required at mid-span to reduce cantilever lengths. Due to the lack of access roads, the foundations consisted of micro shafts grouted into the underlying rock formations [Tassin 2006].

Precast concrete was chosen over cast-in-place segments because the region has a relatively short construction season. By choosing precast concrete, production of the segments could continue during the winter. Additionally, the precast segments were made under plant-controlled conditions which led to high quality concrete.

The progressive scheme is considered feasible and structurally satisfactory for span ranges of from 46 m to 61 m. For these span lengths, a constant depth box girder has proven to be the most economical. Typical box girder bridges have been built with span-to-depth ratios of 18 to 25. Structural aesthetics are generally more pleasing through the use of higher span-to-depth ratios. Considering the beautiful site of Linn Cove, it was decided to use a span-to-depth ratio of 22 to provide a graceful structure. However, after analysis of this cross-section, it was decided to increase the depth of the box and the web thicknesses because the shallower depth structure would have required a significant amount of high strength post-tensioning steel. Figure A.8 shows the final cross-section adopted [Muller 1985].

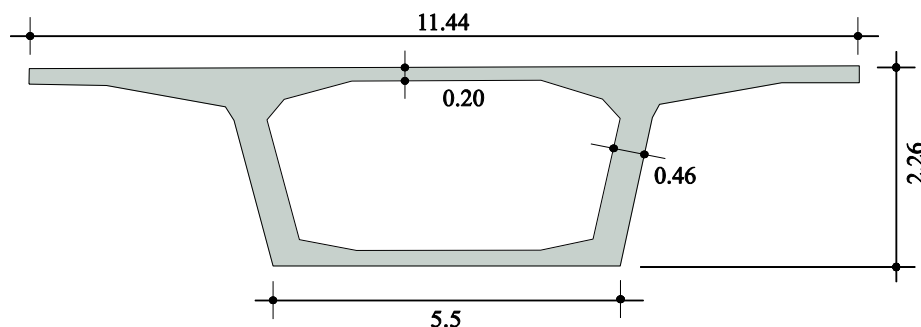


Figure A.8: Typical cross-section of precast segment [Muller 1985]

This bridge is the first segmental structure in the United States to incorporate progressive placing erection. This project proved that precast concrete segmental construction was the right solution for bridges with complex geometry and difficult access. It also showed the adaptability of segmental construction [Tassin 2006].

### **Sunshine Skyway Bridge – 1987, Tampa, USA**

The Sunshine Skyway Bridge in Tampa was the longest concrete cable-stayed bridge in North America, with a 366 m main span, when completed in 1987. The bridge was an extension of the Brotonne Bridge, with a total width of 29 m compared with a width of 19 m for the earlier bridge.

The superstructure consisted of wide single-cell precast concrete segments stiffened by internal struts with a weight reaching 220 tons. Extensive use of precasting was justified by the location of the bridge over water and easy barge access. Superstructure segments for the main bridge and

approach spans, approach piers, and underwater foundations were all fabricated by Pomco at the Port Manatee, Fla., casting yard, 8 km away from the bridge site [Tassin 2006].

There are 333 large roadway segments of 29 m width to accommodate both northbound and southbound spans (Figure A.9). Due to the relatively large width of the segments, internal inclined struts are necessary to properly support the top deck. These struts are precast separately ahead of time to facilitate mass production. Diagonal post-tensioning is also provided to cable stay anchor segments in order to distribute stay forces to the webs. The transverse deck post-tensioning consists of 152 mm diameter strands in 25×76 mm flat polyethylene duct. Also, the base slab is tensioned after the concrete has attained strength of 17 MPa. The large segments are match cast to each adjacent segment using the short line method. A freshly cast segment is moved to the match cast segment. Using an adjustable pallet to the bottom slab, the whole segments is aligned both horizontally and vertically so proper geometric control can be achieved. The balanced cantilever method requires an erection sequence to start at a pier and extend equidistant both ways with a maximum imbalance of one segment thus explaining the first span of 43 m transitioning to the span by span piers, then a series of 73 m spans [Podolny 1986].

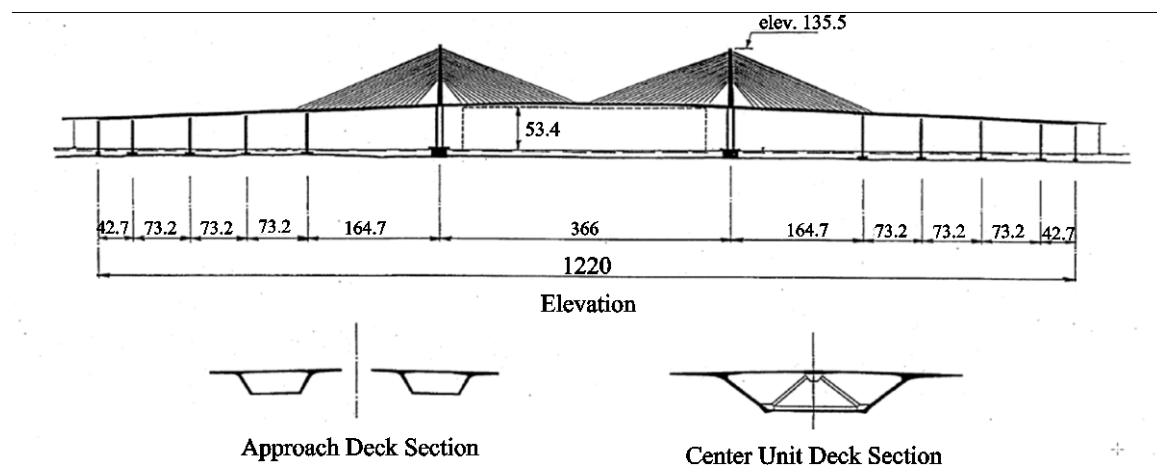


Figure A.9: Precast segmental box girder sections for various portions of Sunshine Skyway Bridge [Sauvageot 2000]

**Cable stayed spans:** To achieve a main span of 366 m, two main pylons of reinforced concrete, 133 m above the water of 73 m above the road surface, provide the vertical support. The cable stayed spans were erected entirely with winches on self-advancing beams, with the stays replacing the longitudinal post-tensioning required in the shorter spans. After closure, the internal continuity strands were stressed to carry their final suspended loads. Each pylon carries 21 stays, anchored in every other (every 7.3 m) but passing freely through individual saddles in the pylon. Made up of multi-wire strand and ranging from 38 to 82 high strength steel strands, the cables are encased in 168 and 219 mm steel pipe, grouted after final stressing [Podolny 1986].

### The metro of Monterrey – 1991, Monterrey, Mexico

In 1991, the 18.7 km long line 1, the first line of the metro of Monterrey (Monterrey), opened to the public in the metropolitan area of Monterrey, Nuevo Leon, Mexico. The precast concrete segmental structure was designed by the late Jean Muller (see Figure A.10). The structure comprises typical simple spans about 27 m long with a maximum span length of 36 m. The box girders have a width of 7.40 m and a depth of 2.13 m. There are 17 elevated stations on the line, and more than 6500 precast concrete bridge segments and 2700 other elements were cast in a specially designed. Segments were match-cast on concrete beds long enough for each complete span, then delivered by trucks to the site, erected span-by-span on movable steel trusses and post-tensioned. The precast concrete box girder segments have pretensioned top slabs.

While this viaduct is an efficient system for transporting people, the existing structure has serious aesthetic deficiencies: wavy joints, rust in the columns, and a lack of uniformity in the color. These problems have prompted negative comments from the citizens and motivated Metrorrey to explore alternative concepts for the line 2 extension.

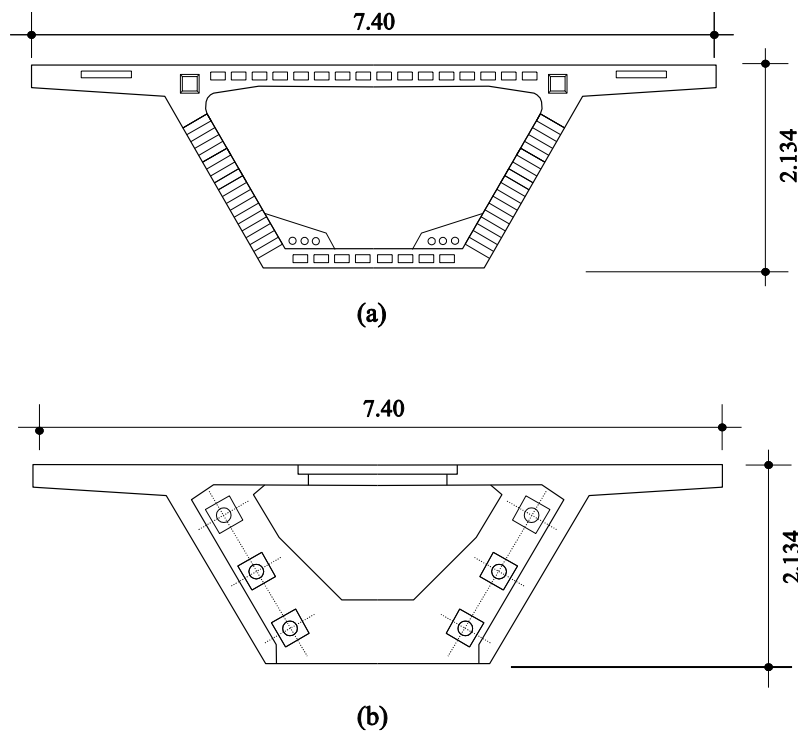


Figure A.10: The first line of the metro of Monterrey: details of (a) typical span segments and (b) pier segments [Mondorf 1993]

Monterrey's line 2 was completed in November 1994. A typical precast concrete segmental simple supported girder has a width of 9.2 m and a span of 37 m. The cross-section was created as shown in Figure A.11. In addition, the cross-section also has the same depth of 1.9 m. The typical span includes nine 3.55 m long typical precast concrete segments and two 2.49 m long pier segments. The concrete strength for the superstructure is 35 MPa. Furthermore, Monterrey required a

minimum of 5 MPa of residual compression for any service load. This viaduct was built with epoxy joints.

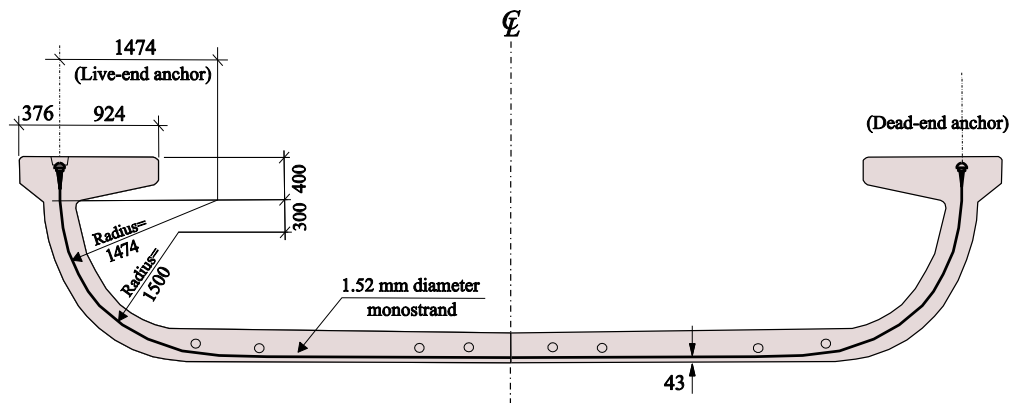


Figure A.11: The second line of the metro of Monterrey: transverse tendon layout and cross-section [Baamonde 2009]

### Second Stage Expressway – 1995, Bangkok, Thailand

The second Stage Expressway in Bangkok, Thailand, was the first large-scale precast concrete segmental project for an elevated highway network. The first phase of the project, Sector A, had 47 km of elevated structures, including mainline, ramps, and interchanges, such as a three-level interchange over the Makkasan swamp. This part of the project was built within three years. Sectors B, C, and D were built later, adding about 53 km of viaducts.

The superstructure consisted of precast segmental concrete box girders with maximum span lengths of 45 m. The spans were simply supported to accommodate differential settlements. All the structures were designed with two types of precast concrete segments, namely, two-lane segments with a maximum width of 12 m, and three-lane segments with a maximum width of 15 m. These sections could be combined with a cast-in-place closure joint in between the wing tips for a maximum width of 60 m. The spans were post-tensioned with external tendons placed inside the box girders. The segments were manufactured in an enormous precasting yard with 50 casting machines 80 km north of Bangkok. They were trucked to the site at night and erected with underslung and overhead trusses. The maximum production reached 100 segments per month, and the spans were typically erected in less than two days. This method of construction was well adapted to the congested urban environment of Bangkok [Tassin 2006].

A typical span is shown in Figure A.12. A standard span has a length of appr. 45 m. It consists of 14 segments. Dry joints are used in this project (no epoxy glue). No continuous reinforcement is provided across the match cast joints between the segments. Due to the external post tensioning, 3 different segments are needed [Takebayashi et al. 1994].

More information on the planning and construction of S.E.S can be found in [Girmscheid 1993].

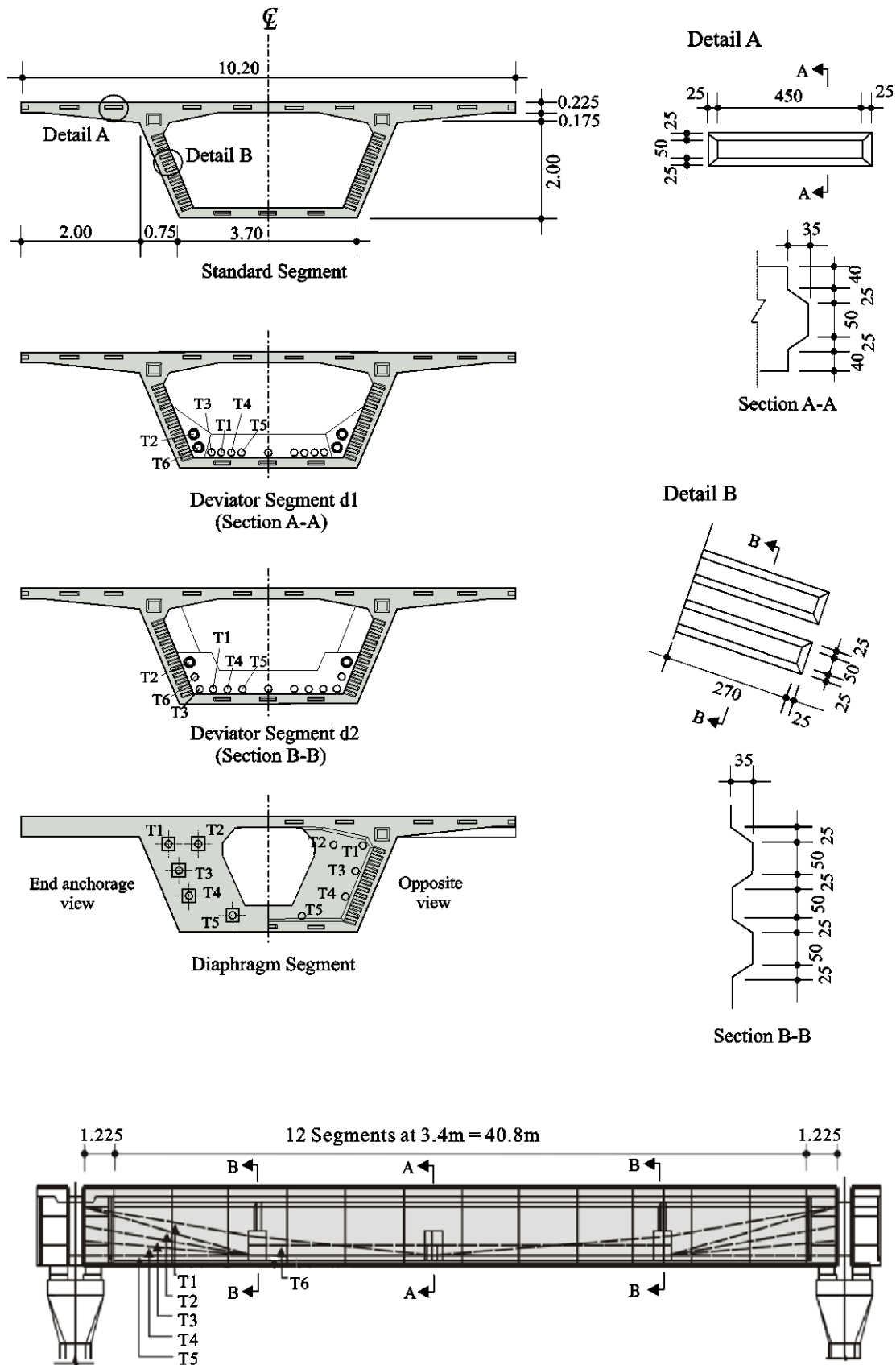


Figure A.12: Cross-sections and shear keys of the segment and tendon layout of the standard span of Second Stag Expressway in Bangkok [Takebayashi et al 1994], [Rombach 2002]

### Confederation Bridge – 1997, Northumberland Strait, Canada

In the field of gigantic bridge projects, the Confederation Bridge was a formidable challenge for design and construction. This 13 km long bridge crosses Canada's Northumberland Strait between Cape Tormentine, New Brunswick, and Borden, Prince Edward Island. Ice is present in the Strait for five months every year, preventing any construction at the bridge site. Minimum span lengths of 250 m were required to facilitate the ice clearing process in the spring. Close coordination was required between the design and construction teams to meet the tight construction schedule and find solutions to the unusual project requirements.

The bridge carries a two-lane road-way and two shoulders. The main bridge includes forty-three 250 m spans and two 165 m transition spans. The vertical clearance for the marine spans is typically 25 m, except for the navigation channel with a clearance of 49 m. The superstructure of the main spans consists of a variable-depth, single-cell concrete box girder.

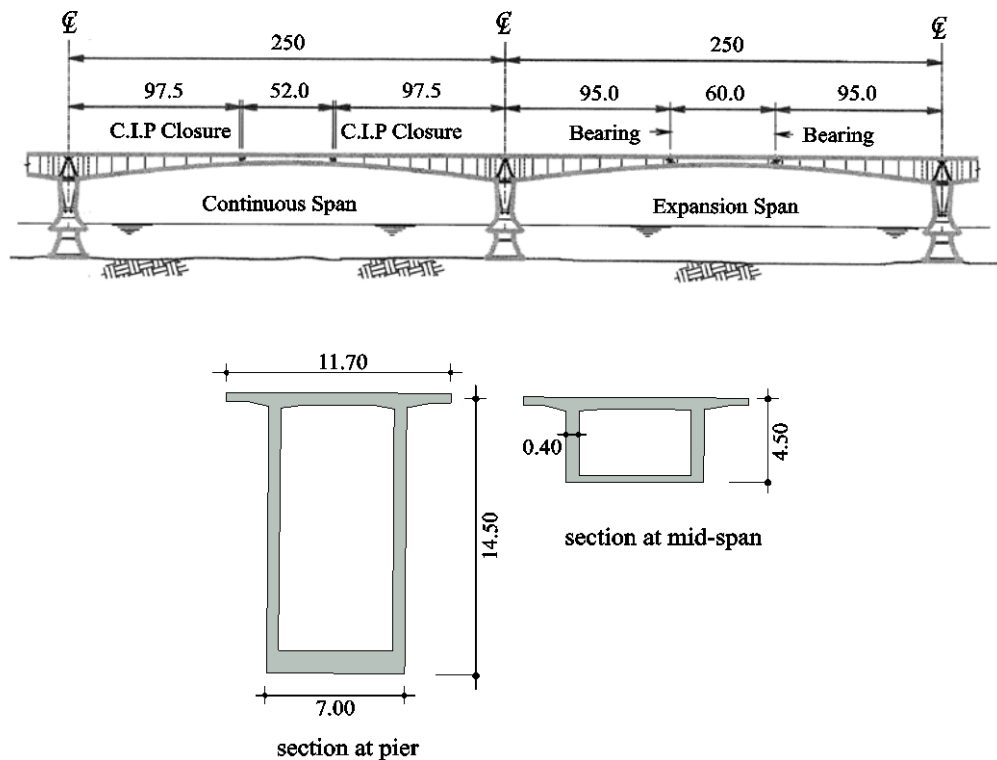


Figure A.13: Cross-sections of the Confederation Bridge [Sauvageot 2000], [Tadros 1995]

The main girder was cast segmentally using a balanced cantilever approach (Figure A.13). Each girder is made up of two precast concrete elements, a 190 m long double cantilever and a 60 m long drop-in girder. The drop-in girder is made continuous every other span. Due to the environmental conditions and construction schedule, all the main bridge elements (pier bases, pier shafts, main girders, and drop-in spans) were fabricated in a casting yard at the extremity of the bridge on the Prince Edward Island side. The bridge was completed in 1997 in record time. Note

that all the substructure and superstructure elements were erected in a period of 12 working months [Tassin 2006], [Tadros 1995].

### **Bang Na-Bang Pli-Bang Pakong Expressway – 2000, Bangkok, Thailand**

The Bang Na-Bang Pli-Bang Pakong Expressway in the South-East of Bangkok is with a 55 km length that at present is the longest segmental bridge in the world (completion 2000). The standard superstructure shows a width of 27.2 m that suffices for 6 lanes. The normal segment signalizes through its large slenderness that was only enabled by arrangement of aslope supports. In addition, the construction work was considerable at the great project. Approximately 1.900.000 m<sup>2</sup> superstructure surface was built in 4 years. Approximately 2600 m of superstructure (1800 segments) was produced per month. In total, 21,320 segments for 6 lanes (Type D6) (Figure A.14) and 18,250 segments for 2 to 3 lanes (Type D2/D3) were required. The segment shows a cross-prestressing in the deck slab and through the webs. An internal passing longitudinal tendon, which is required for the under compression of the joints in the area, is always located at the end of the cantilever plates.

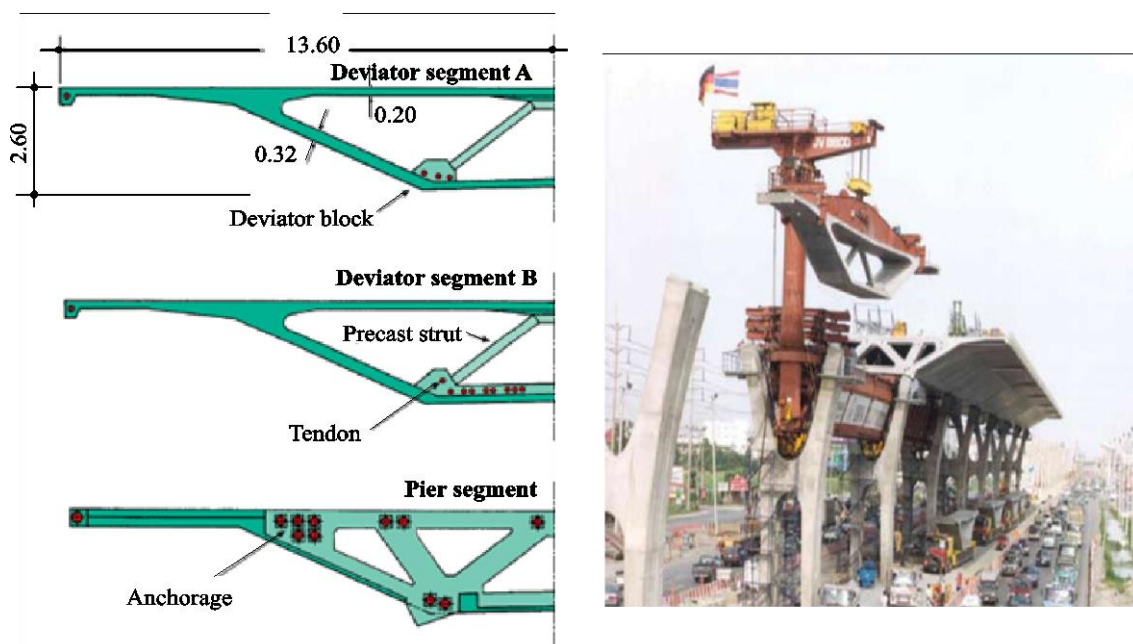


Figure 2.14: Cross-sections (D6 segments) of the Bang Na-Bang Pli-Bang Pakong Expressways, in Bangkok [Brockmann 2000], [Rombach 2003]

The D6 segments are the main part of the expressway structure. They have a width of 27.20 m over six lanes of traffic. For typical segments, their height and length are 2.60 and 2.55 m, respectively; for pier segments, their width is 1.775 m. The weights of typical girder and pier segments are 85 and 100 tonnes, respectively. The unusually slender cross-section has inclined webs and two struts in the middle of the segment. The inclination of the webs accentuates the curvature of the outside of the columns and carries this line to the horizontal plane of the deck. The spans are longitudinally prestressed by 22 tendons. Twenty of these tendons are placed externally in the box and two are placed internally in the edge beam. The transverse post-



tensioning is accomplished not only by the tendons in the top slab, but also by placing them in the webs and bottom slab [Brockmann 2000].

### Precast Box girder with strutted wing slab

*Cantilever Method Bridge over the Sella – 2002, Dolomiten, Italy:* By way of example for a cantilever method bridge, this bridge over the Sella was completed in 2002 (Figure A. 15(a)). The girder height in the span amounts around 3.70 m that corresponds at a maximum span length 106 m of a slenderness  $l/h = 42$ . The box-shaped segments were complemented according to joints closing through in-situ concrete plates and precast struts. Also in Spain, four another bridges were built in the same construction method [Rombach 2003].

*Uchimaki Viaduct – 2005, Shizuoka, Japan:* The Uchimaki Viaduct is a multi-span continuous box girder bridge with strutted wing slabs (Figure A. 19(b)). It is erected progressively by assembling divided parts of the cross-section. The bridge is around 1 km long. And span length is standardized into approx. 50 m in 36 of the 42 spans in total. Span-by-span construction method with precast segments is adopted.

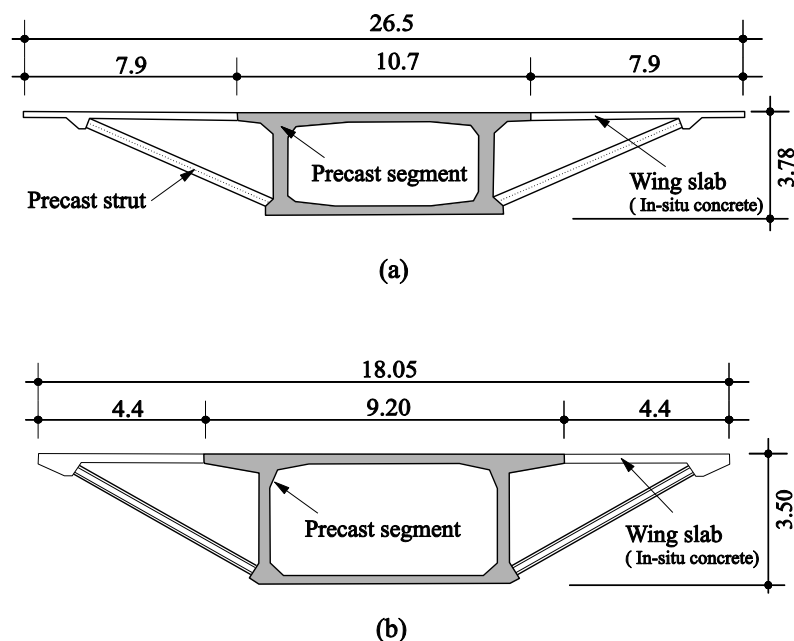


Figure A.15: Cross-sections of (a) Bridge over the Sella [Rombach 2003] and (b) Uchimaki Viaduct [Saito et al. 2001]

### Furukawa Viadukt – 2002, Asahi-cho Mie Pref., Japan

In recent years, numerous segmental bridges were built in Japan. The details can be taken to the conference transcript of the 1.FIB congress in Osaka. In the following, the Furukawa viaduct is accepted. The bridge, that is continuous beam, shows total length of  $34.7+35.7+45.5*9+36.2+35.3=473.8$  m. The U-shaped cross-section with a strut in the cantilever area (see Figure A.16) was developed in order to receive a possible light segment. The segment length could be increased to 2.6 m opposite 1.9 m at a normal hollow box cross-section of the same weight through

the special form whereby appr.7 segments per span were saved. This led to a considerable acceleration of the installation of the precast which are made with an above recumbent scaffold. But disadvantageously, the necessary in-situ concrete addition is for the deck slab. There were precast beams in order to insert the non-formwork. According to the same system, two another bridges were built in Japan [Rombach 2003].

The Furukawa Viaduct is located on the new Meishin Expressway between the Kawagoe and Asahi interchanges, and was built between 1999 and 2002. The viaduct consists of two side-by-side precast, prestressed concrete box girder bridges. It has 41 spans with span lengths ranging from 34 to 45 m (112 to 148 ft.) for a total length of 1,475 m (4,839 ft.). To reduce the weight of each precast segment to 33 tons for transport by road, the traditional top slab of each segment was replaced with a transverse prestressed rib, as shown in figure A.16.

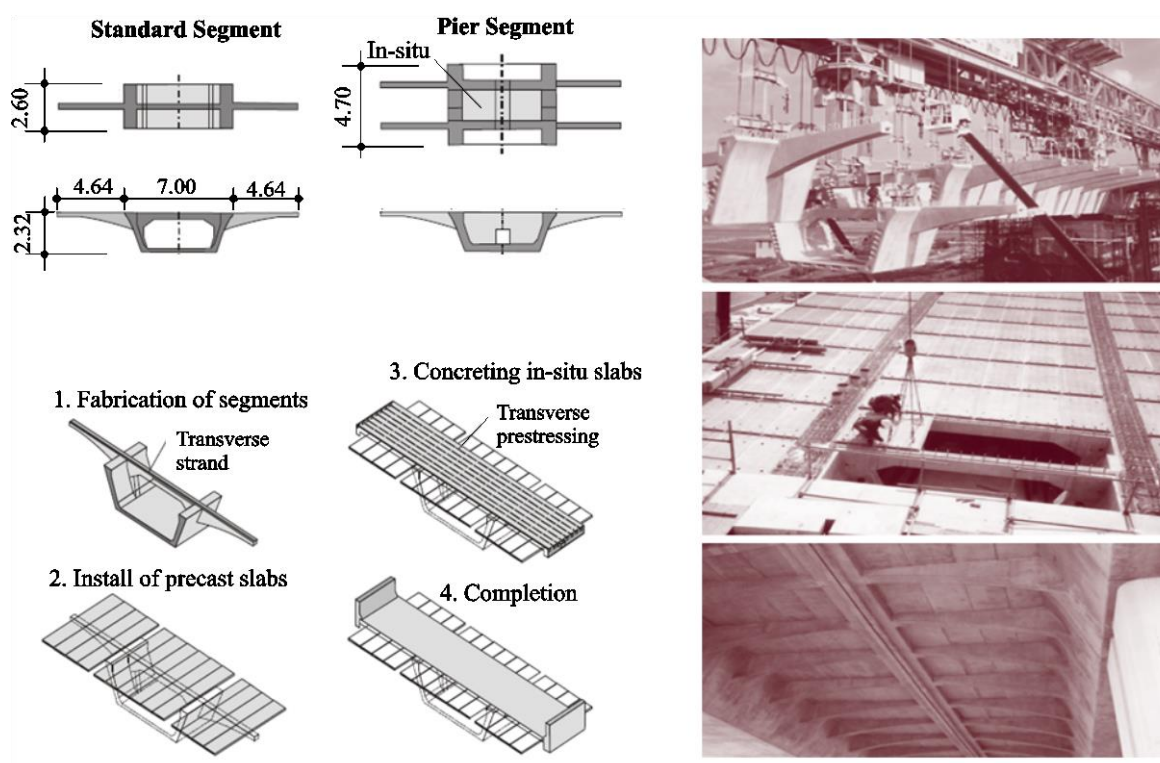


Figure A.16: Segments and fabrication of the superstructure of Furukawa Viaduct [Rombach 2003], [FHWA 2005]

The viaduct was built using the span-by-span method with an overhead truss. A CIP joint is provided between the span segments and the pier segments at both ends of each span. The longitudinal external post-tensioning is located inside the box to permit easy maintenance and replacement. The tendons were stressed in several stages. Precast-prestressed concrete deck panels span longitudinally between the transverse ribs. A CIP topping, which is transversely post-tensioned, is used to complete the system. A second feature to reduce the weight of each segment and to increase durability was the use of concrete with a specified concrete compressive strength of 60 MPa. Because this was the first application of this method, a full-scale test was performed

for each construction phase to ensure safety. This superstructure design concept allows for future deck removal [FHW 2005].

### Segmental bridge of textile reinforced concrete – 2007, Allgäu, Germany

Recently, an interesting segmental bridge had been built in Germany. As very lightweight concrete construction, it was possible to realize prefabricated concrete bridge with a size that was not possible yet due to limits in transport. This pedestrian bridge consists of textile reinforced concrete segments (see Figure A.17). The bridge has a span length of 17.2 m and slenderness of 1/35. Epoxy was used at the joints between segments. The bridge was designed by TU Dresden.

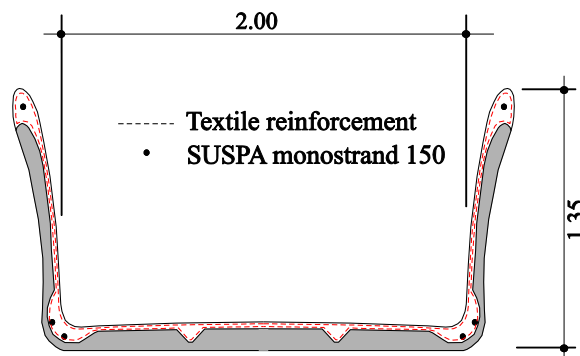


Figure A.17: Cross-section of the Kempton Bridge [Michler 2013]

## **Appendix B**

### **UHPC Shear-key Tests**

## B. 1 UHPC composition

Basic-mixture: **M3Q**

Table B.1: Mix proportion of the UHPC specimens

Material		Volume [dm <sup>3</sup> ]	Weight [kg]	Density [kg/dm <sup>3</sup> ]
Water		186.08	186.075	1.00
Pore Volume		15.00		0.00
Binder	CEM 52,5 R HS-NA (Holcim Sulfo)	253.98	787.332	3.10
	Sika Silicoll P unkompaktiert	75.86	166.900	2.20
admixture	Sika Viskocrete 2810	22.30	23.856	1.07
Aggregate	Quartz Powder Millisil W12	74.09	196.155	2.65
	Quarzsand G32	362.70	961.155	2.65
Fibers	Micro wire fiber	10.00	78.500	7.85
Total		1000.00	2400.151	

\* Steel fibers (stratec): diameter of 0.20 mm/ length of 13 mm

## B. 2 Material properties of UHPC cylinders

### B.2.1 Compressive strength and modulus of elasticity

5 cylinders ( $\phi 150/300$  mm) preserved in normal condition were tested after 104 days.

Table B.2: Test results of cylinders for compressive strength and modulus of elasticity

Cylinder No.	Weight [kg]	Density [kg/m <sup>3</sup> ]	Force [kN]	$f_{c,cyl}$ [N/mm <sup>2</sup> ]	Test of E-modulus				
					$\sigma_o$ [N/mm <sup>2</sup> ]	$\sigma_u$ [N/mm <sup>2</sup> ]	$\epsilon_o$ [mm/m]	$\epsilon_u$ [mm/m]	$E_c$ [N/mm <sup>2</sup> ]
1	12.340	2.373	3.240	183.3	-	-	-	-	-
2	12.605	2.406	3.410	193.0	61.1	0.6	1.203	0.019	51.140
3	12.509	2.384	3.224	182.4	61.1	0.6	1.227	0.016	50.000
5	12.338	2.365	3.114	176.2	61.1	0.6	1.251	0.017	49.068
6	12.418	2.285	3.338	188.9	61.1	0.6	1.206	0.012	50.759
Mean value		2.383		184.8					50.242



Figure B.1: Cylinder failure in compressive strength test

### B.2.2 Tensile strength

2 cylinders ( $\phi 150/300$  mm) preserved in normal condition were tested after 107 days.

Table B.2.3: Test results of cylinders for split tensile strength

Cylinder No.	Weight [kg]	Density [kg/m <sup>3</sup> ]	Force [kN]	$f_{ct,sp}$ [N/mm <sup>2</sup> ]
4	12.338	2.376	905.0	13.06
7	12.591	2.396	893.0	12.74
Mean value		2.390		12.90



Figure B.2: Cylinder failure in split tensile test



### B.3 Fabrication of the test specimens

The fabrication process of the test specimens is as follows:

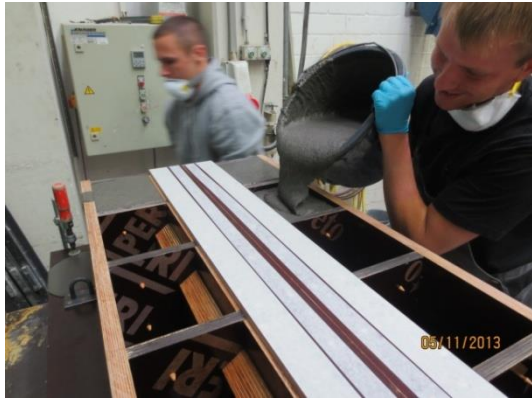


Figure B.3: Concreting for side parts



Figure B.4: Surface after formwork removal at joint



Figure B.5: Aluminium foil as a bond breaker between segments



Figure B.6: Concreting for middle parts



Figure B.7: Formwork on the vibrator



Figure B.8: Finished specimen set after formwork removal



## B.4 Behaviour of the test specimens

### B.4.1 Flat joint test

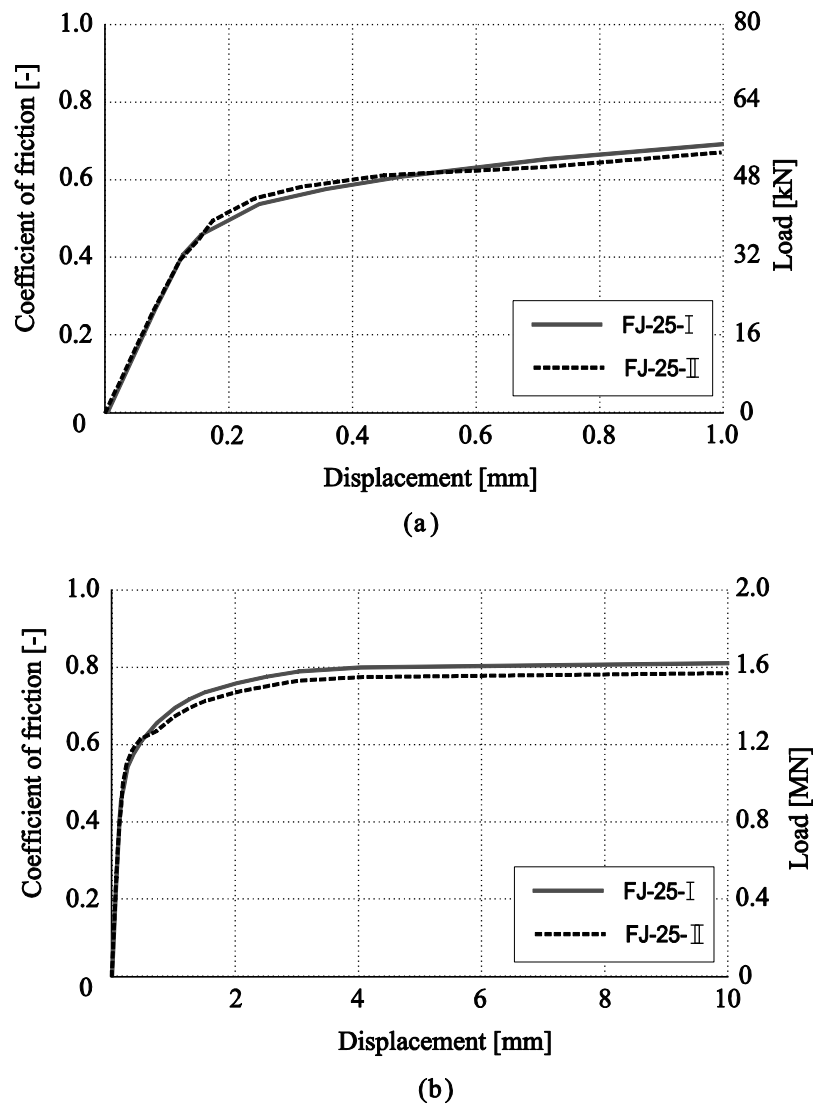
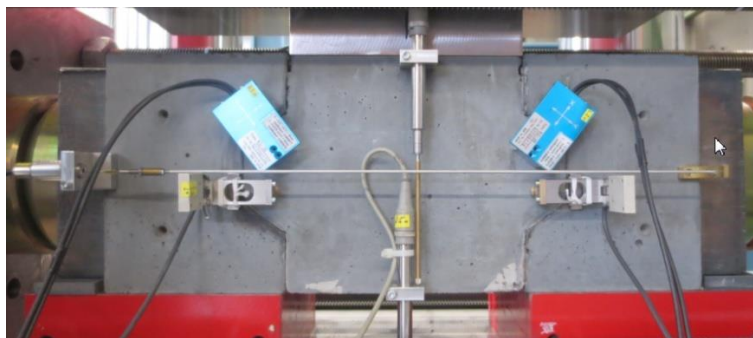
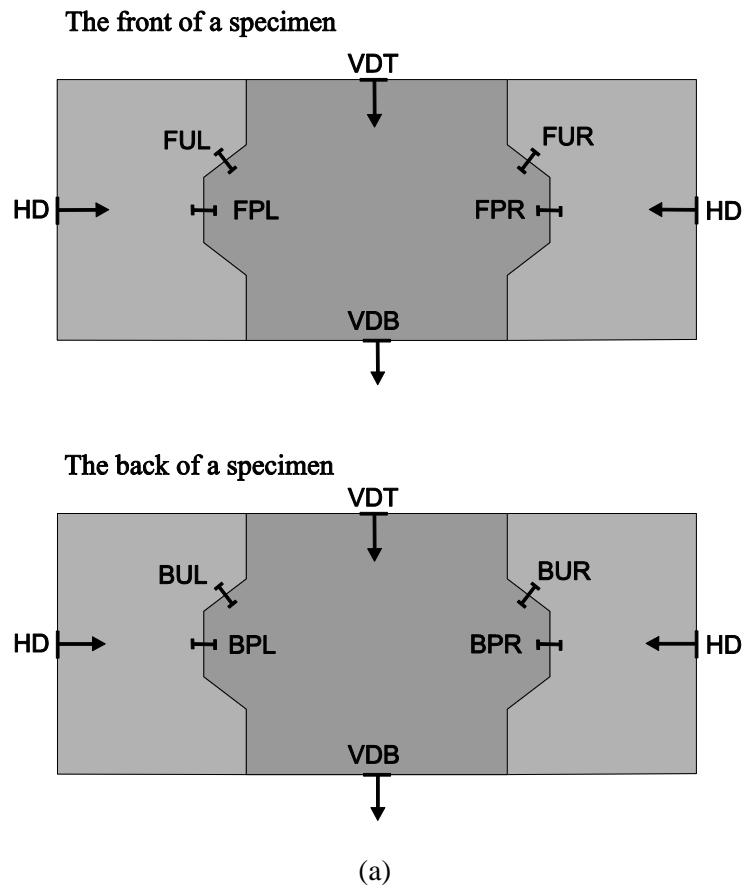


Figure B.9: Coefficient of friction for dry joints of UHPC (a) Relative displacement = 1.0 mm  
(b) relative displacement = 10 mm

## B.4.2 Keyed joint test

### Instrumentation system



(b)

Figure B.10: Instrumentation of dry keyed joint test (a) Position and name of gauges (b) instrumentation set up during the test

### Behaviour of the test specimen: KJ-0-I

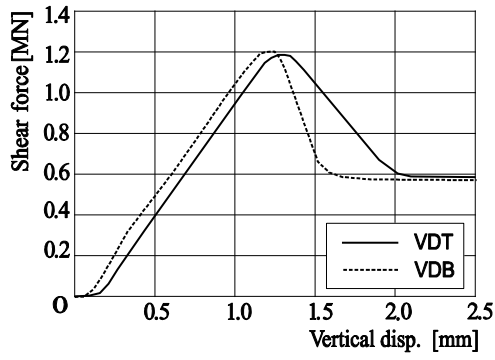


Figure B.11: Load vs. vertical displacement

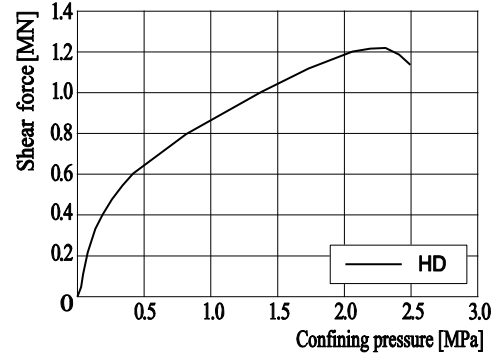


Figure B.12: Variation of confining stress due to increasing load

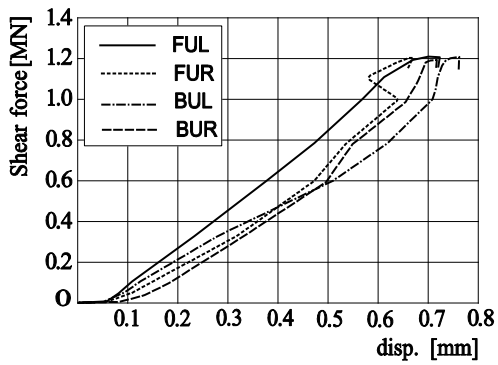


Figure B.13: Variations of joint opening at upper face of key due to increasing load

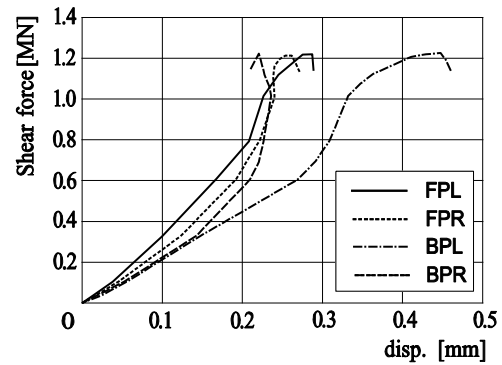


Figure B.14: Variations of joint opening at plane face of key due to increasing load

### Behaviour of the test specimen: KJ-0-II

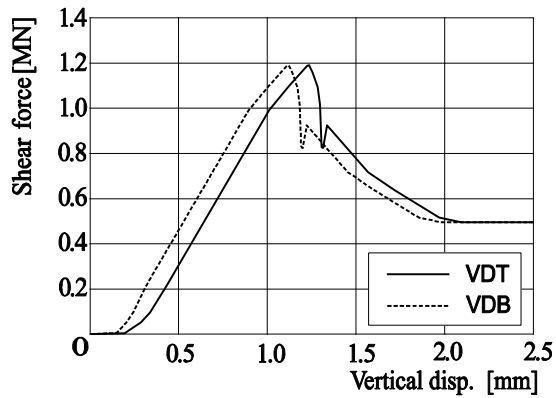


Figure B.15: Load vs. vertical displacement

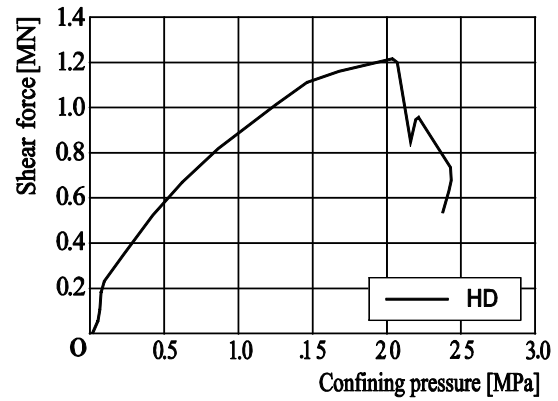


Figure B.16: Variation of confining stress due to increasing load

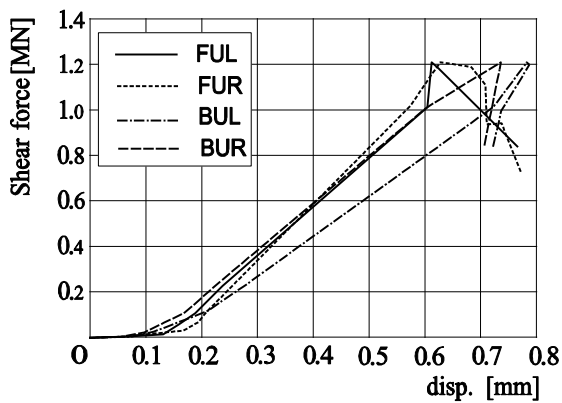


Figure B.17: Variations of joint opening at upper face of key due to increasing load

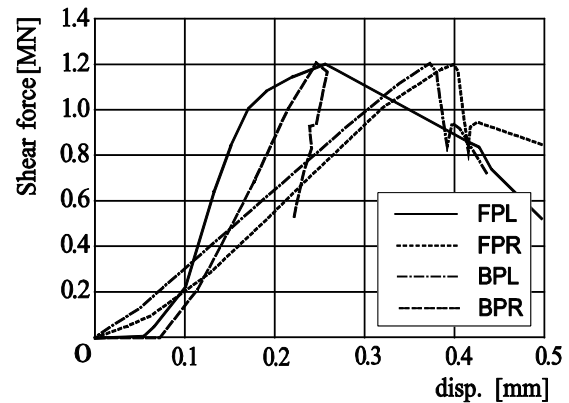


Figure B.18: Variations of joint opening at plane face of key due to increasing load

### Behaviour of the test specimen: KJ-1-I

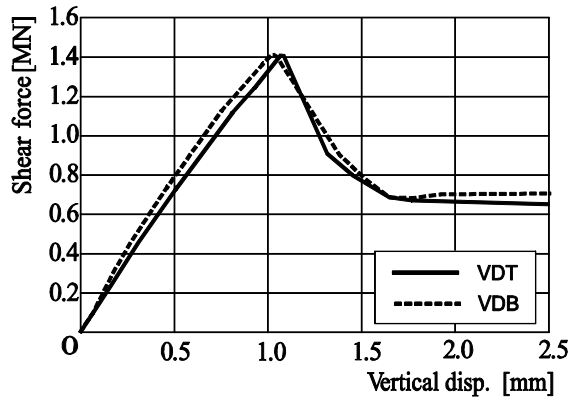


Figure B.19: Load vs. vertical displacement

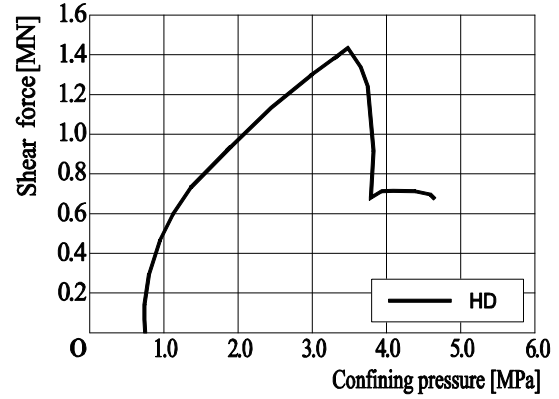


Figure B.20: Variation of confining stress due to increasing load

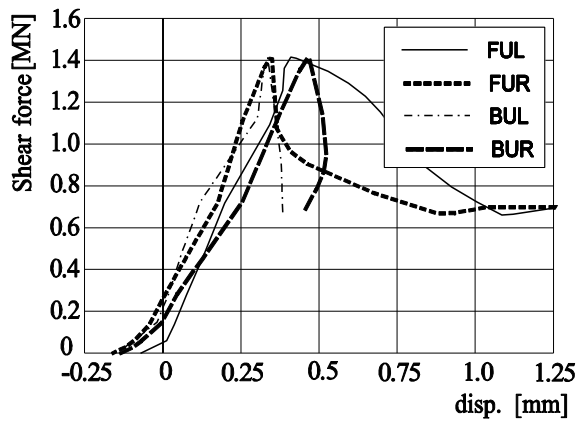


Figure B.21: Variations of joint opening at upper face of key due to increasing load

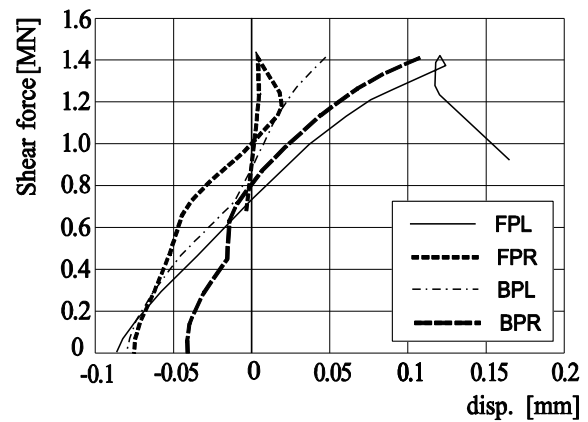


Figure B.22: Variations of joint opening at plane face of key due to increasing load

### Behaviour of the test specimen: KJ-4-I

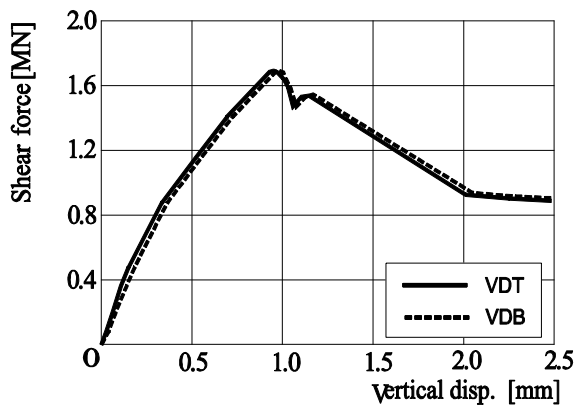


Figure B.23: Load vs. vertical displacement

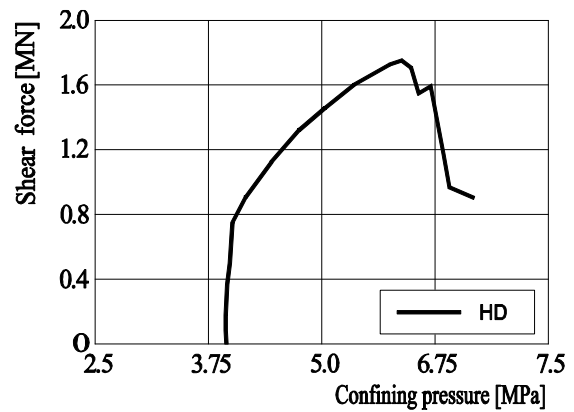


Figure B.24: Variation of confining stress due to increasing load

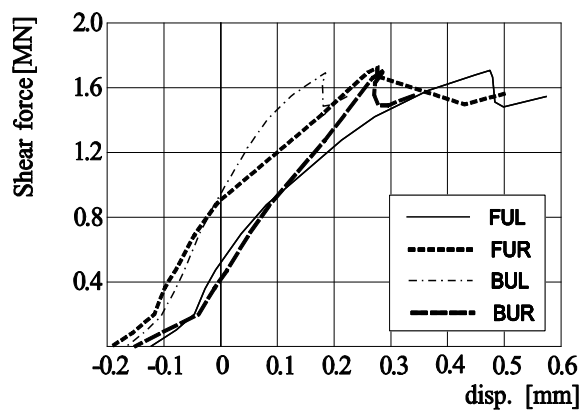


Figure B.25: Variations of joint opening at upper face of key due to increasing load

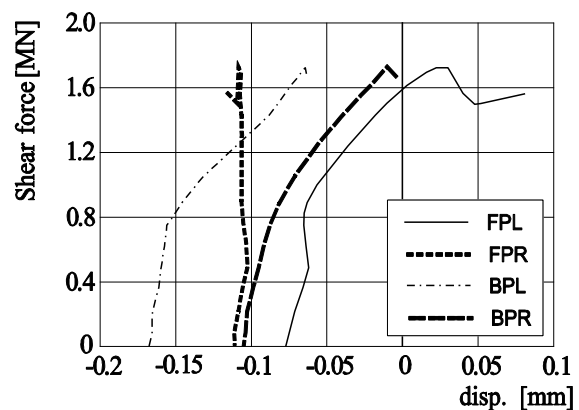


Figure B.26: Variations of joint opening at plane face of key due to increasing load

### Behaviour of the test specimen: KJ-8-I

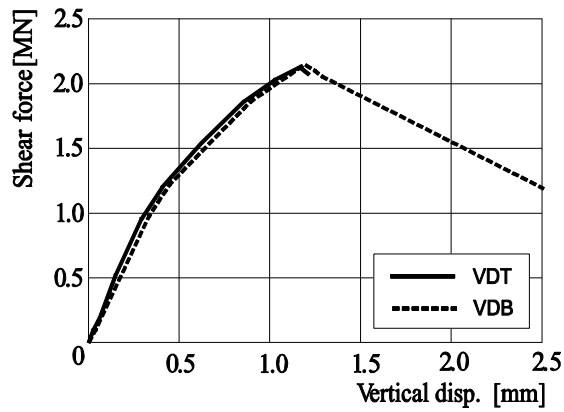


Figure B.27: Load vs. vertical displacement

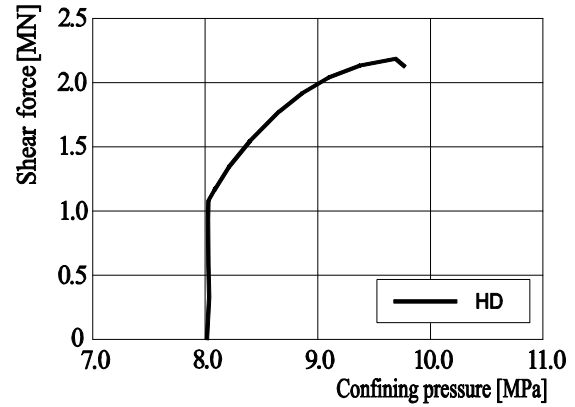


Figure B.28: Variation of confining stress due to increasing load

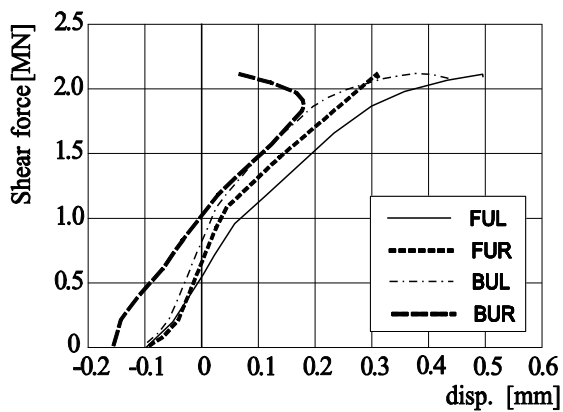


Figure B.29: Variations of joint opening at upper face of key due to increasing load

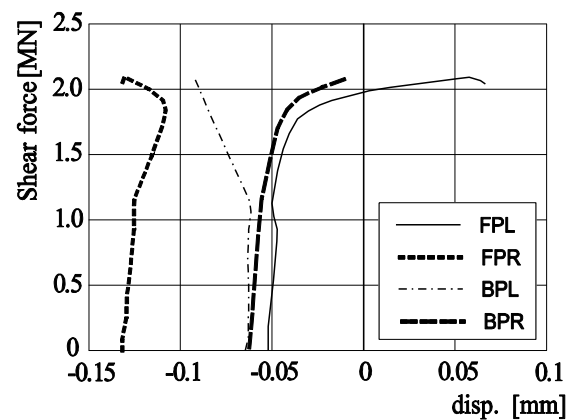


Figure B.30: Variations of joint opening at plane face of key due to increasing load

### Behaviour of the test specimen: KJ-16-I

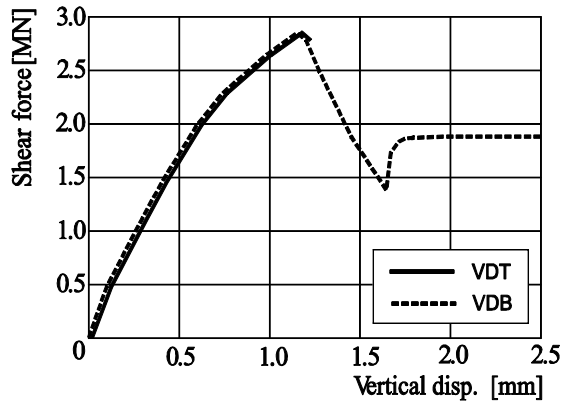


Figure B.31: Load vs. vertical displacement

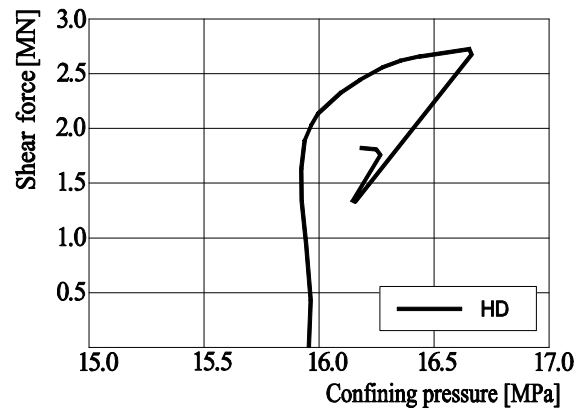


Figure B.32: Variation of confining stress due to increasing load

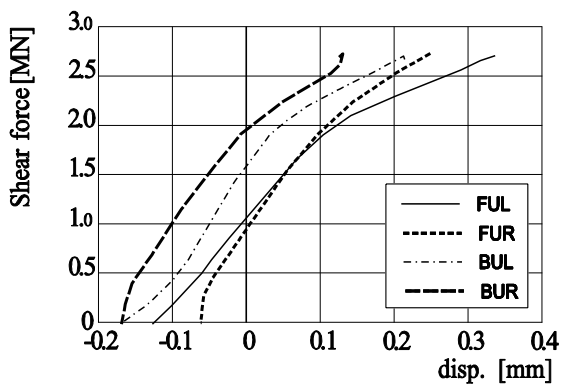


Figure B.33: Variations of joint opening at upper face of key due to increasing load

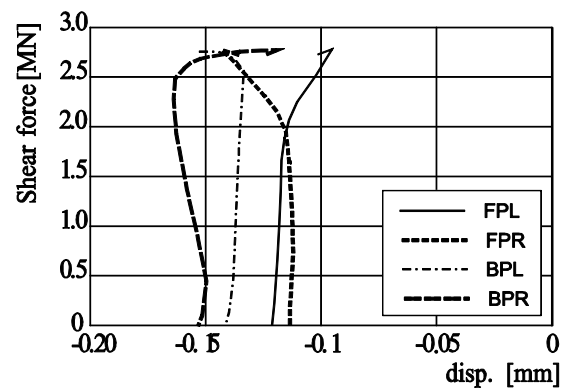


Figure B.34: Variations of joint opening at plane face of key due to increasing load



### Behaviour of the test specimen: KJ-25-I

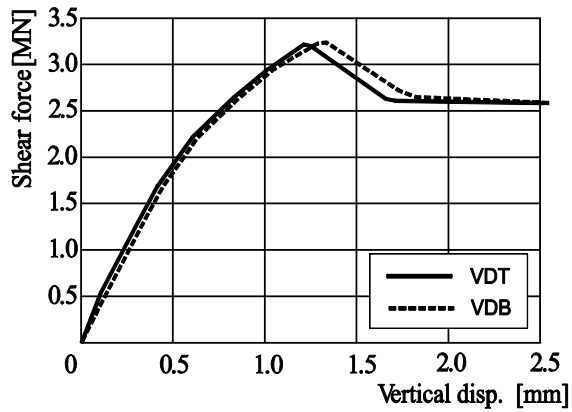


Figure B.35: Load vs. vertical displacement

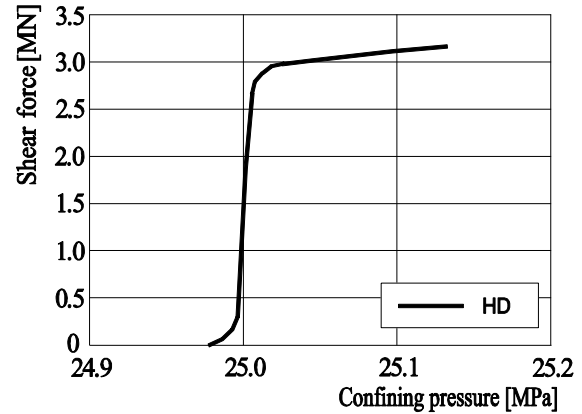


Figure B.36: Variation of confining stress due to increasing load

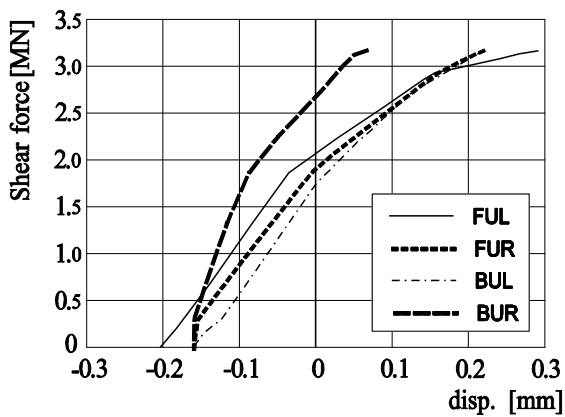


Figure B.37: Variations of joint opening at upper face of key due to increasing load

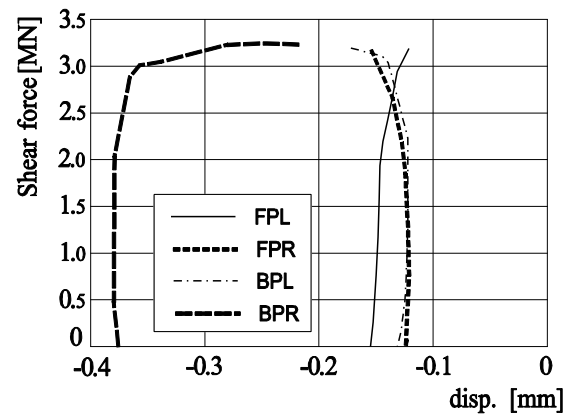


Figure B.38: Variations of joint opening at plane face of key due to increasing load

### Behaviour of the test specimen: KJ-25-II

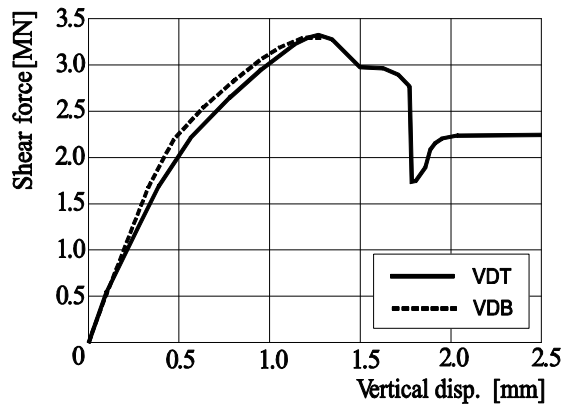


Figure B.39: Load vs. vertical displacement

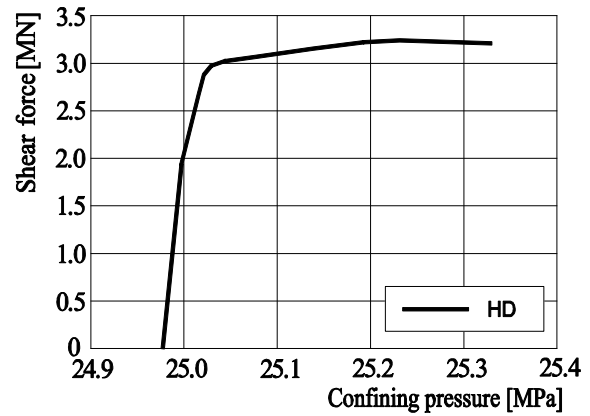


Figure B.40: Variation of confining stress due to increasing load

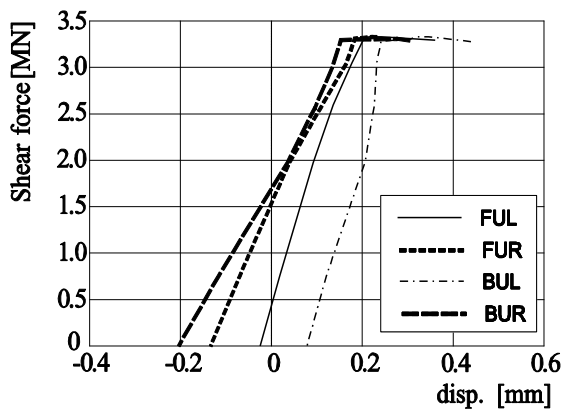
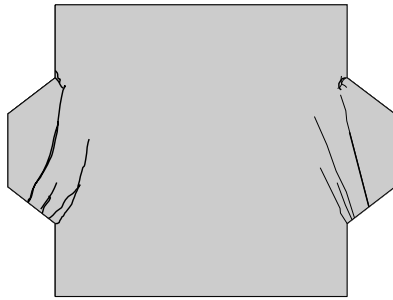
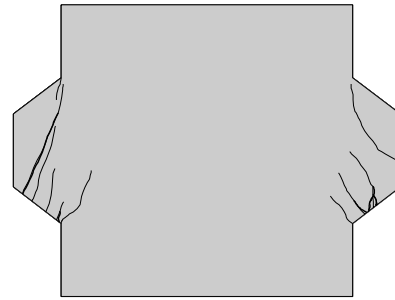


Figure B.41: Variations of joint opening at upper face of key due to increasing load

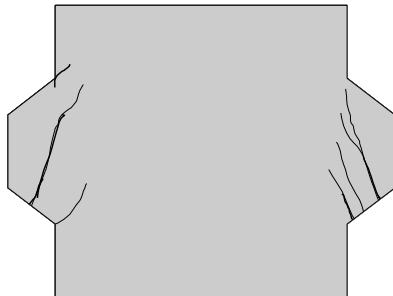
## B.5 Crack pattern of the test specimens



**KJ-0-I**



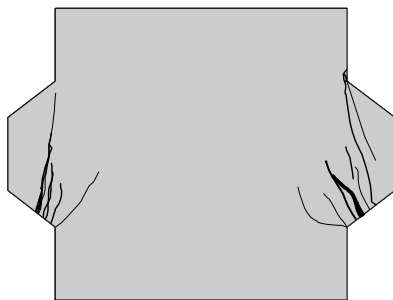
**KJ-0-II**



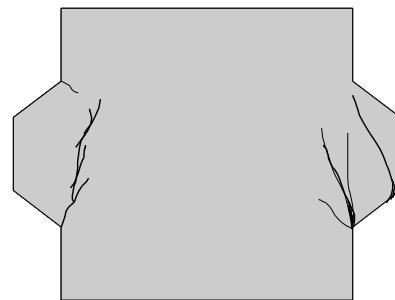
**KJ-1-I**



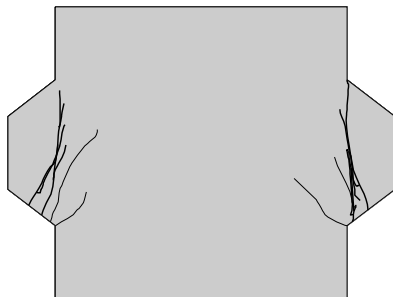
**KJ-4-I**



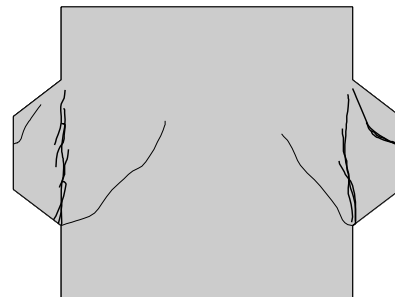
**KJ-8-I**



**KJ-16-I**



**KJ-25-I**



**KJ-25-II**

Figure B.42: Crack pattern after failure of the test specimens

## References

- AASHTO** *Guide Specifications for Design and Construction of Segmental Concrete Bridges*, 2. Edition, Washington, **1999**
- AASHTO** *Standards AASHTO-PCI-ASBI Segmental Box Girder Standards for span-by-span construction*, November, **2002**
- ABAQUS** *Analysis user's Manual*. Version 6.10. © Dassault Systèmes, SIMULIA, 2010
- Abendeh, R.** *Temperature Induced Deformations in Match-Cast Segments and their Effects on Precast Segmental Bridges*. Ph.D. thesis, TU Hamburg-Harburg, **2006**
- ACI Committee 363** *State-of-the-Art Report on High-Strength Concrete*, ACI363R-92, **1997**
- ACI-318-05** *Building Code Requirements for Structural Concrete*. American Concrete Institute, **2005**
- Acker, P., Ulm, F. J.** *UHPFRC: Science-driven material engineering can provide sustainable solution*, Designing and Building with UHPFRC: State of the Art and Development; Wiley, pp. 15-20, **2011**
- Adel-Halim, M. A. H.** *Nonlinear Analysis of a Segmental concrete Bridge by finite Element Method*. Ph.D. Thesis, The Pennsylvania State University, **1982**
- Aeberhard, H. U., Buergi, P., et al.** *External Post-tensioning: Design Considerations VSL External Tendons Examples from Practice*. VSL report series 1. VSL International Ltd., **1992**
- AFGC/SETRA** (Association Française de Génie Civil / Service d'études techniques des routes et autoroutes): *Bétons fibrés à ultra-hautes performances / Ultra High Performance Fibre Reinforced Concretes*, Recommandations provisoires / Interim Recommendations, January, **2002**
- Almansour, H., Lounis, Z.** *Innovative Design of Precast/Prestressed Girder Bridge Superstructures using Ultra High Performance Concrete*, Paper prepared for presentation at the poster session on bridges of the 2008 Annual Conference of the Transportation Association of Canada Toronto, Ontario, **2008**
- Aparicio, A.C., Ramos, G., Casas, J.R.** *Testing of externally prestressed concrete beams*, Engineering Structures 24, **2002**
- Ariyawardena, N.** *Prestressed concrete with Internal or External Tendons: Behaviour and analysis*. Ph.D. Thesis, The University of Calgary, Calgary, Alberta, Canada, July **2000**
- Ariyawardena, N., Ghali, A.** *Design of Precast Prestressed Concrete Members Using External Prestressing* PCI Journal March-April, **2002**

- Baanonde, J. and Benitez, A.** *Monterrey's line 2 extension viaduct: a revolution for light-rail precast concrete segmental bridges*. PCI Journal, pp.175-188, fall, **2009**
- Bache, H. H.** *Ny beton-Ny teknologi*. Alborg Portland, Beton-teknik, **1999**
- Bakhoun, M. M.** *Shear behavior and design of joints in precast concrete segmental bridges*. PhD Thesis, Massachusetts Institute of Technology, **1991**
- Barbier, J.-C.** *Rogerville Viaduct, Normandy - 609 tonnes of PT installed in just 8 months*. VSL News, pp. 4, **1996**
- Beattie, S. M.** *Behavioral improvements in segmental concrete bridge joints though the use of steel fibers*. M.Sc. thesis, Massachusetts Institute of Technology, **1989**
- Behloul, M., Lee, K.C.** *Ductal® Seonyu footbridge*. Structural Concrete, Vol. 4, No. 4, pp. 195-201, December **2003**
- Bernhardt, K., Brameshuber, W., König, G., Krill, A., Zink, M.** *Vorgespannter Hochleistungsbeton: Erstanwendung in Deutschland beim Pilotprojekt Sasbach*. Beton- und Stahlbetonbau 94, No. 5, pp. 216-233, **1999**
- Bertram, G.** *Zum Verbund- und Querkrafttragverhalten von Spannbetonträgern aus Ultrahochfestem Beton*. PhD Thesis, RWTH Aachen Univ., **2012**
- Blais, P.Y., Couture, M.** *Precast, Prestressed Pedestrian Bridge – World's First Reactive Powder concrete Structure*. PCI Journal, Vol. 44, pp. 60-71, Sept/Oct. **1999**
- Bornemann, R., Schmidt, M., Fehling, E., Middendorf, B.** *Ultrahochleistungsbeton – UHFB*. Beton- und Stahlbetonbau 96, Heft 7, pp. 458-467, **2001**
- Breitenbücher, R.** *Developments and applications of high-performance concrete*. Materials and Structure, Vol. 31, pp. 209-215, April **1998**
- Brockmann, C., Rogenhofer, H.** *Bang Na Expressway, Bangkok, Thailand – World's Longest Bridge and Largest Precasting Operation*, PCI Journal, pp.26-38, January-February **2000**
- Buyukozturk, O., Bakhoun, M. M., Beattie, M.** *Shear Behavior of Joints in Precast concrete Segmental Bridges*. ASCE Journal of Structural Engineering, pp. 3380-3401, **1990**
- Casanova, P., Dugat, J., Orange, G.** *“Ductal”: A new generation of Ultra High Performance Fiber Reinforced Concrete*. HPC Symposium, Hong Kong, **2000**
- Combault, J.** *Precast Concrete Segments for Bridges: Fabrication and Assembly – Fundamental Details*. 1st international symposium on bridges and large structures, Brazil, **2008**
- Curbach, M., Speck, K.** *Mehraxiale Festigkeit von duktilem Hochleistungsbeton*. Schriftenreihe des Deutschen Ausschusses für Stahlbeton, Heft 524, Beuth-Verlag, **2003**
- Curbach, M., Speck, K.** *Zweiachiale Druckfestigkeit von ultrahochfestem Beton*. Beton- und

Stahlbetonbau 102, Heft 10, pp. 664-673, **2007**

**DAfStb** (Deutscher Ausschuss für Stahlbeton) *Sachstandsbericht „Ultrahochfester Beton“*. Heft 561, Beuth Verlag, Berlin, **2008**

**DBV** (Deutscher Beton und Bautechnikverein) *Empfehlungen für Segmentfertigteilbrücken mit externen Spanngliedern*. **1999**

**DIN 1045-1** *Tragwerke aus Beton, Stahlbeton und Spannbeton; Teil 1: Bemessung und Konstruktion*. Deutsches Institut für Normung e. V., Berlin, Juli **2001**

**DIN EN 1992-1-1/NA** *Bemessung und Konstruktion von Stahlbeton- und Spannbetontragwerken - Teil 1-1: Allgemeine Bemessungsregeln und Regeln für den Hochbau*, **2011**

**DIN-Fachbericht 101** *Einwirkungen auf Brücken*. DIN Deutsche Institut für Normung, Berlin **2003**

**DIN -Fachbericht 102** *Betonbrücken*. DIN Deutsche Institut für Normung, Berlin, **2003**

**Empelmann, M., Oettel, V.** *UHPFRC Box Girders under Torsion*. Ultra-High Performance Concrete and Nanotechnology in Construction (Proceedings of Hipermant), Schriftenreihe Baustoff- und Massivbau, Vol.19, pp. 517-524, Kassel Univ. press, **2012**

**EN 1992-1-1: 2004** Design of concrete structures – Part 1-1: General rules and rules for buildings. 2004**Fehling E., Schmidt M., Teichmann T., Bunje K., Bornemann R., Middendorf B.** *Entwicklung, Dauerhaftigkeit und Berechnung - Ultrahochfester Beton (UHPC)*, Forschungsbericht DFG FE 497/1-1, Schriftreihe Baustoff- und Massivbau, Band 1, Kassel Univ. press, **2005**

**FIB-Recommendations:** *Practical Design of structural concrete*. FIP-Commission 3 “Practical Design”, Publ.: SETO, London, Sept. 1999. (Distributed by: fib, Lausanne), Sept., **1996**

**Figg, Linda W., Denney Plate, P.E.** *Precast concrete Segmental Bridges-America’s Beautiful and Affordable Icons*. PCI Journal, pp. 26-39, September-October **2004**

**FHWA (The Federal Highway Administration)** *Prefabricated Bridge Elements and Systems in Japan and Europe*. International Technology Exchange Program, pp. 6-7, March **2005**

**FHWA (The Federal Highway Administration)** *Performance of Concrete Segmental and Cable-stayed Bridges in Europe*. International Technology Exchange Program, May **2001**

**Fischer, O., Krill, A.** *The Bang Na Expressway, Bangkok: A Full-Scale Loading Test of a Precast Segmental Box Girder Bridge for Six Lanes of Traffic*, FIP-Symposium 1998, Amsterdam, Structural Concrete 1994-1998, Deutscher Beton Verein e. V., German Group of FIP, pp. 20-25

**Fitik, B., Niedermeier, R., Zilch, K.** *Fatigue Behaviour of Ultra-High Performance Concrete under Cyclic Stress Reversal Loading*. 3<sup>rd</sup> fib International Congress, Washington D.C., **2010**

- Foure, B., Rezende Martins, P. C., Hoang, L. H.** *Problèmes de Sécurité a Rupture et de Modélisation du Comportement des Poutres en Béton a Précontrainte Extérieure*. Annales 491, February, pp. 45-95, **1991**
- Fouré, B., Bouafia, Y., Soubret, R., Thomas, P.** *Shear test on keyed joints between precast segments*. Proceeding of the workshop AFPC, External Prestressing in Structures. Saint-Rémy-Iès-Chevreuse. pp. 297-319, **1993**
- Freyermuth, Clifford L.** *AASHTO-PCI-ASBI Segmental Box Girder Standards: A New Product for Grade Separations and Interchange Bridge*. PCI Journal, pp. 32-42, September-October **1997**
- Freyermuth, Clifford L.** *Ten Years of Segmental Achievements and Projections for the Next Century*. PCI Journal, pp. 36-52, May-June **1999**
- Freytag, B.; Reichel, M.; Sparowitz, L.** *Großversuch Wild-Brücke: Versuchsgestützte Bemessung einer UHPC-Bogenbrücke*. Beton- und Stahlbetonbau 104, Heft 9, **2009**
- Graybeal, B. A.** *Material Property Characterization of Ultra-High performance concrete*. Report No.: FHWA-HRT-06-103, August **2006**
- Graybeal, B. A.** *Flexural Behavior of an Ultrahigh-Performance Concrete I-Girder*. ASCE Journal of Bridge Engineering, pp. 602-610, **2008**
- Graybeal, B. A.** *Structural Behavior of a 2<sup>nd</sup> Generation UHPC Pi-Girder*. TechBrief No.: FHWA-HRT-09-069, **2009**
- Gimsing, N. J.** *History of cable-stayed bridges*. IABSE Conference: Cable-Stayed Bridges – Past, Present and Future, Malmö, Sweden, **1999**
- Girmscheid, G.** *Spannbeton-Hochstraße in Bangkok – Planung der Ausführung*. Beton- und Stahlbetonbau 88, Heft 6, pp.161-166, **1993**
- Hajar, A., Lecointre D.** *Design and construction of the world first Ultra-High Performance Concrete road bridges*. Proceedings of the International Symposium on Ultra High Performance Concrete; Kassel University Press; pp. 39-48, **2004**
- Harris, D. K.** *Characterization of the Punching Shear Capacity of Thin Ultra-High Performance concrete Slabs*. Virginia Transportation Research Council, Report No.: VTRC 05-CR26, June **2005**
- Hense, S.** *Entwicklung und Beschreibung des Tragverhaltens einer modularen Fachwerk-konstruktion aus Hochleistungsbeton*. Ph.D. thesis, Leipzig Univ., **2009**
- Hewson, Nigel R.** *Prestressed Concrete Bridges: Design and Construction*. London, Thomas Telford Ltd., **2003**

**Hewson, Nigel R.** *The use of dry joints between precast segments for bridge decks.* Proceedings of the Institution of Civil Engineer, pp. 177-184, November **1992**

**Hindi, A., MacGregor, R., Kreger, M. E., Breen, J. E.** *Enhancing Strength and Ductility of Post-tensioned Segmental Box Girder Bridges.* ACI Structural Journal, pp. 33-44, January-February **1995**

**JCI** (Japan Prestressed Concrete Engineering Association/ Terada, N., Homma, A., Saito, K. et al.) *Design of Precast Segmental Box Girder Bridge with Strutted Wing Slab.* The 1<sup>st</sup> fib Congress, Concrete structures in the 21st century, Osaka, Japan, Oct., **2002**

**JSCE** *Recommendations for Design and Construction of Ultra High Strength Concrete Structures – Draft.* Japan Society of Civil Engineers, September **2006**

**Kasic, S.** *Tragverhalten von Segmentbauteilen mit interner und externer Vorspannung ohne Verbund.* Ph.D. thesis, Karlsruhe, Heft 48, **2002**

**Keierleber, B., Phares, B. et al.** *Design of Buchanan County, Iowa, Bridge Using Ultra High Performance Concrete and PI Girders.* Proceedings of the 2007 Mid-Continent Transportation Research Symposium, Ames, Iowa, August **2007**

**König, G., Tue N. V., Zink M.** *Hochleistungsbeton - Bemessung, Herstellung und Anwendung.* Ernst & Sohn, Berlin, **2001**

**Koseki, K., Breen, J.,E.** *Exploratory study of shear strength of joints for precast segmental bridges.* Centre for Transportation Research, The Univ. of Texas at Austin, Research report 248-1, September **1983**

**Kreger, M. E., Fenves, G. L., El-Habr, K. C.** *Finite Element Analysis of Externally Post-tensioned Segmental Box Girder Construction.* External Prestressing in Bridges, ACI SP-120, **1990**

**Kupfer, H., Guckenberger, K., Daschner, F.** *Versuche zum Tragverhalten von segmentären Spannbetonträgern - Vergleichende Auswertung für Epoxidharz- und Zementmörtelfugen.* DAfStb Heft 335, Berlin, **1982**

**Lacey, G. C., Breen, J. E.** *State of the Art for Long Span Prestressed Concrete Bridges of Segmental Construction.* PCI Journal, pp.53-77, September-October **1971**

**Leonhardt, F.** *Cable Stayed Bridges with Prestressed Concrete.* PCI Journal - Special Report, Vol. 32, No. 5, September-October **1987**

**Lim, T.Y., Paramasivam, P., and Lee, S. L.** *Analytical model for tensile behavior of steel-fiber concrete.* ACI Materials Journal, pp. 286-298, July-August **1987**

**MacGregor, R., Kreger, M. E., Breen, J. E.** *Strength and Ductility of a Three-Span Externally Post-tensioned Segmental Box Girder Bridge Model.* Research Report 365-3F, Center for Transportation Research, The University of Texas at Austin, January **1989**



- Mansur, M. A., Ong, K. C. G.** *Behavior of reinforced fiber concrete deep beams in shear.* ACI Structural Journal, pp. 98-105, January-February **1991**
- Marković, I.** *High-Performance Hybrid-Fibre Concrete: Development and Utilisation.* Delft Univ., **2006**
- Miller, M. D.** *Durability Survey of Segmental Concrete Bridges.* PCI Journal, pp. 110-123, May-June **1995**
- Mondorf, Paul E.** *Design-Construction of Precast Segmental Elevated Metro Line for Monterrey, Nuevo Leon, Mexico.* PCI Journal, pp. 42-55, March-April **1993**
- Möller, J.** *Rotationsverhalten von verbundlos vorgespannten Segmenttagwerken.* Ph.D. thesis, Karlsruhe, Heft 59, **2006**
- Huang, J.** *Extern vorgespannte Segmentbrücken unter kombinierter Beanspruchung aus Biegung, Querkraft und Torsion.* Schriftenreihe des Instituts für Massivbau und Baustofftechnologie der Universität Karlsruhe, Heft 22, **1994**
- Muller, J.** *Ten years of experience in precast segmental construction.* PCI Journal, pp. 28-6, January- February, **1975**
- Muller, J., Barker, J. M.** *Design and Construction of Linn Cove Viaduct.* PCI Journal, pp. 38-53, September-October **1985**
- Muller, J., Gauthier, Y.** *Ultimate behavior of Precast Segmental Box Girders with External Tendons.* External Prestressing in Bridges, ACI SP-120, **1990**
- Muller, J.** *Design Practice in Europe.* Bridge Engineering Handbook. Ed. Wai-Fah Chen and Lian Duan, Boca Raton: CRC Press, **2000**
- Mutsuyoshi, H., Ichinomiya, T., Sakurada, M., Perera S. V. T. J.** *High-strength concrete for prestressed concrete structures.* CPI Trade Journal for the Concrete Industry, pp. 42-46, August **2010**
- Oettel, V., Empelmann, M.** *Feinprofilierte UHPFRC-Trockenfugen für Segmentbauteile.* Beton- und Stahlbetonbau 108, Heft 7, pp. 487-495, **2013**
- Orgass, M., Klug, Y.** *Fibre Reinforced Ultra-High Strength Concretes.* Proceedings of the First International Symposium on Ultra High Performance Concrete (UHPC), Heft 3, University of Kassel, pp. 637-647, **2004**
- Podolny, W.** *Sunshine Skyway Bridge Closes the Gap.* PCI Journal, pp. 168-176 November-December **1986**
- Podolny, W., Muller, J.** *Construction and Design of Prestressed Concrete Segmental Bridges.* John Wiley & Sons, New York, **1982**

- Rabbat, B. G., Sowlat, K.** *Testing of Segmental Concrete Girders with External Tendons*. PCI Journal, pp. 86-107, March-April **1986**
- Radloff, B. J., Kreger, M. E., Breen J. E.** *Bonding of External Tendons at Deviators*. Center for Transportation Research and the University of Texas at Austin, Report No. FHWA/TX-91+1209-1, **1991**
- Ramirez, G., Macgregor, R., Kreger, M., Roberts-Wollmann, C., Breen, J. E.** *Shear strength of segmental structures*. Proceeding of the workshop AFPC, External Prestressing in Structures. Saint-Rémy-lès-Chevreuse. pp. 297-319, **1993**
- Ramos, G., Aparicio, A. C.** *Ultimate Analysis of Monolithic and Segmental Externally Prestressed Concrete Bridges*. ASCE Journal of Bridge Engineering. Vol. 1, issue 1, February **1996**
- Ralls, M. L., Carrasquillo, R.** *Texas High-Strength Concrete*. Federal Highway Administration, Vol. 57-No. 4, spring **1994**
- Reichel, M., Sparowitz, L., Freytag, B.** *UHPC-Segmental Bridges: Material-based design principles and adapted construction methods*. Proceedings of the Second International Symposium on Ultra High Performance Concrete; Kassel University Press; pp. 779-786, **2008**
- Reichel, M.** *Dünnwandige Segmentfertigteiltbauweisen im Brückenbau aus gefasertem Ultrahochleistungsbeton (UHFB) – Tragverhalten, Bemessung und Konstruktion*. Ph.D. Thesis, TU Graz, **2008**
- Resplendino, J.** *First Recommendation for Ultra-High-Performance-Concretes and examples of application*. Proceedings of the International Symposium on Ultra High Performance Concrete (UHPC), Heft 3, University of Kassel, pp. 79-90, **2004**
- Resplendino, J., Bouteille, S., et al.** *Construction of an overpass on the A51 Motorway, made of a prestressed box beam built with UHPFRC*. In the French technology of concrete, AFGC, The second fib congress, Naples, **2006**
- Resplendino, J.** *Ultra-High Performance Concretes – recent realization and research programs on UHPFRC bridges in France*. Proceedings of the Second International Symposium on Ultra High Performance Concrete (UHPC), Heft 10, University of Kassel, pp. 31-43, **2008**
- Roberts, C., R., Breen, J. E., Kreger, M. E.,** *Measurement Based Revisions for Segmental Bridge Design and Construction Criteria*. Research Report 1234-3F, Center for Transportation Research, The University of Texas at Austin, January **1993**
- Rombach, G., Specker, A.** *Numerical Modelling of Segmental Bridges*. ECCM '99, München **1999**
- Rombach, G., Specker, A.** *Finite Element Analysis of Externally Prestressed Segmental Bridges*. EM 2000, Austin, pp. 21-24, **2000**

- Rombach G.; Specker A.** *Design of Joints in Segmental Hollow Box Girder Bridges*. First FIB Congress 2002, Concrete Structures in the 21<sup>st</sup> Century', Osaka, **2002**
- Rombach, G.** *Precast segmental box girder bridges with external prestressing - design and construction*. INSA Rennes, Feb. **2002**
- Rombach, G., Specker, A.** *Segmentbrücken*. Betonkalender Teil 1 (Bergmeister/Wörner e.d.), Verlag Ernst & Sohn, Berlin, pp. 177-212, **2003**
- Rombach, G.** *Dry joint behaviour of hollow box girder segmental bridges*. Fib Symposium, 'Segmental construction in Concrete' New Delhi, **2004**
- Rombach G., Abende Rae'd** *Temperature induced deformations in match-cast segments*. IABSE Symposium: Metropolitan Habitats and Infrastructure, Shanghai, **2004**
- Rombach G., Abende Rae'd.** *Bow shaped segments in precast segmental bridges*. Engineering Structures 30 (**2008**), pp. 171-179
- Rossi, P. et al.** *Bending and Compressive Behaviors of a New Cement Composite*. Cement and Concrete Research, Vol. 35, No. 1, pp. 27-33, **2005**
- Russell, H. G.** *High Performance Concrete Specifications and Practices for Bridges* NCHRP (National Cooperative Highway Research Program) Synthesis 441, Washington, D.C., **2013**
- Saito, K. et al.** *The Superstructure Design of the Uchimaki Viaduct*. The 11<sup>th</sup> Symposium on Developments in Prestressed Concrete, Japan, November **2001**
- Sauvageot, G.** *Segmental concrete Bridges: Bridge Engineering Handbook*. Ed. Wai-Fah Chen and Lian Duan Boca Raton: CRC Press, **2000**
- Schmidt, M., Bunje, K., Fehling, E., Teichmann T.** *Brückenfamilie aus Ultra-hochfestem Beton in Niestetal und Kassel*. Beton und Stahlbetonbau, Jahrgang 101, Heft 3, pp. 198-204, **2006**
- Schmidt, M., Fehling, E.** *Ultra-High-Performance Concrete: Research, Development and Application in Europe*. Proceeding of SISU of HS/HPC U.S.A, Edited by Henry G. Russell, ACI Advancing Concrete Knowledge, pp. 51, **2005**
- Schoening, J., Pietra, R. d., Hegger, J., Tue, N. V.** *Verbindungen von Fertigteilen aus UHPC*. Bautechnik 90, Heft 5, pp. 304-313, **2013**
- Shushkewich, K. W.** *The Strutted Box Widening Method for Prestressed Concrete Segmental Bridges*. PCI Journal, Vol.48, No.6, November-December **2003**
- Shushkewich, K. W.** *The Strutted Box Widening Method for Prestressed Concrete Segmental Bridges*. Journal of bridge engineering, ASCE, Vol.11, No.1, January-February **2006**
- Shushkewich, K. W.** *Eugène Freyssinet – Invention of Prestressed Concrete and Precast Segmental Construction*. Structural Engineering International, Vol. 22, No. 3, August **2012**

- Spasojevic, A.** *Structural Implications of Ultra-High Performance Fibre-Reinforced Concrete in Bridge Design*. PhD. Thesis, École Polytechnique Fédérale de Lausanne, **2008**
- Specker, A.** *Der Einfluss der Fugen auf die Querkraft- und Torsionstragfähigkeit extern vorgespannter Segmentbrücken*. Ph.D. Thesis, TU Hamburg-Harburg, **2001**
- Sofia, M. J., Homsí, Elie H.** *Fabrication and Erection of Precast Concrete Segmental Boxes for Baldwin Bridge*. PCI Journal, pp. 36-52, November-December **1994**
- SOFiSTiK: SOFiSTiK® Programmdokumentation Servicepack 23**. Sofistik AG, Oberschleisheim, **2011**
- Tadros, G. Lester, B.** *Northumberland's Strait Crossing: Design Development of Precast prestressed Bridge Structure*. PCI Journal, pp. 32-44, September-October **1995**
- Tanaka, Y., Maekawa, K. et al.** *The Innovation and Application of UHPFRC Bridges in Japan, Designing and Building with UHPFRC: State of the Art and Development*; Wiley, pp. 149-187, **2011**
- Takebayashi A., Deeprasertwong K., Leung Y.** *A full-scale destructive test of a precast segmental box girder bridge with dry joints and external tendons*. Proceedings of the Institution of Civil Engineer, pp. 297-315, August **1994**
- Tassin, D. M.** *Jean M. Muller: Bridge Engineer with Flair for the Art Form*. PCI Journal, pp. 2-15, March-April **2006**
- Tassin, D., Dodson, B., Takebayashi, T.** *Analyzing the Ultimate Capacity of a Precast Segmental Box Girder Bridge*. Structural Engineering International, Vol. 6, No. 4, pp. 255-258, **1996**
- Toutlemonde F.** *HPC Applications in France*. LCPC, Division FDOA (Public Works Research Institute, Bridge Structures Department), **2007**
- Tue, N. V., Küchler, M., Schenck, G., Jürgen, R.** *Application of UHPC filled tubes in buildings*. Proceedings of the International Symposium on Ultra High Performance Concrete (UHPC), Heft 3, University of Kassel, pp. 807-817, **2004**
- Tue, N. V., Winkler, M., Freytag, B.** *Connections for precast UHPC part*. CPI-worldwide; Concrete Technology, issue 4, pp. 56-62, **2011**
- Turmo, J., Ramos, G., Aparicio, A.C.** *FEM modelling of unbonded post-tensioned segmental beams with dry joints*. Engineering Structures, Vol. 28, pp. 1852–1863, **2006 (a)**
- Turmo, J., Ramos, G., Aparicio, A.C.** *Shear strength of dry joints of concrete panels with and without steel fibres: Application to precast segmental bridges*. Engineering Structures, Vol. 28, pp. 23–33, **2006 (b)**

- 
- Turmo, J., Ramos, G., Aparicio, A.C.** *Towards a model of dry shear keyed joints: modeling of panel tests*. Computers and Concrete, Vol. 108, No. 5 pp. 469–487, **2012**
- Virlogeux, M.** *External Prestressing Historical and Modern Application*. Proceeding of the workshop AFPC, External Prestressing in Structures. Saint-Rémy-lès-Chevreuse. pp. 13-35, **1993**
- Virlogeux, M.** *Non-linear Analysis of Externally Prestressed Structure*. Proceedings of the FIP Symposium, Jerusalem, pp. 319-340, **1988**
- Watanabe, N., Musha, H., Yoshinaga, K.** *Design and Performance Tests for Bridge using Ultra High Strength Fiber Reinforced Concrete*. 23th US-Japan Bridge Engineering Workshop, November **2007**
- Xercavins, P., Demarthe, D., Shushkewich, K. W.** *Eugène Freyssinet – the Invention of Prestressed Concrete and Precast Segmental Construction*. Eugène Freyssinet website **2008**
- Zhou, X., Mickleborough, N., et al.** *Shear Strength of Joints in Precast Concrete Segmental Bridges*. ACI Structural Journal, Vol. 201, No. 1, pp. 3-11, January-February **2005**
- Zilch, K., Göger, G., et al.** *Fertigteilbrückenbauwerk mit Hochleistungsbeton B85 und verbundloser interner Längsvorspannung (Ortsumgehung Bad Griesbach St 2116)*. Bauingenieur Vol. 76, pp. 157-161, **2001**
- Zilch, K., Pfisterer, H., Müller, A., Hennecke, M.** *Pilotprojekt Buchloe – Brückenbauwerk mit Hochleistungsbeton B85*. Bauingenieur Vol. 74, pp. 370-378, **1999**
- Zilch, K., Zehetmaier, G.** *The Application of HPC in Bridges Structures – Three Pilot Projects*. 6<sup>th</sup> International Symposium on High Strength / High Performance Concrete, **2002**

## Abbreviations

### *Materials*

CRC	Compact Reinforced Cement
FRC	Fibre Reinforced Concrete
HDPE	High-Density Polyethylene
NSC	Normal Strength Concrete
HSC	High Strength Concrete
HPC	High Performance Concrete
OC	Ordinary Concrete
RPC	Reactive Powder Concrete
UHPC	Ultra High Performance Concrete
UHPFRC	Ultra High Performance Fibre Reinforcement Concrete

### *Mechanics*

CDP	Concrete Damaged Plasticity (in Abaqus)
CSC	Concrete Smeared Crack (in Abaqus)
FEM	Finite Element Method
SLS	Serviceability Limit State
ULS	Ultimate Limit State

### *Institutions and Projects*

AASHTO	American Association of State Highway and Transportation Officials
ACI	American Concrete Institute
AFGC	Association Française de Génie Civil
CEBTP	Centre Expérimental de Recherches et d'Etudes du Bâtiment et des Travaux Publics, in France
DAfStb	Deutscher Ausschuss für Stahlbeton / German Association for Reinforced Concrete
DBV	Deutsche Beton- und Bautechnik Verein
TUHH	Technische Universität Hamburg Harburg
SETRA	Service d'Études Techniques des Routes et Autoroutes (Roads and Motorways Department), in France

## Notations

### Latin upper case letters

$A_c$	Cross sectional area of concrete
$A_p$	Cross sectional area of a prestressing tendon or tendons
$E_c$	Tangent modulus of elasticity of normal weight concrete
$E_{cd}$	Design value of modulus of elasticity of concrete
$E_{cm}$	Second modulus of elasticity of concrete
$A_j$	Cross sectional area of the joint (or $A_{joint}$ )
$A_k$	Area of the base of all keys in the failure plane (or $A_{key}$ )
$A_{sm}$	Area of contact between smooth surfaces on the failure plane
$E_p$	Design value of modulus of elasticity of prestressing steel
$EI$	Bending stiffness
$F$	Action
$F_v$	Vertical force
$F_h$	Horizontal force
$F_{v,test}$	Maximum vertical force obtained by the experiment
$F_{h,test}$	Initial horizontal force (without vertical force) in the experiment
$H$	Height or depth of a cross-section
$G$	Elastic shear modulus of the uncracked concrete
$G_k$	Characteristic permanent action
$I$	Second moment of area of concrete section
$L$	Length
$M$	Bending moment
$M_{Ed}$	Design value of the applied internal bending moment
$M_{dec}$	Decompression moment
$N$	Axial force
$P$	Prestressing force
$Q_k$	Characteristic variable action
$V$	Shear force
$V_{Ed}$	Design value of the applied shear force
$V_f$	Volume fraction of steel fibers.
$V_j$	Shear strength of the dry joint [MN]
$V_{j,d}$	Shear design value of the dry joint [MN]
$W_g$	Self-weight per unit length of girder

### Latin lower case letters

$b_k$	Width of shear key
$b_w$	Width of the web
$c$	Factor depending on the indented joints
$e$	Eccentricity before the deformation
$\bar{e}$	Eccentricity after the deformation
$d_k$	Depth of shear key
$f$	Factor for the indentation of the joint
$f_c$	Compressive strength of concrete
$f_{cd}$	Design value of compressive strength of concrete
$f_{ck}$	Characteristic compressive cylinder strength of concrete at 28 days
$f_{ct}$	Characteristic tensile strength of concrete
$f_{ctd}$	Design tensile strength of concrete
$f_{ct,m}$	Mean value of axial tensile strength of concrete
$f_{ctk}$	5% Quantile of the tensile strength (maximum value of the $\sigma$ - $\varepsilon$ curve)
$f_p$	Tensile strength of prestressing steel
$f_{pk}$	Characteristic tensile strength of prestressing steel
$f_{yk}$	Yield strength of prestressing steel
$l_f$	Length of steel fibers
$t$	Member thickness
$v_{Rdi}$	Design shear resistance at the interface
$u, v, w$	Components of the displacement of a point
$z$	Lever arm (distance from centroid axis)
$\epsilon$	Flow potential eccentricity
$\psi$	Dilation angle in the p-q plane

### Greek lower case letters

$\gamma_b$	Partial safety factor (in AFGC/SETRA )
$\gamma_c$	Safety factor for design compressive strength of concrete
$\gamma_{c,UHPC}$	Safety factor for design compressive strength of UHPC
$\gamma_{ct}$	Partial safety factor for the tensile strength of fiber reinforced concrete
$\gamma_f$	Partial safety factor taking into account irregularities in fiber orientation
$\delta$	Displacement
$\varepsilon_c$	Compressive strain in the concrete
$\varepsilon_{cr}$	“fictitious” strain related to crack mouth opening
$\varepsilon_{el}$	Maximum elastic tensile strain
$\varepsilon_{ps}$	Strain of prestressing steel
$\varepsilon_u$	Limited strain in tension of concrete
$\eta_l$	Length efficiency factor for fibers



---

$\eta_o$	Fiber orientation factor
$\theta$	Angle/rotation component
$\lambda$	Slenderness ratio
$\mu$	Coefficient of friction
$\nu$	Poisson's ratio
$\nu$	Strength reduction factor for concrete cracked in shear
$\omega$	Width of joint opening
$\sigma_c$	Compressive stress in the concrete
$\sigma_{b0}$	Initial equibiaxial compressive yield stress
$\sigma_{c0}$	Initial uniaxial compressive yield stress
$\sigma_n$	Normal stress across the joints
$\sigma_p$	Stress in prestressing strand
$\tau$	Shear stress
$\tau_{uf}$	Ultimate bond strength of fibres
$\phi_f$	Diameter of steel fibres



## Curriculum Vitae

Family Name	Shin
Given Name	Jaewoo
Nationality	Korean
Geburtsdatum	12.03.1978
Place of Birth	Seoul, Korea
Civil Status	married, 2 children

03. 1994 – 02. 1997	Myungduk High School in Seoul, Korea
06. 1998 – 10. 2000	Naval military service
09. 1997 – 02. 2005	Student at the Ajou University, Korea; mayor: Civil Engineering Degree: Bachelor of Engineering
03. 2005 – 02. 2007	Student at the Ajou University, Korea; mayor Civil Engineering Degree: Master of Engineering
10. 2009 – 07. 2016	PhD student at the Institute of Concrete Structures, Hamburg University of Technology, Germany Supervisor: Prof. Dr.-Ing. Günter Axel Rombach